Oxidative Medicine and Cellular Longevity

Discovery and Biological Evaluation of Natural Phenolic Antioxidants

Lead Guest Editor: Jie Li
Guest Editors: Keyvan Dastmalchi, Lin-sen Qing, and Pei Luo

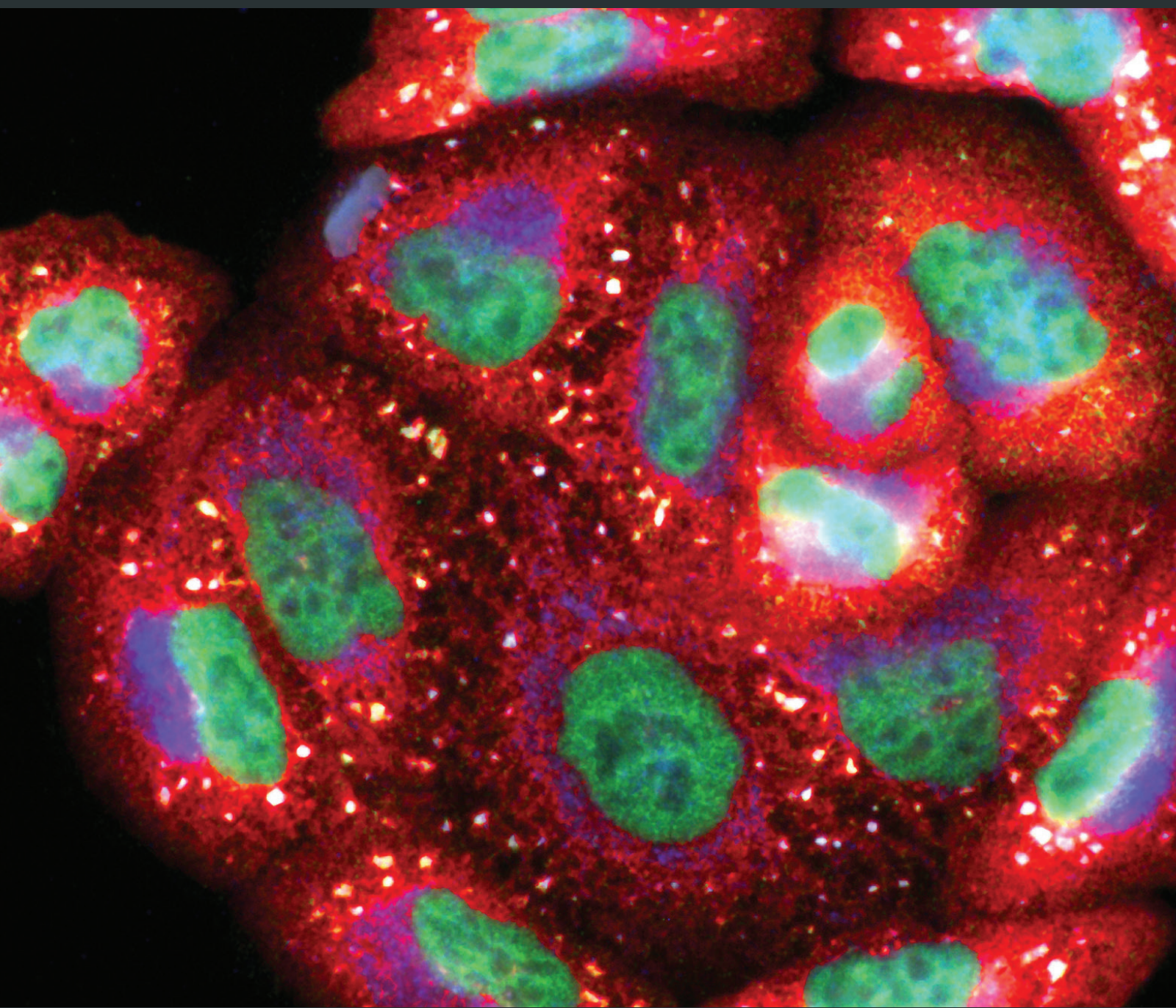

Discovery and Biological Evaluation of Natural Phenolic Antioxidants

Oxidative Medicine and Cellular Longevity

Discovery and Biological Evaluation of Natural Phenolic Antioxidants

Lead Guest Editor: Jie Li
Guest Editors: Keyvan Dastmalchi, Lin-sen Qing, and Pei Luo

Editorial Board

Contents

Hepatoprotective Effect of Polyphenol-Enriched Fraction from *Folium Microcos* on Oxidative Stress and Apoptosis in Acetaminophen-Induced Liver Injury in Mice
Hongtan Wu, Gang Zhang, Lisen Huang, Haiyue Pang, Na Zhang, Yupei Chen, and Gueyhorng Wang
Volume 2017, Article ID 3631565, 14 pages

Hindawi
Oxidative Medicine and Cellular Longevity
Volume 2017, Article ID 2649129, 2 pages
https://doi.org/10.1155/2017/2649129

Editorial

Discovery and Biological Evaluation of Natural Phenolic Antioxidants

Jie Li,[1] Keyvan Dastmalchi,[2] Lin-sen Qing,[3] and Pei Luo[4]

[1]*University of California, San Diego, San Diego, CA, USA*
[2]*The City College of New York, New York, NY, USA*
[3]*Chengdu Institute of Biology, Chinese Academy of Sciences, Chengdu, China*
[4]*Macau University of Science and Technology, Taipa, Macau*

Correspondence should be addressed to Jie Li; jil407@ucsd.edu

Received 25 October 2017; Accepted 26 October 2017; Published 16 November 2017

Oxidative stress results from the imbalance between reactive oxygen or nitrogen species and antioxidants and has been increasingly recognized as a significant contributing factor in the pathogenesis of various disorders, such as pulmonary disorders and cardiovascular diseases. Although well known as antioxidants and widely perceived for their beneficial effects, a large number of phenolic natural products remain underexplored and more evidence is needed to elucidate the molecular mechanisms of different classes of phenolic compounds involved in the potential protective effects against oxidative stress. This special issue aimed to highlight the discovery as well as biological evaluation of natural phenolic antioxidants. From about 20 manuscripts received, we selected 7 primary research articles and 2 reviews that addressed different aspects of those objectives.

X. Ren et al. reported that the role of resveratrol, a phenolic antioxidant, in regulating mitochondrial functions and dynamics during the cardiac aging process involves the Drp1/Parkin/PINK1 signaling pathway. The activation of parkin and PINK1 may be a potential mechanism of resveratrol for treating cardiovascular complications related to aging.

In their primary research article, K. Ji et al. evaluated ginger oleoresin, mainly comprised of phenolic gingerols and shogaols, for their potential to alleviate γ-ray irradiation-induced reactive oxygen species. Besides the direct radiation damage, most of the ionizing radiation- (IR-) induced injuries are caused by generation of reactive oxygen species (ROS). Thus, alleviation of such ROS represents an important means for radiation protection. Their results showed that ginger oleoresin exerted radioprotective effect via the induction of the translocation of Nrf2 to cell nucleus and the subsequent activation of the expression of cytoprotective genes encoding HO-1 and NQO-1, suggesting that ginger oleoresin has a potential as an effective antioxidant and radioprotective agent.

M. Strzemski et al., in their article, studied the chlorogenic acid content, mineral content, total phenolic content, total flavonoid content, and antioxidant activity of three populations of *Carlina vulgaris* L. Among these populations, the flower head extracts obtained from the nonmetallicolous populations were shown to contain the largest amount of chlorogenic acid, a major antioxidant component of this species. Their study suggested *Carlina vulgaris* L. as a source of phytochemicals with antioxidant activity.

The review article by Y. Zhao et al. summarized the recent experimental and limited clinical trial evidence supporting that quercetin, curcumin, and resveratrol, the three selected phenolic compounds, have potential beneficial functions on obesity treatment, through the alleviation of intracellular oxidative stress as one of the possible mechanisms.

A. Papadopoulou et al. observed the reduction of oxidative stress in chickens after the administration of drinking water rich in polyphenolic powder from olive mill waste waters. They evaluated the biomarker in plasma associated with the reduction of oxidative stress and suggested that the

phenolic components from olive mill waste waters could be utilized as a supplement to reduce oxidative stress-induced damage in chicken raising.

In a primary research study, L. Du et al. showed that sea buckthorn paste, a traditional Tibetan medicine with high content of polyphenols and remarkable antioxidant activity, provided significant protection against LPS-induced acute lung injury through maintaining redox homeostasis, with the underlying mechanism involving Nrf2 nuclear translocation and activation.

H. Zhou et al., in their article, revealed that rosmarinic acid attenuated the endothelial dysfunction induced by oxidative stress via the activation of the AMPK/eNOS pathway. They showed that rosmarinic acid cotreatment mitigated the endothelium-dependent relaxation impairments and the oxidative stress induced by H_2O_2 and reversed the downregulation of AMPK and eNOS phosphorylation.

In another review article, L. Yu et al. summarized the recent research development with regard to the cardioprotective effects of salvianolic acid, the major bioactive phenolic constituent of Radix *Salviae miltiorrhizae*. They used the vascular endothelium growth factor, blood vessel density, and myocardial infarct size as the outcome measures for evaluation. Their meta-analysis demonstrated that salvianolic acid can exert cardioprotection effect through promoting angiogenesis in animal models of myocardial infarction.

The article of H. Wu et al. investigated the hepatoprotective effect and underlying mechanisms of the polyphenol-enriched fraction from *Folium Microcos*. Their findings suggested that the hepatoprotective effect of *Folium Microcos* against APAP-induced hepatotoxicity is mainly through dual modification of ROS/MAPKs/apoptosis axis and Nrf2-mediated antioxidant response, which might be attributed to the strong antioxidant activity of phenolic components.

Jie Li
Keyvan Dastmalchi
Lin-sen Qing
Pei Luo

Hindawi
Oxidative Medicine and Cellular Longevity
Volume 2017, Article ID 4175353, 20 pages
https://doi.org/10.1155/2017/4175353

Research Article

Resveratrol Ameliorates Mitochondrial Elongation via Drp1/Parkin/PINK1 Signaling in Senescent-Like Cardiomyocytes

Xuecong Ren,[1,2] Li Chen,[1,2] Jing Xie,[1] Zhifeng Zhang,[1,2] Gengting Dong,[1] Jie Liang,[2] Liang Liu,[1,2] Hua Zhou,[1,2] and Pei Luo[1,2]

[1]*State Key Laboratory of Quality Research in Chinese Medicine, Macau University of Science and Technology, Avenida Wai Long, Taipa, Macau*
[2]*Faculty of Chinese Medicine, Macau University of Science and Technology, Taipa, Macau*

Correspondence should be addressed to Hua Zhou; hzhou@must.edu.mo and Pei Luo; pluo@must.edu.mo

Received 7 April 2017; Revised 26 June 2017; Accepted 5 September 2017; Published 22 October 2017

Academic Editor: Qingping Feng

Resveratrol is widely known for its antiaging properties and exerts cardiovascular protective effects in different experimental models. The role of resveratrol in regulating mitochondrial functions and dynamics during the cardiac aging process remains poorly understood. In this study, the effects of resveratrol on mitochondrial morphology and mitochondrial depolarization and on expressions of Drp1, parkin, PINK1, and LC3 were investigated in H9c2 cells after D-galactose treatment that induced senescent-like cardiomyocytes. The results show that downregulation of Drp1 markedly increased mitochondrial elongation. Senescent-like cardiomyocytes were more resistant to CCCP-induced mitochondrial depolarization, which was accompanied by suppressed expression of parkin, PINK1, and LC3-II. Resveratrol treatment significantly increased Drp1 expression, ameliorated mitochondrial elongation, and increased the mitochondrial translocations of parkin and PINK1. In addition, resveratrol significantly enhanced LC3-II expression and decreased TOM20-labeled mitochondrial content. Resveratrol also suppressed the phosphorylation of parkin and PINK1, which may relate to its abilities to degrade the impaired mitochondria in senescent-like cardiomyocytes. These findings show that suppressing mitochondrial elongation in a Drp1-dependent manner is involved in the effect of resveratrol on attenuating the development of aging cardiomyocytes. Activation of parkin and PINK1 may be a potential mechanism of resveratrol for treating cardiovascular complications related to aging.

1. Introduction

Age-related loss or attenuation of myocardial ischemic preconditioning (IPC) has been studied in animals and humans [1, 2]. Although the dysfunctional IPC mechanisms underlying the aging process remain unclear, there is considerable agreement that mitochondria play a key role in the aging process and that specific defects in mitochondrial function are associated with age-related decline in cardiac efficiency. Alterations of mediator release and/or intracellular pathways mediated by mitochondria may be responsible for the age-related IPC reduction. However, therapeutic intervention via mitochondrial-related mechanisms, such as ATP-sensitive potassium channels (K_{ATP} channels) and permeable transition pore openings [3–5], showed disappointing outcomes in aged hearts [6].

In the past decade, the role of mitochondrial dynamics focusing on organelle fission and fusion has been studied in normal and diseased hearts, and the dysfunction of mitochondrial fission and fusion was well implicated in cardiac death or disease with aging [7–9]. Cardiomyocytes are particularly vulnerable to ischemia due to their high-energy utility and no reserve. Therefore, the tolerance conferred by IPC in aged cardiomyocytes is probably dependent on their ability to maintain mitochondrial dynamism, such as fusion, fission, biogenesis, and selective degradation. The predominant molecular mediator of mitochondrial fission is a member of the dynamin family of GTPases named dynamin-related protein-1 (Drp1) which modulates mitochondrial dynamics. Mitochondrial fragmentation frequently observed in ischemic cardiomyocytes is widely recognized as evidence of increased mitochondrial fission mediated by

Drp1 [10]. Pharmacological inhibition of Drp1 with the Mdivi-1 compound has been suggested to reduce cell death after myocardial infarction [11, 12]. Although a few studies have tested this approach and early results appear promising, the essential requirement of Drp1 in cardiac aging remains elusive. One major challenge in the investigation of mitochondrial fission is to discern the effects of cardiomyocyte senescence from those produced by DNA mutations, metabolism disorders, and excessive ROS (reactive oxygen species) production [13, 14], which contributed to mega, giant, or enlarged mitochondria [15, 16]. Mitochondria with these abnormal dynamics exhibited functional disorders and probably were responsible for the decreased response of aging hearts to IPC.

The selective removal of damaged mitochondria plays a crucial role in maintaining mitochondrial homeostasis maintenance and normal cellular metabolisms of cells. However, a deficiency in mitochondrial fission proteins results in increased activity of senescence-associated β-galactosidase and mitochondrial elongation in aging hearts [17]. Elongated mitochondria display a larger size that increases the difficulty of removal and always presents defective fission. Although whether Drp1 is essential for the selective removal of damaged mitochondria remains unclear, Drp1 is strongly expressed in heart and brain tissues compared to other tissues [18]. There is evidence indicating that cardiac-specific Drp1-knockout mice developed mitochondrial dysfunction and suppressed selective mitochondrial removal [19]. Drp1-mediated mitochondrial fission promoted parkin translocation in cardiomyocytes, which was disturbed by the inhibition of Drp1 [20]. PTEN-inducible kinase 1 (PINK1), a mitochondrial kinase, displayed outer membrane accumulation and initiated parkin translocation in the heart [7], implying that the selective removal of mitochondria in heart tissue is related to PINK1. Based on these previous studies, we hypothesized that the attenuation of abnormal mitochondrial elongation could restore the protective function of IPC in aged hearts by a new mechanism involving Drp1 and parkin.

Resveratrol, a natural polyphenol compound present in several plants, was shown to display antioxidant properties [21] and extend lifespan [22]. Resveratrol was also shown to downregulate lipid peroxidation and upregulate Mn-SOD to decrease oxidative stress in cardiovascular diseases [23]. Resveratrol was reported to restore the cardioprotective effect of IPC on aged hearts by enhancing cardiac function and reducing ischemia/reperfusion-induced cell apoptosis [24]. As a potential activator of sirtuin 1 (SIRT1), resveratrol improved cardiac function through SIRT1-mediated signaling pathways in aged hearts [25]. Moreover, SIRT1 inhibition diminished the preconditioning effect of resveratrol, demonstrating that the SIRT1 pathway was implicated in resveratrol preconditioning [26]. Additionally, several studies have reported the effects of resveratrol on the regulation of mitochondrial morphology and dynamics through Drp1-parkin-PINK1 signaling. Therefore, it is possible that Drp1-parkin-PINK1 signaling could be involved in the abnormal mitochondrial dynamics during cardiac aging and the cardioprotective effect of resveratrol.

In this study, we investigated the mitochondrial dynamic alterations in H9c2 cells in response to D-galactose induction, which was characterized by increased levels of senescence-associated β-galactosidase and BrdU incorporation. D-Galactose intervention generates reactive oxygen species and induces calcium overloading in cardiomyocytes, which are regarded as a potential mechanism in aging research. We explored the roles of mitochondrial depolarization and parkin/PINK1 translocation on elongated mitochondria in D-galactose-induced senescent-like H9c2 cardiomyocytes. To the best of our knowledge, this study is the first to propose a new mechanism of resveratrol, in which it modulates Drp1 to protect against cardiac aging disorders. The new roles of parkin and PINK1 activation required for the elimination of aging mitochondria and their importance in uncovering the antiaging functions of resveratrol are also discussed herein.

2. Materials and Methods

2.1. Cell Culture and Pharmacological Treatments. A rat H9c2 cardiomyocyte cell line, obtained from American Type Cultural Collection (CRL1446, ATCC, USA), was cultured in Dulbecco's modified Eagle's medium (DMEM, Gibco, Oklahoma, USA) supplemented with 10% fetal bovine serum (FBS, Gibco, Oklahoma, USA) and 1% *v*/*v* penicillin/streptomycin (Gibco, Oklahoma, USA) at 37°C in a 5% CO_2 humidity environment. D-Galactose (D-Gal, ≥99%, Sigma, USA) was dissolved in DMEM and given for 48 hours. Carbonyl cyanide 3-chlorophenylhydrazone (CCCP, Sigma, USA) and resveratrol (RSV, purity > 98%, HPLC, Chengdu Conbon Bio-Tech Co. Ltd., Sichuan, China) were dissolved in dimethyl sulfoxide (DMSO, ACROS, USA).

2.2. Senescence-Associated β-Galactosidase Staining. Senescence-associated β-galactosidase staining (CST, USA) was performed according to the manufacturer's protocol. Briefly, cells in a 6-well plate were washed with PBS, fixed for 15 min at room temperature with fixative solution, and incubated for 24 hours with β-galactosidase staining solution in a dry incubator (absence of CO_2). H9c2 cells were observed for the development of blue color under a microscope (100x). The percentage of positive cells was calculated by counting the blue-stained cells and total cells (as a standard) in five randomized fields.

2.3. Cell Viability and Mitochondrial Viability. Cell viability was determined by using the 3-(4,5-dimethylthiazol-2-yl)-2,5-diphenyltetrazolium bromide (MTT, Molecular Probes, USA) assay. An absorbance of 570/650 nm was evaluated by a Multi-Mode Detection Platform (SpectraMax Paradigm, Molecular Devices, USA). For mitochondrial viability, a mitochondrial viability assay reagent (Abcam, UK) was used according to the manufacturer's protocol. Briefly, 5×10^4 cells/ml were seeded in a 96-well plate. After treatment, 100 μl DMEM and 100 μl diluted reagent were added to each well for 4-hour incubation at 37°C. The fluorescent intensity was evaluated at 590 nm with an excitation wavelength of 550 nm. Cell viability and mitochondrial viability were calculated as the ratio to the DMSO group (set as 1.0), respectively.

2.4. Evaluation of Mitochondrial Morphology. H9c2 cells were seeded into a μ-Slide 8-well glass bottom plate (#80826, ibidi, Germany) at a total number of 7500 per well. After treatments of D-galactose (0, 10, 20, and 40 g/l, Sigma, USA) or Mdivi-1 (40 μM, Sigma, USA), the cells were incubated with 50 nM MitoView Red (GeneCopoeia, USA) at 37°C for 30 min. Then, the cells were washed with PBS for three times. Mitochondrial morphology in each group was captured using a confocal microscope (Leica TCS SP8, Germany) equipped with a 63x oil immersion objective. Red fluorescence represents the mitochondria stained by MitoView Red.

2.5. Transmission Electron Microscopy. H9c2 cardiomyocytes were fixed in 2.5% glutaric dialdehyde overnight at 4°C and washed with PBS for three times, then postfixed in 1% osmium tetraoxide for 1-2 hours, dehydrated in a graded series of ethanol concentrations, and embedded in Sparr resin. Sections of 50–70 nm thickness were placed on copper grids that were double-stained with uranyl acetate and lead citrate. Samples were examined with an H-7650 transmission electron microscope (Hitachi, Japan).

2.6. ROS and Calcium Determination. To measure the cellular ROS production and calcium concentration, an H_2DCFDA Cellular ROS Detection Assay Kit (Molecular Probes, USA) and a Fluo-4 AM calcium indicator (Thermo Scientific, USA) were used according to the manufacturers' protocols and determined by BD FACSAria III flow cytometer (BD, USA) analysis. For ROS and calcium determination, Ex 488/Em 530 nm was used. The intensity of each group was calculated by counting 10,000 cells as representation.

2.7. MMP Determination. To measure the mitochondrial membrane potential (MMP), a JC-1 Mitochondrial Membrane Potential Assay Kit (Abcam, Cambridge, UK) was used according to the manufacturer's protocol. The fluorescent images of JC-1 in each group were captured using a confocal microscope by red and green fluorescence. For the quantification of JC-1 intensity, H9c2 cells were seeded in a 96-well black plate with clear bottom. Ex 488/Em 530 nm and Ex 550/Em 600 nm were used, and the MMP was calculated by the ratio of red-to-green fluorescence.

2.8. ATP Content Assay. The ATP level of H9c2 cells was measured by using a Luminescent ATP Detection Assay Kit (Abcam, UK) according to the manufacturer's protocol. The contents of ATP were analyzed from three independent experiments and detected by a Multi-Mode Detection Platform.

2.9. BrdU Incorporation Assay. A BrdU incorporation assay was used to measure the cell proliferation. H9c2 cells were seeded into a μ-Slide 8-well glass bottom plate at a total number of 7500 per well. After treatment, the cells were incubated with medium containing 10 μM BrdU (Sigma, USA) for 24 hours. Then, cells were fixed by 70% ethanol and incubated with 2 M HCl for 30 min at room temperature. 1% BSA was used for blocking, and the cells were incubated with a BrdU primary antibody (1 : 500, Abcam, UK) overnight and with a secondary antibody (1: 250) for 2 hours at room temperature. DAPI (Invitrogen, USA) was stained in the final step. A fluorescent image was detected using a confocal microscope equipped with a 63x oil immersion objective. Blue fluorescence represents DAPI staining, and red fluorescence represents BrdU. Images were analyzed by using the manufacturer's software. The percentage of positive cells was calculated by counting the double-stained cells and total cells (as a standard) in five randomized fields.

2.10. Evaluation of Mitochondrial Respiration. The cellular oxygen consumption rate (OCR) was measured to determine the key parameters of mitochondrial respiration using the Seahorse Bioscience XFp Extracellular Flux Analyzer (Seahorse Bioscience, USA) containing an XFp Cell Mito Stress Test Kit according to the manufacturer's protocol. H9c2 cells were seeded into an XFp cell culture miniplate at a density of 4000 cells/80 μl/well and treated with D-galactose (40 g/l). The sensor cartridge for the XFp analyzer was hydrated in a 37°C non-CO_2 incubator a day before the experiment. For calibration, the sensor cartridge was loaded with 1.5 μM oligomycin (complex V inhibitor) to port A, 2 μM FCCP to port B, and 0.5 μM rotenone/antimycin A (inhibitors of complex I and complex III) to port C. The cellular cultural medium was replaced by 180 μl/well assay medium that was prepared by supplementing XF Base Medium with 5.5 mM glucose, 1 mM pyruvate, and 2 mM L-glutamine (adjusted to pH 7.4) and incubated at 37°C for 1 hour without CO_2. When the calibration was completed, the calibration plate was replaced with a culture miniplate into the calibrated XFp Extracellular Flux Analyzer for the Mito Stress Test. The oxygen consumption rate was calculated to evaluate mitochondrial respiration.

2.11. Immunoblot Analysis. Cells were washed with iced PBS and lysed with RIPA buffer (20 mM Tris-HCl (pH 7.5), 150 mM NaCl, 1 mM Na_2EDTA, 1 mM EGTA, 1% NP-40, 1% sodium deoxycholate, 2.5 mM sodium pyrophosphate, 1 mM beta-glycerophosphate, 1 mM Na_3VO_4, and 1 μg/ml leupeptin, Cell Signaling Technology, USA) containing protease inhibitors (Roche, Basel, Switzerland), then stored on ice for 30 min. The cell lysate was centrifuged at 13,000 rpm at 4°C for 10 min, and the supernatant was collected to a new and clear tube. The protein concentration was determined using a Bio-Rad protein assay kit (Bio-Rad Laboratory, USA). Equal amounts of proteins were boiled and separated with 8% SDS-PAGE gels and transferred to a nitrocellulose membrane (Millipore, Germany). The membrane was blocked with 5% nonfat milk in Tris-buffer saline-Tween 20 (TBST) at room temperature for 1 hour, then incubated overnight at 4°C with primary antibodies of anti-Drp1 (1 : 500, Cell Signaling Technology, USA), anti-Mfn2 (1 : 1000, Cell Signaling Technology, USA), anti-Mfn1 (1 : 500, Abcam, UK), anti-OPA1 (1 : 500, Abcam, UK), anti-Bcl-2 (1 : 500, Cell Signaling Technology, USA), anti-Bax (1 : 500, Cell Signaling Technology, USA), anti-PINK1 (1 : 500, Novus, USA), anti-parkin (1 : 500, Abcam, UK), anti-LC3 (1 : 1000, Cell Signaling Technology, USA), and

anti-TOM20 (1 : 500, Abcam, UK). Membranes were washed in TBST for three times and incubated with a secondary antibody (1 : 1000) for 1 hour at room temperature. Subsequently, the membranes were washed in TBST for three times and detected using the Odyssey Scanner (Licor, USA). Actin (1 : 10,000, Sigma, USA) was used as a loading control.

2.12. Phos-Tag Assay. To detect phosphorylated PINK1 and parkin proteins, 8% polyacrylamide gels containing 25 μM phos-tag acrylamide (Wako Chemicals, USA) and 50 μM $MnCl_2$ were prepared before using. Before electrophoresis, samples were mixed with 1 mM $MnCl_2$. During electrophoresis, cold running buffer was used. After electrophoresis, phos-tag acrylamide gels were washed with transfer buffer containing 1 mM EDTA for 10 min with gentle agitation and then replaced with transfer buffer without EDTA for 10 min with gentle agitation. Proteins were transferred to a nitrocellulose membrane (Millipore, Germany) and analyzed by conventional immunoblotting.

2.13. Immunocytochemistry Analysis. H9c2 cells were seeded into a μ-Slide 8-well glass bottom plate at a total number of 7500 per well. After treatment, cells were washed with PBST (0.1% Tween 20 to PBS) and fixed with 4% PFA (15 min, RT), then permeabilized with 0.1% Triton X-100 (10 min, RT). The cells were washed with PBST for 3 times, blocked with 1% BSA/PBST for 1 hour at room temperature, and incubated with a primary antibody (TOM20 1 : 50, Abcam; parkin 1 : 200, Abcam; and PINK1 1 : 200, Novus) overnight in 4°C. A secondary antibody was used in 1 : 250 in room temperature for 2 hours. A fluorescent image was detected using a confocal microscope equipped with a 63x oil immersion objective.

2.14. Statistical Analysis. Data were analyzed using GraphPad Prism 6.0 (GraphPad Software Inc., San Diego, CA, USA), and all results were expressed as means ± SEM. Dunnett's test of one-way ANOVA was used to analyze difference between 3 or more groups. For two-group analysis, Student's t-test was used. Values with $p < 0.05$ were considered statistically significant.

3. Results

3.1. Resveratrol Attenuated Drp1-Mediated Mitochondrial Elongation in Response to D-Galactose Induction in H9c2 Cells. We examined the morphology of mitochondria in H9c2 cells exposed to D-galactose for 48 hours (Figure 1(a)). The live cell staining dye MitoView Red indicated the changes in the morphology and distribution of mitochondria after different doses of D-galactose induction. The proportion of tubular or thread-like mitochondria was significantly increased in H9c2 cells treated with D-galactose at concentrations of 10, 20, and 40 g/l. After induction with 40 g/l D-galactose, more that 80% of the mitochondria were highly elongated and completely organized into lengthy traveling chains, whereas cells without D-galactose induction displayed short or punctiform mitochondria distributed throughout their cytoplasm. Mitochondria are quite flexible and are directly correlated with the level of cardiomyocyte metabolic activity. Therefore, we wanted to investigate the mechanism underlying mitochondrial elongation or affecting mitochondrial dynamics in response to D-galactose in H9c2 cells. We evaluated fission- or fusion-regulated protein (Mfn1, Mfn2, OPA1, and Drp1) expressions, finding that Drp1 was obviously downregulated after D-galactose induction (Figure 1(b)). Compared with D0 cells (cells treated with 0 g/l D-galactose), the expression levels of Drp1 in D40 cells were significantly decreased. Conversely, there was no change in the expression levels of Mfn1, Mfn2, or OPA1 in response to D-galactose (Figure 1(c)). In addition, we further tested whether Drp1 dominated mitochondrial elongation after D-galactose induction using a selective cell-permeable Drp1 inhibitor (Mdivi-1). Mdivi-1 treatment suppressed Drp1 expression and Drp1-mediated mitochondrial fission and altered mitochondrial elongation even further in H9c2 cells, indicating that mitochondrial elongation induced by D-galactose is partially due to deficient fission machinery caused by Drp1 downregulation.

Next, we examined the effects of resveratrol on mitochondrial morphology in response to D-galactose. H9c2 cells were treated with D-galactose for 48 hours followed by different doses of resveratrol for 12 hours. Interestingly, live cell analysis of the changes in both mitochondrial length and distribution indicated that mitochondrial elongation was ameliorated by resveratrol in a dose-dependent manner (Figure 2(a)). In cells treated with D40 and 100 μM resveratrol (RSV 100), the mitochondria packed tightly into a relatively stable phonotype and their elongation was dramatically diminished compared with that in D40 cells. Quantification of mitochondrial morphology showed that the percentage of cells exhibiting mitochondrial elongation was decreased significantly in cells treated with D40 plus 50 μM or 100 μM RSV cells (Figure 2(b)). We next used transmission electron microscopy to observe mitochondrial morphology changes after D-galactose induction (Figure 2(e)). In the D0 group, most of the mitochondria presented a short- and round-shaped morphology. Most of the mitochondria in D40 cells appeared as long, tubular, and sometimes branched or two-neighbored structures that spread throughout the entire cytoplasm. Notably, some of them were elongated and became the highly interconnected net-like mitochondria (indicated with red arrows). Thus, the structural features of the mitochondrial elongation thus represented abnormal mitochondrial dynamics in response to D-galactose. After resveratrol (100 μM) treatment, we observed a decreased number of elongated mitochondria in H9c2 cells that displayed a tubular or ball-like structure without the connected-like part.

Meanwhile, we evaluated the effects of resveratrol on fission- or fusion-regulated proteins after D-galactose induction and found that resveratrol significantly upregulated Drp1 expressions in a dose-dependent manner (Figure 2(c)). We further analyzed whether resveratrol with or without D-galactose might play roles in cellular toxicity and mitochondrial damage. As shown in Figure 2(d), MTT and fluorescent staining experiments demonstrated that the cell and mitochondrial viabilities were not impaired by 24 hours of 100 μM resveratrol treatment.

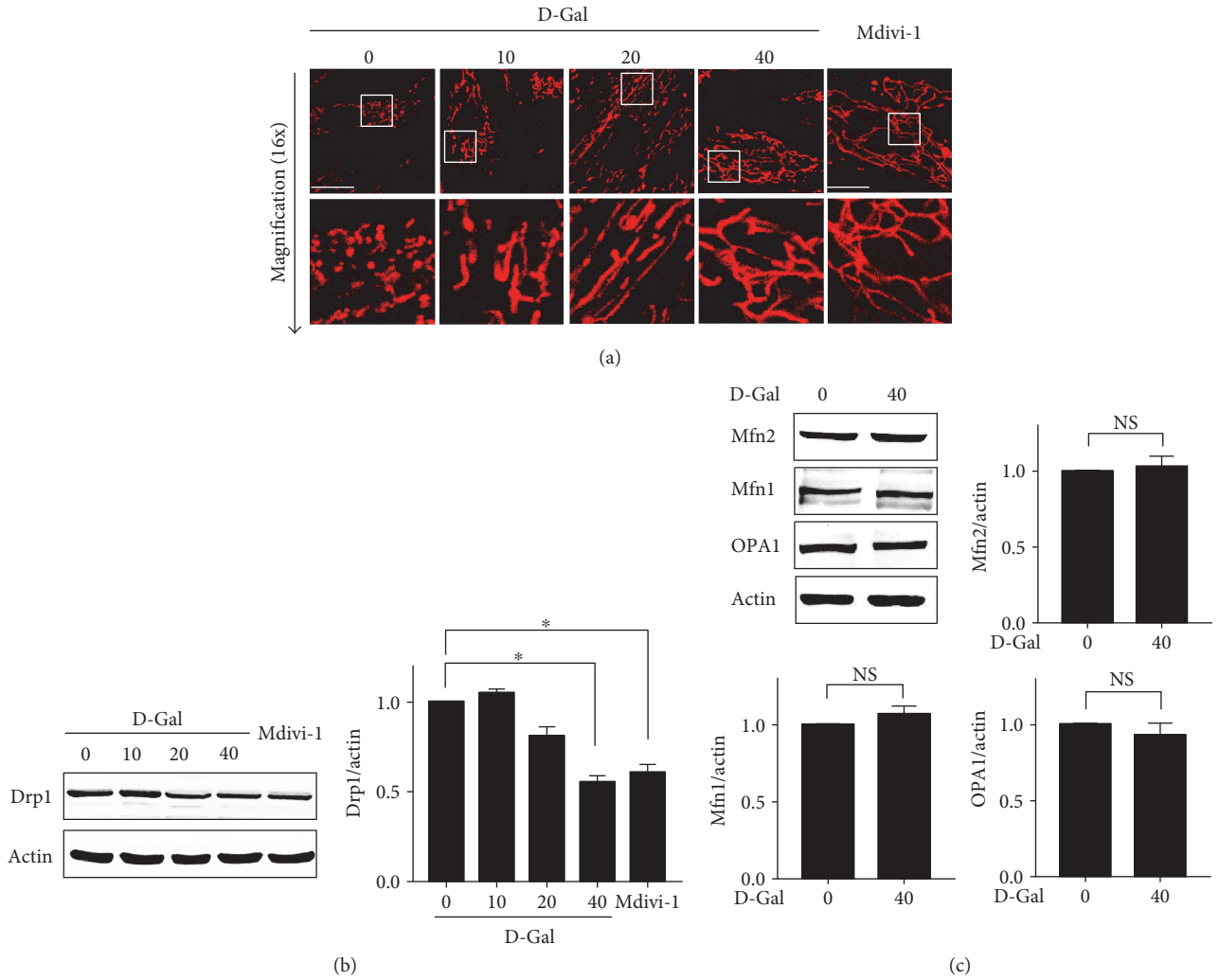

FIGURE 1: Drp1 mediated mitochondrial elongation induced by D-galactose. (a) H9c2 cardiomyocytes were treated with D-galactose (D-Gal; 0, 10, 20, and 40 g/l) and Mdivi-1 (40 μM) for 48 hours, respectively. Mitochondrial morphology was detected using a confocal microscope by MitoView Red staining (upper panels); objective magnification, 63x; white scale bar represents 20 μm. Magnified photographs showed a detail view of the area indicated in the upper panels. (b) Drp1 expressions in H9c2 cells treated with D-galactose and Mdivi-1 were detected by immunoblot analysis. Actin was represented as the loading control. The relative values were normalized to actin. Data ($n = 3$) were shown as the mean ± SEM ($^*p < 0.05$). (c) Mfn1, Mfn2, and OPA1 expressions were detected by immunoblot analysis. Actin was represented as the loading control. The relative values were normalized to actin. Data ($n = 3$) were shown as the mean ± SEM. NS: no significance ($p > 0.05$).

Taken together, these results indicated that Drp1 down-regulation in response to D-galactose caused marked alterations in both mitochondrial length and distribution, revealing obvious elongation morphology. After resveratrol treatment, mitochondrial elongation was decreased, thus ameliorating the characteristic abnormalities in mitochondrial dynamics induced by D-galactose.

3.2. Resveratrol Alleviated Senescent-Like Cell Phenotypes in Response to D-Galactose Induction. Chronic D-galactose administration causes alterations that resembled natural aging in animals [27]. Here, we examined the senescence-related parameters in H9c2 cardiomyocytes in response to D-galactose. First, we performed the senescence-associated β-galactosidase (SA β-Gal) staining, a biomarker for senescent and aging cells. The percentage of positive blue staining in the D40 group increased to 83.16% compared with only 16.16% in the D0 group (Figure 3(a)). To further confirm a cellular senescent-like phenotype in response to D-galactose, the BrdU incorporation assay was performed to evaluate cell proliferation. Fluorescent images show that there was loss of BrdU/DAPI double staining in D40 cells compared with D0 cells. Quantification of cells with double staining showed 44.44% loss of BrdU staining, indicating a reduction in cardiomyocyte proliferation (Figure 3(b)). Furthermore, we used a fluorescent probe to detect the production of reactive oxygen species (ROS) and cellular calcium concentrations. Compared with D0 cells, the ROS productions in D20 and D40 cells were significantly increased (Figure 3(c), 1.71-fold increase in the D40 group compared

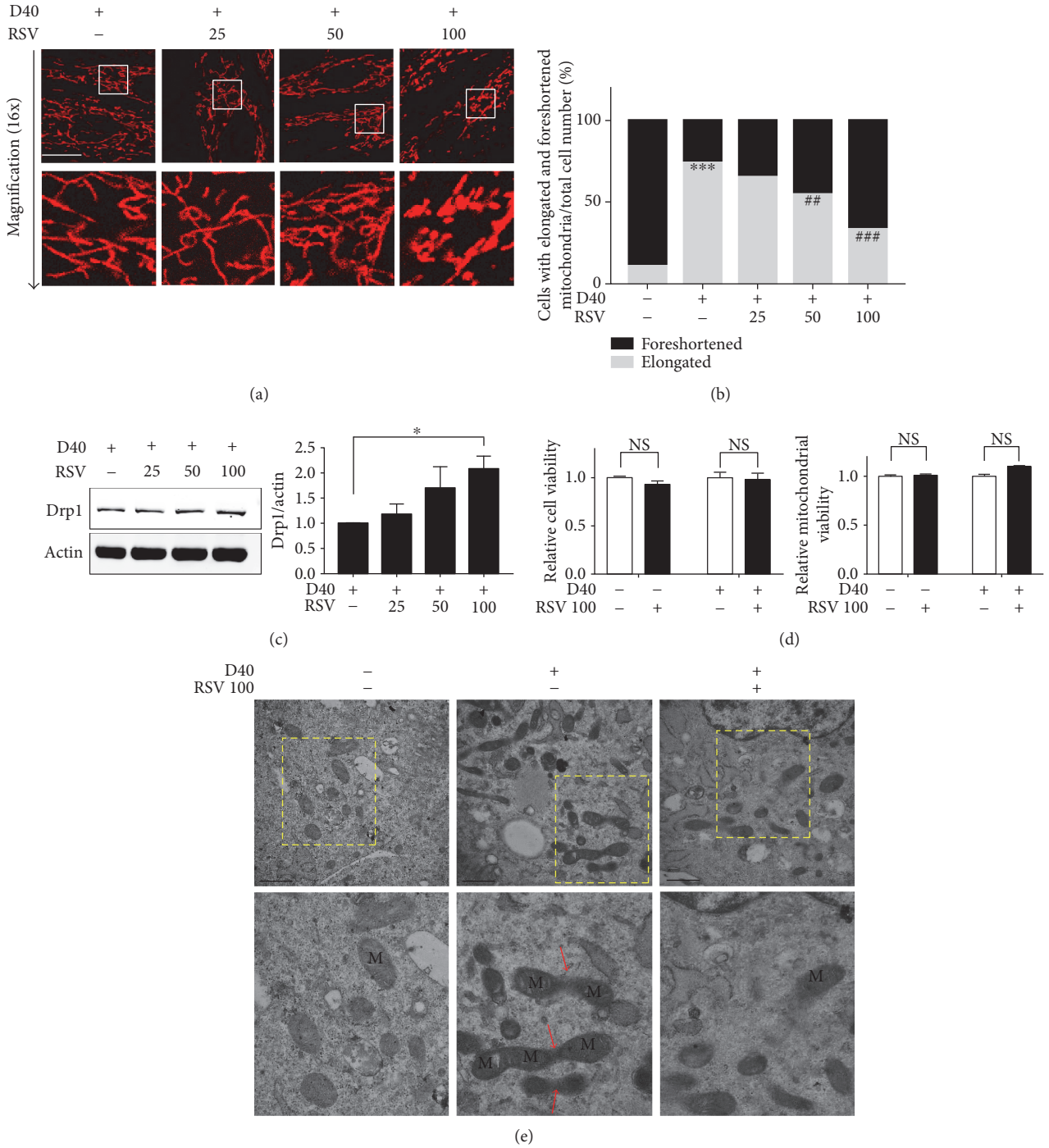

FIGURE 2: The effects of resveratrol on mitochondrial elongation and Drp1 expression. (a) H9c2 cardiomyocytes were treated with resveratrol (RSV; 25, 50, and 100 μM) for 12 hours after 48-hour induction of D-Gal (40 g/l). Mitochondrial morphology was detected using a confocal microscope by MitoView Red staining (upper panels); objective magnification, 63x; scale bar represents 20 μm. Magnified photographs showed a detail view of the area indicated in the upper panels. (b) Quantification of mitochondrial morphology (foreshortened and elongated) in 50 cells from fluorescent images captured by a confocal microscope. Gray bar: cells with elongated mitochondria/total cell number; black bar: cells with foreshortened mitochondria/total cell number. $^{***}p < 0.001$ versus elongated mitochondria in cells without any treatment; $^{\#\#}p < 0.01$ and $^{\#\#\#}p < 0.01$ versus elongated mitochondria in cells treated with D-galactose (40 g/l). (c) The effect of RSV (25, 50, and 100 μM) on Drp1 expressions was detected by immunoblot analysis. Actin was represented as the loading control. The relative values were normalized to actin. Data ($n = 3$) were shown as the mean ± SEM ($^{*}p < 0.05$). (d) The toxic effects of resveratrol (100 μM) on H9c2 cardiomyocytes and mitochondria were evaluated. Data ($n = 3$) were shown as the mean ± SEM; NS: no significance ($p > 0.05$). (e) Electron microscopy analysis (magnification, 25,000x; upper panels) of cells treated with RSV (100 μM) for 12 hours after 48-hour induction of D-Gal (40 g/l). Scale bar represents 1 μm. Magnified photographs showed a detail view of the area indicated in the upper panels. The red arrow indicated the interconnected net-like mitochondria.

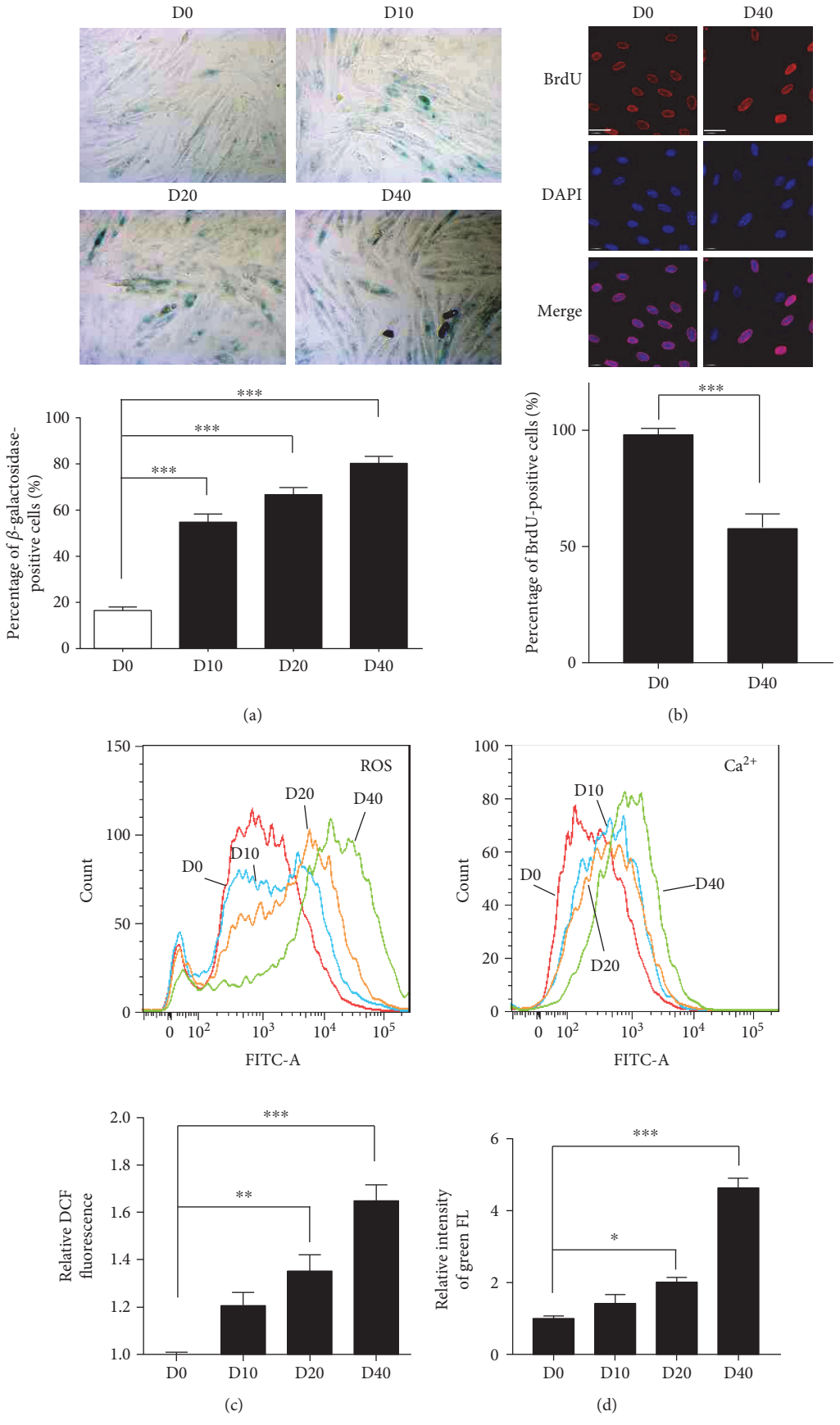

Figure 3: Continued.

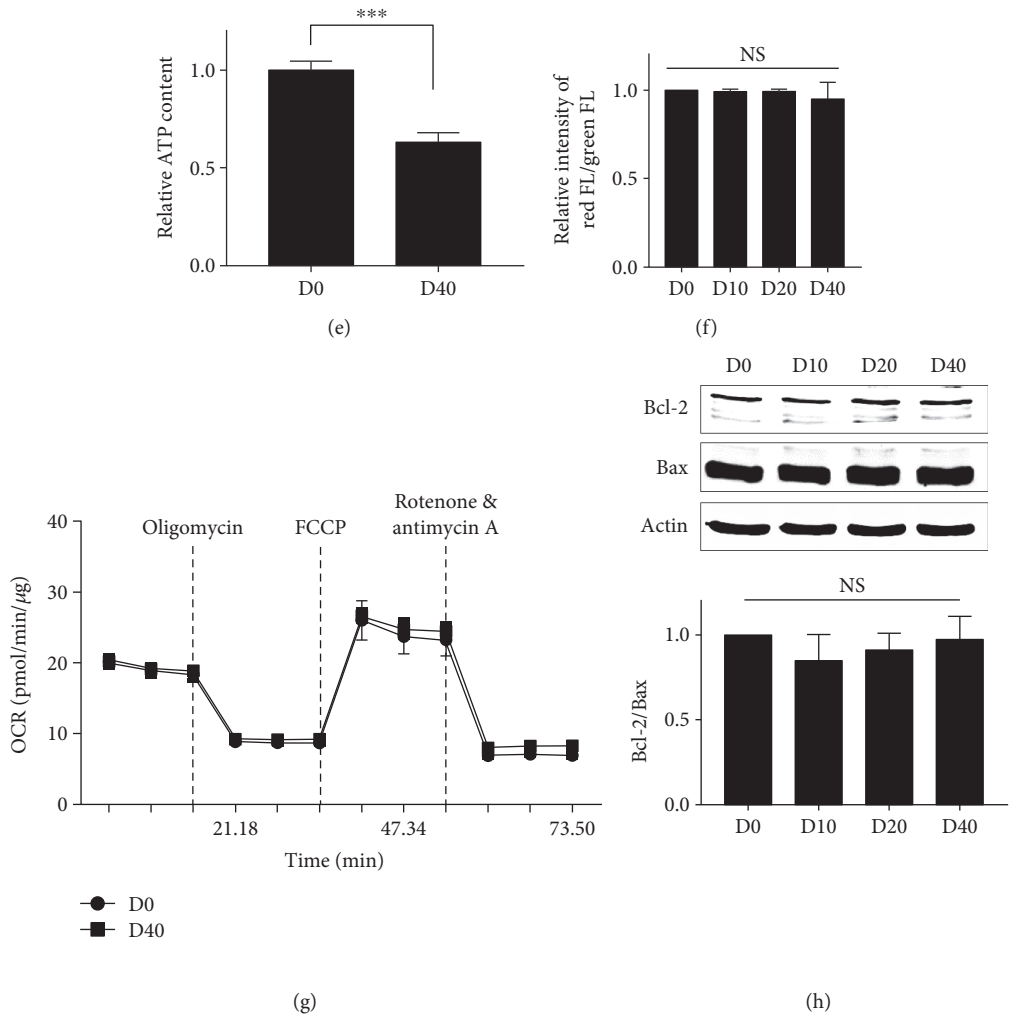

Figure 3: H9c2 cardiomyocytes displayed senescent-like phenotypes induced by D-galactose. (a) H9c2 cardiomyocytes were treated with D-galactose (D-Gal; 0, 10, 20, and 40 g/l). SA-β-Gal activity was detected using a microscope in a bright field with positive blue staining; original magnification, 100x; the percentage of positive staining was analyzed in five randomized fields. Data ($n = 5$) were shown as the mean ± SEM ($^{***}p < 0.001$). (b) BrdU activity was represented by BrdU (red) and DAPI (blue) double staining detected using a confocal microscope; objective magnification, 63x; scale bar represents 40 μm. The percentage of positive staining was analyzed in five randomized fields. Data ($n = 5$) were shown as the mean ± SEM ($^{***}p < 0.001$). H9c2 cardiomyocytes were treated with D-galactose (D-Gal; 0, 10, 20, and 40 g/l). (c) ROS production was evaluated by using H_2DCFDA probe staining, and (d) calcium concentration was evaluated by using Fluo-4 AM staining. Results were detected by flow cytometry. Data ($n = 3$) were shown as the mean ± SEM ($^{*}p < 0.05$, $^{**}p < 0.01$, and $^{***}p < 0.001$). (e) ATP content was detected by the luminescent detection assay. Data ($n = 3$) were shown as the mean ± SEM ($^{***}p < 0.001$). (f) Mitochondrial membrane potential (MMP) was detected using flow cytometry by JC-1 fluorescent dye staining. Data ($n = 3$) were shown as the mean ± SEM; NS: no significance ($p > 0.05$). (g) The H9c2 cardiomyocyte oxygen consumption rate was evaluated using the XFp Cell Mito Stress Test Kit and detected by the Seahorse Bioscience XFp Extracellular Flux Analyzer. (h) Bcl-2 and Bax protein expressions were analyzed by immunoblot analysis and calculated. Actin was represented as the loading control. Data ($n = 3$) were shown as the mean ± SEM; NS: no significance ($p > 0.05$).

with the D0 group). Meanwhile, calcium concentrations in the D20 and D40 were also significantly increased (Figure 3(d), 4.88-fold increase in the D40 group compared with the D0 group). Senescent cardiomyocytes are well-known to display reduced ATP production. Therefore, we examined the ATP content, and the result shows a 38.96% decrease in ATP content in D40 cells compared with D0 cells (Figure 3(e)).

We also wondered whether the elongated mitochondria were damaged in response to D-galactose induction. Therefore, we performed a mitochondrial membrane potential (MMP) assay to explore whether the mitochondria were depolarized which was induced by D-galactose. Interestingly, no significant change was found in the MMP in H9c2 cells induced by D-galactose (Figure 3(f)). In addition, we further detected mitochondrial respiration by testing the oxygen consumption rate. As shown in Figure 3(g), the H9c2 cellular oxygen consumption rate did not obviously change, suggesting that mitochondrial respiratory functionality was not impaired in D40 cells. To further evaluate proapoptotic

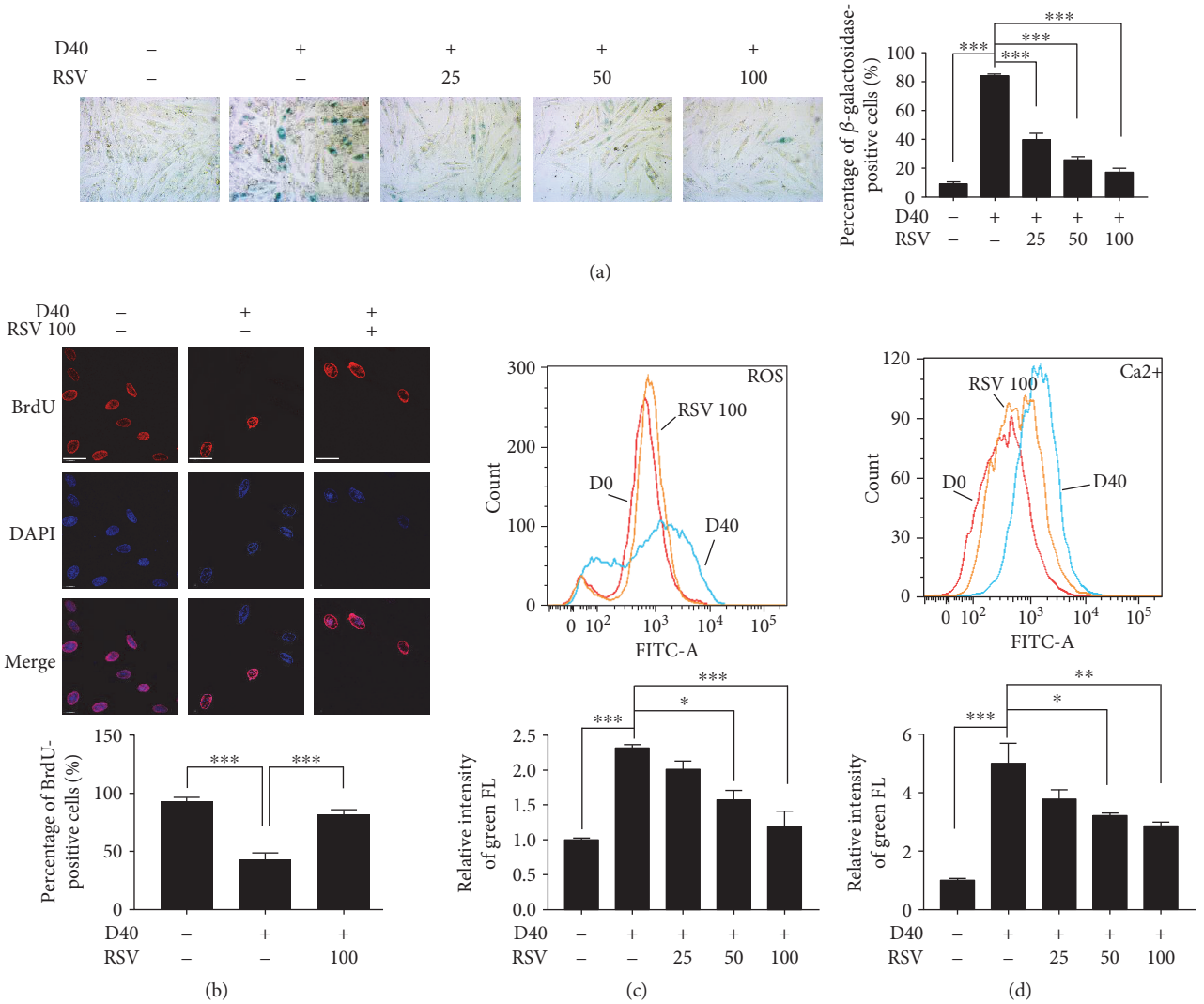

FIGURE 4: The effects of resveratrol on senescent phenotypes of H9c2 cardiomyocytes induced by D-galactose. (a) H9c2 cardiomyocytes were treated with resveratrol (RSV; 25, 50, and 100 μM) for 12 hours after 48-hour induction of D-Gal (40 g/l). SA-β-Gal activity was detected using a microscope in a bright field with positive blue staining; original magnification, 100x; the percentage of positive staining was analyzed in five randomized fields. Data ($n = 5$) were shown as the mean ± SEM ($^{***}p < 0.001$). (b) BrdU activity was represented by BrdU (red) and DAPI (blue) double staining detected using confocal microscopy; objective magnification, 63x; scale bar represented 40 μm. The percentage of positive staining was analyzed in five randomized fields. Data ($n = 5$) were shown as the mean ± SEM ($^{***}p < 0.001$). (c, d) H9c2 cardiomyocytes were treated with resveratrol (RSV; 25, 50, and 100 μM) for 12 hours after 48-hour induction of D-Gal (40 g/l). ROS production was evaluated by using H2DCFDA probe staining, and calcium concentration was evaluated by using Fluo-4 AM staining. Results were detected by flow cytometry. Data ($n = 3$) were shown as the mean ± SEM ($^{*}p < 0.05$, $^{**}p < 0.01$, and $^{***}p < 0.001$).

protein expressions, we analyzed the expressions of Bcl-2 and Bax. No significant changes in the expression levels of Bcl-2 and Bax were detected in response to different doses of D-galactose (Figure 3(h)).

We evaluated the effects of resveratrol on senescent-like phenotypes induced by D-galactose. As shown in Figure 4(a), resveratrol significantly and dose-dependently reduced D-galactose-induced SA β-Gal-positive staining and increased the percentage of BrdU/DAPI double staining (Figure 4(b)). Moreover, resveratrol significantly decreased the ROS production and calcium concentration in response to D-galactose, respectively, in a dose-dependent manner (Figures 4(c) and 4(d)).

Collectively, D-galactose induced cellular senescent-like phenotypes in H9c2 cardiomyocytes, including increased expression of a senescent biomarker, reduced cell proliferation, excessive ROS production, and calcium overloading. Regarding the functional aspect of mitochondria, no changes in the mitochondrial membrane potential or the respiration chain were observed. We also showed that the mitochondrial-mediated apoptotic signaling pathway was not activated. Importantly, resveratrol decreased SA β-Gal activity, increased cellular proliferation, and decreased ROS production and calcium overloading, thus ameliorating D-galactose-induced senescent-like phenotypes in H9c2 cardiomyocytes.

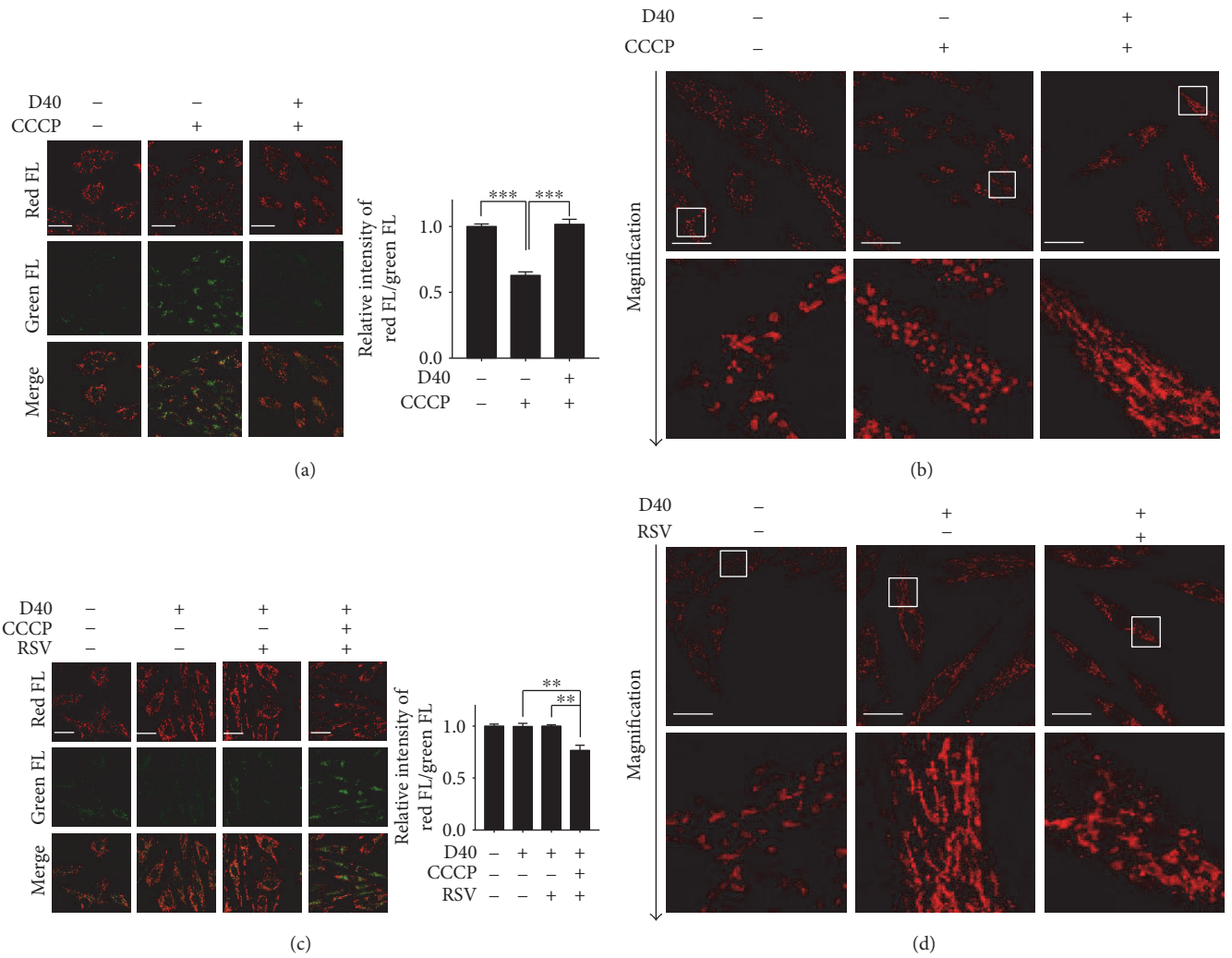

Figure 5: Resveratrol reduced the resistance of elongated mitochondria to CCCP-induced depolarization in H9c2 cells. (a, c) Mitochondrial membrane potential was detected using confocal microscopy by JC-1 fluorescent dye staining. Images were captured by confocal microscopy to show the variations of red and green FL; white scale bar represented 40 μm. The ratio of red/green FL was calculated by the fluorescence microplate assay. Data ($n = 3$) were shown as the mean ± SEM ($^{**}p < 0.01$, $^{***}p < 0.001$). (b, d) Mitochondrial morphology was detected using confocal microscopy (upper panels) by immunostaining with a TOM20 antibody (red); objective magnification, 63x; white scale bar represents 20 μm. Magnified photographs showed a detail view of the area indicated in the upper panels.

3.3. Resveratrol Reduced the Resistance of Elongated Mitochondria to CCCP-Induced Depolarization in Senescent-Like Cardiomyocytes. The mitochondrial membrane potential (MMP) is considered a key sensor and/or effector of intracellular regulatory processes such as apoptosis, redox status, calcium homeostasis, and balance of mitochondrial fusion and fission. We next explored the relationship between mitochondrial depolarization induced by CCCP and mitochondrial elongation after D-galactose induction. We detected the MMP with JC-1 dye using fluorescence microscope- and microplate cytometry-based analyses. Incubating H9c2 cells with CCCP for 3 hours before JC-1 staining indeed increased the intensity of the green fluorescent signal (Figure 5(a), middle panels), indicating significant mitochondrial depolarization. However, we did not observe the CCCP-induced collapse of MMP in the 40 g/l D-galactose-treated H9c2 cells (D40, Figure 5(a), right panels). Using cytometry, we calculated the ratio of red FL to green FL, which represents contributions from both monomers and aggregates of JC-1. Consistent with the results shown in fluorescent images, we also found a decreased red FL/green FL ratio in H9c2 cells after CCCP stimuli, indicating significant loss of MMP. However, there was a significant attenuation of the ability of CCCP to trigger decreased MMP in D40 cells. Meanwhile, we also tested whether the distinct effect of CCCP on D40 cells occurred due to mitochondrial elongation in senescent-like cardiomyocytes. We examined mitochondrial morphological changes in cells exposed to CCCP by immunostaining with an anti-TOM20 antibody (red). Compared with the H9c2 cells without D-galactose induction, CCCP-treated cells contained a higher proportion of short and/or punctate mitochondria, revealing that CCCP leads to mitochondrial fragmentation. Interestingly, the effect of CCCP was not observed in cells

in which mitochondrial elongation was induced by D-galactose, supporting our previous observation that normal or nonelongated mitochondrial morphology was required for CCCP-induced mitochondrial depolarization in cardiomyocytes (Figure 5(b)).

We then postulated that mitochondrial elongation might be an important determination in the MMP-mediated pathway. To determine whether the effects of resveratrol on mitochondrial elongation are involved in mitochondrial depolarization, we examined the MMP alterations and mitochondrial morphology in H9c2 cells after resveratrol treatment. As expected, resveratrol had no direct effect on the loss of MMP in D40 cells. Interestingly, in D40 plus CCCP cells, resveratrol significantly deceased the MMP, suggesting sensitized depolarization to mitochondrial decoupling (Figure 5(c)). Evaluation of mitochondrial morphology by immunostaining with TOM20 further validated the observation that the number of elongated mitochondria was reduced by resveratrol treatment compared with that in D40 cells (Figure 5(d)).

These data suggested that the resistance of mitochondria to CCCP-induced depolarization was likely due to abnormal elongation in D-galactose-induced senescent-like cardiomyocytes. After resveratrol treatment, the mitochondria were more susceptible to depolarization induced by CCCP, which probably resulted from mitochondrial elongation suppression.

3.4. Resveratrol Regulates Parkin/PINK1 Signaling upon Mitochondrial Depolarization in Senescent-Like Cardiomyocytes. First, we detected the parkin mitochondrial translocation by immunostaining with an anti-parkin antibody (green) and an anti-TOM20 antibody (red) using confocal microscopy in the H9c2 cells without D-galactose induction. After incubating the H9c2 cells with CCCP for 3 hours, we observed increased intensity of the yellow fluorescent signal in the merged image (Figure 6(a), second line from the left) compared with that in the cells without CCCP treatment (Figure 6(a), first line from the left). The yellow spots represented the overlaying of green and red fluorescence (FL), indicating that parkin translocated to mitochondria. Next, we examined the activation of PINK1 by immunostaining with an anti-PINK1 antibody (green) and an anti-TOM20 antibody (red). Compared with the H9c2 cells without CCCP treatment (Figure 6(a), second line from the right), the number of yellow dots was increased in the CCCP-treated H9c2 cells, indicating mitochondrial PINK1 translocation (Figure 6(a), first line from the right). We next accessed whether the CCCP-induced mitochondrial translocations of parkin and PINK1 were associated with their upregulations. We analyzed the protein levels of parkin and PINK1 after exposure to a CCCP stimulus. Immunoblot analysis showed that the total protein expression of parkin was not changed significantly (Figure 6(d)). Parkin phosphorylation is a critical step for its mitochondrial translocation in response to CCCP-induced mitochondrial depolarization. We therefore performed immunoblot analysis using an SDS-PAGE gel containing a phos-tag to investigate whether parkin was phosphorylated in H9c2 cells subjected to CCCP. In the phos-tag immunoblot, phosphorylated proteins appeared as slower migrated bands, and a significant increase in band intensity revealed that parkin was phosphorylated in the CCCP-treated cells. Interestingly, the total protein expression level of PINK1 was increased significantly which was induced by CCCP. Meanwhile, we observed an obvious slower PINK1 migration in its phos-tag immunoblot gel, which was potentially reflective of increased PINK1 phosphorylation. These results indicated that both parkin and PINK1 translocated to mitochondria in the presence of CCCP and suggested that higher parkin and PINK1 phosphorylation played a role in their activations.

To further address whether mitochondrial elongation affects the activations of parkin and PINK1 in senescent-like cardiomyocytes, we next investigated the mitochondrial translocation of parkin and PINK1 in the H9c2 cells induced by 40 g/l D-galactose (D40). In the merged images, we did not observe an obvious yellow fluorescent signal in D40 cells not treated with CCCP, indicating that parkin did not translocate to mitochondria (Figure 6(b), first line from the left). Interestingly, the CCCP-induced increase in yellow fluorescence was not detected in D40 cells, suggesting a significant attenuation in the ability of CCCP to trigger the mitochondrial translocation of parkin (Figure 6(b), second line from the left). Next, we analyzed the protein level of parkin induced by CCCP in the D40 cells. Compared with the D40 cells not treated with CCCP treatment, the total parkin expression level did not change significantly in the presence of CCCP (Figure 6(d)). Meanwhile, we also tested whether the CCCP-induced activation of PINK1 was exhibited only in D40 cells. As shown in Figure 6(b), D-galactose treatment did not induce the mitochondrial translocation of PINK1 (second line from the right). We did not observe PINK1 mitochondrial translocation in the D40 cells exposed to CCCP in the merged images (first line from the right). Immunoblot analysis of the PINK1 total protein level showed that its expression did not increase in response to CCCP treatment in the D40 cells. Furthermore, we tested whether the phosphorylation of parkin and PINK1 induced by CCCP was affected by D-galactose induction. In phos-tag immunoblots, we did not observe significant levels of phosphorylated parkin and PINK1 induced by CCCP in D40 cells. These data demonstrated that the CCCP-induced activation of parkin and PINK1 was decreased in the D40 cells, suggesting that mitochondrial depolarization induced by CCCP might be required for the activation of parkin and PINK1.

We next investigated the effects of resveratrol on the expressions of parkin and PINK1 in the D40 cells. First, resveratrol did not induce parkin mitochondrial translocation in D0 cells (Figure 6(c), second line from the left). Then, we examined parkin mitochondrial translocation in the D40 cells treated with resveratrol. In the merged images, we observed significantly increased yellow fluorescence signal intensity after 12 hours of resveratrol treatment (Figure 6(c), second line from the right). Interestingly, the number of colocalized yellow dots was increased in the presence of CCCP, suggesting that resveratrol increased

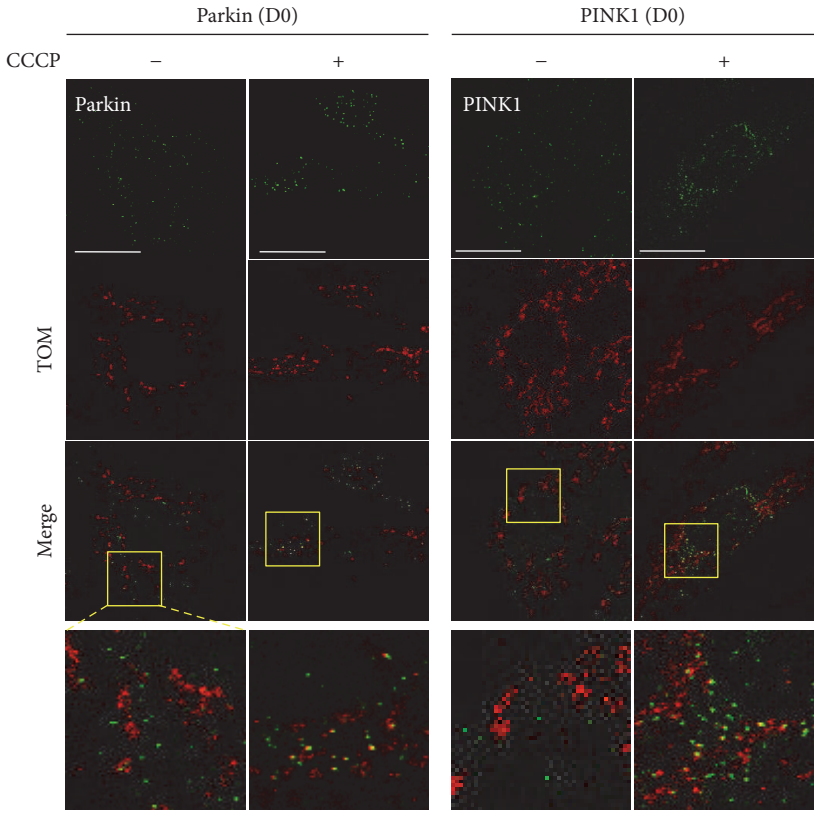

(a)

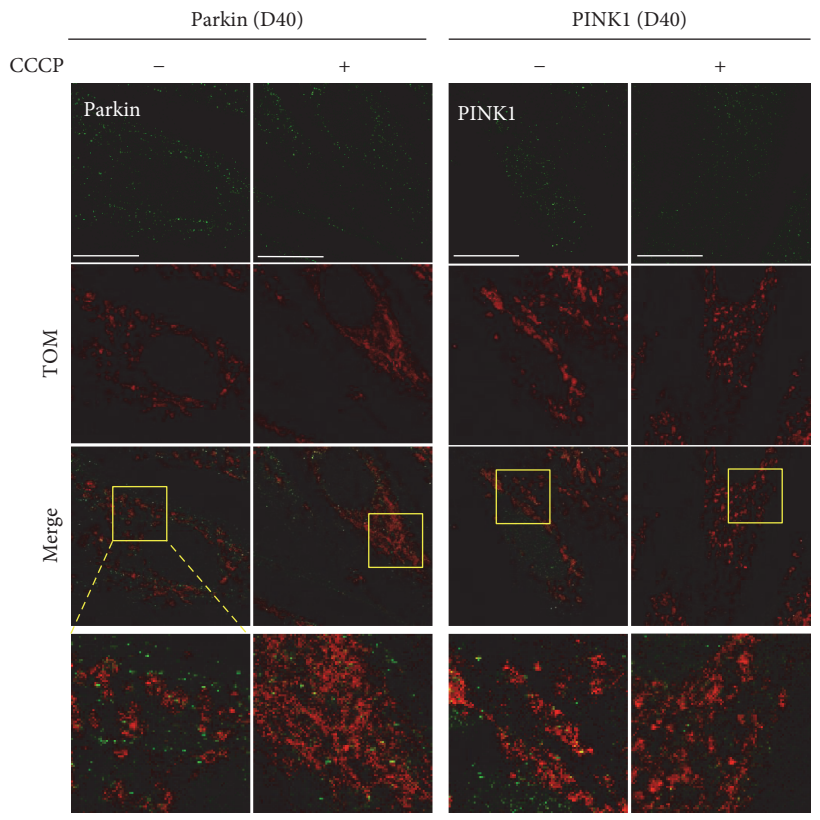

(b)

Figure 6: Continued.

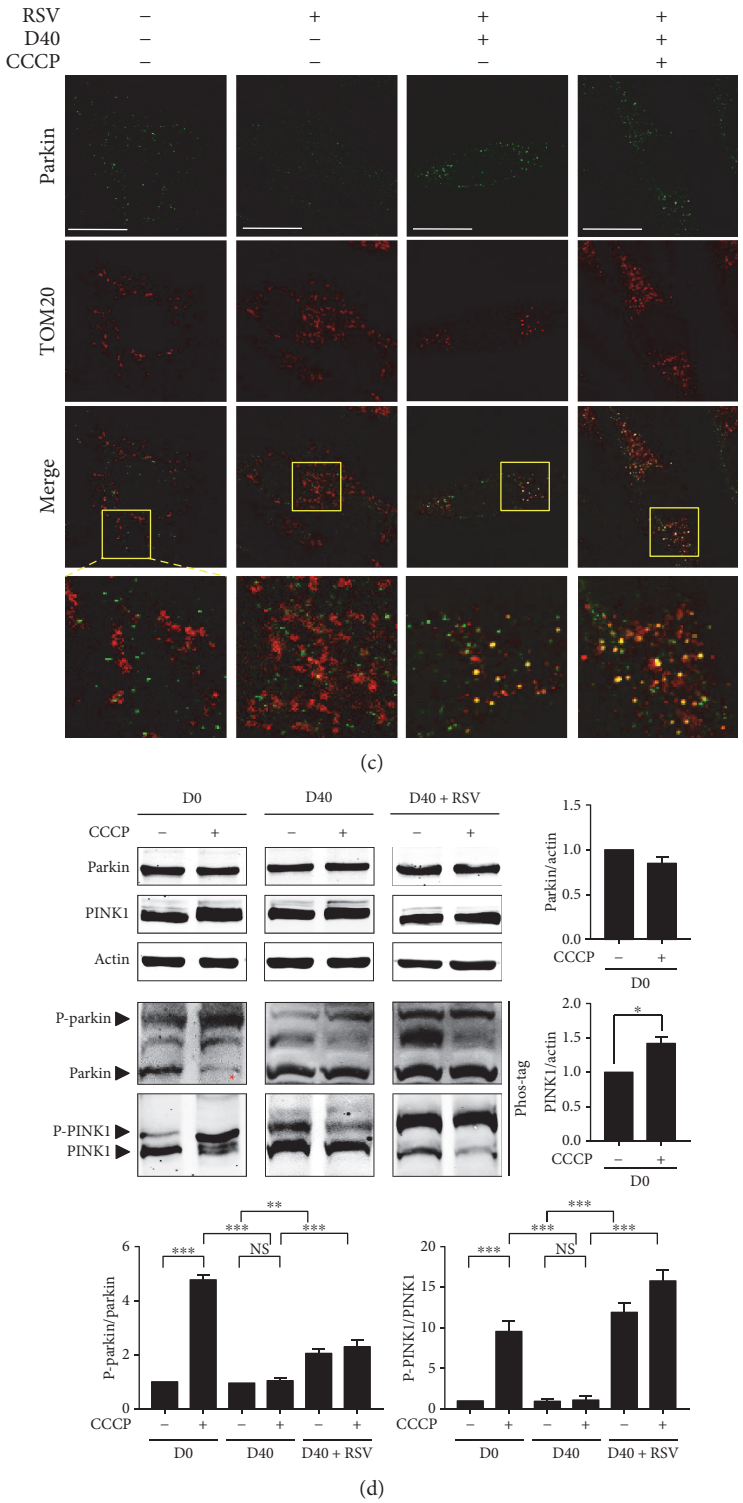

Figure 6: Resveratrol regulated the activity of parkin/PINK1 signaling upon mitochondrial depolarization in H9c2 cells in response to D-galactose induction. (a, b, c) Parkin and PINK1 expressions were detected using confocal microscopy by immunofluorescence analysis; objective magnification, 63x; scale bar represents 20 μm. Colocalization of parkin (or PINK1) (green) and TOM20 (red) was shown in magnified images. The yellow fluorescence represented the overlap of red and green fluorescence. (d) Parkin and PINK1 protein expressions were detected by immunoblot analysis and calculated. Actin was represented as the loading control. Phosphorylation of parkin and PINK1, respectively, was detected by immunoblot analysis with phos-tag and incubated with anti-parkin and anti-PINK1 primary antibodies. The upper binds (slow migration binds) indicated by the black arrow showed phosphorylated proteins. Data ($n = 3$) were shown as the mean ± SEM ($^{*}p < 0.05$, $^{**}p < 0.01$, and $^{***}p < 0.001$).

CCCP-induced parkin mitochondrial translocation in the D40 cells (Figure 6(c), first line from the right). Moreover, after resveratrol treatment, the total expression levels of parkin and PINK1 were not significantly changed in response to CCCP induction in D40 cells. Therefore, we speculated whether parkin and PINK1 phosphorylation increased in response to resveratrol. As shown in Figure 6(d), phosphorylated parkin and PINK1 expressions were detected and showed a significant increase in D40 cells and D40 plus CCCP cells after resveratrol treatment, suggesting that parkin phosphorylation and PINK1 phosphorylation were implicated in parkin mitochondrial translocation induced by resveratrol in H9c2 cells.

Taken together, the CCCP-induced activation of parkin and PINK1 was suppressed in senescent-like H9c2 cardiomyocytes, most likely due to the resistance of elongated mitochondria to depolarization. After resveratrol treatment, parkin translocated to mitochondria due to the phosphorylation of parkin and PINK1.

3.5. Resveratrol Regulates LC3-Mediated Autophagy Induced by CCCP in Senescent-Like Cardiomyocytes. As an E3 ubiquitin ligase, parkin is targeted to damaged mitochondria and mediates its selective removal via damaged protein degradation by autophagosomes or lysosome. We therefore examined the LC3-II/LC3-I conversion induced by CCCP in the H9c2 cells and calculated the ratio of LC3-II to LC3-I by immunoblot analysis. Figure 7(a) shows that CCCP (80 μM) treatment for 3 hours significantly increased the expression of LC3-II in D0 cells (left panels). In D40 cells, we observed that the increased expression of LC3-II after CCCP treatment was significantly lower than that in D0 cells (middle panels). As shown in Figure 7(b), the ratio of LC3-II to LC3-I was increased by approximately 10-fold and 5-fold in D0 and D40 cells, respectively, in the presence of CCCP. Resveratrol treatment significantly increased the expression of LC3-II (Figure 7(a), right panels), and the ratio of LC3-II increased more than 10-fold in RSV plus CCCP-treated D40 cells. This result implied that the suppression of parkin and PINK1 contributed to the reduced activity of LC3-II in D-galactose-treated H9c2 cardiomyocytes. Resveratrol enhanced the ability of CCCPs to upregulate LC3-II expression, suggesting that it affected LC3-mediated autophagy.

We also investigated whether RSV affected the TOM20-labeled mitochondria in H9c2 cells treated with CCCP. After 24 hours of treatment with CCCP, the expression of TOM20 was downregulated significantly in the D0 cells (Figure 7(c), left panels). The relative expression intensity was calculated, and the results in Figure 7(d) show that the expression of TOM20 was downregulated by approximately 50% in D0 cells treated with CCCP for 24 hours. Meanwhile, in the D40 cells, the expression of TOM20 did not change significantly after CCCP induction (Figure 7(c), middle panels). Interestingly, the expression of TOM20 was significantly downregulated by CCCP in the D40 cells treated with resveratrol (Figure 7(c), right panels), indicating that the effect of resveratrol is probably involved in the mitochondrial autophagy process that was disturbed by D-galactose in H9c2 cells. To confirm the loss of mitochondrial content, we visualized the mitochondria using fluorescence staining by MitoView Red and calculated the fluorescence intensity. In D0 cells, the morphology of mitochondria significantly changed to very short, fragmented spots after CCCP induction. The mitochondrial distribution was observed in parts of the cytoplasm, although some disappeared (Figure 7(e), left panels). The intensity of the mitochondrial fluorescence staining dye was significantly decreased, indicating the loss of mitochondrial content (Figure 7(f), left panel). Although the mitochondria were obviously fragmented in D40 plus CCCP cells, no significant loss of mitochondrial content could be detected (Figures 7(e) and 7(f), middle panels). Interestingly, after resveratrol treatment, the mitochondrial content was significantly decreased in D40 plus CCCP cells (Figures 7(e) and 7(f), right panels).

4. Discussion

In our study, mitochondrial dynamic abnormalities were found and most mitochondria became tubular or thread-like in response to D-galactose induction. The major regulators of mitochondrial morphology were fission and fusion proteins, suggesting that mitochondrial elongation is probably caused by the imbalance of fission and fusion [28]. Immunoblot analysis showed that Drp1 might be the major factor contributing to mitochondrial elongation induced by D-galactose. Mdivi-1 was a mitochondrial fission inhibitor that induced mitochondrial elongation by inhibiting fission machinery [12]. Our study showed that the mitochondria were elongated and the expression of Drp1 was downregulated in response to Mdivi-1 induction. Compared with the cells induced by Mdivi-1, D-galactose-treated cells showed similar mitochondrial morphology and Drp1 expression, suggesting that mitochondrial elongation induced by D-galactose was partially due to defective fission. Regarding fusion proteins, 40 g/l D-galactose induction did not alter the expressions of Mfn1, Mfn2, or OPA1. A study by Neuspiel et al. showed that mitofusin 2 (Mfn2) acted as a signaling GTPase to induce mitochondrial fusion and protected against permeability transition [29], suggesting that Mfn2-mediated mitochondrial fusion enhances the endurance of cardiomyocytes to depolarization. However, specific Mfn2 knockout produced enlarged mitochondria that exhibited impaired respiratory function [30]. In addition, independent of Mfn2 promoting fusion, this protein played a critical role in culling damaged mitochondria [9]. Therefore, the roles of Mfn2 in the formation of enlarged mitochondria are complex and not fully elucidated. In our study, Drp1-mediated fission played a major role in mitochondrial elongation in response to D-galactose induction. Resveratrol significantly decreased the mitochondrial elongation in H9c2 cells, thus attenuating the characteristic mitochondrial dynamic abnormalities induced by D-galactose.

Previous studies have evaluated several parameters to show the effects of D-galactose on cellular senescence, such as advanced glycation end products (AGEs), superoxide dismutase (SOD), and telomeres [13, 31–33]. Because cellular senescence is a very complex process that is not fully elucidated, here, we analyzed the senescent-like phenotypes

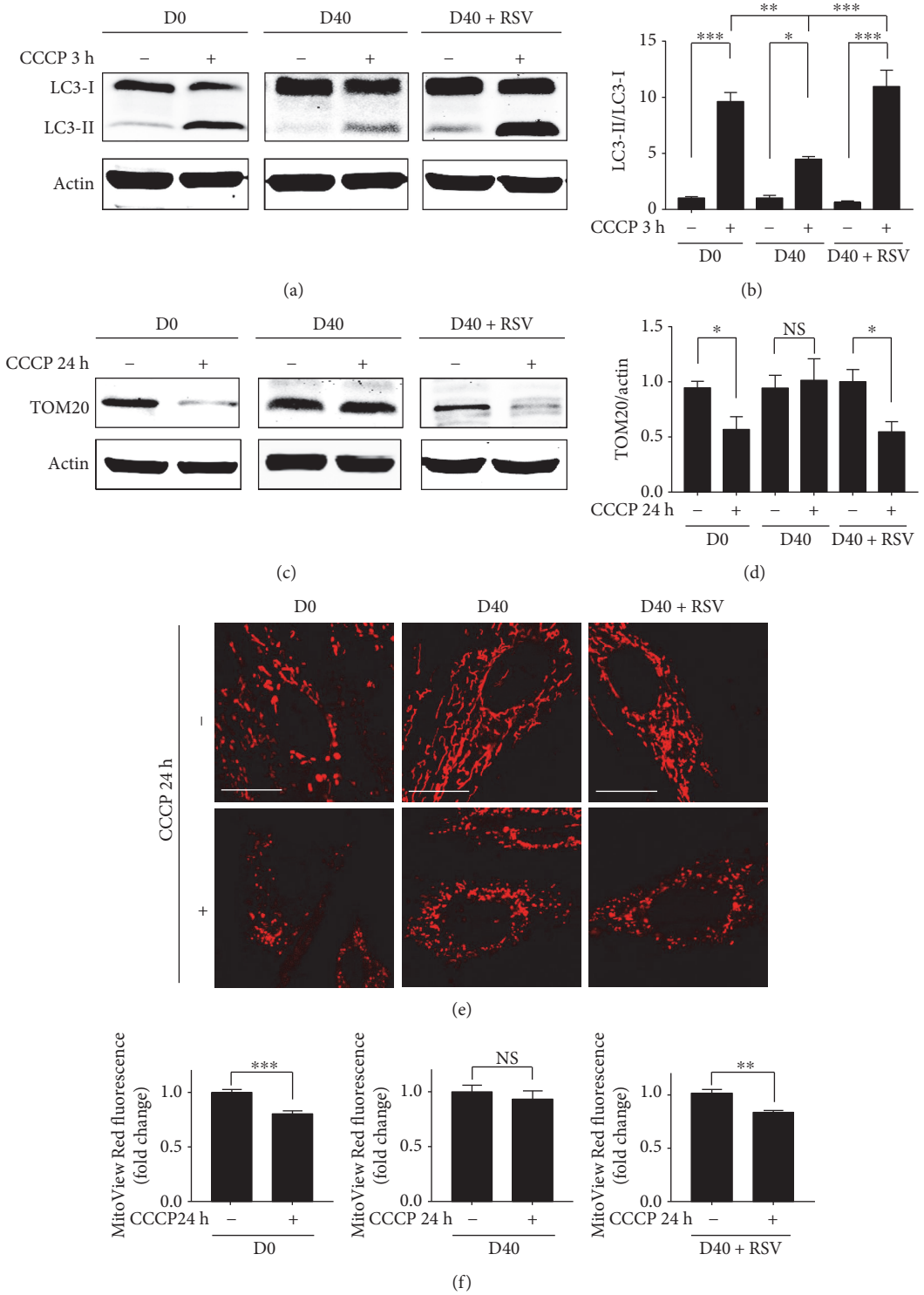

Figure 7: Resveratrol regulated the LC3-mediated autophagy induced by CCCP in D-galactose-induced H9c2 cells. (a) LC3-I and LC3-II expressions in H9c2 cells treated with CCCP (80 μM) for 3 hours were detected by immunoblot analysis. Actin was represented as the loading control. (b) The relative values of LC3-II/LC3-I expressions were calculated. Data ($n = 3$) were shown as the mean ± SEM ($^{*}p < 0.05$, $^{**}p < 0.01$, and $^{***}p < 0.001$). (c) TOM20 expressions in H9c2 cells treated with CCCP (80 μM) for 24 hours were detected by immunoblot analysis. Actin was represented as the loading control. (d) The relative values of TOM20 expressions were normalized to actin. Data ($n = 3$) were shown as the mean ± SEM ($^{*}p < 0.05$); NS: no significance ($p > 0.05$). (e) H9c2 cardiomyocytes were treated with CCCP (80 μM) for 24 hours. Mitochondrial morphology was detected using confocal microscopy by MitoView Red staining; objective magnification, 63x; white scale bar represented 20 μm. (f) Quantification of MitoView Red staining dye was assessed by the fluorescence microplate assay. Data ($n = 3$) were shown as the mean ± SEM ($^{**}p < 0.01$, $^{***}p < 0.001$); NS: no significance ($p > 0.05$).

in H9c2 cardiomyocytes in response to D-galactose by evaluating senescence-associated β-galactosidase activity, a biomarker for cellular senescence or organ aging [34]. For cellular senescence and proliferation [35], we observed reduced cell proliferation by the BrdU incorporation assay. Furthermore, several other metabolism disorder indicators, such as intracellular calcium overloading, enhanced ROS production enhancement, and decreased levels of ATP production, were found in H9c2 cardiomyocytes induced by D-galactose. Taken together, D-galactose induction increased the activity of senescence-associated β-galactosidase and reduced cellular proliferation, thus inducing senescent-like phenotypes in H9c2 cardiomyocytes. Moreover, H9c2 cells displayed excessive ROS production and intracellular calcium overloading induced by D-galactose. Aging cardiomyocytes produced damaged and enlarged mitochondria that exhibit excessive ROS and mutated respiratory function genes and proteins, which make them more difficult to selectively remove than smaller mitochondria [6]. Therefore, we further evaluated the mitochondrial membrane potential and respiration in response to D-galactose. D-galactose induction did not change the MMP and oxygen consumption rate, implying that the mitochondrial function was not impaired. Further analysis of expressions of Bcl-2 and Bax suggested that the mitochondrial-mediated apoptotic signaling pathway was not activated. Further evaluations of resveratrol on senescent-like phenotypes induced by D-galactose showed that resveratrol significantly reduced SA β-Gal-positive staining and increased the percentage of BrdU/DAPI double-positive staining. In addition, resveratrol significantly decreased the ROS production and calcium concentration in response to D-galactose, respectively, in a dose-dependent manner.

Mitochondrial elongation with abnormal dynamics was shown to alter small molecular activation and/or intracellular pathways, including the balance of fusion and fission and the selective removal of damaged mitochondria, probably contributing to the reduction of IPC in the development of cardiac aging. Drp1-mediated mitochondrial fission is considered a potential upstream effector for subsequent selective removal of mitochondria [20]. Evidence showed that decreased Drp1 expression damaged mitochondria, thus increasing cardiomyocyte apoptosis and suppressing glucose deprivation-induced autophagosome formation and autophagic flux. Ikeda et al. applied mitochondrial-targeted Keima fluorescence to monitor the maturation of autophagosomes to lysosomes by detecting excitation spectra peaking in acidic pH conditions. The CCCP-induced positive staining of Keima on mitochondria was not detected in cardiomyocytes transduced with Ad-shDrp1, suggesting that Drp1 was necessary for mitochondrial autophagic removal. More direct evidence that Drp1 downregulation decreased the number of autophagosomes and autophagosomes containing mitochondria in response to glucose deprivation was detected by electron microscopy. Moreover, the authors also investigated the autophagic flux in Drp1-CKO mice. In Drp1-CKO mice, the activity of LC3-II was suppressed and the autophagic flux was present under both physical and chemical stimuli in the heart [19]. This result leads to the hypothesis that Drp1-mediated fission machinery probably dominates the separation of damaged mitochondrial components. Drp1-mediated mitochondrial fission was shown to segregate damaged components for selective elimination and to recruit parkin to mitochondria to maintain their integrity. Suppression of Drp1 reduced the mitochondrial translocation of parkin [20]. Parkin, an E3 ubiquitin ligase, was required in this process to promote Drp1-dependent mitochondrial fragmentation [36]. Furthermore, PINK1, a serine-threonine kinase that collaborates with parkin to regulate mitochondrial programmed clearance, was related to Drp1-mediated mitochondrial fission [37]. A prevalent signaling pathway implicated in selective mitochondrial removal was determined to be mediated by the parkin and PINK1 proteins [38]. Mitochondrial depolarization activated the outer membrane localization of PINK1 and drove cytosolic parkin recruitment [39, 40]. To investigate whether Drp1-mediated mitochondrial elongation in senescent-like cardiomyocytes suppressed selective mitochondrial removal, CCCP was used to induce mitochondrial depolarization and parkin and PINK1 activation.

CCCP is a conventional compound that causes mitochondrial depolarization and induces parkin mitochondrial translocation. In our study, no CCCP-induced mitochondrial depolarization was found in H9c2 cells in response to D-galactose. Interestingly, the mitochondria retained their elongated morphology in the presence of CCCP, indicating that elongated mitochondria exhibited resistance to CCCP-induced mitochondrial depolarization. Additionally, resveratrol ameliorated abnormal mitochondrial elongation by upregulating the expression of Drp1 in D-galactose-treated cardiomyocytes. Therefore, resveratrol probably could enhance the ability of CCCP to induce mitochondrial depolarization. After resveratrol treatment, the mitochondria were depolarized which was induced by CCCP in D-galactose-treated H9c2 cardiomyocytes. Next, we explored the activation of parkin and PINK1 to determine whether the resistance of elongated mitochondria to CCCP-induced depolarization would affect parkin mitochondrial translocation. Our results showed that parkin translocated to mitochondria in response to CCCP induction. However, we did not observe significant parkin mitochondrial translocation in D-galactose-treated cells that were resistant to CCCP-induced depolarization. Meanwhile, the results of PINK1 expression analysis by immunostaining showed that its activation was reduced, suggesting that the defective parkin and PINK1 mitochondrial translocations were implicated in the resistance of D-galactose-treated cells to CCCP-induced mitochondrial depolarization. Furthermore, PINK1-mediated parkin phosphorylation and PINK1 autophosphorylation were essential for the mitochondrial translocation of parkin upon mitochondrial depolarization [41, 42]. To examine the phosphorylation of parkin and PINK1, we applied SDS-PAGE gels containing a phos-tag to specifically separate the phosphorylated proteins for detection using immunoblot analysis. The phos-tag gel showed that the phosphorylation levels of parkin and PINK1 were enhanced in response to CCCP induction. However, the increased levels of phosphorylation were not observed in

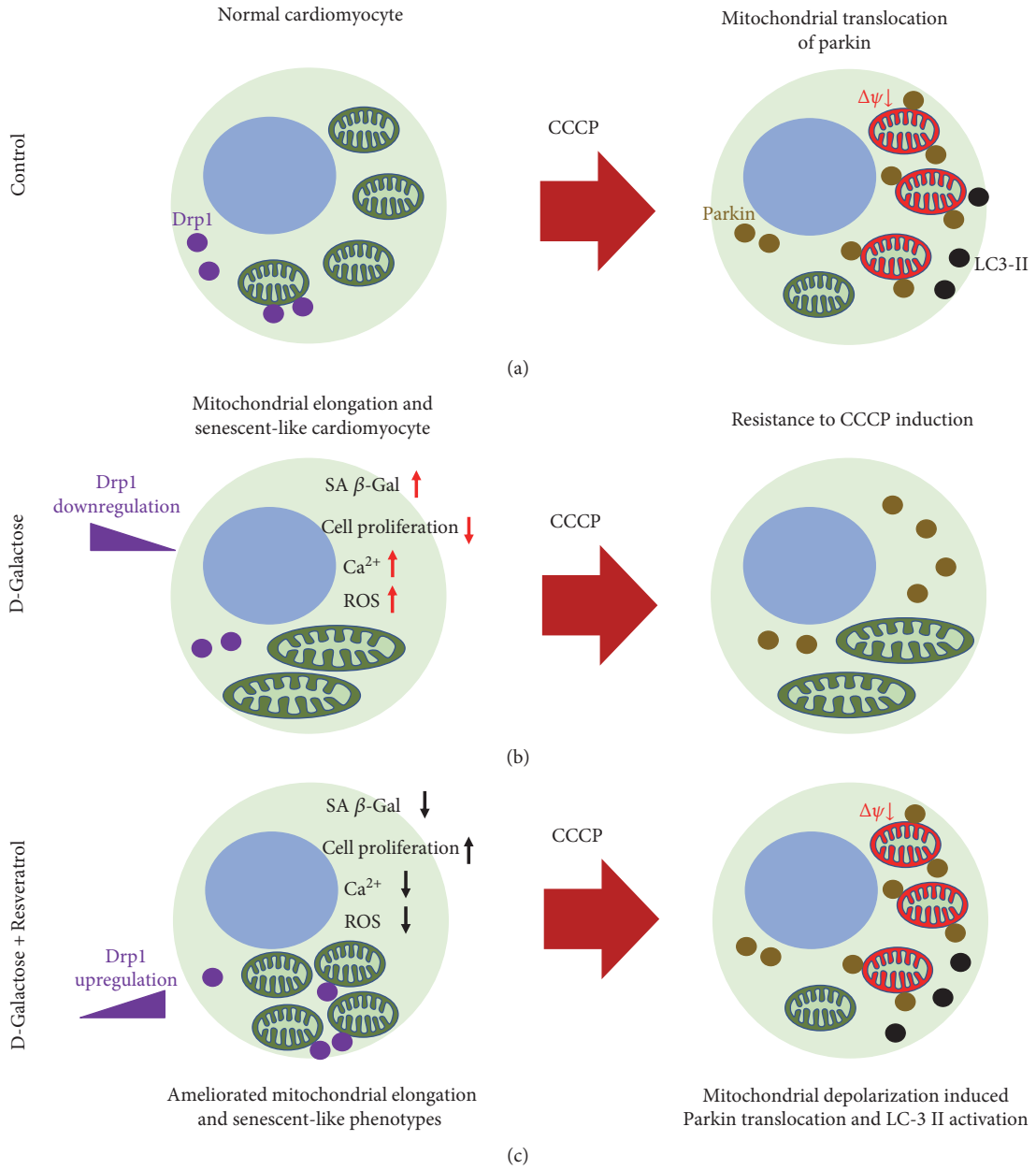

Figure 8: The schematic representation proposed the effect of resveratrol on mitochondrial elongation in D-galactose-induced cardiomyocytes. (a) Control, (b) D-galactose, and (c) D-galactose + resveratrol.

the cells induced by D-galactose, indicating that the phosphorylation of parkin by PINK1 was reduced and suggesting that Drp1-mediated mitochondrial elongation attenuated the activations of parkin and PINK1. Furthermore, CCCP-induced LC3-II protein upregulation and loss of mitochondrial content were suppressed in senescent-like cardiomyocytes, possibly, due to the attenuated activation of parkin.

Mutations in genes encoding the parkin and PINK1 proteins were first identified in the pathogenesis of Parkinson's diseases and determined to be involved in the underlying mechanisms of several other major neurodegenerative diseases [43, 44]. Decreased mitochondrial membrane potential and impaired respiratory chain were found in parkin-mutant patients and PINK1-mutant patients [45, 46]. Defective dysfunctional mitochondrial removal was revealed in the progress of neurodegenerative diseases with the absence of functional parkin and PINK1 [47, 48]. The potential mechanism elucidated by researchers was that the functional interaction of parkin and PINK1 displayed the clearance of dysfunctional mitochondria [49]. Despite the epidemiological association between Parkinson's diseases and heart failure, the indispensable roles of parkin and PINK1 for normal heart function have come under intense attack in the past decade. Evidence showed that deficient parkin protein levels in mice enhanced their sensitivity to cardiac infarction and larger infarct sizes [50]. Decreased PINK1 protein levels led to impaired mitochondrial function and redox homeostasis in cardiac dysfunction [51]. Moreover, the translocation

of parkin to damaged mitochondria was disturbed in aged hearts. The overexpression of parkin ameliorated cardiac aging and maintained mitochondrial integrity [52]. In addition, Huang et al.'s study showed that parkin was involved in the cardioprotection of ischemic preconditioning and short-term hypoxia increased parkin mitochondrial translocation in cardiomyocytes [53]. These studies indicated that parkin plays a critical role in mitochondrial integrity in aging hearts, and defective parkin mitochondrial translocation might be a possible reason for the loss or attenuation of cardiac ischemic preconditioning.

Resveratrol is a polyphenol compound that functions in age-related disorders [54]. Resveratrol can reportedly improve cardiac function in failing hearts by activating the SIRT1 protein level and improving AMPK expression [55]. The effect of resveratrol on mitochondria has been studied for years. Resveratrol was shown to exhibit multiple effects on mitochondrial mass, mtDNA content, and upregulation of the biogenetic factor of PGC-1α, supporting the role of resveratrol against myocardial ischemia/reperfusion injury by decreasing ROS generation and inhibiting mPTP opening [56]. Meanwhile, resveratrol has been shown to exhibit protective effects against oxidative stress by modulating mitochondrial biogenesis in an SIRT3-dependent manner after activating AMPK-PGC-1α-ERRα signaling [57]. Notably, our study is the first to investigate the effects of resveratrol on mitochondrial dynamics. Morphological studies of mitochondria by live cell staining and ultrastructural detection demonstrated that resveratrol ameliorated mitochondrial elongation by upregulating Drp1 expression. Therefore, our study provided a new viewpoint in the effects of resveratrol on mitochondrial dynamic imbalance, suggesting that the potential mechanisms of resveratrol antiaging properties are probably related to mitochondrial dynamics (Figure 8). Meanwhile, resveratrol increased the level of mitochondrial depolarization, perhaps by ameliorating mitochondrial elongation. For decades, few studies have explored the effects of resveratrol on parkin and PINK1 protein expressions and the signaling pathways in which they are involved. Recently, Das et al. showed that raised resveratrol exhibited the potential effects on a Sirt1-Sirt3-Foxo3-PINK1-PARKIN signaling network during ischemia/reperfusion injury [58]. Although their study provided promising insight into the effective mechanisms of resveratrol that involve parkin and PINK1, fully understanding the roles of resveratrol on the functional activation of parkin and PINK1 in different pathological processes still needs to be accomplished. Promisingly, our study showed that resveratrol significantly induced parkin mitochondrial translocation in senescent-like H9c2 cardiomyocytes by regulating the phosphorylation of parkin and PINK1. Furthermore, resveratrol upregulated the expression of LC3-II and decreased the mitochondrial content in D-galactose-induced cells, suggesting that it affected LC3-mediated autophagy.

5. Conclusion

In summary, our study characterized mitochondrial dynamic disorders in H9c2 cardiomyocytes that presented cellular senescent-like phenotypes in response to D-galactose induction. We observed marked mitochondrial elongation by Drp1-mediated fission disorders. Interestingly, D-galactose-treated cardiomyocytes showed resistance to mitochondrial depolarization, and their mitochondrial morphology exhibited elongation in response to CCCP induction. Importantly, the natural polyphenol compound resveratrol ameliorated mitochondrial elongation by enhancing Drp1 expression and increasing the level of mitochondrial depolarization, suggesting that mitochondrial elongation is partly implicated in depolarization resistance. Furthermore, the reduced activations of parkin and PINK1, including mitochondrial translocation and protein phosphorylation, in response to CCCP induction were found in senescent-like cardiomyocytes. Finally, resveratrol upregulated the mitochondrial translocation of parkin, activated the phosphorylation of parkin and PINK1, and upregulated the LC3-II activity, providing a new pharmacological approach for further studies of the mechanisms of Drp1 and parkin-PINK1 signaling.

Abbreviations

IPC: Ischemic preconditioning
ATP: Adenosine triphosphate
$K_{ATP:}$ ATP-sensitive potassium channels
MMP: Mitochondrial membrane potential
ROS: Reactive oxygen species
Mfn1: Mitofusin 1
Mfn2: Mitofusin 2
OPA1: Optic atrophy 1
Drp1: Dynamin-related protein-1
Mdivi-1: Mitochondrial division inhibitor 1
PINK1: PTEN-inducible kinase 1
SIRT1: Sirtuin 1
Bcl-2: B-cell lymphoma 2
Bax: Bcl-2-associated X
RSV: Resveratrol
CCCP: Carbonyl cyanide 3-chlorophenylhydrazone
BrdU: Bromodeoxyuridine
LC3: Microtubule-associated protein 1A/1B light chain 3.

Conflicts of Interest

The authors declare that there is no conflict of interests regarding the publication of this paper.

Acknowledgments

This research was supported by the Macao Science and Technology Development Fund (Project nos.: 073/2011/A3 and 052/2013/A2).

References

[1] P. Abete, F. Cacciatore, G. Testa et al., "Ischemic preconditioning in the aging heart: from bench to bedside," *Ageing Research Reviews*, vol. 9, no. 2, pp. 153–162, 2010.

[2] P. Abete, G. Testa, F. Cacciatore et al., "Ischemic preconditioning in the younger and aged heart," *Aging and Disease*, vol. 2, no. 2, pp. 138–148, 2011.

[3] T. Vanden Hoek, L. B. Becker, Z. H. Shao, C. Q. Li, and P. T. Schumacker, "Preconditioning in cardiomyocytes protects by attenuating oxidant stress at reperfusion," *Circulation Research*, vol. 86, no. 5, pp. 541–548, 2000.

[4] E. Murphy and C. Steenbergen, "Mechanisms underlying acute protection from cardiac ischemia-reperfusion injury," *Physiological Reviews*, vol. 88, no. 2, pp. 581–609, 2008.

[5] G. Heusch, "Molecular basis of cardioprotection: signal transduction in ischemic pre-, post-, and remote conditioning," *Circulation Research*, vol. 116, no. 4, pp. 674–699, 2015.

[6] K. Boengler, R. Schulz, and G. Heusch, "Loss of cardioprotection with ageing," *Cardiovascular Research*, vol. 83, no. 2, pp. 247–261, 2009.

[7] G. W. Dorn 2nd and R. N. Kitsis, "The mitochondrial dynamism-mitophagy-cell death interactome: multiple roles performed by members of a mitochondrial molecular ensemble," *Circulation Research*, vol. 116, no. 1, pp. 167–182, 2015.

[8] G. W. Dorn 2nd, "Mitochondrial dynamism and heart disease: changing shape and shaping change," *EMBO Molecular Medicine*, vol. 7, no. 7, pp. 865–877, 2015.

[9] G. W. Dorn 2nd, "Mitochondrial dynamism and cardiac fate–a personal perspective," *Circulation Journal*, vol. 77, no. 6, pp. 1370–1379, 2013.

[10] R. Zepeda, J. Kuzmicic, V. Parra et al., "Drp1 loss-of-function reduces cardiomyocyte oxygen dependence protecting the heart from ischemia-reperfusion injury," *Journal of Cardiovascular Pharmacology*, vol. 63, no. 6, pp. 477–487, 2014.

[11] W. W. Sharp, Y. H. Fang, M. Han et al., "Dynamin-related protein 1 (Drp1)-mediated diastolic dysfunction in myocardial ischemia-reperfusion injury: therapeutic benefits of Drp1 inhibition to reduce mitochondrial fission," *The FASEB Journal*, vol. 28, no. 1, pp. 316–326, 2014.

[12] S. B. Ong, S. Subrayan, S. Y. Lim, D. M. Yellon, S. M. Davidson, and D. J. Hausenloy, "Inhibiting mitochondrial fission protects the heart against ischemia/reperfusion injury," *Circulation*, vol. 121, no. 18, pp. 2012–2022, 2010.

[13] D. Bernhard and G. Laufer, "The aging cardiomyocyte: a mini-review," *Gerontology*, vol. 54, no. 1, pp. 24–31, 2008.

[14] S. Siddiqi and M. A. Sussman, "Cardiac hegemony of senescence," *Current Translational Geriatrics Experimental Gerontology Reports*, vol. 2, no. 4, pp. 247–254, 2013.

[15] D. Dutta, R. Calvani, R. Bernabei, C. Leeuwenburgh, and E. Marzetti, "Contribution of impaired mitochondrial autophagy to cardiac aging: mechanisms and therapeutic opportunities," *Circulation Research*, vol. 110, no. 8, pp. 1125–1138, 2012.

[16] U. T. Brunk and A. Terman, "The mitochondrial-lysosomal axis theory of aging: accumulation of damaged mitochondria as a result of imperfect autophagocytosis," *European Journal of Biochemistry*, vol. 269, no. 8, p. 2002, 1996.

[17] E. J. Lesnefsky, Q. Chen, and C. L. Hoppel, "Mitochondrial metabolism in aging heart," *Circulation Research*, vol. 118, no. 10, pp. 1593–1611, 2016.

[18] M. Tong and J. Sadoshima, "Mitochondrial autophagy in cardiomyopathy," *Current Opinion in Genetics & Development*, vol. 38, pp. 8–15, 2016.

[19] Y. Ikeda, A. Shirakabe, Y. Maejima et al., "Endogenous Drp1 mediates mitochondrial autophagy and protects the heart against energy stress," *Circulation Research*, vol. 116, no. 2, pp. 264–278, 2015.

[20] Y. Lee, H. Y. Lee, R. A. Hanna, and A. B. Gustafsson, "Mitochondrial autophagy by Bnip3 involves Drp1-mediated mitochondrial fission and recruitment of parkin in cardiac myocytes," *American Journal of Physiology: Heart and Circulatory Physiology*, vol. 301, no. 5, pp. H1924–H1931, 2011.

[21] R. Sgarbanti, D. Amatore, I. Celestino et al., "Intracellular redox state as target for anti-influenza therapy: are antioxidants always effective?," *Current Topics in Medicinal Chemistry*, vol. 14, no. 22, pp. 2529–2541, 2014.

[22] D. R. Valenzano, E. Terzibasi, T. Genade, A. Cattaneo, L. Domenici, and A. Cellerino, "Resveratrol prolongs lifespan and retards the onset of age-related markers in a short-lived vertebrate," *Current Biology*, vol. 16, no. 3, pp. 296–300, 2006.

[23] A. Carrizzo, M. Forte, A. Damato et al., "Antioxidant effects of resveratrol in cardiovascular, cerebral and metabolic diseases," *Food and Chemical Toxicology*, vol. 61, pp. 215–226, 2013.

[24] H. Zheng, H. Guo, Y. Hong, F. Zheng, and J. Wang, "The effects of age and resveratrol on the hypoxic preconditioning protection against hypoxia-reperfusion injury: studies in rat hearts and human cardiomyocytes," *European Journal of Cardio-Thoracic Surgery*, vol. 48, no. 3, pp. 375–381, 2015.

[25] T. K. Sin, A. P. Yu, B. Y. Yung et al., "Modulating effect of SIRT1 activation induced by resveratrol on Foxo1-associated apoptotic signalling in senescent heart," *The Journal of Physiology*, vol. 592, no. 12, pp. 2535–2548, 2014.

[26] A. P. Raval, K. R. Dave, and M. A. Perez-Pinzon, "Resveratrol mimics ischemic preconditioning in the brain," *Journal of Cerebral Blood Flow & Metabolism*, vol. 26, no. 9, pp. 1141–1147, 2006.

[27] Z. F. Zhang, S. H. Fan, Y. L. Zheng et al., "Purple sweet potato color attenuates oxidative stress and inflammatory response induced by D-galactose in mouse liver," *Food and Chemical Toxicology*, vol. 47, no. 2, pp. 496–501, 2009.

[28] C. L. Hoppel, B. Tandler, H. Fujioka, and A. Riva, "Dynamic organization of mitochondria in human heart and in myocardial disease," *The International Journal of Biochemistry & Cell Biology*, vol. 41, no. 10, pp. 1949–1956, 2009.

[29] M. Neuspiel, R. Zunino, S. Gangaraju, P. Rippstein, and H. McBride, "Activated mitofusin 2 signals mitochondrial fusion, interferes with Bax activation, and reduces susceptibility to radical induced depolarization," *The Journal of Biological Chemistry*, vol. 280, no. 26, pp. 25060–25070, 2005.

[30] S. Lee, F. H. Sterky, A. Mourier et al., "Mitofusin 2 is necessary for striatal axonal projections of midbrain dopamine neurons," *Human Molecular Genetics*, vol. 21, no. 22, pp. 4827–4835, 2012.

[31] X. Song, M. Bao, D. Li, and Y. M. Li, "Advanced glycation in D-galactose induced mouse aging model," *Mechanisms of Ageing and Development*, vol. 108, no. 3, pp. 239–251, 1999.

[32] S. C. Ho, J. H. Liu, and R. Y. Wu, "Establishment of the mimetic aging effect in mice caused by D-galactose," *Biogerontology*, vol. 4, no. 1, pp. 15–18, 2003.

[33] A. Lechel, A. Satyanarayana, Z. Ju et al., "The cellular level of telomere dysfunction determines induction of senescence or apoptosis *in vivo*," *EMBO Reports*, vol. 6, no. 3, pp. 275–281, 2005.

[34] A. Gutierrez-Fernandez, C. Soria-Valles, F. G. Osorio et al., "Loss of MT1-MMP causes cell senescence and nuclear defects

which can be reversed by retinoic acid," *The EMBO Journal*, vol. 34, no. 14, pp. 1875–1888, 2015.

[35] C. Franceschi, "Cell proliferation, cell death and aging," *Aging Clinical and Experimental Research*, vol. 1, no. 1, pp. 3–15, 1989.

[36] L. Buhlman, M. Damiano, G. Bertolin et al., "Functional interplay between parkin and Drp1 in mitochondrial fission and clearance," *Biochimica et Biophysica Acta (BBA) - Molecular Cell Research*, vol. 1843, no. 9, pp. 2012–2026, 2014.

[37] H. Deng, M. W. Dodson, H. Huang, and M. Guo, "The Parkinson's disease genes *pink1* and *parkin* promote mitochondrial fission and/or inhibit fusion in *Drosophila*," *Proceedings of the National Academy of Sciences of the United States of America*, vol. 105, no. 38, pp. 14503–14508, 2008.

[38] E. S. Vincow, G. Merrihew, R. E. Thomas et al., "The PINK1-parkin pathway promotes both mitophagy and selective respiratory chain turnover in vivo," *Proceedings of the National Academy of Sciences of the United States of America*, vol. 110, no. 16, pp. 6400–6405, 2013.

[39] K. Okatsu, M. Kimura, T. Oka, K. Tanaka, and N. Matsuda, "Unconventional PINK1 localization to the outer membrane of depolarized mitochondria drives parkin recruitment," *Journal of Cell Science*, vol. 128, no. 5, pp. 964–978, 2015.

[40] M. Lazarou, S. M. Jin, L. A. Kane, and R. J. Youle, "Role of PINK1 binding to the TOM complex and alternate intracellular membranes in recruitment and activation of the E3 ligase parkin," *Developmental Cell*, vol. 22, no. 2, pp. 320–333, 2012.

[41] K. Shiba-Fukushima, Y. Imai, S. Yoshida et al., "PINK1-mediated phosphorylation of the parkin ubiquitin-like domain primes mitochondrial translocation of parkin and regulates mitophagy," *Scientific Reports*, vol. 2, p. 1002, 2012.

[42] K. Okatsu, T. Oka, M. Iguchi et al., "PINK1 autophosphorylation upon membrane potential dissipation is essential for parkin recruitment to damaged mitochondria," *Nature Communications*, vol. 3, p. 1016, 2012.

[43] T. Kitada, S. Asakawa, N. Hattori et al., "Mutations in the parkin gene cause autosomal recessive juvenile parkinsonism," *Nature*, vol. 392, no. 6676, pp. 605–608, 1998.

[44] E. M. Valente, P. M. Abou-Sleiman, V. Caputo et al., "Hereditary early-onset Parkinson's disease caused by mutations in *PINK1*," *Science*, vol. 304, no. 5674, pp. 1158–1160, 2004.

[45] H. Mortiboys, K. J. Thomas, W. J. Koopman et al., "Mitochondrial function and morphology are impaired in *parkin*-mutant fibroblasts," *Annals of Neurology*, vol. 64, no. 5, pp. 555–565, 2008.

[46] A. Y. Abramov, M. Gegg, A. Grunewald, N. W. Wood, C. Klein, and A. H. Schapira, "Bioenergetic consequences of PINK1 mutations in Parkinson disease," *PLoS One*, vol. 6, no. 10, article e25622, 2011.

[47] C. W. Zhang, L. Hang, T. P. Yao, and K. L. Lim, "Parkin regulation and neurodegenerative disorders," *Frontiers in Aging Neuroscience*, vol. 7, p. 248, 2016.

[48] H. Chen and D. C. Chan, "Mitochondrial dynamics–fusion, fission, movement, and mitophagy–in neurodegenerative diseases," *Human Molecular Genetics*, vol. 18, no. R2, pp. R169–R176, 2009.

[49] S. Geisler, K. M. Holmstrom, D. Skujat et al., "PINK1/parkin-mediated mitophagy is dependent on VDAC1 and p62/SQSTM1," *Nature Cell Biology*, vol. 12, no. 2, pp. 119–131, 2010.

[50] D. A. Kubli, X. Zhang, Y. Lee et al., "Parkin protein deficiency exacerbates cardiac injury and reduces survival following myocardial infarction," *The Journal of Biological Chemistry*, vol. 288, no. 2, p. 915, 2013.

[51] F. Billia, L. Hauck, F. Konecny, V. Rao, J. Shen, and T. W. Mak, "PTEN-inducible kinase 1 (PINK1)/Park6 is indispensable for normal heart function," *Proceedings of the National Academy of Sciences of the United States of America*, vol. 108, no. 23, pp. 9572–9577, 2011.

[52] A. Hoshino, Y. Mita, Y. Okawa et al., "Cytosolic p53 inhibits parkin-mediated mitophagy and promotes mitochondrial dysfunction in the mouse heart," *Nature Communications*, vol. 4, p. 2308, 2013.

[53] C. Huang, A. M. Andres, E. P. Ratliff, G. Hernandez, P. Lee, and R. A. Gottlieb, "Preconditioning involves selective mitophagy mediated by parkin and p62/SQSTM1," *PLoS One*, vol. 6, no. 6, article e20975, 2011.

[54] S. J. Park, F. Ahmad, A. Philp et al., "Resveratrol ameliorates aging-related metabolic phenotypes by inhibiting cAMP phosphodiesterases," *Cell*, vol. 148, no. 3, pp. 421–433, 2012.

[55] X. S. Gu, Z. B. Wang, Z. Ye et al., "Resveratrol, an activator of SIRT1, upregulates AMPK and improves cardiac function in heart failure," *Genetics and Molecular Research*, vol. 13, no. 1, pp. 323–335, 2014.

[56] E. Fan and K. Zhang, "Targeting resveratrol to mitochondria for cardiovascular diseases," *Recent Patents on Cardiovascular Drug Discovery*, vol. 5, no. 2, pp. 97–102, 2010.

[57] M. R. de Oliveira, S. F. Nabavi, A. Manayi, M. Daglia, Z. Hajheydari, and S. M. Nabavi, "Resveratrol and the mitochondria: from triggering the intrinsic apoptotic pathway to inducing mitochondrial biogenesis, a mechanistic view," *Biochimica et Biophysica Acta (BBA) - General Subjects*, vol. 1860, no. 4, pp. 727–745, 2016.

[58] S. Das, G. Mitrovsky, H. R. Vasanthi, and D. K. Das, "Antiaging properties of a grape-derived antioxidant are regulated by mitochondrial balance of fusion and fission leading to mitophagy triggered by a signaling network of Sirt1-Sirt3-Foxo3-PINK1-PARKIN," *Oxidative Medicine and Cellular Longevity*, vol. 2014, Article ID 345105, 10 pages, 2014.

Hindawi
Oxidative Medicine and Cellular Longevity
Volume 2017, Article ID 1480294, 12 pages
https://doi.org/10.1155/2017/1480294

Research Article

Ginger Oleoresin Alleviated γ-Ray Irradiation-Induced Reactive Oxygen Species via the Nrf2 Protective Response in Human Mesenchymal Stem Cells

Kaihua Ji,[1] Lianying Fang,[1] Hui Zhao,[2] Qing Li,[1] Yang Shi,[3] Chang Xu,[1] Yan Wang,[1] Liqing Du,[1] Jinhan Wang,[1] and Qiang Liu[1]

[1]*Tianjin Key Laboratory of Radiation Medicine and Molecular Nuclear Medicine, Department of Radiobiology, Institute of Radiation Medicine of Chinese Academy of Medical Science, Tianjin 300192, China*
[2]*Tianjin Key Laboratory of Food and Biotechnology, School of Biotechnology and Food Science, Tianjin University of Commerce, Tianjin 300134, China*
[3]*Tsingdao Lihe Exact Science & Technology Co. Ltd., Tsingdao 266111, China*

Correspondence should be addressed to Qiang Liu; liuqiang@irm-cams.ac.cn

Received 23 May 2017; Revised 27 July 2017; Accepted 20 September 2017; Published 18 October 2017

Academic Editor: Pei Luo

Unplanned exposure to radiation can cause side effects on high-risk individuals; meanwhile, radiotherapies can also cause injury on normal cells and tissues surrounding the tumor. Besides the direct radiation damage, most of the ionizing radiation- (IR-) induced injuries were caused by generation of reactive oxygen species (ROS). Human mesenchymal stem cells (hMSCs), which possess self-renew and multilineage differentiation capabilities, are a critical population of cells to participate in the regeneration of IR-damaged tissues. Therefore, it is imperative to search effective radioprotectors for hMSCs. This study was to demonstrate whether natural source ginger oleoresin would mitigate IR-induced injuries in human mesenchymal stem cells (hMSCs). We demonstrated that ginger oleoresin could significantly reduce IR-induced cytotoxicity, ROS generation, and DNA strand breaks. In addition, the ROS-scavenging mechanism of ginger oleoresin was also investigated. The results showed that ginger oleoresin could induce the translocation of Nrf2 to cell nucleus and activate the expression of cytoprotective genes encoding for HO-1 and NQO-1. It suggests that ginger oleoresin has a potential role of being an effective antioxidant and radioprotective agent.

1. Introduction

Radiation from natural or artificial sources is a common phenomenon in our daily life [1]. However, abnormal exposure to radiation can cause side effects on individuals who are involved in nuclear mishaps, attack cleanup crews, astronauts, nuclear power plant workers, and some medical professionals whom could be professionally or accidentally exposed to radiation [2]. Furthermore, radiation therapy used as one of the most important therapy strategies for human malignancy can also injure the normal cells and tissues surrounding the tumor [3]. It represents a cause of treatment toxicity and a limiting factor for dose, volume, and technique of radiation therapy.

Human mesenchymal stem cells (hMSCs) which reside in the mesenchymal stroma are an important population of cells [4]. hMSCs were first isolated from bone marrow and could be found in almost all human organs and tissues such as kidney, vascular tissue, adipose tissue, skin, umbilical cord, and placenta [5–7]. These cells possess stem cell-like characteristics including self-renewal and multilineage differentiation into mesenchymal and nonmesenchymal lineages [8]. hMSCs have been proved to participate in the regeneration of ionizing radiation-damaged tissues. However, hMSCs themselves can also be damaged by ionizing radiation [9]. When irradiated in vitro with increasing doses, the human bone-derived MSC was reported with the phenomenon of greatly reduced self-renewal, proliferation, and differentiation

capabilities [10]. Thus, there is an urgent need for exploring natural effective radioprotectors which could be used to protect normal cells, especially hMSCs when exposed to radiation.

Radiation-induced damages are mediated directly by DNA single-strand breaks, DNA double-strands breaks, and chromosome damage and indirectly due to the production of reactive oxygen species (ROS) [1, 11–13]. ROS makes a large part of contributions to radiation-induced damages, so much of the efforts in the past were made in exploring potential natural antioxidants without obvious side effects to ameliorate radiation-induced toxicities [14]. Many naturally occurring phenolic compounds, such as bioactive substances in plants, grape seed proanthocyanidins, tea polyphenol, curcumin, and ginger oleoresin, have been reported to possess antioxidant properties [15–20]. Ginger (*Zingiber officinale* Roscoe, Zingiberaceae) is one of the most widely consumed spice and condiment for foods and beverages [21]. It has also been used as a remedy for common cold, motion sickness, nausea, digestive disorders, rheumatism, indigestion, and osteoarthritis for a long time in traditional oriental medicine [22]. Ginger oleoresin is a complex mixture which is extracted from Zingiberaceae and is rich in gingerols and shogaols. [6]-Gingerol, [6]-shogaols, and their derivatives are considered as chemopreventive candidates against ROS stress and cancer due to their property of activating the Nrf2-ARE signaling pathway in different types of human cells [23–26]. Furthermore, many researches have reported that [6]-gingerol can prevent UVB or gamma radiation-induced cell damage both in vitro and in vivo [27, 28]. Nrf2, which is regarded as a redox-sensitive prosurvival transcription factor, is maintained at a very low level through Keap1-mediated ubiquitylation and subsequent proteasome-mediated degradation. However, when cells are exposed to oxidative situation, the level of Nrf2 rises, meanwhile Nrf2 translocates into the cell nucleus and binds to the antioxidant response element (ARE) located in the promoter region of cytoprotective genes and upregulates their transcription [29]. The Nrf2 target genes can encode proteins with diverse cellular functions including intracellular redox-balancing proteins such as heme oxygenase-1 (HO-1) and glutamate-cysteine ligase that eliminate ROS and maintain the cellular redox capacity and phase II detoxifying enzymes such as NAD(P)H:quinone oxidoreductase 1 (NQO-1) [29].

Ginger oleoresin, which is extracted from ginger by a supercritical CO_2 fluid-extracted method, is a nonvolatile pungent mixture [30]. Ginger oleoresin is mainly composed of gingerols and shogaols [30]. Therefore, we hypothesized that ginger oleoresin may be a potent radioprotective agent in hMSCs cells via Nrf2 protective response. In the present study, we evaluated that ginger oleoresin can protect hMSCs against radiation-inducing cell damage. Based on these findings, we further verified the radioprotective molecular mechanism of ginger oleoresin focusing on the roles of Nrf2 and its target antioxidant enzymes.

2. Materials and Methods

2.1. Cell Culture. Human mesenchymal stem cells (hMSCs) were obtained from the National Engineering Research Center (NERC) of China, cultured in Dulbecco's modified Eagle's medium-F12 (Hyclone, Logan, UT, USA) containing 10% fetal bovine serum (Gibco, Carlsbad, CA, USA) and antibiotics (100 U/mL penicillin and 100 μg/mL streptomycin) (Invitrogen, Carlsbad, CA, USA) in an atmosphere with 5% CO_2 at 37°C and passaged every two days.

2.2. Treatment with Ginger Oleoresin and Irradiation Schedule. Ginger oleoresin was presented by Tianjin University of Commerce and diluted in the equal volume of dimethyl sulfoxide (DMSO) (Dingguo, BJ, China) to prepare the stock solution. Then, the stock solution was further diluted to the required concentration using cell culture medium. For cytotoxicity determination of ginger oleoresin, hMSCs were exposed to 10^{-3}, 10^{-4}, 10^{-5}, and 10^{-6} g/mL ginger oleoresin and cultured for 24 h, 48 h, and 72 h. For radioprotective effect determination, hMSCs were pretreated with 10^{-4} g/mL ginger oleoresin and cultured for 2 h followed by exposure to γ-rays at the Irradiation Center. After irradiation, the cells were subsequently incubated for 24 h. ^{137}Cs was used as the irradiation source (AECL, Canada). hMSCs cells (±ginger oleoresin in medium) were irradiated at a dose of 4 Gy. DMSO was used as a vehicle control. hMSCs + ginger oleoresin without γ-ray irradiation were also studied.

2.3. Cell Viability Assay. To detect cell viability, the 3-(4,5-dimethylthia-zol-2-yl)-2,5-diphenyltetrazolium bromide (MTT) (Solarbio, Beijing, China) assay was performed [31]. MTT can be reduced to purple formazan in the mitochondria of living cells. The absorbance of formazan solution can be quantified by a spectrophotometer, and hence, this method can be applied to assess the cytoprotective ability and the toxicity of ginger oleoresin based on the viability of cells. For toxicity test, hMSCs cells (5×10^3 cells/well) were seeded in a 96-well plate and treated with the indicated dose of ginger oleoresin for the indicated time period. For cytoprotective determination, hMSCs were seeded in a 96-well plate and pretreated with 10^{-4} g/mL ginger oleoresin or the same volume of DMSO and cultured for 2 h before exposure to 4 Gy γ-rays. Then, the hMSCs cells were cultured for 24 h and added 10 μL MTT (5 mg/mL) solution. The cells were incubated at 30°C for 4 h. The supernatants were discarded, and then 150 μL DMSO was added. The cell viability was determined by measuring the absorbance at 492 nm on a multifunctional microplate reader (BioTek, Winooski, VT).

2.4. Intracellular ROS Measurements. Measurements of intracellular ROS levels were performed using the 2′,7′-dichlorodihydrofluoroscein diacetate ($DCFH_2$-DA) (Sigma, USA) method [32]. $DCFH_2$-DA is able to diffuse through the cell membrane and be hydrolysed by intracellular esterases to produce $DCFH_2$. The nonfluorescent $DCFH_2$ is oxidized by intracellular ROS and results in fluorescent DCF. The treated cell samples (hMSCs, hMSCs + ginger oleoresin, hMSCs + γ-ray irradiation, and hMSCs + ginger oleoresin + γ-ray irradiation) were incubated in the presence of 10 μM $DCFH_2$-DA in DMEM-F12 medium at 37°C for 20 min and then washed three times with DMEM-F12 medium to remove the extracellular $DCFH_2$-DA. The fluorescence values of DCF

inside the cells were monitored to evaluate and detect intracellular ROS by excitation at 498 nm and emission 530 nm using a flow cytometer (BriCyte E6, Mindray, Shenzhen, China) and inverted fluorescence microscope (Leica DMI3000B, German).

2.5. Comet Assay. The DNA damage in an individual cell was measured by using the gel electrophoresis-based comet assay [33]. Under alkaline conditions, the negatively charged DNA supercoils with broken ends were able to migrate toward the anode during electrophoresis. But the DNA supercoils without breaks prevented migration. For comet assay, hMSCs were pretreated with 10^{-4} g/mL ginger oleoresin and cultured for 2 h followed by exposure to γ-rays at the Irradiation Center. After irradiation, the cells were subsequently incubated for 24 h. The comet assay was performed as described before [33]. Briefly, the treated cell samples were applied to prepare single-cell suspensions using trypsin disaggregation. The single-cell suspensions (30 μL) were mixed with low melting point agarose gel (70 μL) (Promega, Madison, WI). The mixture drop was added to a slide with agarose gel (Biowest, Nuaille, France) and then was lysed. Subsequently, the cells were exposed to alkali for DNA unwinding and electrophoresis. After electrophoresis, the slides were neutralized, stained with ethidium bromide (EB), and observed using a fluorescence microscope (ETLPSE 90i, Nikon, Japan). The result images were analyzed using CASP software.

2.6. Quantitative Real-Time PCR. After treatment with or without ginger oleoresin and γ-ray irradiation, cells were cultured for 24 h. RNA extraction, cDNA synthesis, and quantitative real-time PCR were performed as described before [34]. The total RNA in each group was isolated using Trizol reagent (Invitrogen, Carlsbad, CA) following the manufacturer's protocol, and equal amounts of RNA were reverse transcribed to cDNA using a PrimeScript RT reagent kit (Takara, Dalian, China). *Nrf2*, *HO-1*, *NQO-1*, and *GAPDH* mRNA transcription levels were determined using Fast Start Universal SYBR Green Master (Roche, Indianapolis, IN). The sequences of primers used in this study are listed in Table 1. The quantitative real-time PCR data presented are relative mRNA levels normalized to GAPDH, and the value from the untreated control group was set as 1.

2.7. Immunoblotting Analysis. After cells were treated as described above and incubated for 24 h, the expression levels of Nrf2, HO-1, NQO-1, TBP, and TUBLIN were detected using immunoblotting assay. Briefly, cells were lysed with RIPA protein extraction reagent (Bestbio, Shanghai, China) to extract the total protein. The protein concentrations of the extracts were measured by using a bicinchoninic acid kit (Beyotime, Beijing, China) according to the manufacturer's instructions. Equal amounts of extracts were fractionated by SDS-PAGE, and then they were transferred to nitrocellulose membranes (Millipore, Massachusetts, USA). After being transferred, the proteins on the nitrocellulose membranes were blotted with the antibodies indicated. Nrf2, HO-1, NQO-1, TBP, and TUBLIN primary antibodies were purchased from Abcam (Abcam, Cambridge, UK). The intensities of protein bands were measured using Quantity One software (Bio-rad, Hercules, CA).

Table 1: List of primers used for QRT-PCR.

Gene	Sequence (5′-3′)
Nrf2	(Forward) TCAGCGACGGAAAGAGTATGA
	(Reverse) CCACTGGTTTCTGACTGGATGT
HO-1	(Forward) AGAGGGAATTCTCTTGGCTGGCTT
	(Reverse) ATGCCATAGGCTCCTTCCTCCTTT
NQO-1	(Forward) AGGAAGAGCTAATAAATCTCTTCTTTGCTG
	(Reverse) TCATATTGCAGATGTACGGTGTGGATTTAT
GADPH	(Forward) TGACTTCAACAGCGACACCCA
	(Reverse) CACCCTGTTGCTGTAGCCAAA

2.8. Determination of Nuclear Levels of Nrf2. Nuclear levels of Nrf2 were determined by immunofluorescence assay and immunoblotting assay. For immunofluorescence assay, the cells were fixed with 4% paraformaldehyde; and the cell membranes were disrupted using 0.3% TrintonX-100 after the cells were treated and incubated. Subsequently, the cells were labelled with Nrf2 antibody and secondary antibody IgG. Then, the cells were stained with DAPI for nuclear staining. The stained cells were examined using an EVOS inverted fluorescence microscope (Thermo Fisher, MA, USA). Overlay images were recorded by superimposing simultaneous images from two different channels. For immunoblotting assay, the proteins in the cytoplasm and nucleus were isolated using NE-PER Nuclear and Cytoplasmic extraction reagent (Thermo Scientific, Waltham, USA).

2.9. siRNA Knockdown Studies. Nrf2 siRNA was used for knocking down Nrf2 in hMSCs to explore whether the antioxidant effect of ginger oleoresin was through the Nrf2 pathways. RNA interference assay was performed as described before [35]. Briefly, 7×10^4 cells were inoculated into a 6-well plate and 1.8 mL fresh medium was replaced for every well. Then, 2 nmol siRNA (GenePharma, Suzhou, China) mixed with 5 μL Lipofectamine 2000 RNAiMAX Reagent (Thermo Scientific, Waltham, USA) and 193 μL Opti-MEM reduced serum culture medium (Thermo Scientific, Waltham, USA) were added into each well. Cells were further cultured for 1~3 days for transfection and gene knockdown. Knockdown hMSCs were treated with or without ginger oleoresin for 2 h followed by a radiation dose of 4 Gy and incubated for 24 h. MTT assay was used to detect whether the radiation protection effect of ginger oleoresin was lost in Nrf2-silenced hMSCs. Cells were further subjected to RNA extraction for quantitative real-time PCR assay and protein extraction for Western blot assay.

2.10. Statistical Analysis. Data are represented as means ± standard deviations. Statistical analysis was performed using SPSS 19.0 software. Student's *t*-test was performed for the analysis of differences between the two groups. $p < 0.05$ was indicated as statistically significant.

3. Results

3.1. Toxicity of Ginger Oleoresin to Human Mesenchymal Stem Cells (hMSCs). We firstly used the MTT method to evaluate the toxicity of ginger oleoresin to human mesenchymal stem cells (hMSCs) and to determine the treatment doses. As shown in Figure 1, when cells were treated with ginger oleoresin for 24 h, 48 h, and 72 h, there was no significant cell toxicity below 10^{-4} g/mL, but 10^{-3} g/mL was toxic. Therefore, the concentration of 10^{-4} g/mL was chosen for the subsequent bioassays.

3.2. Ginger Oleoresin Significantly Protected Human Mesenchymal Stem Cells against Radiation-Induced Cytotoxicity. The protection conferred by ginger oleoresin against radiation-induced cytotoxicity was evaluated. Human mesenchymal stem cells (hMSCs) were pretreated with 10^{-4} g/mL ginger oleoresin for 2 h before γ-ray irradiation. As shown in Figure 2(a), we demonstrated that the pretreatment of hMSCs cells with ginger oleoresin before radiation significantly increased cell survival rates as compared to cells treated with radiation alone. To our knowledge, the homeostasis of cellular redox status is very important for maintaining the normal functions of cells [36], and ionizing radiation is known to modulate the cellular redox status via inducing the production of reactive oxygen species [1]. The effect of ginger oleoresin to modulate cellular redox status was then evaluated by monitoring changes in ROS levels using DCFH-DA assay. As observed in a fluorescence microscope (Figure 2(b)) and measured in flow cytometry (Figure 2(c)), treatment with 4 Gy γ-ray irradiation alone significantly increased the intracellular level of ROS (248.40 $\pm$ 10.13) compared to the untreated control group (101.70 $\pm$ 1.72), which could be reverted by pretreatment with 10^{-4} (g/mL) ginger oleoresin (130.70 $\pm$ 4.99), while this dose of ginger oleoresin alone had no obvious effect on ROS levels (129.00 $\pm$ 13.96). These results indicated that ginger oleoresin is able to enhance intracellular redox capacity and inhibit γ-ray irradiation-induced oxidative stress. In addition, ionizing radiation is very harmful to cells through inducing widespread biomolecule damages, such as DNA, protein, and lipid damages [37], among which DNA damage is the most important target of IR. Protection of ginger oleoresin to DNA damage was investigated via comet assay. As shown in Figure 3, the radiated human mesenchymal stem cells (hMSCs) resulted in an increase in the levels of all comet parameters (tail DNA%, tail length, and tail moment), whereas pretreatment of ginger oleoresin before radiation inhibited the increase of these parameters significantly. These results indicated the protective effect of ginger oleoresin on IR-induced DNA damage.

3.3. Ginger Oleoresin Induced the Enhancement of Antioxidant Pathway in Human Mesenchymal Stem Cells (hMSCs). Kelch-like ECH-associated protein 1- (Keap1-) nuclear factor erythroid 2-related factor 2- (Nrf2-) antioxidant response element (ARE) pathway is reported as one of the most important defense mechanisms against oxidative stress [38]. Then, we tested the ability of ginger oleoresin to induce Nrf2 and downstream genes encoding for heme oxygenase-1 (HO-1) and NAD(P)H:quinone oxidoreductase 1(NQO-1) in mRNA level via qRT-PCR and protein level via Western blotting. As shown in Figure 4(a), ginger oleoresin enhanced the transcription of Nrf2 very weakly, and the results were not statistically significant ($p > 0.05$). However, the mRNA levels of HO-1 and NQO-1 were significantly induced by ginger oleoresin, especially for the group treated with ginger oleoresin and IR. And the variation pattern of Nrf2, HO-1, and NQO-1 at protein levels was consistent with that of mRNA levels (Figure 4(b)). These data indicated that ginger oleoresin induced the enhancement of the antioxidant pathway in mesenchymal stem cells not by activating the expression of Nrf2.

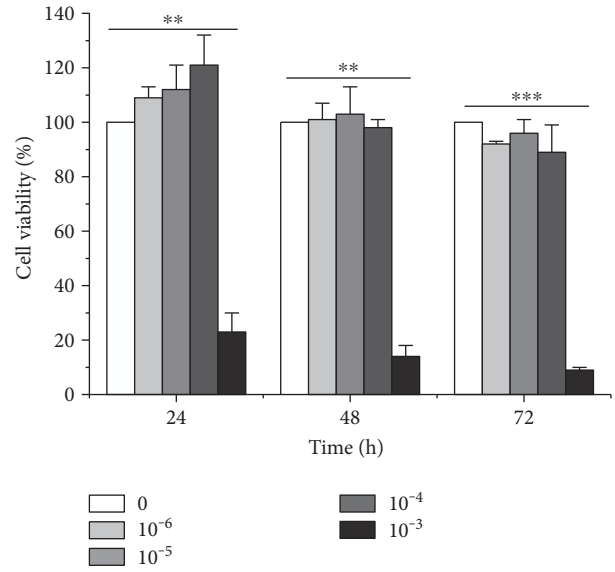

Figure 1: Cytotoxicity of ginger oleoresin in human mesenchymal stem cells (hMSCs) for 24, 36, and 48 h. Cell viability was measured using the MTT assay. The results are the mean $\pm$ SD of three experiments, each in triplicate. $^{**}p < 0.01$ 10^{-3} g/mL treated versus control. $^{***}p < 0.001$ 10^{-3} g/mL treated versus control.

3.4. Knocking Down Nrf2 Significantly Abrogated the Ginger Oleoresin Radiation Protective Effect and Induced Antioxidant Pathway in hMSCs. To further test the role of Nrf2 in the radiation protective effect of ginger oleoresin on hMSCs, Nrf2 knockdown assay was carried out. hMSCs were transfected with Nrf2 siRNA or scrambled siRNA to create a knockdown or negative control. After 3 days, transfected cells with ablated Nrf2 were treated as described above (with or without ginger oleoresin and with or without irradiation) and were further monitored for the cell viability, transcription, and expression of Nrf2, HO-1, and NQO-1 by MTT, qRT-PCR, and immunoblotting, respectively. When pretreated with ginger oleoresin and then irradiation, the cell viability of hMSCs was significantly higher than that treated with irradiation alone (Figure 5) which was consistent with the abovementioned Figure 2(a). The result suggested that ginger oleoresin has a protective effect on hMSCs. However, the radiation protective effect of ginger oleoresin on hMSCs

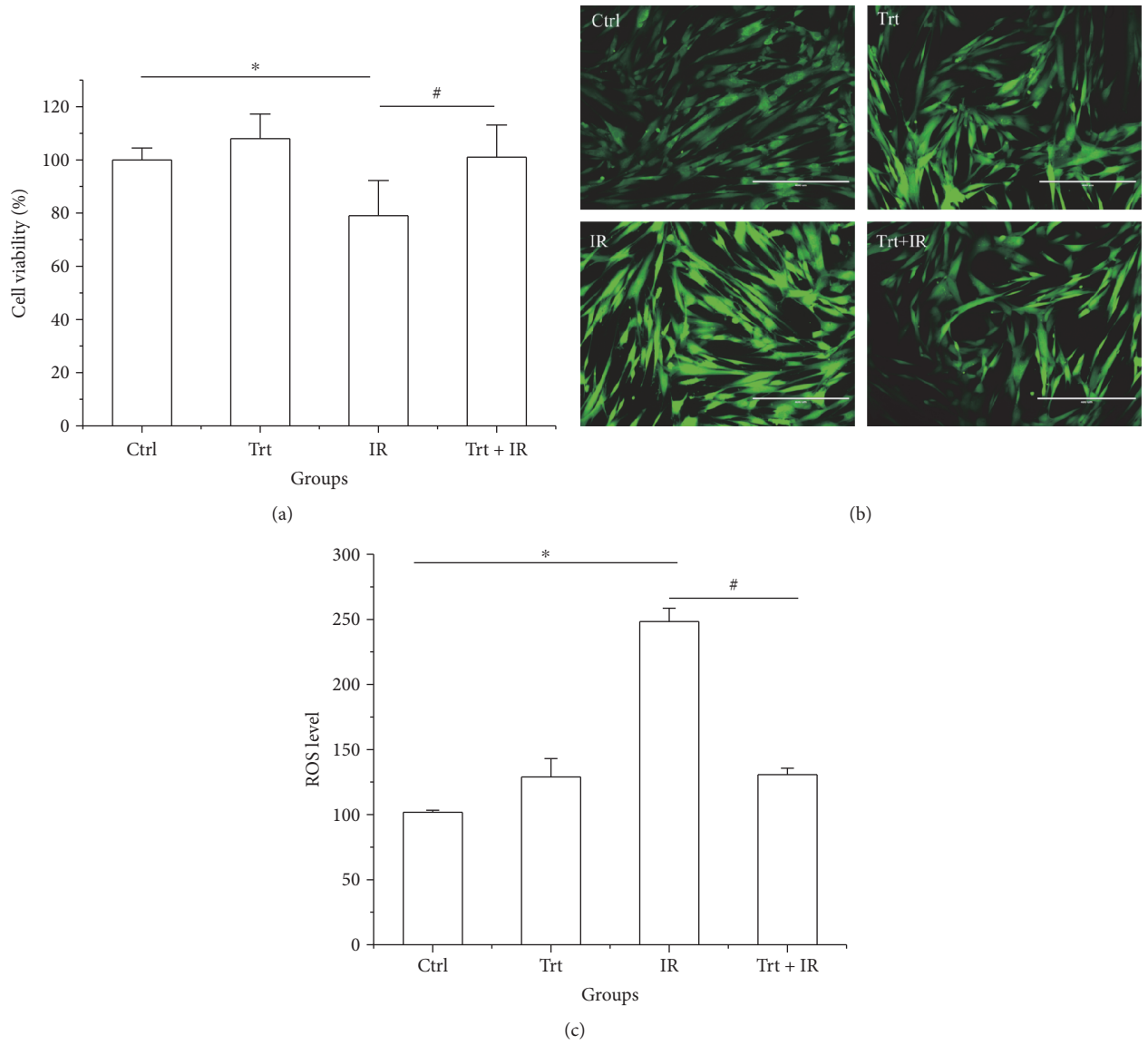

Figure 2: Ginger oleoresin increased the cell viability and reduced the γ-ray irradiation-induced ROS level in hMSCs. Cell viability was measured using the MTT assay (a). The level of ROS was measured using DCF fluorescence with a fluorescence microscope (b) and flow cytometry (c). Cells were untreated (Ctrl) or treated with ginger oleoresin (10^{-4} g/mL) (Trt) and γ-ray irradiation (4 Gy) (IR) or pretreated with ginger oleoresin (10^{-4} g/mL) and then γ-ray irradiation (4 Gy) (Trt + IR). Results are expressed as mean ± SD ($n = 4$). $^{*}p < 0.05$ IR versus untreated control (Ctrl). $^{\#}p < 0.05$ Trt + IR versus IR.

was lost when Nrf2 was knocked down (Figure 5). In addition, as shown in Figures 6(a), 6(b), and 6(c), when pretreated with ginger oleoresin and then irradiation, the mRNA levels of HO-1 and NQO-1 genes were significantly increased compared to those treated with irradiation alone. Interestingly, knocking down the Nrf2 pathway significantly abrogated the transcription of HO-1 and NQO-1 genes. Further, reduction of NQO-1 expression was also observed when the Nrf2 gene was knocked down (Figure 6(d)). These results confirmed that Nrf2 functions as a central regulator for HO-1 and NQO-1 activation. All these data illuminated that ginger oleoresin may play a radiation protective effect on hMSCs through Nrf2 and its induced antioxidant pathway.

3.5. Ginger Oleoresin Mediated the Nuclear Translocation of Nrf2. Many reports have suggested that Nrf2 is stabilized, increased, and translocated into the nucleus under oxidation conditions [29]. Because of the central role of the Nrf2 pathway to regulate the expression of HO-1 and NQO-1, we hypothesized that ginger oleoresin might promote the nuclear translocation of Nrf2 in hMSCs. To test this, we analyzed the distribution of Nrf2 in the cytoplasm and the nucleus of hMSCs using immunofluorescence assay. As shown in Figure 7(a), when cells were treated with or without ginger oleoresin alone or combined with irradiation, the red fluorescence of TRIC-Nrf2 cannot form a clear nucleus structure. When merged with blue fluorescence of a DAPI-stained

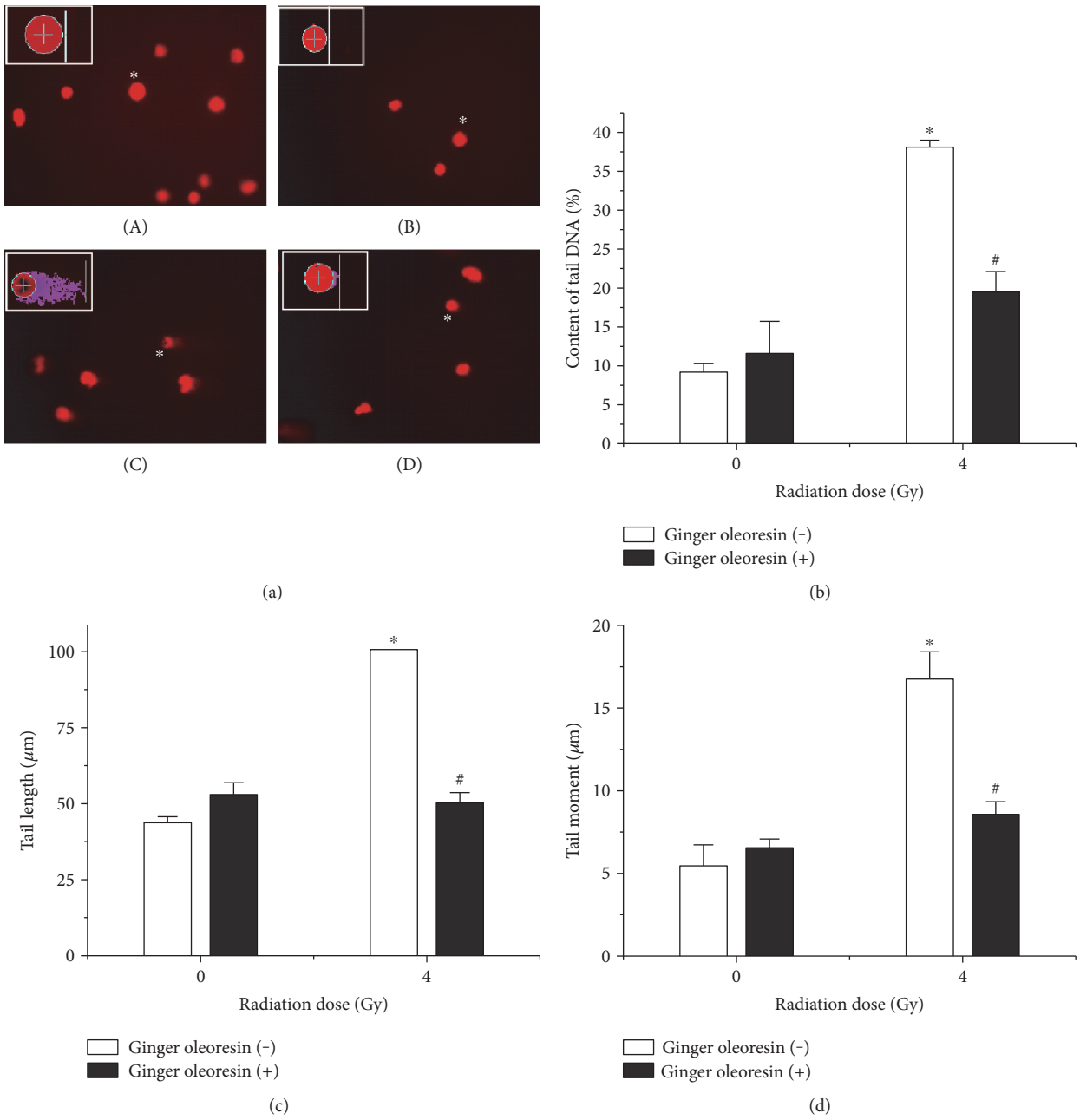

Figure 3: Ginger oleoresin reduced the IR-induced DNA strand breaks in hMSCs. The levels of DNA strand breaks were assayed by comet assay. (a) Representative micrographs—(A): untreated group; (B): treated with ginger oleoresin only; (C): treated with IR only; and (D): pretreated with ginger oleoresin and then with IR. (b) Tail DNA%. (c) Tail length. (d) Tail moment. Results are expressed as mean ± SD ($n = 4$). $^{*}p < 0.05$ IR versus untreated control (Ctrl). $^{\#}p < 0.05$ ginger oleoresin + IR versus IR.

nucleus, the red fluorescence was not observed in the cell nucleus. When cells were pretreated with ginger oleoresin and irradiated with γ-ray radiation, the TRIC-Nrf2 red fluorescence formed a clear nucleus structure located on the blue fluorescence of the DAPI-stained nucleus (Figure 7(a)). To further demonstrate the nuclear translocation of Nrf2, we extracted the cytoplasm proteins and the nucleus protein of cells which were treated with γ-ray irradiation alone or pretreated with ginger oleoresin then γ-ray irradiation, respectively. Subsequently, the Nrf2 of the cytoplasm and nucleus was detected using immunoblotting. Consistent with the immunofluorescence results, when pretreated with ginger oleoresin, the Nrf2 levels in the cell nucleus increased (Figure 7(b)). These results suggested that ginger oleoresin induced the nucleus translocation of Nrf2.

4. Discussion

In the current study, we show that ginger oleoresin treatment prevents IR-induced cell injury and reduces IR-induced ROS generation in hMSCs (Figure 2). Radiation exposure from medical diagnosis, cancer therapy, nuclear exposure, and

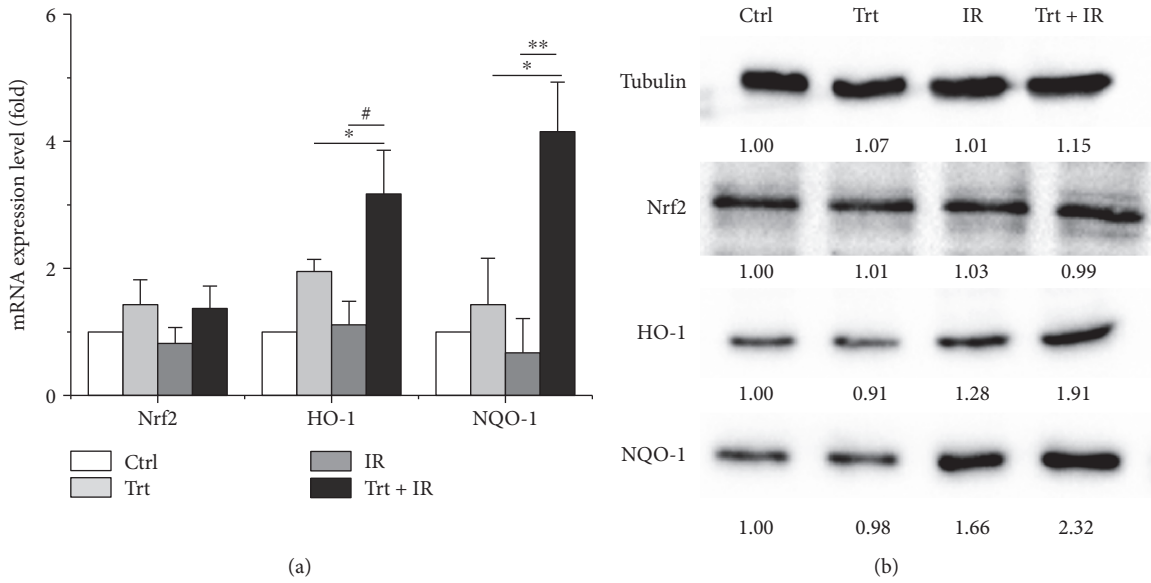

Figure 4: Expression properties of Nrf2 and its downstream genes encoding for HO-1 and NQO-1 in hMSCs when untreated (Ctrl) or treated with ginger oleoresin alone (Trt) and ionizing radiation alone (IR) or pretreated with ginger oleoresin and then ionizing radiation (Trt + IR). (a) mRNA levels. Results are expressed as mean ± SD ($n = 3$). $^{*}p < 0.05$ Trt + IR versus Trt. $^{\#}p < 0.05$ Trt + IR versus IR. $^{**}p < 0.01$ Trt + IR versus IR. (b) Protein levels.

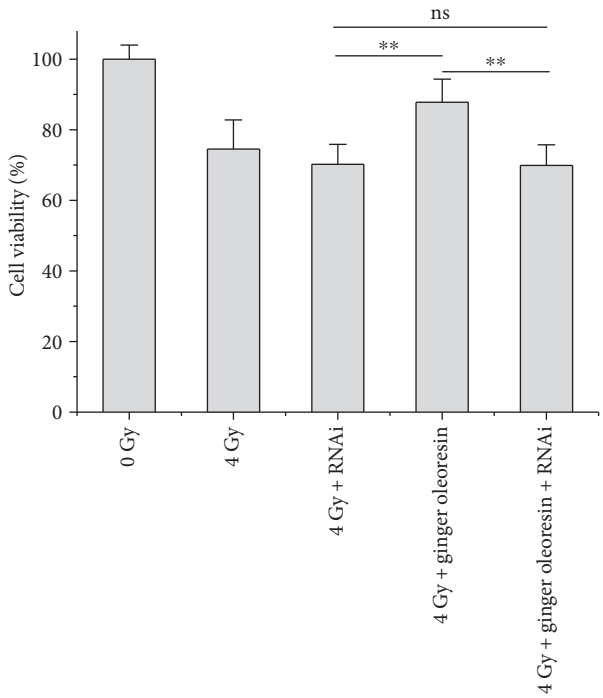

Figure 5: Knocking down Nrf2 reversed the radiation protective effect of ginger oleoresin on hMSCs. Results are expressed as mean ± SD ($n = 5$). $^{**}p < 0.01$.

spaces flight is a kind of physical stress that increases the oxidative pressure and leads to the disturbance of cellular redox homeostasis through increasing the production of reactive oxygen species [39]. High levels of ROS can result in further oxidative damage of DNA, lipids, and protein and induce the activation of apoptotic pathway [40], so maintenance of cellular redox homeostasis is important to maintain cell viability and normal physiological responses [14]. There were studies showing that the natural source of ginger oleoresin could protect against oxidative pressure and damages. [6]-Gingerol, a major constituent of ginger oleoresin, has been found to possess many diverse pharmacologic effects including antioxidant, anti-inflammatory, and anticancer activities [23, 40, 41]. Besides, [6]-shogaol, another component of ginger oleoresin, was suggested to exhibit the most potent of antioxidant and anti-inflammatory properties in RAW 264.7 cells, although its content was much lower than gingerols [23, 42]. On the basis of the above research, it thus seems receivable that the hMSCs cell protection effects against IR by ginger oleoresin are due to the suppression of ROS production induced by IR.

Additionally, it is well known that DNA is one of the major targets of ROS. In our current study, ginger oleoresin was proved to be able to protect hMSCs against IR-induced DNA double-strand breaks. The result from comet assay demonstrates that treatment of hMSCs by ginger oleoresin can greatly reduce radiation-induced DNA damages (Figure 3). However, the molecular mechanism of ginger oleoresin on ROS scavenging in hMSCs remains unknown. Many investigators have shown that redox-sensitive prosurvival transcription factor Nrf2 plays a primary role in scavenging the ROS [38, 43]. Consequently, the Nrf2 signaling pathway is firstly taken into account for the ROS-scavenging ability of ginger oleoresin. In the present study, the cytoprotective genes encoding for HO-1 and NQO-1 were induced on both mRNA and protein levels when pretreated with ginger oleoresin and then ionizing radiation; however, the expression of the key regulatory factor Nrf2 was observed to be not obviously changed (Figure 4). To

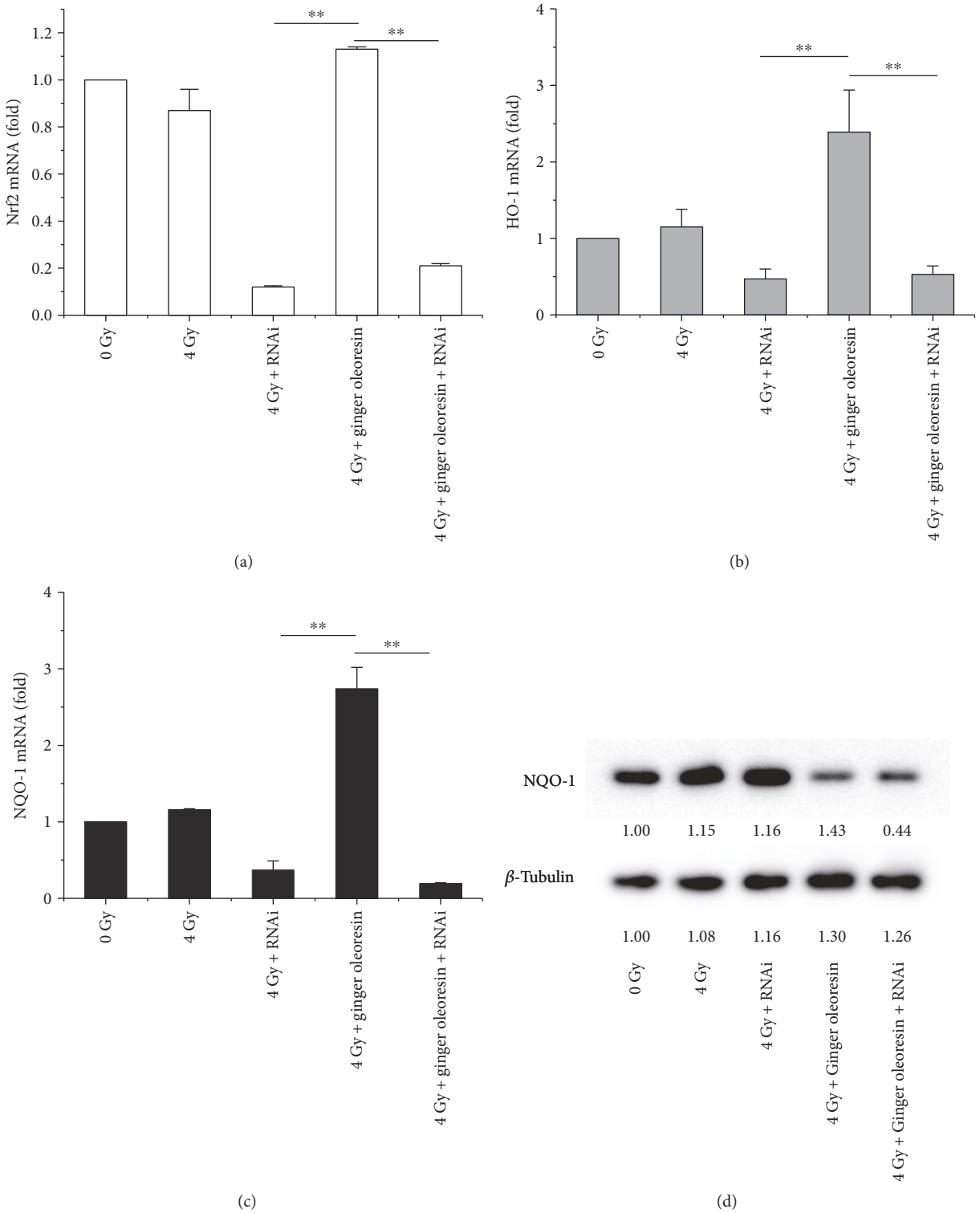

Figure 6: Knocking down Nrf2 reversed the activation of HO-1 and NQO-1 offered by ginger oleoresin in hMSCs when cotreated with ionizing radiation. (a) mRNA levels of Nrf2. (b) mRNA levels of HO-1. (c) mRNA levels of NQO-1. (d) Protein levels of NQO-1. Results are expressed as mean ± SD ($n = 3$). $^{**}p < 0.01$.

further investigate the role of Nrf2 on the radiation protective effect on hMSCs and the induction of HO-1 and NQO-1, siRNA knocking down of Nrf2 was introduced. Our data highlighted that the radiation protective effect was lost (Figure 5), and the expression of HO-1 and NQO-1 was significantly decreased when Nrf2 was knocking down (Figure 6), confirming the critical role of Nrf2 on radiation protective effect on hMSCs and regulating the downstream

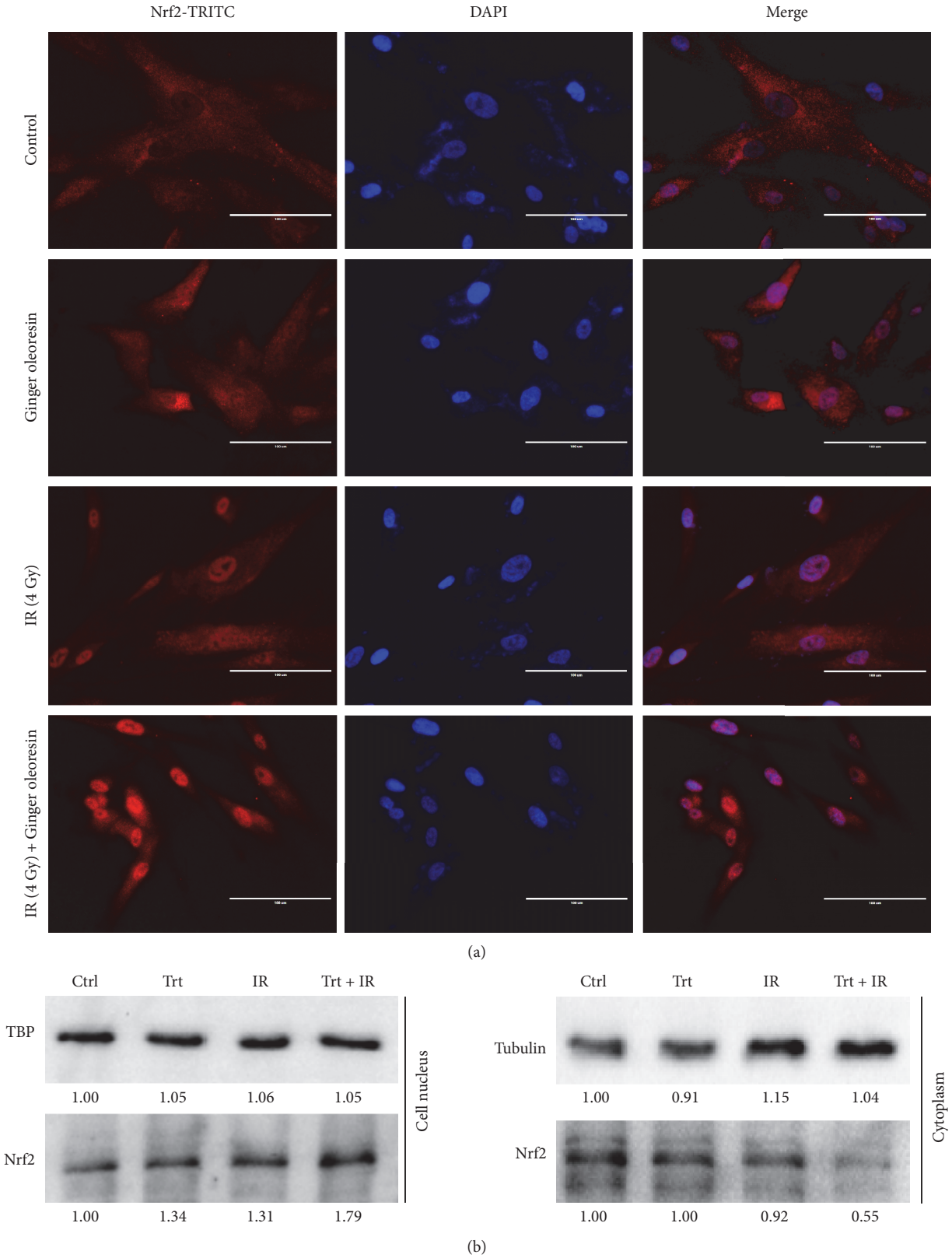

Figure 7: Ginger oleoresin induced nucleus translocation of Nrf2 in hMSCs when treated with ionizing radiation. (a) hMSCs when not treated or treated with ginger oleoresin alone or treated with ionizing radiation alone or pretreated with ginger oleoresin and then with ionizing radiation were stained with TRITC-labelled anti-Nrf2 antibody and DAPI. Nrf2-TRITC (left), DAPI (mid), merge (right) are shown. (b) Distribution of Nrf2 in the cytoplasm or nucleus in hMSCs. When pretreated with ginger oleoresin and then ionizing radiation, Nrf2 in the nucleus was increased.

gene expression. As the Nrf2 expression was not responsible for its regulatory function, we hypothesized that the activation of Nrf2 may be through its translocation into the cell nucleus. On the basis of this consideration, the distribution and positioning of Nrf2 were analyzed by immunofluorescence and immunoblotting. Our data clearly showed that the ginger oleoresin induced the translocation of Nrf2 into the cell nucleus to activate the Nrf2 signaling pathway (Figure 7). Interestingly, we also observed that the nuclear levels of Nrf2 in hMSCs were not increased when cells were treated with ginger oleoresin alone but significantly increased when cells were treated with ginger oleoresin and radiation. Nrf2 has been proved to be maintained at a low level through Keap1-mediated ubiquitylation and 26S proteasome-mediated degradation. However, Nrf2 is stabilized, and Nrf2 levels rise when cells are exposed to electrophiles or oxidants [29]. In our study, it is perhaps that Nrf2 was bounded by Keap1 and could not translocate into the cell nucleus by ginger oleoresin when treated with ginger oleoresin alone. Nevertheless, Nrf2 was released and stabilized when exposed to irradiation. Then, the stabilized Nrf2 can be translocated into the cell nucleus by ginger oleoresin. These results suggested that the ginger oleoresin could alleviate γ-ray irradiation-induced reactive oxygen species (ROS) via the Nrf2 protective response in human mesenchymal stem cells (hMSCs).

In line with our experimental finding, [6]-gingerol has been reported to protect against UVB-induced ROS production and COX-2 expression in vitro and vivo [27]. Meanwhile, ginger essential oil and [6]-shogaol have recently been certified to protect against γ-ray irradiation-induced oxidative stress, clastogenic damage, and intestinal mucosa injury in mice [44, 45]. Compared to the above studies, our data extend previous findings and further confirm the protective effect of ginger oleoresin on hMSCs under IR conditions. Given the important role of hMSCs in the repair of radiation-induced tissue damage, our current study has a more important significance for radiation protection. Besides, we further investigated the molecular mechanism of ginger oleoresin to reduce IR-induced ROS generation, which is found to be regulated through the translocation of Nrf2.

In summary, ginger oleoresin pretreatment prevents IR-induced cell injury in hMSCs via reducing IR-induced ROS production, which are related to the nuclear translocation of Nrf2 and its regulation of downstream gene expression of HO-1 and NQO-1. Our study paves the way for prospective drug development of ginger oleoresin as natural resources against IR-induced injury. However, it should be noted that the scavenging ability of ginger oleoresin should be further elucidated *in vivo*.

Conflicts of Interest

The authors have no competing interests to disclose.

Authors' Contributions

Kaihua Ji and Lianying Fang contributed equally to this work.

Acknowledgments

This study was supported by the National Natural Science Foundation of China (31670859), Natural Science Foundation of Tianjin (15KPXM01SF056), Fundamental Research Funds for CAMS & PUMC (2016ZX310068, 2016ZX310198, 2016RC310019, and 2016RC310017), PUMC Youth Fund and the Fundamental Research Funds for the Central Universities (3332016100), and Research Funds for the Innovation Team of IRM-CAMS (1650).

References

[1] J. A. Reisz, N. Bansal, J. Qian, W. Zhao, and C. M. Furdui, "Effects of ionizing radiation on biological molecules-mechanisms of damage and emerging methods of detection," *Antioxidants & Redox Signaling*, vol. 21, no. 2, pp. 260–292, 2014.

[2] A. C. Munteanu, V. Uivarosi, and A. Andries, "Recent progress in understanding the molecular mechanisms of radioresistance in *Deinococcus* bacteria," *Extremophiles*, vol. 19, no. 4, pp. 707–719, 2015.

[3] C. Ostrau, J. Hülsenbeck, M. Herzog et al., "Lovastatin attenuates ionizing radiation-induced normal tissue damage in vivo," *Radiotherapy and Oncology*, vol. 92, pp. 492–499, 2009.

[4] R. Hass, C. Kasper, S. Böhm, and R. Jacobs, "Different populations and sources of human mesenchymal stem cells (MSC): a comparison of adult and neonatal tissue-derived MSC," *Cell Communication and Signaling*, vol. 9, no. 12, pp. 1–12, 2011.

[5] L. Moroni and P. M. Fornasari, "Human mesenchymal stem cells: a bank perspective on the isolation, characterization and potential of alternative sources for the regeneration of musculoskeletal tissues," *Journal of Cellular Physiology*, vol. 228, no. 4, pp. 680–687, 2013.

[6] O. Parolini, F. Alviano, G. P. Bagnara et al., "Concise review: isolation and characterization of cells from human term placenta: outcome of the first international workshop on placenta derived stem cells," *Stem Cells*, vol. 26, no. 2, pp. 300–311, 2008.

[7] A. Can and S. Karahuseyinoglu, "Concise review: human umbilical cord stroma with regard to the source of fetus-derived stem cells," *Stem Cells*, vol. 25, no. 11, pp. 2886–2895, 2007.

[8] D. M. Patel, J. Shah, and A. S. Srivastava, "Therapeutic potential of mesenchymal stem cells in regenerative medicine," *Stem Cells International*, vol. 2013, Article ID 496218, 15 pages, 2013.

[9] N. H. Nicolay, Y. Liang, R. Lopez Perez et al., "Mesenchymal stem cells are resistant to carbon ion radiotherapy," *Oncotarget*, vol. 6, no. 4, pp. 2076–2087, 2014.

[10] S. Singh, F. R. Kloss, R. Brunauer et al., "Mesenchymal stem cells show radioresistance in vivo," *Journal of Cellular and Molecular Medicine*, vol. 16, no. 4, pp. 877–887, 2012.

[11] J. Kobayashi, H. Fujimoto, J. Sato et al., "Nucleolin participates in DNA double-strand break-induced damage response through MDC1-dependent pathway," *PLoS One*, vol. 7, no. 11, article e49245, 2012.

[12] D. Slade and M. Radman, "Oxidative stress resistance in *Deinococcus radiodurans*," *Microbiology and Molecular Biology Reviews*, vol. 75, no. 1, pp. 133–191, 2011.

[13] N. Hamada and Y. Fujimichi, "Classification of radiation effects for dose limitation purposes: history, current situation and future prospects," *Journal of Radiation Research*, vol. 55, no. 4, pp. 629–640, 2014.

[14] L. Gambhir, "1,4-Naphthoquinone, a pro-oxidant, ameliorated radiation induced gastro-intestinal injury through perturbation of cellular redox and activation of Nrf2 pathway," *Drug Discoveries & Therapeutics*, vol. 10, no. 2, pp. 93–102, 2016.

[15] Y. Huang, H. Zhao, K. Cao et al., "Radioprotective effect of grape seed proanthocyanidins in vitro and in vivo," *Oxidative Medicine and Cellular Longevity*, vol. 2016, Article ID 5706751, 7 pages, 2016.

[16] Z. M. Chen and Z. Lin, "Tea and human health: biomedical functions of tea active components and current issues," *Journal of Zhejiang University Science B*, vol. 16, no. 2, pp. 87–102, 2015.

[17] S. Z. Moghadamtousi, H. A. Kadir, P. Hassandarvish, H. Tajik, S. Abubakar, and K. Zandi, "A review on antibacterial, antiviral, and antifungal activity of curcumin," *BioMed Research International*, vol. 2014, Article ID 186864, 12 pages, 2014.

[18] B. B. Aggarwal, S. C. Gupta, and B. Sung, "Curcumin: an orally bioavailable blocker of TNF and other pro-inflammatory biomarkers," *British Journal of Pharmacology*, vol. 169, no. 8, pp. 1672–1692, 2013.

[19] A. H. Rahmani, M. A. Al Zohairy, S. M. Aly, and M. A. Khan, "Curcumin: a potential candidate in prevention of cancer via modulation of molecular pathways," *BioMed Research International*, vol. 2014, Article ID 761608, 15 pages, 2014.

[20] R. Wilken, M. S. Veena, M. B. Wang, and E. S. Srivatsan, "Curcumin: a review of anti-cancer properties and therapeutic activity in head and neck squamous cell carcinoma," *Molecular Cancer*, vol. 10, no. 1, p. 12, 2011.

[21] B. White, "Ginger: an overview," *American Family Physician*, vol. 75, pp. 1689–1691, 2007.

[22] M. S. Baliga, R. Haniadka, M. M. Pereira et al., "Update on the chemopreventive effects of ginger and its phytochemicals," *Critical Reviews in Food Science and Nutrition*, vol. 51, pp. 499–523, 2011.

[23] S. Dugasani, M. R. Pichika, V. D. Nadarajah, M. K. Balijepalli, S. Tandra, and J. N. Korlakunta, "Comparative antioxidant and anti-inflammatory effects of [6]-gingerol, [8]-gingerol, [10]-gingerol and [6]-shogaol," *Journal of Ethnopharmacology*, vol. 127, pp. 515–520, 2010.

[24] Y. J. Surh, J. K. Kundu, and H. K. Na, "Nrf2 as a master redox switch in turning on the cellular signaling involved in the induction of cytoprotective genes by some chemopreventive phytochemicals," *Planta Medica*, vol. 74, no. 13, pp. 1526–1539, 2008.

[25] A. Giudice, C. Arra, and M. C. Turco, "Review of molecular mechanisms involved in the activation of the Nrf2-ARE signaling pathway by chemopreventive agents," *Methods in Molecular Biology*, vol. 647, pp. 37–74, 2010.

[26] K. S. Chun, J. Kundu, J. K. Kundu, and Y. J. Surh, "Targeting Nrf2-Keap1 signaling for chemoprevention of skin carcinogenesis with bioactive phytochemicals," *Toxicology Letters*, vol. 229, no. 1, pp. 73–84, 2014.

[27] D.-M. Chung, S. M. Nasir Uddin, J.-H. Kim, and J. K. Kim, "[6]-Gingerol prevents gamma radiation-induced cell damage in $HepG_2$ cells," *Journal of Radioanalytical and Nuclear Chemistry*, vol. 305, pp. 323–328, 2015.

[28] J. K. Kim, Y. Kim, K. M. Na, Y. J. Surh, and T. Y. Kim, "[6]-Gingerol prevents UVB-induced ROS production and COX-2 expression in vitro and in vivo," *Free Radical Research*, vol. 41, no. 5, pp. 603–614, 2007.

[29] M. C. Jaramillo and D. D. Zhang, "The emerging role of the Nrf2-Keap1 signaling pathway in cancer," *Genes & Development*, vol. 27, pp. 2179–2191, 2013.

[30] Y. Q. Tao, Y. Shi, S. M. Zhang et al., "A new process of extracting oleoresin ginger from ginger by critical-state liquid CO_2," *Advanced Materials Research*, vol. 699, pp. 212–216, 2013.

[31] T. F. Slater, B. Sawyer, and U. Straeuli, "Studies on succinate tetrazolium reductase systems III points of coupling of four different tetrazolium salts," *Biochimica et Biophysica Acta*, vol. 77, pp. 383–393, 1963.

[32] K. Hafer, K. S. Iwamoto, and R. H. Schiestl, "Refinement of the dichlorofluorescein assay for flow cytometric measurement of reactive oxygen species in irradiated and bystander cell populations," *Radiation Research*, vol. 169, pp. 460–468, 2008.

[33] J. Li, Y. Wang, D. U. Liqing et al., "Nested PCR for mtDNA 4977bp deletion and comet assay for DNA damage- a combined method for radiosensitivity evaluation of tumor cells," *Oncology Letters*, vol. 7, pp. 1083–1087, 2014.

[34] R. S. Patwardhan, R. Checker, D. Sharma, V. Kohli, K. I. Priyadarsini, and S. K. Sandur, "Dimethoxycurcumin, a metabolically stable analogue of curcumin, exhibits anti-inflammatory activities in murine and human lymphocytes," *Biochemical Pharmacology*, vol. 82, pp. 642–657, 2011.

[35] S. E. Mohr, J. A. Smith, C. E. Shamu, R. A. Neumüller, and N. Perrimon, "RNAi screening comes of age: improved techniques and complementary approaches," *Nature Reviews Molecular Cell Biology*, vol. 15, pp. 591–600, 2014.

[36] V. Adler, Z. Yin, K. D. Tew, and Z. Ronai, "Role of redox potential and reactive oxygen species in stress signaling," *Oncegene*, vol. 18, pp. 6104–6111, 1999.

[37] W. Zhao and M. E. C. Robbins, "Inflammation and chronic oxidative stress in radiation-induced late normal tissue injury: therapeutic implications," *Current Medicinal Chemistry*, vol. 16, no. 2, pp. 130–143, 2009.

[38] S. Magesh, Y. Chen, and L. Q. Hu, "Small molecule modulators of Keap1-Nrf2-ARE pathway as potential preventive and therapeutic agents," *Medicine Research Reviews*, vol. 32, no. 4, pp. 687–726, 2012.

[39] P. Li, Q. L. Zhao, L. H. Wu et al., "Isofraxidin, a potent reactive oxygen species (ROS) scavenger, protects human leukemia cells from radiation-induced apoptosis via ROS/mitochondria pathway in p53-independent manner," *Apoptosis*, vol. 19, no. 6, pp. 1043–1053, 2014.

[40] N. Nigam, K. Bhui, S. Prasad, J. George, and Y. Shukla, "[6]-Gingerol induced reactive oxygen species regulated mitochondrial cell death pathway in human epidermoid carcinoma A431 cells," *Chemico-Biological Interactions*, vol. 181, pp. 77–84, 2009.

[41] E. C. Kim, J. K. Min, T. Y. Kim et al., "[6]-Gingerol, a pungent ingredient of ginger, inhibits angiogenesis in vitro and in vivo," *Biochemical and Biophysical Research Communications*, vol. 335, pp. 300–308, 2005.

[42] Y. Yonei, H. Ōhinata, R. Yoshida, Y. Shimizu, and C. Yokoyama, "Extraction of ginner flavor with liquid or supercritical carbon dioxide," *Journal of Supercritical Fluids*, vol. 8, pp. 156–161, 1995.

[43] S. B. Kim, R. K. Pandita, U. Eskiocak et al., "Targeting of Nrf2 induces DNA damage signaling and protects colonic epithelial cells from ionizing radiation," *Proceedings of the National Academy of Sciences of the United States of America*, vol. 109, pp. E2949–E2955, 2012.

[44] K. Jeena, V. B. Liju, V. Ramanath, and R. Kuttan, "Protection against whole body γ-irradiation induced oxidative stress and clastogenic damage in mice by ginger essential oil," *Asian Pacific Journal of Cancer Prevention*, vol. 17, no. 3, pp. 1325–1332, 2016.

[45] J. Wang, M. Yao, Y. Wang et al., "6-Shogaol ameliorates injury to the intestinal mucosa and increases survival after high-dose abdominal irradiation," *Journal of Functional Foods*, vol. 36, pp. 63–71, 2017.

Hindawi
Oxidative Medicine and Cellular Longevity
Volume 2017, Article ID 1891849, 10 pages
https://doi.org/10.1155/2017/1891849

Research Article

Carlina vulgaris L. as a Source of Phytochemicals with Antioxidant Activity

Maciej Strzemski,[1] Magdalena Wójciak-Kosior,[1] Ireneusz Sowa,[1] Daniel Załuski,[2] Wojciech Szwerc,[1] Jan Sawicki,[1] Ryszard Kocjan,[1] Marcin Feldo,[3] and Sławomir Dresler[4]

[1]*Department of Analytical Chemistry, Medical University of Lublin, Chodźki 4a, 20-093 Lublin, Poland*
[2]*Department of Pharmacognosy, Ludwik Rydygier Collegium Medicum, Nicolaus Copernicus University, Marie Curie-Skłodowska 9, 85-094 Bydgoszcz, Poland*
[3]*Department of Vascular Surgery, Medical University of Lublin, Staszica 11, 20-081 Lublin, Poland*
[4]*Department of Plant Physiology, Institute of Biology and Biochemistry, Maria Curie-Skłodowska University, Akademicka 19, 20-033 Lublin, Poland*

Correspondence should be addressed to Maciej Strzemski; maciej.strzemski@poczta.onet.pl
and Sławomir Dresler; slawomir.dresler@poczta.umcs.lublin.pl

Received 8 June 2017; Revised 17 August 2017; Accepted 6 September 2017; Published 18 October 2017

Academic Editor: Jie Li

The methanol extracts from three populations of *Carlina vulgaris* L. were examined for the chlorogenic acid content, mineral content, total phenolic content (TPC), total flavonoid content (TFC), and antioxidant activity. Two populations originated from natural nonmetallicolous habitats (NN (populations from Nasiłów) and NP (populations from Pińczów)), and one metallicolous population (MB) was collected from Bolesław waste heap localized at the place of former open-cast mining of Ag-Pb and Zn-Pb ores dating back to the 13th century and 18th century, respectively. The level of Zn, Pb, Cd, Fe, Ni, and Mn was significantly higher in the root and leaves of MB plants as a result of soil contaminations compared to those of the NN and NP ones. The highest antioxidant potency has been showed by the plants growing in a nonmetallicolous habitat. The flower head extracts obtained from the nonmetallicolous populations also contained the largest amount of chlorogenic acid, whereas the lowest was determined in the roots (ca. 2–3.5 mg/g and 0.2–0.4 mg/g of air-dry weight, resp.). These studies provide important information on the influence of a habitat on the quality of herbal materials and the content of the biologically active primary and secondary metabolites.

1. Introduction

Free radicals that are constantly generated in the human body cause oxidative stress. The ratio of free radicals may be increased by the factors such as drugs, chlorinated compounds, deficiency of natural antioxidants, tobacco, and pollution. Despite naturally occurring antioxidant systems in the human body, free radicals cause lipid, protein, and DNA oxidation. These damages at the molecular level may influence the etiology of diseases, such as cancer, atherosclerosis, diabetes, neurodegenerative disorders, and aging-related diseases. Some evidence indicates that the diet rich in antioxidants may be protective against abovementioned diseases [1–3].

One of the special sources of antioxidants is plant-based natural phenolic compounds. Phenolic compounds, known as nonnutritional ingredients in food, constitute one of the most widely occurring groups of phytochemicals with a wide range of physiological properties. They are components of many herbs, fruits, and vegetables, which are associated with the health benefits after their consumption. A clinical trial and epidemiological studies have established that a dietary intake of fruits is strongly associated with a reduced risk of the civilization diseases.

In the human body, they play as antiallergenic, antiatherogenic, anti-inflammatory, antimicrobial, antioxidant, and antithrombotic agents. However, their health benefits also depend on their absorption and metabolism, which in turn are determined by their structure, molecular size and solubility in cell wall structure, location of glycosides in cells, and binding of phenolic compounds within the food matrix [4].

Plants belonging to the *Carlina* L. genus (Asteraceae) which comprises over 30 species found in Europe and Asia are rich in antioxidants. Since hundreds of years, some of them have been used in traditional medicine in many countries, for example, in Italy, in Spain, in Hungary, in the Balcan countries, and in Poland. They are used for medicinal and nutritional purposes. They act as diuretic, diaphoretic, stomachic, or antibiotic agents. Extracts are used externally in the treatment of skin diseases. Regarding the chemical composition of *Carlina* spp., reports are scarce and include mainly pentacyclic triterpenes and essential oil. The Strzemski et al.'s previous studies revealed that the *Carlina* spp. contain a high amount of triterpenes (lupeol, lupeol acetate, α-amyrin, β-amyrin, β-amyrin acetate, oleanolic acid, and ursolic acid) [5–9]. There is no information about phenolic acids and minerals and the antioxidant activity of different *Carlina* spp. growing wildly in Poland. As part of a program to search for bioactive constituents from *Carlina* species, this study was focused on the establishment of phenolic compounds (phenolic acids, TPC, and TFC), mineral content, and antioxidant properties of *Carlina vulgaris* L. Moreover, the differences between the populations from a natural habitat and from a postindustrial area contaminated with heavy metals were investigated.

2. Experimental

2.1. Plant Material. Fifty-two specimens of *Carlina vulgaris* L. (Asteraceae) were collected from three different sites in Poland. Two populations were from Nasiłów (NN, $n = 22$) and Pińczów (NP, $n = 11$), and one population (MB, $n = 19$) originated from a contaminated metalliferous area in Bolesław. The coordinates of sites and exemplary plant photos are presented in Figure 1. The plants were collected at the first half of August 2016. Taxa were identified on the basis of the monographs "*Lebensgeschichte der Gold - und Silberdisteln*" [10] and "*Polish Plants*" [11]. All plant samples were deposited at the Department of Plant Physiology, Institute of Biology and Biochemistry, Maria Curie-Skłodowska University, Poland.

2.2. Chemicals and Reagents. Chlorogenic acid standard (≥95%), 2,2′-azino-bis(3-ethylbenzothiazoline-6-sulphonic acid) (ABTS), 2,2-diphenyl-1-picrylhydrazyl (DPPH), Folin–Ciocalteau reagent, trolox, aluminum chloride, suprapure nitric acid (65%), and solution of metal standards (1000 ppm) were purchased from Sigma (St. Louis, MO, USA). Methanol, trifluoroacetic acid (TFA), and HPLC-grade acetonitrile were from Merck (Darmstadt, Germany). Water was deionized and purified by Ultrapure Millipore Direct-Q® 3UV-R (Merck, Darmstadt, Germany).

2.3. Analysis of Metal Content. Dried and pulverized roots, leaves, and flower heads (0.1000 g) were mineralized using 10 mL of mixture $HNO_3 : H_2O$ (2 : 8, *v*/*v*) in TOPwave apparatus (Analytik Jena AG, Jena, Germany). Mineralization parameters are given in Table S1 in Supplementary Material available online at https://doi.org/10.1155/2017/1891849. The analysis of metal content was conducted using a high-resolution continuum source atomic absorption spectrometer (HR CS AAS) (contrAA® 700, Analytik Jena, Germany) in an electrothermal graphite furnace mode for Ag, Cd, Co, Cr, Cu, Fe, Mn, Mo, Ni, and Pb and using a C_2H_2/air flame technique for Zn. The validation parameters are summarized in Table S2.

2.4. Extract Preparation. Methanol extracts were prepared according to the previously published procedure [6]. Dried and pulverized roots, leaves, and flower heads (0.5000 g) were extracted four times with methanol (4×10 mL) using ultrasonic bath (4×15 min). The obtained extracts were combined, concentrated, and filled up with methanol to 10 mL.

2.5. Spectroscopic Measurement. The assay was carried out using a Bio-Rad Benchmark Plus microplate spectrometer (Bio-Rad, Hercules, CA, USA). Antioxidant capacities of methanol extracts were determined with the use of 2-azino-bis(3-ethylbenzthiazoline-6-sulphonic acid) (ABTS) and 2,2-diphenyl-1-picrylhydrazyl (DPPH) and expressed as trolox equivalent per gram of air-dry weight (mg TE/g ADW). The total phenolic content (TPC) was established using the Folin–Ciocalteau reagent, and total flavonoid content (TFC) was analyzed based on the reaction with aluminum chloride. TPC and TFC were expressed as equivalent of gallic acid (mg GAE/g ADW) and rutin (mg RUE/g ADW), respectively. All experiments were performed in triplicate.

2.6. High-Performance Liquid Chromatography (HPLC). Chromatographic determination was performed on VWR Hitachi Chromaster 600 chromatograph set coupled with a diode array detector (DAD) (Merck, Darmstadt, Germany) and C18 column Kinetex (10 cm × 4.0 mm i.d., 2.6 μm particle size) (Phenomenex, Torrance, CA, USA). The condition of extract separation was based on literature [12]. A mixture of acetonitrile with 0.025% TFA (solvent A) and water with 0.025% TFA (solvent B) was used as a mobile phase. The gradient program was as follows: 0–8 min (A, 0%; B, 100%), 8–33 min (A, 0–11%; B, 100–89%), 33–38 min (A, 11%; B, 89%), and 38–60 min (A, 11–70%; B, 89–30%). The eluent flow rate was 1.0 mL/min. The column temperature was 25°C. The data were collected in a wavelength range from 200 to 400 nm. The analytes were identified by comparing the retention times and *m*/*z* values obtained with mass spectrometry (MS) analysis using a micrOTOF-Q II mass spectrometer (Bruker Daltonics, Bremen, Germany). The quantitative analysis was conducted at analytical wavelength characteristic for the investigated compounds using an external calibration method.

Figure 1: Coordinates of origin sites and exemplary photos of the investigated *Carlina vulgaris* L. plants.

2.7. Statistical Analysis. Analysis of variance (one-way ANOVA) was applied to the evaluation of difference between the populations. Differences were determined using Fisher's least significance difference test at the 0.05 probability level. Statistical analysis was carried out using Statistica ver. 12 (StatSoft Inc., 2014).

3. Results and Discussion

Since the environmental conditions may affect significantly the composition and antioxidant properties of a plant, in our work, the three populations from different sites were investigated. Two of them originated from

Table 1: Content of metal in leaves, flower heads, and roots of *C. vulgaris* growing in different sites (mg/kg of ADW).

Elements	Leaves			Flower heads			Roots		
	MB	NN	NP	MB	NN	NP	MB	NN	NP
Zn	1458.5 ± 277.7^{a}	46.6 ± 4.6^{b}	89.0 ± 11.5^{b}	100.6 ± 22.8^{a}	0.1 ± 0.1^{b}	3.3 ± 1.6^{b}	1576 ± 249^{a}	26.5 ± 6.1^{b}	20.5 ± 3.7^{b}
Cd	28.74 ± 2.89^{a}	0.13 ± 0.09^{b}	0.41 ± 0.08^{b}	6.59 ± 1.04^{a}	0.08 ± 0.01^{b}	1.13 ± 1.05^{b}	18.73 ± 2.25^{a}	0.11 ± 0.02^{b}	0.21 ± 0.05^{b}
Pb	78.45 ± 21.71^{a}	0.73 ± 0.07^{b}	6.13 ± 2.56^{b}	0.34 ± 0.21^{a}	0.07 ± 0.01^{a}	0.81 ± 0.51^{a}	179.3 ± 17.1^{a}	0.97 ± 0.38^{b}	1.73 ± 0.41^{b}
Cr	1.61 ± 0.44^{a}	0.48 ± 0.11^{b}	0.74 ± 0.15^{ab}	1.40 ± 1.20^{a}	0.02 ± 0.02^{a}	0.13 ± 0.02^{a}	1.78 ± 0.15^{a}	2.41 ± 0.43^{a}	1.16 ± 0.12^{a}
Ni	0.98 ± 0.34^{a}	0.03 ± 0.02^{b}	0.18 ± 0.06^{b}	0.83 ± 0.46^{b}	1.11 ± 0.17^{ab}	1.67 ± 0.25^{a}	1.00 ± 0.09^{a}	0.24 ± 0.09^{b}	0.09 ± 0.06^{b}
Mn	77.54 ± 9.19^{a}	10.63 ± 0.61^{b}	27.64 ± 3.87^{b}	23.30 ± 5.87^{a}	4.39 ± 0.42^{b}	14.69 ± 2.60^{a}	79.59 ± 6.98^{a}	19.22 ± 6.88^{b}	17.11 ± 3.99b
Mo	1.61 ± 0.37^{b}	4.73 ± 0.10^{a}	0.05 ± 0.05^{b}	0.99 ± 0.34^{b}	2.73 ± 0.91^{a}	0.23 ± 0.12^{b}	36.0 ± 20.4^{a}	28.9 ± 12.0^{a}	nd*
Co	0.27 ± 0.05^{b}	0.12 ± 0.01^{c}	0.43 ± 0.08^{a}	0.05 ± 0.02^{b}	0.03 ± 0.01^{b}	0.15 ± 0.04^{a}	0.31 ± 0.03^{a}	0.13 ± 0.02^{b}	0.24 ± 0.04^{a}
Cu	45.98 ± 10.22^{a}	35.49 ± 3.41^{a}	26.18 ± 2.68^{a}	43.89 ± 5.10^{a}	69.1 ± 21.36^{a}	46.82 ± 6.14^{a}	67.84 ± 8.79^{a}	50.43 ± 5.51^{a}	75.9 ± 25.3^{a}
Fe	2165.5 ± 516.6^{a}	702.3 ± 193.3^{b}	353.6 ± 54.0^{b}	162.2 ± 79.2^{a}	9.5 ± 3.2^{b}	8.2 ± 1.4^{b}	3945 ± 738^{a}	2057 ± 519^{b}	989 ± 228^{b}
Ag	0.22 ± 0.04^{a}	0.06 ± 0.03^{b}	0.09 ± 0.03^{b}	0.05 ± 0.02^{a}	0.07 ± 0.03^{a}	0.04 ± 0.01^{a}	0.51 ± 0.10^{a}	0.03 ± 0.00^{b}	0.04 ± 0.02^{b}

Means ± SE. According to Fisher's test ($p < 0.05$), the values followed by different letters within the same plant organ and metal are significantly different, the values followed by the same letter are not significantly different, and "ab" indicates that there is no difference between values followed by a and b letters. *Not detectable.

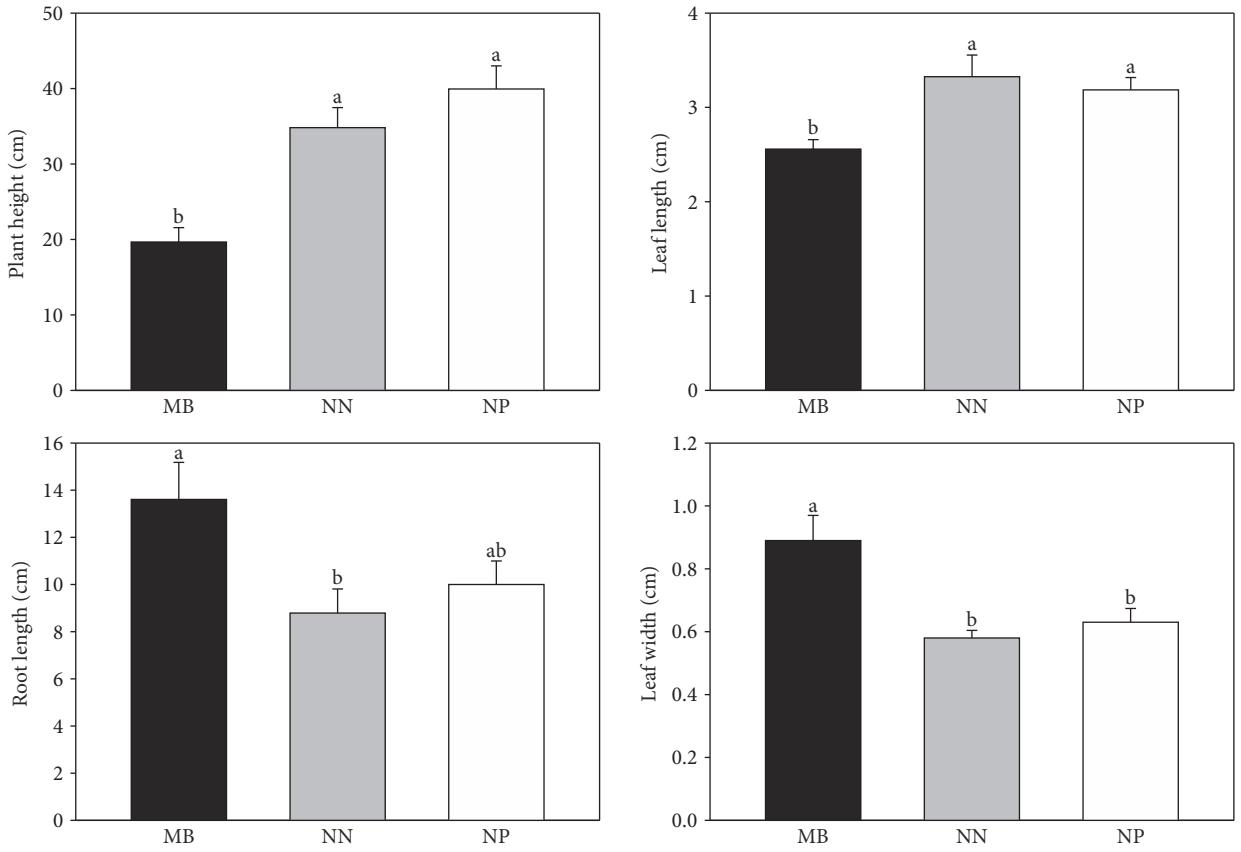

Figure 2: Morphometric parameters obtained for leaves and roots of the investigated *C. vulgaris* populations (NN—from Nasiłów, NP—from Pińczów, and MB—from a metalliferous area in Bolesław). Data are means ± SE. According to Fisher's test ($p < 0.05$), the values followed by different letters are significantly different, the values followed by the same letter are not significantly different, and "ab" indicates that there is no difference between values followed by a and b letters.

natural habitats (NN and NP—nonmetallicolous), and one (MB—metallicolous) was collected from Bolesław waste heap localized at the place of former open-cast mining of Ag-Pb and Zn-Pb ores dating back to the13th century and 18th century, respectively. The analysis of soil from Bolesław revealed the increased level of Zn, Cd, and Pb [13], and metal stress may induce [14] or inhibit [15] the production of plant antioxidants. The relationships of variables such as metal content, morphometric parameters, antioxidant activity, and total phenolic and flavonoid content were studied with the use of principal component analysis (PCA).

3.1. Metal Content. Microelements and toxic metals were determined in the investigated plant populations. The results are presented in Table 1.

For most metals, the differences of their content between the populations from natural habitats were only slight or statistically insignificant. The amount of Zn, Cr, Mo, Co, and Mn was in the range typically found in plants [16]. However, *C. vulgaris* showed the ability to accumulate Fe and Cu, especially in the root. The level of Fe reached even to 2000 mg/kg and Cu content was above 50 mg/kg, while the values in the other plants usually ranged from 75 to 400 and from 5 to 20 mg/kg, respectively. In turn, the high variation of heavy metal content between the metallicolous population from Bolesław (MB) and the nonmetallicolous populations (NN and NP) has been noticed. As expected, the level of Zn, Pb, Cd, Fe, Ni, and Mn was significantly higher in the root and leaves of MB plants as a result of soil contaminations compared to those of the NN and NP. Particularly, high differences were observed for the content of Pb, Zn, and Cd; the concentration was from several to even few hundredfold higher in the MB population. In MB flower heads, the amount of these metals was also increased; however, it was about 10-fold lower than that in MB leaves and roots. The restricted translocation of heavy metals to generative plant organs is common phenomena occurring in numerous species [16]. The differences in distribution of metals between the MB and NN/NP populations were also observed. In reference populations, the concentration of Cr in roots was 2-3-fold higher than that in leaves whereas accumulation of Zn was higher in leaves. In turn, in MB plants, there were no statistically significant differences between Cr and Zn content in the root and leaves. The translocation of metals in plants exposed to excess of Ni, Pb, and Cd was also reported by Pandey and Sharma [17]. The concentration of Fe was significantly increased in all parts of MB plants

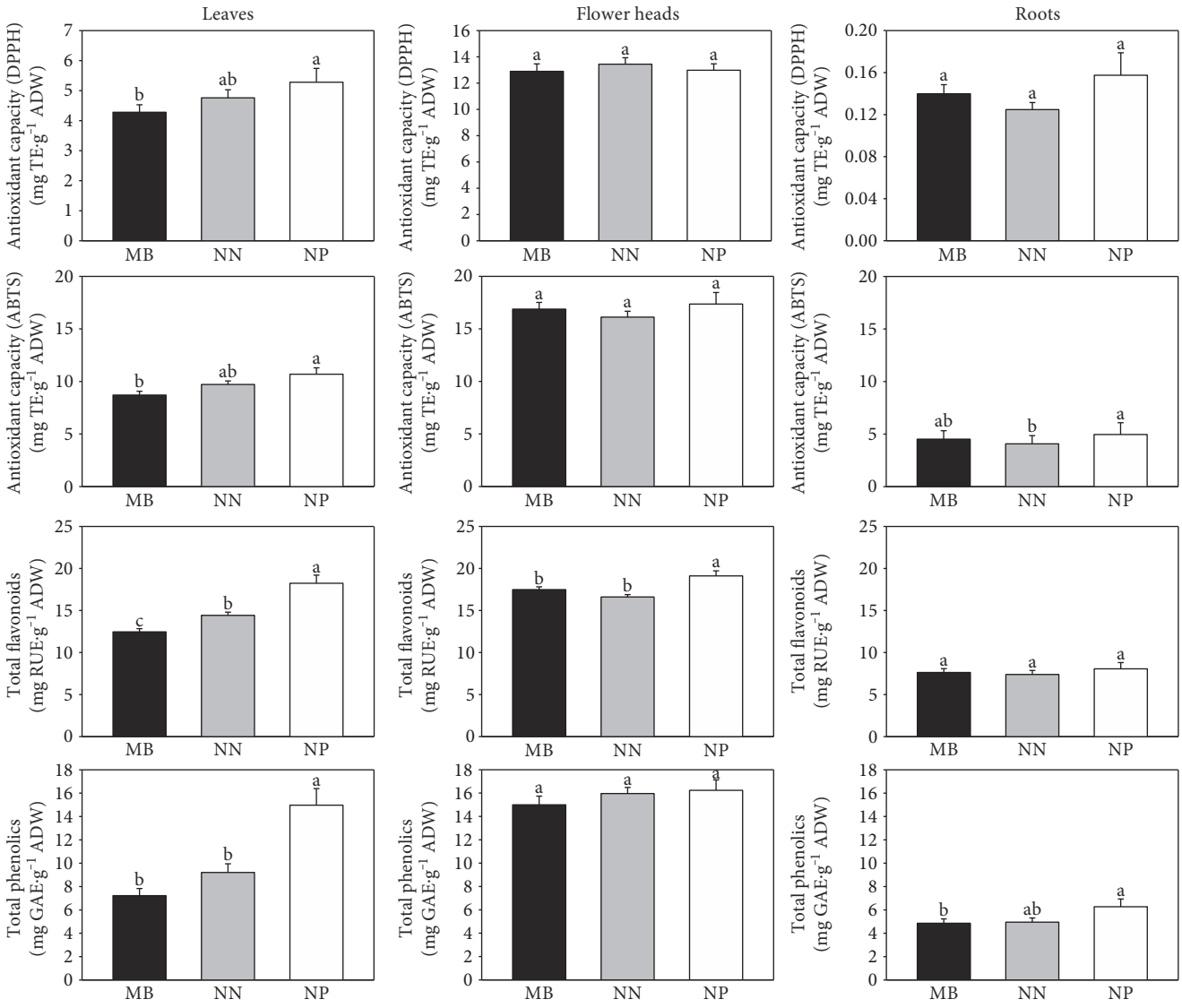

Figure 3: Comparison of antioxidant activity, TPC, and TFC obtained for the different parts of the *C. vulgaris* plant (NN—population from Nasiłów, NP—population from Pińczów, and MB—population from a metalliferous area in Bolesław). Data are means ± SE. According to Fisher's test ($p < 0.05$), the values followed by different letters are significantly different, the values followed by the same letter are not significantly different, and "ab" indicates that there is no difference between values followed by a and b letters.

compared to those of NP/NN; however, plants are able to accumulate a much higher amount of Fe without a toxic effect [18]. The differences between the amount of Cu and Cr in the metallicolous and NP/NN populations were not statistically significant. For Co and Mo, slight differences were observed; however, it was not linked with postindustrial contamination.

Metal ions have a diverse influence on plants. Cadmium and lead belong to the typical toxic components which cause a cellular damage and disturb cellular homeostasis [17, 19, 20]. Zn, Mn, Fe, Co, and Ni are essential for plant growth and development because they are involved in various physiological processes, such as enzyme activation, absorption, and translocation, and may play an important role in the adaptive responses of plant cells under environmental stresses [16, 21, 22]. They are also essential for human as valuable components of plant-derived products affecting their biological properties.

3.2. Morphometric Parameters. The excess of metals in a growth environment may cause the adverse process in a plant, such as chlorosis, necrotic leaf spots, and the other morphological alterations. The tolerance on a decreased level of metals is highly dependent on the plant species, cultivars, or genotypes within a species [23]. In our investigation, the leaf length and width, flower head diameter, number of flower heads and leaves per plant, and root length and plant height were compared between the MB, NN, and NP populations. The results are presented in Figure 2.

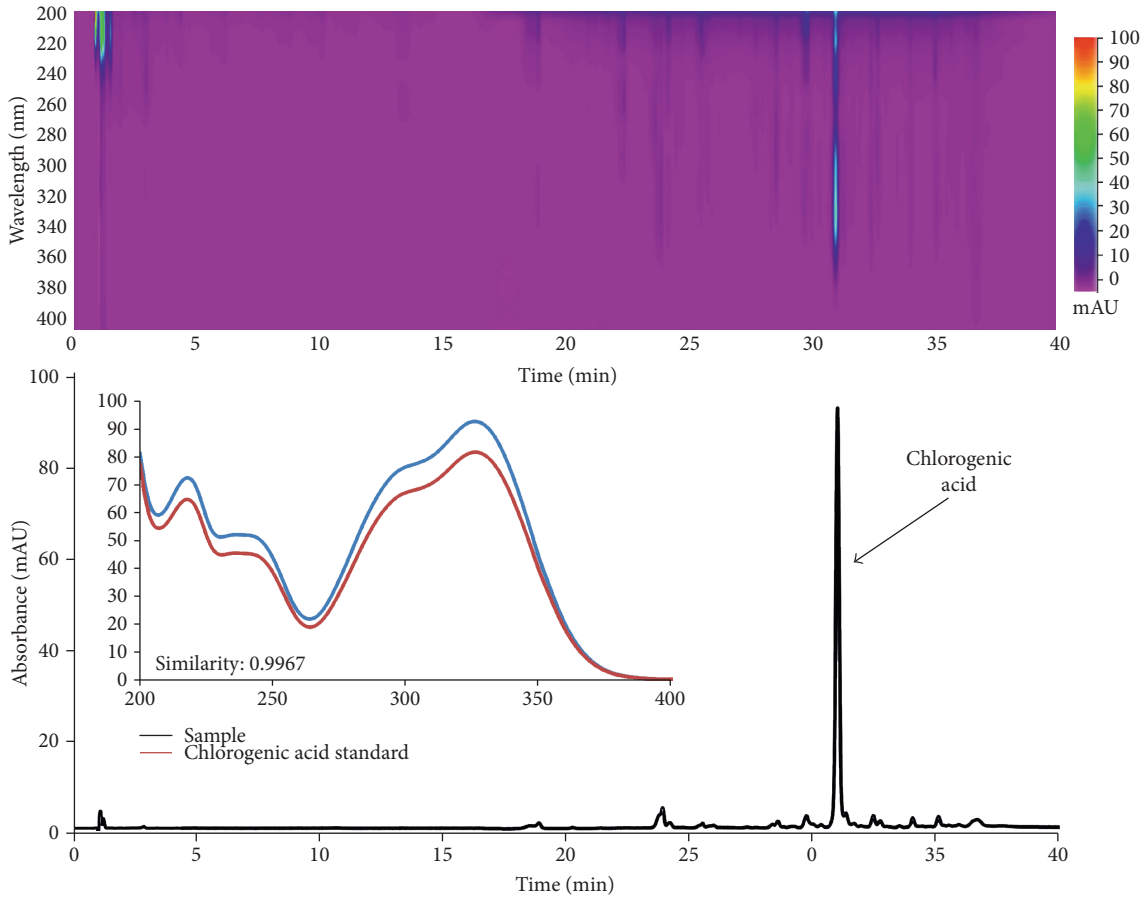

Figure 4: An exemplary 2D and 3D chromatogram of the extract from *C. vulgaris* leaves and UV spectrum of chlorogenic acid standard and compound identified in the extract.

The diameter and number of flower heads and leaves were similar for all tested populations (Figure S1); however, the other morphological parameters differed significantly. MB plants were about 2-fold lower, and they had shorter and wilder leaves and longer roots compared to reference populations. The differentiation in morphological features between the metallicolous and NN/NP populations is observed by numerous researchers. For example, in plants exposed to Pb chronic stress, roots are usually longer or/and thicker and Pb is cumulated in their outer part to prevent generative organs [24, 25]. The content of Cd, Pb, Zn, and Ni in the MB population significantly exceeded the values typically found in the other plants, and it affected the plant morphology.

3.3. Antioxidant Activity: Total Phenolic Content (TPC) and Total Flavonoid Content (TFC). Plant and plant-based products may be a rich source of polyphenols, which act as antioxidants, and therefore, they are helpful in preventing oxidative stress [1]. The antioxidant activity and the total phenolic and flavonoid content for *C. vulgaris* were established using a spectrophotometric technique. The comparison of results obtained for the different parts of the plant was presented in Figure 3.

As it can be seen, the aboveground part of *C. vulgaris* had significant antioxidant activity. The highest ability to scavenge free radical was noted for flower head extracts, and it was more than 2-fold higher compared to that for the leaf extract. In turn, root extracts exhibited the lowest activity, and it may be explained by generally lower production of antioxidants in the underground part of the plant. No or only slight differences between the investigated populations were observed, and it showed that chronic multimetallic stress had no influence on the antioxidant activity. These findings are in accordance with the results obtained by Dresler et al. [15, 25]. Generally, minor differentiation of TPC and TFC values between the investigated populations was observed for root and flower head extracts. As expected, the highest mean TPC and TFC were obtained for flower heads (15.4 and 18.3 mg/g, resp.) whereas for the root, both values were the lowest (5.8 and 8.2, resp.). The differences between the populations were clearly visible for leaf extracts. The highest TPC and TFC were determined for NP plants; in turn, for the MB population, the values were significantly lower. It suggested that chronic stress decreased the level of polyphenolics. Moreover, the high correlation between TPC/TFC, TPC and DPPH/ABTS, and TFC and DPPH/ABTS was obtained ($r > 0.79$, $r > 0.61$, and $r > 0.68$, resp.). The detailed correlation data are presented in Table S3.

3.4. HPLC Analysis. Phenolic acids and their derivatives are considered one of the main groups of plant secondary

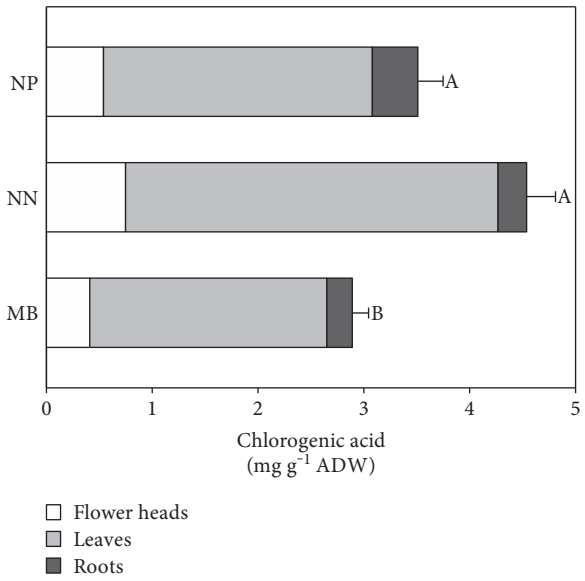

Figure 5: Content of chlorogenic acid in different populations of *C. vulgaris* (NN—population from Nasiłów, NP—population from Pińczów, and MB—population from a metalliferous area in Bolesław). Data are means ± SE. According to Fisher's test ($p < 0.05$), the values followed by different letters are significantly different and the values followed by the same letter are not significantly different.

metabolites with significant antioxidant activity [26]. HPLC of phenolic acids in *C. vulgaris* plant extracts was conducted using an experimentally elaborated gradient elution program which enabled the separation of common plant phenolics [12]. The analysis revealed that chlorogenic acid was a predominant compound found in all parts of the plant. In few samples, caffeic and protocatechuic acids also occurred; however, their contents were slight (below the limit of quantification). The example of the obtained chromatogram is presented in Figure 4.

Quantification of chlorogenic acid was performed based on the linear regression equation ($y = 124454737.80 \times -36813$, $r = 0.9997$). The calibration curve was constructed on the basis of the relationship between peak areas and standard concentrations at 5 concentration levels ($n = 5$).

The results are demonstrated in Figure 5.

Our research revealed that *C. vulgaris* plants are a rich source of chlorogenic acid. Its amount was higher than that in *C. acaulis* and *C. acalifolia* [26]. As it can be seen, the highest content of chlorogenic acid was in the flower heads whereas the lowest was determined in the roots (ca. 2-3.5 mg/g ADW and 0.2–0.4 mg/g ADW, resp.). Moreover, the populations from a natural habitat (NP and NN) contained significantly higher total content of chlorogenic acid compared to the metallicolous population (MB). The differences may be caused by the ability to chelate metal ions by polyphenols with at least two hydroxyl groups in the phenolic ring [27]. Therefore, chlorogenic acid may be bonded in complex, and thus, the amount of its free form is decreased. The antioxidant activity of *C. vulgaris* was statistically significantly correlated with the content of chlorogenic acid; however, the correlation between chlorogenic acid and TPC was

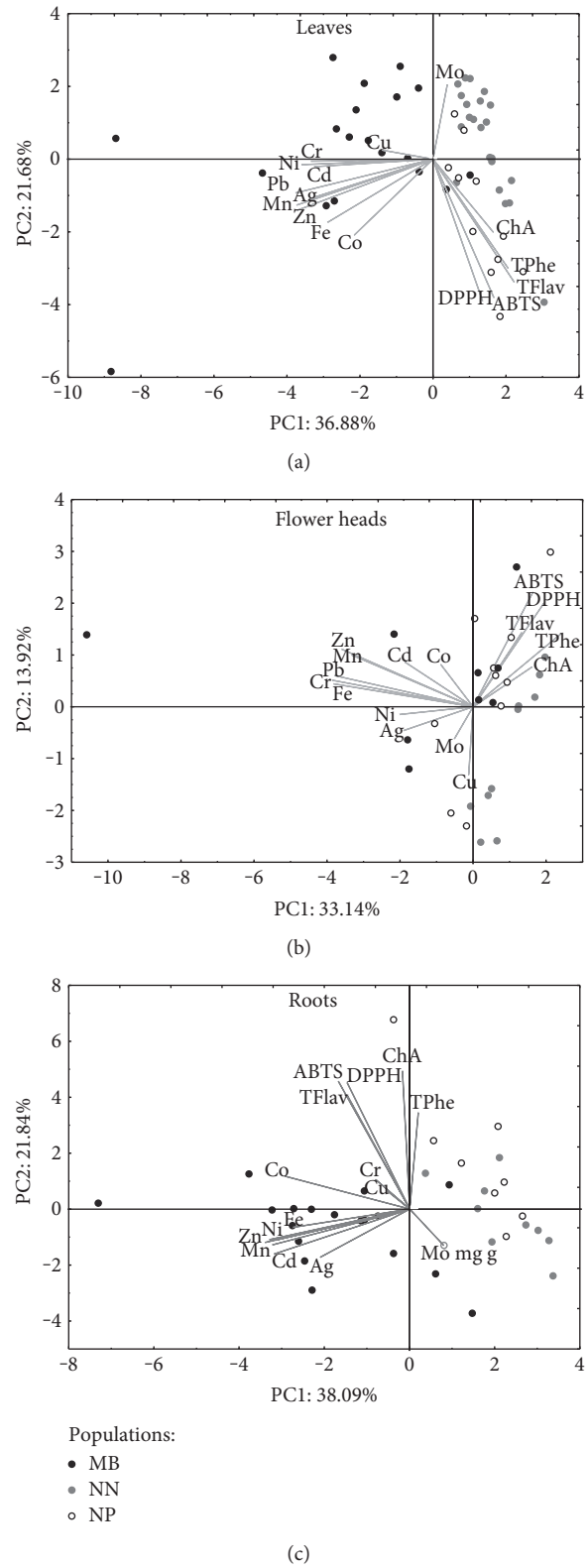

Figure 6: Scatter plot of the PCA of antioxidant capacity, chlorogenic acid concentration (ChA), metal content, and total flavonoid and phenolic content in the investigated populations of *C. vulgaris* (NN—population from Nasiłów, NP—population from Pińczów, and MB—population from a metalliferous area in Bolesław).

lower, and it suggests the presence of other phenolics in plants with lower antioxidant capacity.

3.5. Multivariate Comparison between the Investigated Populations. The multivariate comparison between the populations is presented in Figure 6.

The performed principal component analysis (PCA) of leaf and root data showed a clear separation between the metallicolous and nonmetallicolous populations (Figures 6(a) and 6(c)). It was noted that the variations among the studied plants were explained by the first two components and represented 60, 46, and 58% of the total variance for leaves, flower heads, and roots, respectively. The first components (in the analysis of all plant organs) were largely negatively determined by heavy metal concentration (except Mo in the leaves and the roots) and these separated plants collected from heavy metal-contaminated and heavy metal-noncontaminated areas (particular leaf and root data analysis) (Figures 5(a) and 5(c)), while PC2 was generally loadings on the secondary metabolites and antioxidant capacity data (positive in the flower heads and roots and negative in the leaf data) and generally showed (leaf data) (Figure 5(a)) difference between the MB and NP populations.

4. Conclusion

Our results demonstrate that *C. vulgaris* is rich in polyphenols and minerals. The species growing in noncontaminated areas contain more chlorogenic acid and possess higher antioxidant activity; thus, these species may become ingredients of herbal teas or natural products where a high amount of phytochemicals and minerals is needed. The results obtained in this study confirm an importance of the plants' growth conditions for the safety and quality of the herbal material.

Conflicts of Interest

The authors declare no competing financial interests.

References

[1] M. Ahmed, M. I. Khan, M. R. Khan, N. Muhammad, A. U. Khan, and R. A. Khan, "Role of medicinal plants in oxidative stress and cancer," *Scientific Reports*, vol. 2, pp. 641–643, 2013.

[2] M. S. Cooke, "Special issue on DNA oxidation: mechanisms, measurement and consequences," *Free Radicals Research*, vol. 46, no. 4, pp. 365-366, 2012.

[3] Ł. Cieśla, J. Kryszeń, A. Stochmal, W. Oleszek, and M. Waksmundzka-Hajnos, "Approach to develop a standardized TLC-DPPH test for assessing free radical scavenging properties of selected phenolic compounds," *Journal Pharmaceutical Biomedical Analysis*, vol. 70, pp. 126–135, 2012.

[4] D. H. Watson, *Performance Functional Foods-Woodhead Publishing in Food Science and Technology*, Woodhead Publishing, Cambridge, UK, 2003.

[5] M. Strzemski, M. Wójciak-Kosior, I. Sowa et al., "Chemical composition of plant Carlina species," *TEKA Archives of the Commission of Medical Sciences*, vol. 4, pp. 57–62, 2016.

[6] M. Strzemski, M. Wójciak-Kosior, I. Sowa et al., "*Carlina* species as a new source of bioactive pentacyclic triterpenes," *Industrial Crops and Products*, vol. 94, pp. 498–504, 2016.

[7] S. Dordevic, S. Petrovic, S. Dobric et al., "Antimicrobial, anti-inflammatory, anti-ulcer and antioxidant activities of *Carlina acanthifolia* root essential oil," *Journal of Ethnopharmacology*, vol. 109, no. 3, pp. 458–463, 2007.

[8] C. Guarino, L. De Simone, and S. Santoro, "Ethnobotanical study of the Sannio area, Campania, Southern Italy," *Ethnobotany Research Applications*, vol. 6, pp. 255–317, 2008.

[9] M. A. Bonet, M. Parada, A. Selga, and J. Valle's, "Studies on pharmaceutical ethnobotany in the regions of L'Alt empordà and Les Guilleries (Catalonia, Iberian Peninsula)," *Journal of Ethnopharmacology*, vol. 68, no. 1–3, pp. 145–168, 1999.

[10] H. Meusel and A. Kästner, *Lebensgeschichte der Gold - und Silberdisteln. Monographie der Mediterran – mitteleuropaischen Compositen-Gattung Carlina*, Springer-Verlag, Wien, Austria, New York, USA, 1994.

[11] W. Szafer, S. Kulczyński, and B. Pawłowski, *Polish Plants*, State Scientific Publishing, Warsaw, Poland, 1976.

[12] I. Sowa, R. Paduch, M. Strzemski et al., "Proliferative and antioxidant activity of *Symphytum officinale* root extract," *Natural Product Research*, pp. 1–5, 2017.

[13] M. Wójcik, P. Sugier, and G. Siebielec, "Metal accumulation strategies in plants spontaneously inhabiting Zn-Pb waste deposits," *Science of the Total Environment*, vol. 487, pp. 313–322, 2014.

[14] M. Wójciak-Kosior, I. Sowa, T. Blicharski et al., "The stimulatory effect of strontium ions on phytoestrogens content in *Glycine max* (L.) Merr," *Molecules*, vol. 21, pp. 1–90, 2016.

[15] S. Dresler, E. Rutkowska, W. Bednarek et al., "Selected secondary metabolites in *Echium vulgare* L. populations from nonmetalliferous and metalliferous areas," *Phytochemistry*, vol. 133, pp. 4–14, 2017.

[16] A. Kabata-Pendias and A. B. Mukherjee, *Trace Elements from Soil to Human*, Springer-Verlag, Berlin, Heidelberg, Germany, 2007.

[17] N. Pandey and C. P. Sharma, "Effect of heavy metals Co^{2+}, Ni^{2+}, and Cd^{2+} on growth and metabolism of cabbage," *Plant Science*, vol. 163, no. 4, pp. 753–758, 2002.

[18] G. R. Rout and S. Sahoo, "Role of iron in plant growth and metabolism," *Reviews in Agricultural Science*, vol. 3, pp. 1–24, 2015.

[19] P. Sharma and R. S. Dubey, "Lead toxicity in plants," *Brazilian Journal of Plant Physiology*, vol. 17, pp. 35–52, 2005.

[20] P. Mohanpuria, N. K. Rana, and S. K. Yadav, "Cadmium induced oxidative stress influence on glutathione metabolic genes of *Camellia sinensis* (L.) O. Kuntze," *Environmental Toxicology*, vol. 22, no. 4, pp. 368–374, 2007.

[21] H. F. Li, C. Gray, C. Mico, F. J. Zhao, and S. P. McGrath, "Phytotoxicity and bioavailability of cobalt to plants in a range of soils," *Chemosphere*, vol. 75, no. 7, pp. 979–986, 2009.

[22] S. K. Yadav, "Heavy metals toxicity in plants: an overview on the role of glutathione and phytochelatins in heavy metal stress tolerance of plants," *South African Journal of Botany*, vol. 76, no. 2, pp. 167–179, 2010.

[23] S. D. Ebbs and L. V. Kochian, "Toxicity of zinc and copper to Brassica species: implications for phytoremediation," *Journal of Environmental Quality*, vol. 26, pp. 776–781, 1997.

[24] M. Wierzbicka and M. Pielichowska, "Adaptation of *Biscutella laevigata* L, a metal hyperaccumulator, to growth on a zinc–lead waste heap in southern Poland: I: differences between waste-heap and mountain populations," *Chemosphere*, vol. 54, no. 11, pp. 1663–1674, 2004.

[25] S. Dresler, M. Wójciak-Kosior, I. Sowa, G. Stanisławski, I. Bany, and M. Wójcik, "Effect of short-term Zn/Pb or long-term multi-metal stress on physiological and morphological parameters of metallicolous and nonmetallicolous *Echium vulgare* L. populations," *Plant Physiology and Biochemistry*, vol. 115, pp. 380–389, 2017.

[26] S. Đordevic, V. Tadic, S. Petrovic et al., "Bioactivity assays on *Carlina acaulis* and *C. acanthifolia* root and herb extracts," *Digest Journal of Nanomaterials and Biostructures*, vol. 7, pp. 1213–1222, 2012.

[27] S. Quideau, D. Deffieux, C. Douat-Casassus, and L. Pouységu, "Plant polyphenols: chemical properties, biological activities, and synthesis," *Angewandle Chemie International Edition*, vol. 50, no. 3, pp. 586–621, 2011.

Hindawi
Oxidative Medicine and Cellular Longevity
Volume 2017, Article ID 1459497, 8 pages
https://doi.org/10.1155/2017/1459497

Review Article

The Beneficial Effects of Quercetin, Curcumin, and Resveratrol in Obesity

Yueshui Zhao,[1] Bo Chen,[2] Jing Shen,[1] Lin Wan,[3] Yinxin Zhu,[4] Tao Yi,[5] and Zhangang Xiao[1,6]

[1]*Laboratory of Molecular Pharmacology, Department of Pharmacology, School of Pharmacy, Southwest Medical University, Luzhou, Sichuan, China*
[2]*Experiment Center for Medical Science Research, Kunming Medical University, Kunming, Yunnan, China*
[3]*Department of Hematology and Oncology, The Children's Hospital of Soochow, Jiangsu, China*
[4]*Department of Gastroenterology, The Third Affiliated Hospital of Soochow University, Changzhou, Jiangsu, China*
[5]*School of Chinese Medicine, Hong Kong Baptist University, Kowloon, Hong Kong*
[6]*Key Laboratory of Medical Electrophysiology of Ministry of Education, School of Pharmacy, Southwest Medical University, Luzhou, Sichuan, China*

Correspondence should be addressed to Zhangang Xiao; xzg555898@hotmail.com

Received 7 April 2017; Revised 20 July 2017; Accepted 2 August 2017; Published 24 August 2017

Academic Editor: Lin-sen Qing

Over the past two decades, obesity has been one of the major public health concerns in most countries. In the search for new molecules that could be used for the treatment of obesity, good perspectives have been opened up for polyphenols, a class of natural bioactive phytochemicals. Experimental and limited clinical trial evidence supports that some polyphenols such as quercetin, curcumin, and resveratrol have potential benefit functions on obesity treatment. This brief review focuses on the main functions of the above-named polyphenols on adipose tissue. These polyphenols may play beneficial effects on adipose tissue under obese condition by alleviating intracellular oxidative stress, reducing chronic low-grade inflammation, inhibiting adipogenesis and lipogenesis, and suppressing the differentiation of preadipocytes to mature adipocytes.

1. Introduction

Over the past decades, obesity has been one of the major public health threats in most developed countries and in an increasing number of developing countries [1]. Obesity is caused by the imbalance between energy intake and expenditure, which promotes the hypertrophy of adipocytes and results in adipose tissue dysfunction [2]. It is well known that obesity is a strong risk factor for type 2 diabetes mellitus (T2DM) and cancer, and T2DM is linked to the development of cardiovascular diseases, such as hypertension and atherosclerosis [3, 4]. Furthermore, obesity was associated with higher disability rates and mortality rates in the elderly [5]. A better understanding of the molecular basis of obesity will lead to establish strategies for prevention and treatment of obesity.

Adipose tissue is composed of many kinds of cell types, including adipocytes, macrophages, endothelial cells, and stem cells. In addition, as the major energy storage organ, adipose tissue also is a very important endocrine organ [6]. To maintain the function on energy regulation, adipose tissue produces adipokines, such as adiponectin and leptin, and proinflammatory cytokines, such as tumor necrosis factor- (TNF-) α and interleukin- (IL-) 1β [6]. Under normal physiological lean state, when the body takes excessive energy, adipose tissue can be rapidly enlarged by increasing the adipocyte size (hypertrophy) and numbers (hyperplasia), which were accompanied by an increase of blood vessels (angiogenesis) to supply more oxygen (O_2) and nutrients to the whole tissue [7]. However, under pathological obese state, adipose tissue will undergo a process named "adipose tissue remodeling," which was characterized by reduced angiogenesis,

increased hypoxia levels and extra cellular matrix (ECM) levels, and induced higher levels of immune cell infiltration and subsequently induced a low-grade chronic inflammation. All of these pathological events will lead to adipocyte dysfunction, cell death, and systemic insulin resistance [7].

There are two types of adipose tissue, white adipose tissue and brown adipose tissue. The excess energy was mainly stored in the white adipose tissue in the form of triglycerides (TAGs). The function of brown adipose tissue is to directly transfer energy from nutrients to heat by uncoupling protein (UCP) 1, which mediates uncoupling of oxidative phosphorylation from ATP synthesis (conferred thermogenesis) [8–10]. *In vitro* and *in vivo* studies demonstrated that the activation of brown adipocytes is an effective and efficient way for excess energy metabolism [11–15]. Human studies showed that activation of brown-like adipocytes is a potential way to counteract obesity [12, 13, 16–19].

Oxidative stress is referred to an event resulting from the imbalance between the intracellular oxidation system and reduction system, the redox system [20]. The imbalance between oxidant and antioxidant enzymes/substrates will result in a series of oxidation-reduction reactions, which will subsequently induce cytotoxicity by inducing cellular stress responses and stimulating cell death [21]. A series of studies have revealed that oxidative stress is related to the development of obesity. Excess levels of reactive oxygen species (ROS) might lead to the dysfunction of mitochondria by inhibiting respiration process and result in a reduction on the energy expenditure in adipocytes and conversely enhance the energy storage in adipose tissue [22]. Oxidative stress also suppresses the endocrine functions of adipose tissue by disrupting the secretion of adipokines such as adiponectin [23]. Antioxidants can protect cells from oxidative stress by trapping free radicals and restoring cell functions. In recent years, chemical antioxidants derived from natural plants, which are named as "phytochemicals," have gained interest by researchers for preventing and treating diseases, including obesity and obesity-related metabolic diseases [24–29].

Among the phytochemicals studied, researchers pay more attention on polyphenols, which are derived from diet food such as vegetables and fruits, as well as beverages such as juice, coffee, and tea [30–35]. Studies showed that polyphenols such as quercetin, curcumin, and resveratrol exerted beneficial effects on lipid and energy metabolism and potential body weight change. In this review, we will focus on the roles of and the mechanisms of polyphenols including quercetin, curcumin, and resveratrol and on obesity and adipose tissue function.

2. Quercetin

Quercetin is the most abundant of flavonoids and is found in vegetables, fruits, tea, and wine [36].

2.1. Effects on Cell Culture Models of Obesity. The first *in vitro* study investigating the potential antiobesity effect of quercetin on obesity was performed on primary adipocytes. Kuppusamy and Das found that quercetin induced lipolysis of primary rat adipocytes in a dose- and time-dependent manner by increasing cyclic adenosine monophosphate (cAMP) levels and hormone-sensitive lipase (HSL) activity [37]. In addition to the inductive effect on lipolysis, quercetin can also suppress lipogenesis by reducing the incorporation rate of fatty acids into adipocyte triacylglycerols in rat fat pads [38] and by inhibiting the gene expression levels of fatty acid synthase (FAS) and the activity of acetyl-CoA carboxylase (ACC) [39]. Quercetin also can inhibit adipogenesis by decreasing gene expression levels of the key adipogenic factors peroxisome proliferator-activated receptor γ (PPARγ) and CCAAT/enhancer binding protein α (C/EBP α) [39]. Recently, using hypertrophied 3T3-L1 adipocyte model, Herranz-López et al. showed that quercetin can rapidly reduce the intracellular ROS levels, which was correlated with the higher levels of quercetin metabolite [40]. Moreover, in human SGBS adipocytes, quercetin can significantly reduce levels of adipokines ANGPTL4, adipsin, and PAI-1 as well as of glycolysis-associated enzymes ENO2, PFKP, and PFKFB4, all of which are associated with obesity and adipose tissue dysfunction [41]. Adipocyte browning is a promising strategy for the prevention of obesity [14, 42–44]. In 3T3-L1 adipocytes, quercetin (50 μM) induced the expression of brown adipocyte-specific genes such as UCP-1 and cell death-inducing DNA fragmentation factor-alpha-like effector A (CIDEA) by the activation of AMP-activated protein kinase (AMPK) [45], which is a key checkpoint to control the energy balance in adipocytes by suppressing the activity of ACC; as a result, the levels of lipid in adipocytes were decreased [46].

2.2. Effects on Animal Models of Obesity. Animal studies showed that quercetin can protect mice or rats from high-fat diet- (HFD-) induced body weight gain and adipose tissue accumulation [47–49]. In HFD-fed mouse model, Stewart et al. showed that quercetin can transiently increase energy expenditures which may relate to the upregulation of UCP-1 [49]. In HFD-fed rat model, quercetin suppressed adipogenesis by reducing the key adipogenic factor C/EBP α gene expression levels and reduced lipogenesis by downregulating the gene levels of FAS and ACC [50]. Quercetin also has anti-inflammatory effects on adipose tissue. Stewart et al. found that long-time treatment with quercetin can reduce the levels of inflammatory markers IFNγ, TNFα, IL-1, and IL-4 in mice [49]. Quercetin suppresses the accumulation and activation of immune cell and improves mitochondrial functions in adipose tissue of HFD-induced obese mice by increasing the levels of oxidative stress-sensitive transcription factor and antioxidant enzymes [51]. Moreover, Dong et al. found that quercetin attenuated mast cell and macrophage infiltration into epididymis adipose tissues (EATs) through the AMPK α1-silent information regulator (SIRT) 1 pathway in HFD-fed mice [52]. In Wistar rats, quercetin suppressed the expression of oxidative stress and inflammatory markers, including nuclear factor kappa B (NF-κB), nuclear factor-related factor- (Nrf-) 2, and heme oxygenase- (HO-) 1 [53]. In another study, quercetin (10 mg/kg of body weight) improved the inflammatory status of visceral adipose tissue by suppressing the expression of TNF-α and enhancing the levels of adiponectin, which indicates the recovery of the

functions of the adipose tissue, in obese Zucker rats, a genetically obese rat model [48].

2.3. Human Studies and Clinical Trials Using Quercetin to Treat Obesity. Although many cell culture and animal studies focused on the beneficial effects of quercetin in obesity, there are only a limited number of human studies and clinical trials that have been performed to evaluate the effects of quercetin on obesity treatment. In a 12-week, randomized, double-blind, placebo-controlled study, Lee et al. demonstrated that quercetin (100 mg/day/subject) significantly decreased the total body fat, particularly in the percentage of fat in the arm, and decreased the body mass index (BMI) of overweight or obese subjects [54]. Another study evaluated the effects of quercetin on obesity in overweight-obese subjects with various apolipoprotein E (APOE) genotypes; the authors reported that quercetin (150 mg/day/subject) decreased the waist circumference and triacylglycerol concentration [55]. In addition to these findings, one study showed that 12-week of onion extract (quercetin-rich extract) intake decreased body weight, percentage of body fat, and BMI of 10 female university students [56]. However, another study reported that 12-week of onion extract intake has no effect on body fat composition and BMI of the female university students [57], indicating that the experiment period of the study is important for the effects of the onion extracts on body weight change. Currently, there is one clinical trial that is still under phase II stage investigation; the purpose of this study is to investigate whether quercetin changes the absorption of glucose by the body in obese subjects and obese diabetic subjects [58]. Although quercetin suppressed oxidative stress in obese rodent models [51, 53], Shanely et al. reported that quercetin has no effect on oxidative stress and antioxidant capacity during a 12-week consuming period of high doses of quercetin (500 or 1000 mg/day/subject) in obese subjects [59]. Future research need to further investigate the bioactive effects and bioavailability of quercetin in the treatment of obesity.

3. Curcumin

Curcumin is derived from and is the most bioactive polyphenol in the spice turmeric [60]. Curcumin exerts several biological functions including antioxidation, anti-inflammation, and antiangiogenesis in different organs including adipose tissue [60].

3.1. Effects on Cell Culture Models of Obesity. Curcumin may have a significant effect on adipogenesis. In primary human adipocytes and murine 3T3-L1 adipocytes, curcumin treatment suppressed the expression of adipogenic genes peroxisome proliferator-activated receptor γ (PPARγ) and C/EBP α [61]. In addition to the antiadipogenic effects, curcumin also suppresses the differentiation of preadipocytes to mature adipocytes. Ahn et al. demonstrated that curcumin inhibited 3T3-L1 adipocyte differentiation by inhibiting activities of mitogen-activated protein kinases including ERK, JNK, and p38 [62]. Another report showed that the inhibition effect of curcumin on adipocyte differentiation might have been mediated by the suppression of PPARγ expression in a dose-dependent manner in human adipocytes [63]. Moreover, curcumin also showed anti-inflammatory effects. Curcumin pretreatment inhibited the secretion of monocyte chemoattractant protein- (MCP-) 1, a proinflammatory cytokine, from 3T3-L1 adipocytes [64].

3.2. Effects on Animal Models of Obesity. Curcumin showed beneficial effects on body weight reduction and energy metabolism. Two weeks of high dietary curcumin supplementation feeding in rats reduced epididymal adipose tissue and increased fatty acid β-oxidation, indicating the increase of energy expenditure after curcumin treatment [65]. Curcumin also showed anti-inflammatory functions. In HFD-induced obesity and in genetic obesity (ob/ob mice) models, curcumin reduced adipose tissue inflammation by reducing macrophage infiltration into adipose tissue and by increasing adiponectin production [66, 67]. Curcumin also showed antioxidant effects. Dietary curcumin (0.2–1 g/100 g diet) suppressed high-fat-induced lipid accumulation in epididymal adipose tissue [65].

3.3. Human Studies and Clinical Trials Using Curcumin to Treat Obesity. Unlike the studies on the effects of curcumin in cells or animals, studies on obese subjects are limited. The first clinical trial using curcumin for obesity treatment was conducted by Mohammadi et al. [68]. In this study, obese subjects were treated with a commercial formulation of curcumin (C3 Complex®, 1 g/day) supplemented with a bioavailability enhancer, piperine (5 mg/day) for a month. Although there were no changes in weight, body mass index (BMI), or body fat, serum triglyceride levels were significantly decreased after curcumin treatment, indicating the improvement of insulin actions [68]. In another randomized, double-blind, crossover trial, Ganjali and Sahebkar showed that 30-day treatment of C3 Complex (500 mg/day) plus piperine (5 mg/day) reduced serum levels of inflammatory cytokines IL-1β and IL-4 of obese individuals [69], indicating the anti-inflammatory activity of curcumin in obesity therapy. Moreover, oral curcumin supplementation (1 g/day for 30 days) was effective in reducing oxidative stress burden in obese individuals [70].

Although curcumin has been used for clinical trials in obesity treatment, the multifaceted pharmacological nature of curcumin and its pharmacokinetics and the side effects of curcumin in obesity therapy need to be carefully investigated. The recommended maximum daily usage of curcumin is 1 mg/kg body weight by a joint report of the World Health Organization and the Food and Agriculture Organization [71]. However, a few studies showed that the chronic use of curcumin can cause liver toxicity [72] and high doses of curcumin can induce gastrointestinal upset, inflamed skin, and chest tightness in a phase II trial in patients with advanced pancreatic cancer [73].

4. Resveratrol

Resveratrol (3,5,4′-trihydroxytrans-stilbene) is a small polyphenolic compound, which was well known as constituent

of red grapes, red wine, peanuts, and ground nuts [74, 75]. Resveratrol showed antioxidant and anti-inflammatory actions [76] and showed beneficial effects in preventing the development of many diseases including obesity and diabetes [77].

4.1. Effects on Cell Culture and Ex Vivo Adipose Tissue Culture Models of Obesity. Resveratrol can inhibit adipogenesis by reducing the stability and transcriptional activity of PPARγ [78, 79] and prevent triglyceride accumulation via enhancing the expression of sirtuin1 (Sirt1), which is an important molecular target regulating cellular energy metabolism and mitochondrial homeostasis [80] in 3T3-L1 adipocytes. Moreover, resveratrol enhanced lipolytic activity in human and rat adipocytes; this effect was mediated by β-adrenergic activation and the induction of cAMP levels [81, 82]. In addition, to enhance lipolysis, resveratrol also can inhibit lipogenesis by downregulating the expression of lipogenic genes in human adipocytes [83]. Kang et al. found that resveratrol pretreatment suppressed secretion of TNF-α and IL-6 from 3T3-L1 adipocytes and inhibited the activation of inflammatory-related proteins such as extracellular receptor-activated kinase (ERK) and NF-kappaB (NF-κB), indicating that resveratrol has anti-inflammatory effects in adipocytes [84]. In human adipocytes, resveratrol reversed IL-1β-stimulated expression of proinflammatory adipokines including IL-6, IL-8, monocyte chemoattractant protein- (MCP-) 1, and plasminogen activator inhibitor- (PAI-) 1 [85, 86]. Moreover, reports showed that resveratrol inhibited adipose tissue inflammation by downregulating the protein levels of IL-6, IL-8, MCP-1, and the inflammatory-related adipokine leptin in human adipose tissue *in vitro* [86, 87].

4.2. Effects on Animal Models of Obesity. Dietary treatment of rodents with resveratrol protected mice against HFD-induced body weight gain and obesity by increasing energy expenditure which was partly mediated by stimulating intracellular mitochondrial functions (fatty acid oxidation) in adipose tissue and by the suppression of fatty acid synthesis [88–90] and by inducing brown-like adipocyte formation in white adipose [91–94]. The *in vitro* anti-inflammatory effect of resveratrol was also confirmed in animal models. In mice, resveratrol attenuated HFD-induced inflammation of WAT by downregulating the protein levels of proinflammatory cytokines TNF-α, IFN-α, IFN-β, and IL-6 [89]. In addition, resveratrol reduced adipose tissue macrophage infiltration [95] and prevented the suppression of the production of regulatory T cells (Tregs, the negative regulators of inflammation) [96] in HFD-induced obese mice. In Zucker rats, resveratrol suppressed the protein levels of IL-6 and the activity of NF-κB in adipose tissue by reducing macrophage infiltration [97]. Interestingly, Jimenez-Gomez et al. showed that resveratrol showed similar effects on high-fat-treated adult rhesus monkey model as effects on HFD-induced obese rodent models, suppressed the activation of NF-κB, and decreased the mRNA levels of IL-6, TNF-α, IL-1β, and adiponectin in the visceral adipose tissue of high-fat-treated monkey model [98]. Resveratrol also showed antioxidant effect in animal models. Lv et al. found that resveratrol attenuated diet-induced oxidative stress in epididymal white adipose tissue partly by the reduction of Sirt1 and manganese superoxide dismutase (Sod2) levels [99].

4.3. Clinical Trials Using Resveratrol to Treat Obesity. Although several clinical trials that examine the effect of resveratrol on obesity are currently ongoing (see http://clinicaltrials.gov) or have finished (see Review [100]), none of them were designed specifically to test the effects of resveratrol on body weight change of obese subjects. In a randomized double-blind cross-over study, Timmers et al. showed that 150 mg/day of resveratrol treatment increased energy expenditure, reduced serum inflammatory markers, and decreased adipose tissue lipolysis and plasma fatty acid and glycerol levels of obese men [101]. In another study, Konings et al. investigated the effects of 30 days resveratrol treatment (150 mg/day) on the adipocyte size and gene expression patterns in obese men. The authors found that resveratrol treatment decreased the size of abdominal subcutaneous adipocytes [102]. However, another report showed that high levels of resveratrol supplementation treatment had no effect on energy expenditure, adipose tissue content, and metabolic events [103]. The reason for the reversed results obtained from the two reports may possibly lie in the administered doses of resveratrol they used for obesity treatment. The latter report used 1500 mg/day for the trial [103]; this dose was ten times of the dose Konings et al. used in the study [102].

5. Concluding Remarks

In the search for new molecules that could be used for the treatment of obesity, good perspectives have been opened up for polyphenols. Current knowledge from cell cultures and animal models suggests that polyphenols, including quercertin, curcumin, and resveratrol, play beneficial effects under obese condition potentially by alleviating intracellular oxidative stress, reducing chronic low-grade inflammation, inhibiting adipogenesis and lipogenesis, and suppressing the differentiation of preadipocytes to mature adipocytes. Although investigators have obtained limited results from clinical trials, there is still no sufficient data to support the high-dose and long-term usage of these polyphenols in obesity treatment.

Conflicts of Interest

The authors declare no conflict of interest.

Authors' Contributions

Yueshui Zhao and Bo Chen contributed equally to this work.

Acknowledgments

This study is supported by grants from the National Natural Science Foundation of China (Grant nos. 81503093, 81602166, and 81672444) and the Natural Science Foundation of Jiangsu Province (BK2014086).

References

[1] Obesity: preventing and managing the global epidemic. Report of a WHO consultation," *World Health Organization Technical Report Series*, vol. 894, no. i-xii, pp. 1–253, 2000.

[2] K. Sun, J. Tordjman, K. Clement, and P. E. Scherer, "Fibrosis and adipose tissue dysfunction," *Cell Metabolism*, vol. 18, no. 4, pp. 470–477, 2013.

[3] V. Cifarelli and S. D. Hursting, "Obesity, diabetes and cancer: a mechanistic perspective," *International Journal of Diabetology & Vascular Disease Research*, vol. 2015, Supplement 4, 2015.

[4] Y. Matsuzawa, I. Shimomura, T. Nakamura, Y. Keno, K. Kotani, and K. Tokunaga, "Pathophysiology and pathogenesis of visceral fat obesity," *Obesity Research*, vol. 3, Supplement 2, pp. 187s–194s, 1995.

[5] V. B. Kalish, "Obesity in older adults," *Primary Care*, vol. 43, no. 1, pp. 137–144, ix, 2016.

[6] S. E. Wozniak, L. L. Gee, M. S. Wachtel, and E. E. Frezza, "Adipose tissue: the new endocrine organ? A review article," *Digestive Diseases and Sciences*, vol. 54, no. 9, pp. 1847–1856, 2009.

[7] K. Sun, C. M. Kusminski, and P. E. Scherer, "Adipose tissue remodeling and obesity," *The Journal of Clinical Investigation*, vol. 121, no. 6, pp. 2094–2101, 2011.

[8] M. Chondronikola, E. Volpi, E. Børsheim et al., "Brown adipose tissue activation is linked to distinct systemic effects on lipid metabolism in humans," *Cell Metabolism*, vol. 23, no. 6, pp. 1200–1206, 2016.

[9] B. Cannon and J. Nedergaard, "Brown adipose tissue: function and physiological significance," *Physiological Reviews*, vol. 84, no. 1, pp. 277–359, 2004.

[10] R. Oelkrug, E. T. Polymeropoulos, and M. Jastroch, "Brown adipose tissue: physiological function and evolutionary significance," *Journal of Comparative Physiology B, Biochemical, Systemic, and Environmental Physiology*, vol. 185, no. 6, pp. 587–606, 2015.

[11] C. E. Varela, A. Rodriguez, M. Romero-Valdovinos et al., "Browning effects of (-)-epicatechin on adipocytes and white adipose tissue," *European Journal of Pharmacology*, 2017.

[12] B. Thyagarajan and M. T. Foster, "Beiging of white adipose tissue as a therapeutic strategy for weight loss in humans," *Hormone Molecular Biology and Clinical Investigation*, 2017.

[13] P. C. Dinas, A. Valente, M. Granzotto et al., "Browning formation markers of subcutaneous adipose tissue in relation to resting energy expenditure, physical activity and diet in humans," 2017.

[14] N. J. Song, S. H. Chang, D. Y. Li, C. J. Villanueva, and K. W. Park, "Induction of thermogenic adipocytes: molecular targets and thermogenic small molecules," *Experimental & Molecular Medicine*, vol. 49, no. 7, article e353, 2017.

[15] V. Ryu, E. Zarebidaki, H. Elliott Albers, B. Xue, and T. J. Bartness, "Short photoperiod reverses obesity in Siberian hamsters via sympathetically induced lipolysis and browning in adipose tissue," *Physiology & Behavior*, 2017.

[16] B. Halpern, M. C. Mancini, and A. Halpern, "Brown adipose tissue: what have we learned since its recent identification in human adults," *Arquivos Brasileiros de Endocrinologia e Metabologia*, vol. 58, no. 9, pp. 889–899, 2014.

[17] W. D. Marken Lichtenbeltvan, J. W. Vanhommerig, N. M. Smulders et al., "Cold-activated brown adipose tissue in healthy men," *The New England Journal of Medicine*, vol. 360, no. 15, pp. 1500–1508, 2009.

[18] M. Saito, Y. Okamatsu-Ogura, M. Matsushita et al., "High incidence of metabolically active brown adipose tissue in healthy adult humans: effects of cold exposure and adiposity," *Diabetes*, vol. 58, no. 7, pp. 1526–1531, 2009.

[19] V. Ouellet, S. M. Labbe, D. P. Blondin et al., "Brown adipose tissue oxidative metabolism contributes to energy expenditure during acute cold exposure in humans," *The Journal of Clinical Investigation*, vol. 122, no. 2, pp. 545–552, 2012.

[20] C. M. Grant, "Metabolic reconfiguration is a regulated response to oxidative stress," *Journal of Biology*, vol. 7, no. 1, p. 1, 2008.

[21] G. Bjorklund and S. Chirumbolo, "Role of oxidative stress and antioxidants in daily nutrition and human health," *Nutrition (Burbank, Los Angeles County, Calif.)*, vol. 33, pp. 311–321, 2017.

[22] T. Wang, Y. Si, O. S. Shirihai et al., "Respiration in adipocytes is inhibited by reactive oxygen species," *Obesity (Silver Spring, Md.)*, vol. 18, no. 8, pp. 1493–1502, 2010.

[23] M. Matsuda and I. Shimomura, "Roles of oxidative stress, adiponectin, and nuclear hormone receptors in obesity-associated insulin resistance and cardiovascular risk," *Hormone Molecular Biology and Clinical Investigation*, vol. 19, no. 2, pp. 75–88, 2014.

[24] R. Mopuri and M. S. Islam, "Medicinal plants and phytochemicals with anti-obesogenic potentials: a review," *Biomedicine & Pharmacotherapy = Biomedecine & Pharmacotherapie*, vol. 89, pp. 1442–1452, 2017.

[25] Y. Tang and R. Tsao, "Phytochemicals in quinoa and amaranth grains and their antioxidant, anti-inflammatory, and potential health beneficial effects: a review," *Molecular Nutrition & Food Research*, vol. 61, no. 7, 2017.

[26] J. Martel, D. M. Ojcius, C. J. Chang et al., "Anti-obesogenic and antidiabetic effects of plants and mushrooms," *Nature Reviews Endocrinology*, vol. 13, no. 3, pp. 149–160, 2017.

[27] N. N. Sun, T. Y. Wu, and C. F. Chau, "Natural dietary and herbal products in anti-obesity treatment," *Molecules (Basel, Switzerland)*, vol. 21, no. 10, 2016.

[28] M. Balaji, M. S. Ganjayi, G. E. Hanuma Kumar, B. N. Parim, R. Mopuri, and S. Dasari, "A review on possible therapeutic targets to contain obesity: the role of phytochemicals," *Obesity Research & Clinical Practice*, vol. 10, no. 4, pp. 363–380, 2016.

[29] Y. J. Zhang, R. Y. Gan, S. Li et al., "Antioxidant phytochemicals for the prevention and treatment of chronic diseases," *Molecules (Basel, Switzerland)*, vol. 20, no. 12, pp. 21138–21156, 2015.

[30] S. S. Deshpande, S. K. Sathe, and D. K. Salunkhe, "Chemistry and safety of plant polyphenols," *Advances in Experimental Medicine and Biology*, vol. 177, pp. 457–495, 1984.

[31] L. Vamos-Vigyazo, "Polyphenol oxidase and peroxidase in fruits and vegetables," *Critical Reviews in Food Science and Nutrition*, vol. 15, no. 1, pp. 49–127, 1981.

[32] E. Haslam, T. H. Lilley, Y. Cai, R. Martin, and D. Magnolato, "Traditional herbal medicines—the role of polyphenols," *Planta Medica*, vol. 55, no. 1, pp. 1–8, 1989.

[33] C. Rice-Evans, "Plant polyphenols: free radical scavengers or chain-breaking antioxidants?," *Biochemical Society Symposium*, vol. 61, pp. 103–116, 1995.

[34] J. A. Dominguez Avila, J. Rodrigo Garcia, G. A. Gonzalez Aguilar, and L. A. Rosade la, "The antidiabetic mechanisms of polyphenols related to increased glucagon-like peptide-1 (GLP1) and insulin signaling," *Molecules (Basel, Switzerland)*, vol. 22, no. 6, 2017.

[35] J. Teixeira, D. Chavarria, F. Borges et al., "Dietary polyphenols and mitochondrial function: role in health and disease," *Current Medicinal Chemistry*, 2017.

[36] R. J. Nijveldt, E. Noodvan, D. E. Hoornvan, P. G. Boelens, K. Norrenvan, and P. A. Leeuwenvan, "Flavonoids: a review of probable mechanisms of action and potential applications," *The American Journal of Clinical Nutrition*, vol. 74, no. 4, pp. 418–425, 2001.

[37] U. R. Kuppusamy and N. P. Das, "Effects of flavonoids on cyclic AMP phosphodiesterase and lipid mobilization in rat adipocytes," *Biochemical Pharmacology*, vol. 44, no. 7, pp. 1307–1315, 1992.

[38] T. Motoyashiki, T. Morita, and H. Ueki, "Involvement of the rapid increase in cAMP content in the vanadate-stimulated release of lipoprotein lipase activity from rat fat pads," *Biological & Pharmaceutical Bulletin*, vol. 19, no. 11, pp. 1412–1416, 1996.

[39] J. Ahn, H. Lee, S. Kim, J. Park, and T. Ha, "The anti-obesity effect of quercetin is mediated by the AMPK and MAPK signaling pathways," *Biochemical and Biophysical Research Communications*, vol. 373, no. 4, pp. 545–549, 2008.

[40] M. Herranz-López, I. Borras-Linares, M. Olivares-Vicente, J. Galvez, A. Segura-Carretero, and V. Micol, "Correlation between the cellular metabolism of quercetin and its glucuronide metabolite and oxidative stress in hypertrophied 3T3-L1 adipocytes," *Phytomedicine: International Journal of Phytotherapy and Phytopharmacology*, vol. 25, pp. 25–28, 2017.

[41] A. Leiherer, K. Stoemmer, A. Muendlein et al., "Quercetin impacts expression of metabolism- and obesity-associated genes in SGBS adipocytes," *Nutrients*, vol. 8, no. 5, p. 282, 2016.

[42] C. R. Yeo, M. Agrawal, S. Hoon et al., "SGBS cells as a model of human adipocyte browning: a comprehensive comparative study with primary human white subcutaneous adipocytes," *Scientific Reports*, vol. 7, no. 1, p. 4031, 2017.

[43] S. Carobbio, V. Pellegrinelli, and A. Vidal-Puig, "Adipose tissue function and expandability as determinants of lipotoxicity and the metabolic syndrome," *Advances in Experimental Medicine and Biology*, vol. 960, pp. 161–196, 2017.

[44] M. Okla, J. Kim, and K. Koehler, "Dietary factors promoting brown and beige fat development and thermogenesis," *Advances in Nutrition (Bethesda, Md.)*, vol. 8, no. 3, pp. 473–483, 2017.

[45] S. G. Lee, J. S. Parks, and H. W. Kang, "Quercetin, a functional compound of onion peel, remodels white adipocytes to brown-like adipocytes," *The Journal of Nutritional Biochemistry*, vol. 42, pp. 62–71, 2017.

[46] X. Zhou, J. Xu, Y. Shi, and J. M. Ye, "Discovery of novel antidiabetic drugs by targeting lipid metabolism," *Current Drug Targets*, vol. 16, no. 12, pp. 1372–1380, 2015.

[47] C. Liang, M. E. Oest, and M. R. Prater, "Intrauterine exposure to high saturated fat diet elevates risk of adult-onset chronic diseases in C57BL/6 mice," *Birth Defects Research Part B, Developmental and Reproductive Toxicology*, vol. 86, no. 5, pp. 377–384, 2009.

[48] L. Rivera, R. Moron, M. Sanchez, A. Zarzuelo, and M. Galisteo, "Quercetin ameliorates metabolic syndrome and improves the inflammatory status in obese Zucker rats," *Obesity (Silver Spring, Md.)*, vol. 16, no. 9, pp. 2081–2087, 2008.

[49] L. K. Stewart, J. L. Soileau, D. Ribnicky et al., "Quercetin transiently increases energy expenditure but persistently decreases circulating markers of inflammation in C57BL/6J mice fed a high-fat diet," *Metabolism: Clinical and Experimental*, vol. 57, no. 7, Supplement 1, pp. S39–S46, 2008.

[50] J. Moon, H. J. Do, O. Y. Kim, and M. J. Shin, "Antiobesity effects of quercetin-rich onion peel extract on the differentiation of 3T3-L1 preadipocytes and the adipogenesis in high fat-fed rats," *Food and Chemical Toxicology: An International Journal Published for the British Industrial Biological Research Association*, vol. 58, pp. 347–354, 2013.

[51] M. Kobori, Y. Takahashi, M. Sakurai et al., "Quercetin suppresses immune cell accumulation and improves mitochondrial gene expression in adipose tissue of diet-induced obese mice," *Molecular Nutrition & Food Research*, vol. 60, no. 2, pp. 300–312, 2016.

[52] J. Dong, X. Zhang, L. Zhang et al., "Quercetin reduces obesity-associated ATM infiltration and inflammation in mice: a mechanism including AMPKalpha1/SIRT1," *Journal of Lipid Research*, vol. 55, no. 3, pp. 363–374, 2014.

[53] S. K. Panchal, H. Poudyal, and L. Brown, "Quercetin ameliorates cardiovascular, hepatic, and metabolic changes in diet-induced metabolic syndrome in rats," *The Journal of Nutrition*, vol. 142, no. 6, pp. 1026–1032, 2012.

[54] J.-S. Lee, Y.-J. Cha, K.-H. Lee, and J.-E. Yim, "Onion peel extract reduces the percentage of body fat in overweight and obese subjects: a 12-week, randomized, double-blind, placebo-controlled study," *Nutrition Research Practice*, vol. 10, no. 2, pp. 175–181, 2016.

[55] M. Pfeuffer, A. Auinger, U. Bley et al., "Effect of quercetin on traits of the metabolic syndrome, endothelial function and inflammation in men with different APOE isoforms," *Nutrition, Metabolism, and Cardiovascular Diseases: NMCD*, vol. 23, no. 5, pp. 403–409, 2013.

[56] Y. K. Yang and S. P. Kim, "The effect of onion extract intake for 12 weeks on blood lipid and obesity index in obese university women," *Korean Journal of Sports Sciences*, vol. 22, pp. 955–962, 2013.

[57] K. H. Lee, H. J. Lee, E. J. Park, and K. I. Jeon, "Effect of onion extracts on serum lipid and antioxidant status in healthy university female," *Korean Journal of Community Nutrition*, vol. 2, 2008.

[58] Trials.gov C, "Investigating the use of quercetin on glucose absorption in obesity, and obesity with type 2 diabetes," 2017, http://clinicaltrials.gov/show/NCT00065676, 2013.

[59] R. A. Shanely, A. M. Knab, D. C. Nieman, F. Jin, S. R. McAnulty, and M. J. Landram, "Quercetin supplementation does not alter antioxidant status in humans," *Free Radical Research*, vol. 44, no. 2, pp. 224–231, 2010.

[60] A. S. Strimpakos and R. A. Sharma, "Curcumin: preventive and therapeutic properties in laboratory studies and clinical trials," *Antioxidants & Redox Signaling*, vol. 10, no. 3, pp. 511–545, 2008.

[61] C. Y. Kim, T. T. Le, C. Chen, J. X. Cheng, and K. H. Kim, "Curcumin inhibits adipocyte differentiation through modulation of mitotic clonal expansion," *The Journal of Nutritional Biochemistry*, vol. 22, no. 10, pp. 910–920, 2011.

[62] J. Ahn, H. Lee, S. Kim, and T. Ha, "Curcumin-induced suppression of adipogenic differentiation is accompanied by activation of Wnt/beta-catenin signaling," *American Journal of Physiology Cell Physiology*, vol. 298, no. 6, pp. C1510–C1516, 2010.

[63] M. Gurnell, "Peroxisome proliferator-activated receptor gamma and the regulation of adipocyte function: lessons from human genetic studies," *Best Practice & Research Clinical Endocrinology & Metabolism*, vol. 19, no. 4, pp. 501–523, 2005.

[64] H. M. Woo, J. H. Kang, T. Kawada, H. Yoo, M. K. Sung, and R. Yu, "Active spice-derived components can inhibit inflammatory responses of adipose tissue in obesity by suppressing inflammatory actions of macrophages and release of monocyte chemoattractant protein-1 from adipocytes," *Life Sciences*, vol. 80, no. 10, pp. 926–931, 2007.

[65] A. Asai and T. Miyazawa, "Dietary curcuminoids prevent high-fat diet-induced lipid accumulation in rat liver and epididymal adipose tissue," *The Journal of Nutrition*, vol. 131, no. 11, pp. 2932–2935, 2001.

[66] W. Shao, Z. Yu, Y. Chiang et al., "Curcumin prevents high fat diet induced insulin resistance and obesity via attenuating lipogenesis in liver and inflammatory pathway in adipocytes," *PLoS One*, vol. 7, no. 1, article e28784, 2012.

[67] S. P. Weisberg, R. Leibel, and D. V. Tortoriello, "Dietary curcumin significantly improves obesity-associated inflammation and diabetes in mouse models of diabesity," *Endocrinology*, vol. 149, no. 7, pp. 3549–3558, 2008.

[68] A. Mohammadi, A. Sahebkar, M. Iranshahi et al., "Effects of supplementation with curcuminoids on dyslipidemia in obese patients: a randomized crossover trial," *Phytotherapy Research: PTR*, vol. 27, no. 3, pp. 374–379, 2013.

[69] S. Ganjali and A. Sahebkar, "Investigation of the effects of curcumin on serum cytokines in obese individuals: a randomized controlled trial," *The Scientific World Journal*, vol. 2014, Article ID 898361, 6 pages, 2014.

[70] A. Sahebkar, A. Mohammadi, A. Atabati et al., "Curcuminoids modulate pro-oxidant-antioxidant balance but not the immune response to heat shock protein 27 and oxidized LDL in obese individuals," *Phytotherapy Research: PTR*, vol. 27, no. 12, pp. 1883–1888, 2013.

[71] Evaluation of certain food additives," WHO Technical Report Series, 891, WHO, Geneva, 2000.

[72] M. Liddle, C. Hull, C. Liu, and D. Powell, "Contact urticaria from curcumin," *Dermatitis: Contact, Atopic, Occupational, Drug*, vol. 17, no. 4, pp. 196-197, 2006.

[73] N. Dhillon, B. B. Aggarwal, R. A. Newman et al., "Phase II trial of curcumin in patients with advanced pancreatic cancer," *Clinical Cancer Research: An Official Journal of the American Association for Cancer Research*, vol. 14, no. 14, pp. 4491–4499, 2008.

[74] M. Meydani and S. T. Hasan, "Dietary polyphenols and obesity," *Nutrients*, vol. 2, no. 7, pp. 737–751, 2010.

[75] U. Stervbo, O. Vang, and C. Bonnesen, "A review of the content of the putative chemopreventive phytoalexin resveratrol in red wine," *Food Chemistry*, vol. 101, no. 2, pp. 449–457, 2007.

[76] J. Burns, T. Yokota, H. Ashihara, M. E. Lean, and A. Crozier, "Plant foods and herbal sources of resveratrol," *Journal of Agricultural and Food Chemistry*, vol. 50, no. 11, pp. 3337–3340, 2002.

[77] W. J. Spuyvan der and E. Pretorius, "Is the use of resveratrol in the treatment and prevention of obesity premature?," *Nutrition Research Reviews*, vol. 22, no. 2, pp. 111–117, 2009.

[78] Z. E. Floyd, Z. Q. Wang, G. Kilroy, and W. T. Cefalu, "Modulation of peroxisome proliferator-activated receptor gamma stability and transcriptional activity in adipocytes by resveratrol," *Metabolism*, vol. 57, no. 7, Supplement 1, pp. S32–S38, 2008.

[79] S. Rayalam, J. Y. Yang, S. Ambati, M. A. Della-Fera, and C. A. Baile, "Resveratrol induces apoptosis and inhibits adipogenesis in 3T3-L1 adipocytes," *Phytotherapy Research: PTR*, vol. 22, no. 10, pp. 1367–1371, 2008.

[80] H. Imamura, D. Nagayama, N. Ishihara et al., "Resveratrol attenuates triglyceride accumulation associated with upregulation of Sirt1 and lipoprotein lipase in 3T3-L1 adipocytes," *Molecular Genetics and Metabolism Reports*, vol. 12, pp. 44–50, 2017.

[81] K. Szkudelska, L. Nogowski, and T. Szkudelski, "Resveratrol, a naturally occurring diphenolic compound, affects lipogenesis, lipolysis and the antilipolytic action of insulin in isolated rat adipocytes," *The Journal of Steroid Biochemistry and Molecular Biology*, vol. 113, no. 1-2, pp. 17–24, 2009.

[82] S. Gomez-Zorita, K. Treguer, J. Mercader, and C. Carpene, "Resveratrol directly affects in vitro lipolysis and glucose transport in human fat cells," *Journal of Physiology and Biochemistry*, vol. 69, no. 3, pp. 585–593, 2013.

[83] P. Fischer-Posovszky, V. Kukulus, D. Tews et al., "Resveratrol regulates human adipocyte number and function in a Sirt1-dependent manner," *The American Journal of Clinical Nutrition*, vol. 92, no. 1, pp. 5–15, 2010.

[84] L. Kang, W. Heng, A. Yuan, L. Baolin, and H. Fang, "Resveratrol modulates adipokine expression and improves insulin sensitivity in adipocytes: relative to inhibition of inflammatory responses," *Biochimie*, vol. 92, no. 7, pp. 789–796, 2010.

[85] J. Olholm, S. K. Paulsen, K. B. Cullberg, B. Richelsen, and S. B. Pedersen, "Anti-inflammatory effect of resveratrol on adipokine expression and secretion in human adipose tissue explants," *International Journal of Obesity (2005)*, vol. 34, no. 10, pp. 1546–1553, 2010.

[86] I. Zagotta, E. Y. Dimova, K. M. Debatin, M. Wabitsch, T. Kietzmann, and P. Fischer-Posovszky, "Obesity and inflammation: reduced cytokine expression due to resveratrol in a human in vitro model of inflamed adipose tissue," *Frontiers in Pharmacology*, vol. 6, p. 79, 2015.

[87] K. B. Cullberg, J. Olholm, S. K. Paulsen et al., "Resveratrol has inhibitory effects on the hypoxia-induced inflammation and angiogenesis in human adipose tissue in vitro," *European Journal of Pharmaceutical Sciences: Official Journal of the European Federation for Pharmaceutical Sciences*, vol. 49, no. 2, pp. 251–257, 2013.

[88] S. J. Cho, U. J. Jung, and M. S. Choi, "Differential effects of low-dose resveratrol on adiposity and hepatic steatosis in diet-induced obese mice," *The British Journal of Nutrition*, vol. 108, no. 12, pp. 2166–2175, 2012.

[89] S. Kim, Y. Jin, Y. Choi, and T. Park, "Resveratrol exerts anti-obesity effects via mechanisms involving down-regulation of adipogenic and inflammatory processes in mice," *Biochemical Pharmacology*, vol. 81, no. 11, pp. 1343–1351, 2011.

[90] M. Lagouge, C. Argmann, Z. Gerhart-Hines et al., "Resveratrol improves mitochondrial function and protects against metabolic disease by activating SIRT1 and PGC-1alpha," *Cell*, vol. 127, no. 6, pp. 1109–1122, 2006.

[91] C. R. Ku, Y. H. Cho, Z. Y. Hong et al., "The effects of high fat diet and resveratrol on mitochondrial activity of brown adipocytes," *Endocrinology and Metabolism (Seoul, Korea)*, vol. 31, no. 2, pp. 328–335, 2016.

[92] G. Alberdi, V. M. Rodriguez, J. Miranda, M. T. Macarulla, I. Churruca, and M. P. Portillo, "Thermogenesis is involved in the body-fat lowering effects of resveratrol in rats," *Food Chemistry*, vol. 141, no. 2, pp. 1530–1535, 2013.

[93] N. Arias, C. Pico, M. Teresa Macarulla et al., "A combination of resveratrol and quercetin induces browning in white adipose tissue of rats fed an obesogenic diet," *Obesity (Silver Spring, Md.)*, vol. 25, no. 1, pp. 111–121, 2017.

[94] S. Wang, X. Liang, Q. Yang et al., "Resveratrol induces brown-like adipocyte formation in white fat through activation of AMP-activated protein kinase (AMPK) alpha1," *International Journal of Obesity (2005)*, vol. 39, no. 6, pp. 967–976, 2015.

[95] B. T. Jeon, E. A. Jeong, H. J. Shin et al., "Resveratrol attenuates obesity-associated peripheral and central inflammation and improves memory deficit in mice fed a high-fat diet," *Diabetes*, vol. 61, no. 6, pp. 1444–1454, 2012.

[96] B. Wang, J. Sun, X. Li et al., "Resveratrol prevents suppression of regulatory T-cell production, oxidative stress, and inflammation of mice prone or resistant to high-fat diet-induced obesity," *Nutrition Research (New York, N.Y.)*, vol. 33, no. 11, pp. 971–981, 2013.

[97] S. Gomez-Zorita, A. Fernandez-Quintela, A. Lasa, E. Hijona, L. Bujanda, and M. P. Portillo, "Effects of resveratrol on obesity-related inflammation markers in adipose tissue of genetically obese rats," *Nutrition (Burbank, Los Angeles County, Calif.)*, vol. 29, no. 11-12, pp. 1374–1380, 2013.

[98] Y. Jimenez-Gomez, J. A. Mattison, K. J. Pearson et al., "Resveratrol improves adipose insulin signaling and reduces the inflammatory response in adipose tissue of rhesus monkeys on high-fat, high-sugar diet," *Cell Metabolism*, vol. 18, no. 4, pp. 533–545, 2013.

[99] Z. M. Lv, Q. Wang, Y. H. Chen, S. H. Wang, and D. Q. Huang, "Resveratrol attenuates inflammation and oxidative stress in epididymal white adipose tissue: implications for its involvement in improving steroidogenesis in diet-induced obese mice," *Molecular Reproduction and Development*, vol. 82, no. 4, pp. 321–328, 2015.

[100] S. Timmers, M. K. Hesselink, and P. Schrauwen, "Therapeutic potential of resveratrol in obesity and type 2 diabetes: new avenues for health benefits?," *Annals of the New York Academy of Sciences*, vol. 1290, pp. 83–89, 2013.

[101] S. Timmers, E. Konings, L. Bilet et al., "Calorie restriction-like effects of 30 days of resveratrol (resVida™) supplementation on energy metabolism and metabolic profile in obese humans," *Cell Metabolism*, vol. 14, no. 5, pp. 612–622, 2011.

[102] E. Konings, S. Timmers, M. V. Boekschoten et al., "The effects of 30 days resveratrol supplementation on adipose tissue morphology and gene expression patterns in obese men," *International Journal of Obesity (2005)*, vol. 38, no. 3, pp. 470–473, 2014.

[103] M. M. Poulsen, P. F. Vestergaard, B. F. Clasen et al., "High-dose resveratrol supplementation in obese men. An investigator-initiated, randomized, placebo-controlled clinical trial of substrate metabolism, insulin sensitivity, and body composition," *Diabetes*, vol. 62, no. 4, pp. 1186–1195, 2013.

Hindawi
Oxidative Medicine and Cellular Longevity
Volume 2017, Article ID 8273160, 10 pages
https://doi.org/10.1155/2017/8273160

Research Article

Enhancement of Antioxidant Mechanisms and Reduction of Oxidative Stress in Chickens after the Administration of Drinking Water Enriched with Polyphenolic Powder from Olive Mill Waste Waters

Aliki Papadopoulou,[1] Konstantinos Petrotos,[2] Dimitrios Stagos,[1] Konstantinos Gerasopoulos,[1] Antonios Maimaris,[3] Haralampos Makris,[3] Ioannis Kafantaris,[1] Sotiria Makri,[1] Efthalia Kerasioti,[1] Maria Halabalaki,[4] Vincent Brieudes,[4] Georgia Ntasi,[5] Stylianos Kokkas,[2] Pavlos Tzimas,[6] Panagiotis Goulas,[3] Alexander M. Zakharenko,[7] Kirill S. Golokhvast,[7] Aristidis Tsatsakis,[8] and Demetrios Kouretas[1]

[1]*Department of Biochemistry and Biotechnology, University of Thessaly, Viopolis, 41500 Larissa, Greece*
[2]*Department of Biosystems Engineering, Technical Education Institute of Thessaly, 41110 Larissa, Greece*
[3]*Department of Animal Production, Technical Education Institute of Thessaly, 41110 Larissa, Greece*
[4]*Department of Pharmacognosy and Natural Products Chemistry, Faculty of Pharmacy, University of Athens, Panepistimiopolis Zografou, 15771 Athens, Greece*
[5]*PharmaGnose S.A., Papathanasiou 24, 34100 Eyboia, Greece*
[6]*Department of Agricultural Engineering Technologists, Technical Education Institute of Thessaly, 41110 Larissa, Greece*
[7]*Scientific Educational Centre of Nanotechnology, Far Eastern Federal University, Engineering School, 10 Pushkinskaya Street, 690950 Vladivostok, Russia*
[8]*Laboratory of Toxicology, School of Medicine, University of Crete, 71003 Heraklion, Greece*

Correspondence should be addressed to Demetrios Kouretas; dkouret@uth.gr

Received 14 May 2017; Revised 21 July 2017; Accepted 26 July 2017; Published 24 August 2017

Academic Editor: Jie Li

The aim of the study was to examine the effects of a polyphenolic powder from olive mill wastewater (OMWW) administered through drinking water, on chickens' redox status. Thus, 75 chickens were divided into three groups. Group A was given just drinking water, while groups B and C were given drinking water containing 20 and 50 μg/ml of polyphenols, respectively, for 45 days. The antioxidant effects of the polyphenolic powder were assessed by measuring oxidative stress biomarkers in blood after 25 and 45 days of treatment. These markers were total antioxidant capacity (TAC), protein carbonyls (CARB), thiobarbituric acid reactive species (TBARS) and superoxide dismutase activity (SOD) in plasma, and glutathione (GSH) and catalase activity in erythrocytes. The results showed that CARB and TBARS were decreased significantly in groups B and C, and SOD decreased in group B compared to that in group A. TAC was increased significantly in group C and GSH was increased in group B, while catalase activity was increased in groups B and C compared to that in group A. In conclusion, this is the first study showing that supplementation of chickens with polyphenols from OMWW through drinking water enhanced their antioxidant mechanisms and reduced oxidative stress-induced damage.

1. Introduction

Free radicals are atoms, molecules, or ions that have unpaired valence electrons [1]. Free radicals such as reactive oxygen species (ROS) are produced in living organisms either from normal essential metabolic processes or from external sources (e.g., exposure to X-rays, air pollutants, and industrial chemicals) [2]. Due to the unpaired electrons, free radicals are very reactive species and their overproduction can cause damage to all biological macromolecules such as DNA, proteins, and lipids, thus resulting in cell damage and subsequently in manifestation of pathological conditions [1]. Oxidative stress is defined as an imbalance between the production of free radicals and the ability of the organism to detoxify them or counteract their harmful effects through neutralization by antioxidants and is responsible for the cause of several diseases [1, 2]. Several studies have suggested that oxidative stress in farm animals may be involved in pathological conditions affecting animal production and welfare [3]. For example, the hot and humid environment in aviaries may cause heat-induced oxidative stress in chickens, which in turn reduces growth and meat quality [4]. Thus, administration of natural antioxidant compounds to chickens has been proposed as a means for reducing the oxidative stress-induced adverse effects [5–7]. Polyphenols are bioactive phytochemical compounds and mostly studied due to their antioxidant properties. Polyphenols are secondary metabolites and act defensively in plants against pathogens and UV-mediated stress [8]. They are divided mainly into four groups according to their chemical structure, flavonoids, phenolic acids, stilbenes, and lignans [8]. Many studies have suggested that polyphenols' antioxidant activity may improve the well-being of living organisms and protect against several diseases [9–11]. Moreover, polyphenol consumption causes lower toxicity and fewer side effects than other chemical compounds used for prevention from diseases [12].

One of the polyphenols' sources is olive oil obtained from olive tree fruit (*Olea europaea* L.). The main polyphenolic compounds found in olive oil are tyrosol, hydroxytyrosol, oleuropein, and pinoresinol, exhibiting potent antioxidant properties [13, 14]. For example, olive oil-supplemented diet has been shown to protect chicken skeletal muscle from heat stress-induced oxidative stress [15]. Moreover, byproducts of olive oil production such as olive mill wastewater (OMWW) contain polyphenols (e.g., p-coumaric acid, homovanillic acid, caffeic acid, protocatechuic acid, 3,4-dihydroxymandelic acid, vanillic acid, and ferulic acid) with antioxidant activity [16–18]. In previous studies, we have demonstrated that administration of feed supplemented with polyphenols from OMWW improved the redox status in chickens and pigs [7, 19]. However, polyphenols from OMWW byproducts have not been so far administered to chickens through water supply. Polyphenols' supplementation through water or feed may affect differently their absorption and consequently their bioavailability and bioactivities' potency. Thus, in the present study, water-diluted polyphenolic powder from OMWW was administered to broiler chickens. Then, the possible enhancement of antioxidant mechanisms or the protection of macromolecules from ROS-induced damage was assessed by measuring oxidative stress biomarkers in broilers' blood.

2. Materials and Methods

2.1. Polyphenolic Powder Description. The product with the name MEDOLIVA® is produced according to an established patented procedure (patent application number: 20120100569—Greek Industrial Property Organization), for obtaining polyphenols from OMWW based on the use of ceramic membrane microfiltration using clean vegetable waters from olive mills. The product comes in a liquid form which is stable and safe without the use of conservatives. The polyphenolic liquid product is transformed into powder, using maltodextrin as nanoencapsulation material, through the freeze dryer technology.

2.2. HPLC Analysis for the Identification of Polyphenols of Medoliva Powder. All HPLC analyses were carried out on a Hitachi Co-Japan system (Japan) equipped with a quaternary pump L-2130, column thermostat L-2300, and diode array L-2455 detector. The column used was a Pinnacle II RP C18 (150 mm × 4.6 mm) with a guard column of Kromasil 100-5 C18 (3.0 × 4.6 mm). Injection was by means of a Hitachi Elite LaChrom Autosampler L-2200 with a 20 μl fixed loop. For the chromatographic analyses, HPLC grade water was used, whereas all HPLC solvents were filtered prior to use through cellulose acetate membranes of 0.45 μM pore size. Chromatographic data were acquired and processed using Agilent EZChrom Elite software (Agilent, CA, USA).

For the preparation of the sample analyzed by HPLC, 10 ml of the sample solution was extracted four times with HPLC grade ethyl acetate, and then the solvent was evaporated and the remaining organic phase was dissolved in 4 ml of HPLC grade methanol and collected to HPLC type glass bottles for further analysis.

The HPLC analysis was carried out at 40°C (maintained by the column thermostat) using samples of 20 μl, which were directly injected by means of a Hitachi Elite LaChrom Autosampler L-2200. The gradient eluted consisted of solvent A [obtained by the addition of 3% acetic acid in 20 mM sodium acetate aqueous solution, pH 3.2] and solvent B (acetonitrile, CH_3CN). Run time was set at 28 min with a constant flow rate at 1.0 ml/min in accordance with the following gradient time table: at zero time, 100% A; after 3 min, the pumps were adjusted to 88% A and 12% B; at 10 min, 79% A and 21% B; at 12 min, 61% A and 39% B; at 18 min, 46% A and 54% B; at 25 min, 40% A and 60% B; and finally, at 28 min, 100% B. The analysis was monitored at 280 nm for oleuropein, hydroxytyrosol, and tyrosol and at 355 nm for flavonols simultaneously. Three replicate experiments were carried out for each sample examined. Peaks were identified by comparing their retention time and UV-vis spectra with the reference compounds, and data were quantitated using the corresponding curves of the reference compounds as standards. All standards were dissolved in methanol.

2.3. Assessment of the Total Polyphenolic Content (TPC). The TPC of the Medoliva powder was determined in accordance with a modified version of the Folin-Ciocalteu method [20].

Initially, 1 gr of powder was added to 20 ml of extraction solution (80% *v*/*v* ethanol, 20% distilled water containing 1% HCl). The mixture was added to a 50 ml flask and centrifuged at 3000 rpm for 20 min. Then, the supernatant solution was added to a 50 ml volumetric flask that was filled with distilled water until the final volume. Afterwards, 5 ml of the solution was transferred to a volumetric flask of 25 ml that was filled with water until the final volume.

After the above preparation, 1.6 ml of sample was added to a tube along with 0.3 ml of 20% Na_2CO_3 deionized water and 0.1 ml of Folin-Ciocalteu reagent. The mixture was allowed to stand at room temperature for 2 h. Absorbance was measured at 725 nm versus a blank. The results are expressed as gallic acid equivalents using the standard curve (absorbance versus concentration) prepared from authentic gallic acid.

2.4. Animals. The experiment was reviewed and approved by the institutional review board and the appropriate state authority. Seventy-five broiler chickens (Hubbard-Sasso hybrid), 15 days old, were purchased from "Bloutsos" aviary (Trikala, Greece). Chickens were housed under controlled environmental conditions (12-hour light/dark cycle, temperature 18–21°C, and humidity 50–70%). Then, they were randomly divided into three experimental groups (25 chickens per group) as follows: group A, chickens were given fresh tap water without polyphenolic powder; group B, chickens were given polyphenols dissolved in water at a concentration of 200 μg/ml powder (equals to 20 μg/ml of polyphenols); and group C, chickens were given polyphenols dissolved in water at a concentration of 500 μg/ml powder (equal to 50 μg/ml of polyphenols). The Medoliva powder was instantly soluble in the water, as it was prepared by freeze drying. The concentrations of 200 and 500 μg/ml did not cause a solubility problem. The addition of the powder to the water was made at a daily basis, and for this reason, there was no problem of stability. Chickens' weight was monitored every five days throughout the 45 days of the experiment. Moreover, feed and water consumption were recorded at a daily basis.

2.5. Blood Collection. Blood samples were drawn at the age of 40 days (i.e., after 25 days of treatment) and 60 days (i.e., after 45 days of treatment). 4 ml of blood was collected from the brachial vein of each chicken and placed into 5 ml aseptic EDTA tubes. Blood samples were centrifuged immediately at 1370*g* for 10 min at 4°C, and the plasma was collected and used for measuring total antioxidant capacity (TAC), thiobarbituric acid reactive species (TBARS), and protein carbonyls (CARB). The packed erythrocytes were lysed with distilled water (1 : 1 *v*/*v*), inverted vigorously, and centrifuged at 4020*g* for 15 min at 4°C, and the erythrocyte lysate was collected for the measurement of reduced glutathione (GSH) and catalase activity.

2.6. Oxidative Stress Biomarkers. Glutathione (GSH) was measured according to the method of [21]. In particular, 20 μl of erythrocyte lysate, treated with 5% trichloroacetic acid (TCA), was mixed with 660 μl of 67 mM sodium potassium phosphate (pH 8.0) and 330 μl of 1 mM 5,5-dithiobis-2-nitrobenzoate (DTNB). The samples were incubated in the dark at room temperature for 45 min, and the absorbance was read at 412 nm. GSH concentration was calculated on the basis of a calibration curve made using commercial standards.

Catalase activity was determined using the method of [22]. Briefly, 4 μl of erythrocyte lysate (diluted 1 : 10) was added to 2991 μl of 67 mM sodium potassium phosphate (pH 7.4), and the samples were incubated at 37°C for 10 min. A total of 5 μl of 30% hydrogen peroxide was added to the samples, and the change in absorbance was immediately read at 240 nm for 1.5 min. Calculation of catalase activity was based on the molar extinction coefficient of H_2O_2.

The determination of superoxide dismutase (SOD) activity was based on the method of nitroblue tetrazolium salt (NBT) according to Oberley and Spitz [23]. More specifically, this assay included a negative control made by mixing 800 μl of SOD buffer [1 mM diethylenetriaminepentaacetic acid (DETAPAC) in 0.05 M potassium phosphate buffer (pH 7.8); 1 U catalase; 5.6×10^{-5} M NBT; 10^{-4} M xanthine] with 100 μl of 0.05 M potassium phosphate buffer. Subsequently, ~60 mU of xanthine oxidase (XO) was added and the rate of increase in absorbance was measured at 560 nm for 3.5 min. In the test samples, 100 μl of plasma was added to 800 μl of SOD buffer followed by the addition of ~60 mU of XO and the rate of increase in absorbance was measured for 3.5 min at 560 nm. Calculation of SOD activity in the test samples was based on the percent inhibition of the rate of increase in absorbance. The rate of increase in absorbance (A) per minute for the negative control and for the tested samples was determined by formula (1), and the percentage inhibition for each sample was calculated using formula (2):

$$\frac{\Delta A_{560\,\mathrm{nm}}}{\mathrm{min}} = \frac{A_{560\,\mathrm{nm}}\,\mathrm{final} - A_{560\,\mathrm{nm}}\,\mathrm{initial}}{3.5\,\mathrm{min}}, \tag{1}$$

$$\%\,\mathrm{Inhibition} = \left[\frac{\Delta\left(\left(A_{560\,\mathrm{nm}}\right)/\left(\mathrm{min}_{\mathrm{negative\ control}}\right)\right) - \Delta\left(\left(A_{560\,\mathrm{nm}}\right)/\left(\mathrm{min}_{\mathrm{sample}}\right)\right)}{\Delta\left(\left(A_{560\,\mathrm{nm}}\right)/\left(\mathrm{min}_{\mathrm{negative\ control}}\right)\right)}\right] \times 100. \tag{2}$$

The determination of TAC was based on the method of [24]. Briefly, 20 μl of plasma was added to 480 μl of 10 mM sodium potassium phosphate (pH 7.4) and 500 μl of 0.1 mM 2,2-diphenyl-1-picrylhydrazyl (DPPH) free radical, and the samples were incubated in the dark for 30 min at room temperature. The samples were centrifuged for 3 min at 20,000*g*, and the absorbance was read at 520 nm. TAC is presented as mmol of DPPH reduced to 2,2-diphenyl-1-picrylhydrazine (DPPH : H) by the antioxidants of plasma.

For the determination of TBARS, a slightly modified assay of [25] was used. According to this method, 100 μl of plasma was mixed with 500 μl of 35% TCA and 500 μl of

Tris-HCl (200 mmol/L; pH 7.4) and incubated for 10 min at room temperature. 1 ml Na_2SO_4—thiobarbituric acid (TBA) solution—was added, and the samples were incubated at 95°C for 45 min. The samples were cooled on ice for 5 min and were vortexed after 1 ml of 70% TCA was added. The samples were centrifuged at 15,000g for 3 min, and the absorbance of the supernatant was read at 530 nm. A baseline shift in absorbance was taken into account by running a blank along with all samples during the measurement. Calculation of TBARS concentration was based on the molar extinction coefficient of malondialdehyde.

CARB were determined based on the method of [26]. In this assay, 50 μl of 20% TCA was added to 50 μl of plasma. This mixture was incubated in an ice bath for 15 min and centrifuged at 15,000g for 5 min at 4°C. The supernatant was discarded, and 500 μl of 14 mM 2,4-dinitrophenyl hydrazine (DNPH) dissolved in 2.5 N HCl for the sample or 500 μl of 2.5 N HCl for the blank was added in the pellet. The samples were incubated in the dark at room temperature for 1 h, with intermittent vortexing every 15 min, and were centrifuged at 15,000g for 5 min at 4°C. The supernatant was discarded, and 1 ml of 10% TCA was added, vortexed, and centrifuged at 15,000g for 5 min at 4°C. The supernatant was discarded, and 1 ml of ethanol-ethyl acetate (1 : 1 v/v) was added, vortexed, and centrifuged at 15,000g for 5 min at 4°C. This washing step was repeated twice. The supernatant was discarded, and 1 ml of 5 M urea (pH 2.3) was added, vortexed, and incubated at 37°C for 15 min. The samples were centrifuged at 15,000g for 3 min at 4°C, and the absorbance was read at 375 nm. Calculation of CARB concentration was based on the molar extinction coefficient of DNPH. Total plasma protein was assayed using a Bradford reagent (Sigma-Aldrich Ltd.).

2.7. Determination of Hydroxytyrosol in Chickens' Plasma by Mass Spectrometry. For all plasma samples, a preparation was carried out before the measurement of hydroxytyrosol. Briefly, 100 μl of plasma was thawed and 480 μl of acetonitrile, 60 μl of methanol, and 60 μl of purified water were added. Subsequently, the blurred sample due to protein precipitation was centrifuged at 12000 rpm for 10 min, and the supernatants were evaporated to dryness. Finally, with 100 μl of methanol/water 1 : 1, the samples were reconstituted and at first were subjected to chromatographic separation and then analyzed at UPLC-TQD-MS/MS.

For chromatographic separation, ultra high-performance liquid chromatography system (EVOQ™, Bruker, Bremen) was employed. Mobile phases consisted of (A) deionized water with 0.1% formic acid and (B) acetonitrile (LC-MS grade). The samples (5 μl) were injected to a Waters HSS (2.1 × 100 mm, 1.8 μm) analytical column with 95.0% mobile phase B at a flow rate of 0.4 ml/min for 2 min. The mobile phase composition was increased to 10% B and held for 6 min before returning to 95% B for other 3.0 min to reequilibrate. Total run time injection-to-injection was 11 min. Column oven temperature was maintained at 40°C throughout.

After chromatographic separation, the eluate was directed into EVOQ triple quadrupole mass spectrometer.

Table 1: Polyphenolic composition and total polyphenolic content (TPC) of Medoliva powder.

Polyphenols	
Hydroxytyrosol	0.50[a]
Tyrosol	0.55
Caffeic acid	0.02
p-Coumaric acid	0.04
TPC	100.00

[a]All values are mg/g powder. TPC: total polyphenolic content (as mg gallic acid/g powder).

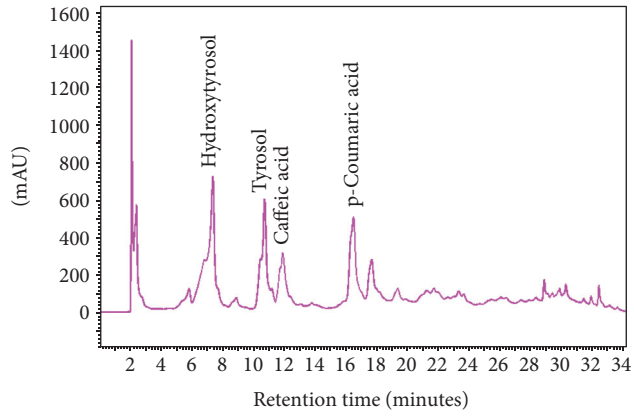

Figure 1: HPLC polyphenolic profile of Medoliva powder.

The mass spectrometer was operated in the negative electrospray ionization mode, the spray voltage was maintained at 4000 V, and the cone temperature was 250°C, although the heated probe temperature was 300°C. The probe and the nebulizer gas flow (nitrogen) were 30 arbs and 50 arbs, respectively. The transition of hydroxytyrosol (153.10 to 123.10 m/z) was monitored in the multiple reaction monitoring (MRM) mode with a scan time of 50 ms with collision energy of 12 eV. The calibration curve of hydroxytyrosol used for its determination consisted of six points (0.1, 0.5, 1.0, 5.0, 10.0, and 50.0 ng/ml).

2.8. Statistical Analysis. Data were analyzed by one-way ANOVA. The level of statistical significance was set at $p < 0.05$. All results are expressed as mean ± SD. Data were analyzed using SPSS, version 13.0 (SPSS Inc., Chicago, Il).

3. Results

3.1. Total Polyphenolic Content and Composition of Medoliva Powder. The TPC of the Melidova powder was 100 mg GAE/g powder (Table 1). In Figure 1, the HPLC of the polyphenolic profile of Medoliva powder is presented. From the polyphenols used as standards, four polyphenols were identified, hydroxytyrosol, tyrosol, caffeic acid, and p-coumaric acid, and their quantities were 0.50, 0.55, 0.02, and 0.04 mg/g of Medoliva powder, respectively (Table 1).

3.2. Assessment of Chickens' Weight. Chickens' weight was monitored throughout the experiment. Groups B and C

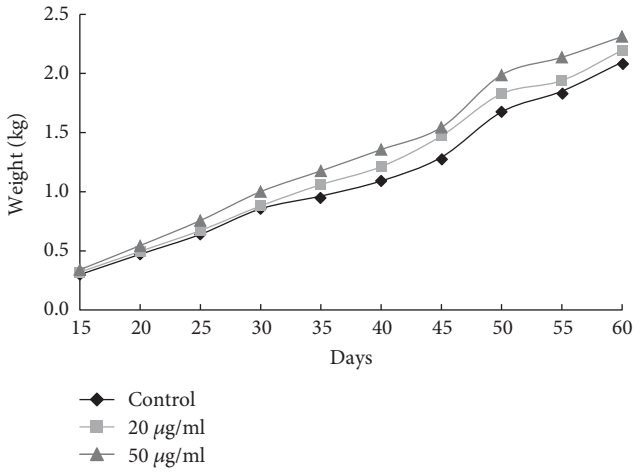

Figure 2: Chicken weight in relation to the days after birth.

showed an increase in weight compared to the control group, but it was not statistically significant (Figure 2). In addition, there were not significant differences in feed consumption between the different groups (data not shown). Likewise, water consumption did not differ significantly between the different groups (Table 2).

3.3. Assessment of Oxidative Stress Markers in Chickens' Blood. Regarding oxidative stress markers' measurements, all of them showed that polyphenolic powder administration through water supply improved the redox status of the broiler chickens. Specifically, CARB levels were decreased significantly in groups B and C, compared to the control group (Figure 3(a)). Group C exhibited the highest decrease in CARB levels by 44.7 and 33.8% at days 25 and 45, respectively (Figure 3(a)). In group B, there was a decrease in protein carbonyl levels by 26.1% at 25 days (Figure 3(a)). Moreover, the decrease in CARB levels was dose dependent, since there was significant reduction of CARB in group C (high dose) at both 25 and 45 days compared to group B (low dose) (Figure 3(a)).

Like protein carbonyls, TBARS levels in plasma were decreased significantly in groups B and C, compared to the control group (Figure 3(b)). Group C exhibited the greatest decrease in TBARS levels by 34.1 and 19.4%, at 25 and 45 days of treatment, respectively. In group B, TBARS were decreased by 19.1% at 25 days (Figure 3(b)). Moreover, at 25 days of treatment, there was a dose-dependent decrease in TBARS, since they were significantly lower in group C (high dose) compared to group B (low dose) (Figure 3(b)). Also, there was a time-dependent effect of the administration of polyphenols from OMWW, since in both groups B and C, TBARS were significantly lower at 45 days compared to 25 days (Figure 3(b)).

TAC in plasma was increased significantly in group C by 13.9 and 19.5% at 25 and 45 days of treatment, respectively (Figure 3(c)).

There was also a significant increase in GSH levels in erythrocytes in group B, where GSH levels were increased by 50.9% at 25 days (Figure 4(b)). Moreover, GSH levels were increased time dependently in both B and C groups (Figure 4(b)).

Table 2: Water consumption by the chickens during the experiment.

	Group A (control)	Group B	Group C
15–40 d after birth	229±67[a]	225 ± 18	233 ± 24
41–60 d after birth	362 ± 12	355 ± 21	358 ± 19

[a]Water consumption (ml) by each chicken per day. Values indicate mean ± SD. $^{*}p < 0.05$, significant differences from the control (there was not any significant difference between groups).

Furthermore, the administration of polyphenolic powder increased catalase activity in erythrocytes. Group C demonstrated the highest increase in catalase activity by 38.4 and 30.2% at days 25 and 45, respectively (Figure 4(a)). In group B, the catalase activity was increased by 27.6 and 24.0% at days 25 and 45, respectively (Figure 4(a)). In addition, in both groups B and C, polyphenols from OMWW time dependently increased catalase activity (Figure 4(a)). There was also a dose-dependent increase of catalase activity at 25 days (Figure 4(a)).

Regarding SOD activity in plasma, at 25 days of treatment, the enzyme activity was decreased significantly by 30.4 and 33.8% in B and C groups, respectively, compared to that in the control (Figure 5), while, at 45 days of treatment, there were not significant differences in SOD activity between the control and treatment groups (Figure 5). Moreover, in group C, SOD activity was lower at 25 days of treatment by 26.5% compared to that at 45 days (Figure 5).

Finally, it was interesting that in the control group, the chickens at 25 days of treatment (i.e., 40 days post birth) had significantly higher CARB and TBARS levels and lower GSH levels than the chickens at 45 days of treatment (i.e., 60 days post birth) (Figures 3(a), 3(b), and 4(b)).

3.4. Assessment of Hydroxytyrosol in Chickens' Plasma. The mass spectrometry analysis showed that, in group C, the hydroxytyrosol levels were 349.5 pg/ml plasma (Table 3). In group B, the concentration of hydroxytyrosol was below the lower limit of quantitation (100 pg/ml), while as expected, in the control group, it was not detected (lower limit of detection was 30 pg/ml) (Table 3).

4. Discussion

In a previous study, we have shown that supplementation of feed with polyphenols from OMWW enhanced the antioxidant mechanisms and decreased oxidative stress-induced damage in broiler chickens [7]. As known, oxidative stress may be the etiological factor for several diseases in farm animals [3]. Thus, the aim of the present study was to administer polyphenols from OMWW through water supply to chickens, as an easier way than administration through feed. For example, in order to increase the time storage and to improve the bioavailability of feed supplemented with OMWW, silage corn should be made, a laborious and time-consuming process [7]. However, the preparation for the supplementation of polyphenolic powder from OMWW through water requires only its dilution. The effects of water supplied with polyphenols from OMMW on the chickens'

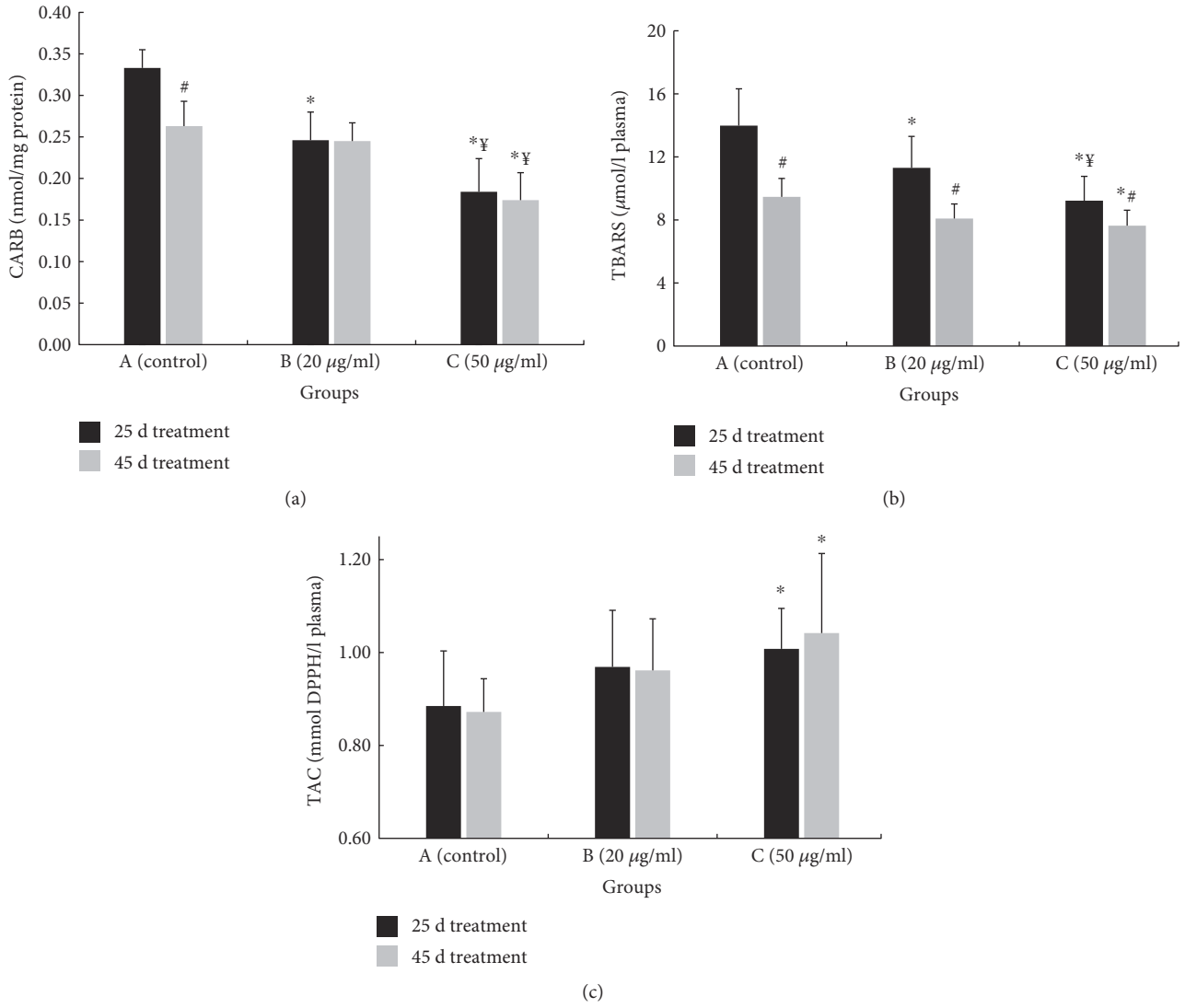

Figure 3: Effects on oxidative stress markers: (a) CARB, (b) TBARS, and (c) TAC, in the plasma of chickens after treatment for 25 and 45 days with water (group A; control) or water containing polyphenols at 20 μg/ml (group B) or at 50 μg/ml (group C). *Significantly different from the value of the control group at the same sampling time ($p < 0.05$). #Significant differences between the values of the same group, measured at different sampling times ($p < 0.05$). ¥Significant differences between the values of B and C groups, measured at the same sampling time ($p < 0.05$).

redox status were assessed by measuring oxidative stress markers in blood.

The results showed that the administration of water supplied with polyphenols from OMWW enhanced the antioxidant mechanisms in chickens. Specifically, TAC, an indicator of the total antioxidant capacity, was increased in the plasma of the chicken group given water supplied with OMWW, compared to that of the control. Especially, there was a significant increase in TAC after the administration of the high dose (i.e., 50 μg/ml of polyphenols) of OMWW for both 25 and 45 days treatment. Interestingly, hydroxytyrosol, a major polyphenol found in OMWW, has been shown to increase nuclear factor (erythroid-derived 2)-like2 (Nrf2) expression and nuclear translocation, where it stimulated the transcription of antioxidant and detoxifying enzymes in the mouse heart [27].

The abovementioned increase in TAC could be attributed, at least in part, to the OMWW-induced increase of antioxidant molecules such as catalase enzyme activity in erythrocytes. Catalase catalyzes the decomposition of hydrogen peroxide to water and oxygen. Thus, catalase prevents the formation of the hydroxyl radical, one of the most common and potent free radicals in living organisms, from hydrogen peroxide through the Fenton reaction [1]. Interestingly, OMWW-induced increase in catalase activity was both time- and dose-dependent suggesting a major role of this enzyme for OMWW's antioxidant effects. Hamden et al. [28] have demonstrated that OMWW extract increased catalase activity in rat plasma, liver, and kidney. Moreover, hydroxytyrosol, one of the main polyphenols present in OMWW, has been shown to increase catalase activity as well as mRNA and protein expression through phosphorylation

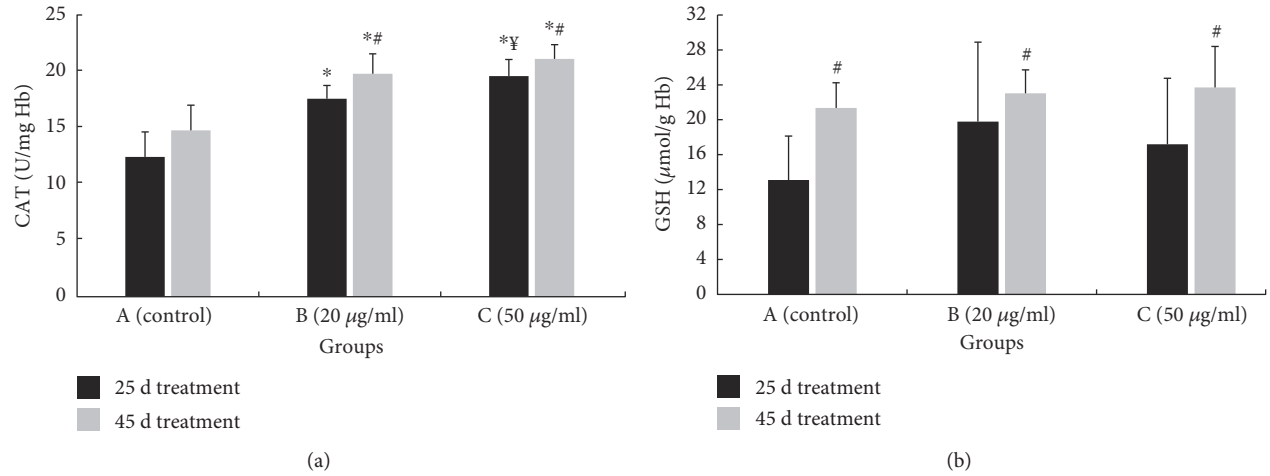

Figure 4: Effects on oxidative stress markers: (a) catalase activity (CAT) and (b) GSH in erythrocytes of chickens after treatment for 25 and 45 days with water (group A; control) or water containing polyphenols at 20 μg/ml (group B) or at 50 μg/ml (group C). *Significantly different from the value of the control group at the same sampling time ($p < 0.05$). #Significant differences between the values of the same group, measured at different sampling times ($p < 0.05$). ¥Significant differences between the values of B and C groups, measured at the same sampling time ($p < 0.05$).

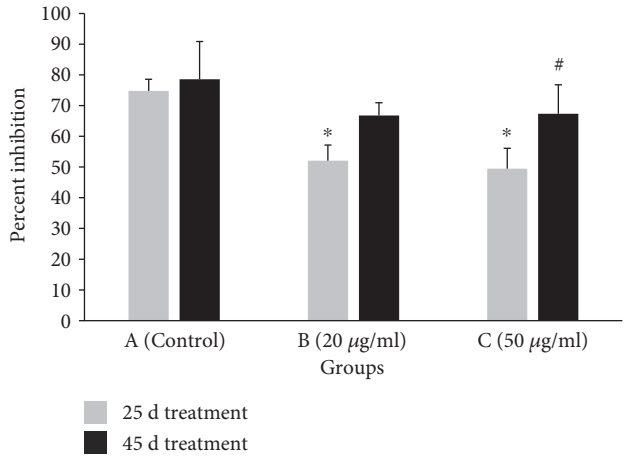

Figure 5: Nitroblue tetrazolium salt (NBT) assay of superoxide dismutase (SOD) activity in chicken plasma. Percent inhibition of superoxide production from 100 μl of chicken plasma after treatment for 25 and 45 days with water (group A; control) or water containing polyphenols at 20 μg/ml (group B) or at 50 μg/ml (group C). Percent inhibition indicates the amount by which the plasma samples inhibited NBT reduction relative to a nonplasma containing control reaction. *Significantly different from the value of the control group at the same sampling time ($p < 0.005$). #Significant differences between the values of the same group, measured at different sampling times ($p < 0.05$).

Table 3: Quantification of hydroxytyrosol in chickens' plasma.

Experimental groups	Hydroxytyrosol (pg/ml)
Group A (control)	<LLOD
Group B	349.5
Group C	<LLOQ

LLOD: lower limit of detection (30 pg/ml); LLOQ: lower limit of quantitation (100 pg/ml).

of AMP-activated protein kinase (AMPK) leading to activation of FOXO3a transcription factor in porcine pulmonary artery endothelial cells [29].

Apart from the catalase activity, the effects of OMWW on SOD activity, an antioxidant enzyme that catalyzes the dismutation of the superoxide anion into hydrogen peroxide and molecular oxygen, in plasma, were examined. The results showed that the water supplied with OMWW decreased SOD activity, especially at 25 days treatment. Other studies have also reported that administration of olive oil polyphenols decreased SOD activity in human and rat plasma [30, 31]. It has been suggested that olive oil polyphenols such as hydroxytyrosol and tyrosol reduce SOD activity by acting as direct scavengers of superoxide anion, that is, it is a kind of compensation mechanism [32, 33]. In contrast, Tufarelli et al. [34] have demonstrated that extra virgin olive oil rich in polyphenols increased SOD activity in chicken liver. Likewise, olive oil polyphenols have been shown to increase SOD activity in rat liver and heart [35, 36]. It seems that the effect of olive oil polyphenols on SOD activity may be tissue specific. In addition, Pajovic et al. [37] have reported that the administration of olive oil to rats affected differently cytosol superoxide dismutase (CuZnSOD) and mitochondrial superoxide dismutase (MnSOD) even in the same tissue.

GSH in erythrocytes was another important antioxidant molecule that was increased after the administration of polyphenols from OMWW through water supply. However, OMWW's effect on GSH was peculiar, that is, there was only significant increase after administration of the low dose (i.e., 20 μg/ml of polyphenols) of OMWW in the chickens at the younger age (after 25 days treatment or 40 days post birth). This finding was in accordance with our previous one observed after the administration of OMWW to chickens through feeding [7]. In this study, feed supplemented with OMWW increased also GSH levels in chickens only at a younger age [7]. As we and others have stated previously, an explanation

for this effect may be that polyphenols from OMWW increase GSH at a younger age when the endogenous GSH levels are low, but they had no effect or even reduced GSH in broilers at an older age when chickens' organism can produce by itself efficient GSH [5, 7, 38]. The molecular mechanisms accounting for polyphenols from OMWW-induced increase in GSH levels may be as follows: (i) increase in enzymes being responsible for GSH synthesis (e.g., g-glutamylcysteine ligase and GSH synthetase) [39], (ii) reserve GSH from reaction with free radicals by their direct scavenging [18], and (iii) increase in glutathione reductase (GR) activity (GR regenerates GSH from GSSG) [40].

The abovementioned enhancement of antioxidant mechanisms after the administration of polyphenols from OMWW through water supply may account for the protection from oxidative stress-induced damage. In particular, protein oxidation in plasma as indicated by CARB was lower in the chicken group drinking water containing polyphenols from OMWW compared to that in the control group. This protection was dose dependent after both 25 and 45 days treatments, indicating that it was more intense in the chicken group receiving the high dose of polyphenols from OMWW. The protection of proteins from oxidative stress-induced damage is important, since protein oxidation can impede protein function or lead to destruction of cellular organelles [1]. Specifically, it has been found that 82 mitochondrial proteins have been damaged in chicken skeletal muscle by oxidative stress induced by heat stress [15, 41].

Apart from protein oxidation, drinking water containing polyphenols from OMWW reduced lipid peroxidation in chicken plasma as shown by decrease in TBARS compared to control. Importantly, like protein oxidation, decrease in lipid peroxidation was dose dependent after 25 days treatment, while it was time dependent at both low and high dose of polyphenols from OMWW. It has been demonstrated that climatic stressors such as high dust and NH_3 levels and low ambient temperature caused lipid peroxidation in chickens [42, 43]. Decrease in lipid peroxidation is considerable in chicken farming, since oxidation of lipids has been associated with lower food intake and egg production [44]. Interestingly, polyphenols such as hydroxytyrosol, verbascoside, and isoverbascoside found in OMWW have been shown to reduce lipid peroxidation [45, 46].

Two different doses, 20 and 50 μg/ml of polyphenols from OMWW, were used in the present study. All the tested oxidative stress markers, apart from GSH, suggested that the high dose of the polyphenolic powder was more effective for improving chickens' redox status. Another interesting finding was that the chickens of control groups at a younger age had higher oxidative stress (e.g., CARB and TBARS) and lower antioxidant mechanisms (e.g., GSH and catalase activity) than the older chickens. This conforms to our observations from previous studies in chickens and lambs [7, 47]. The high sensitivity to oxidative stress of chickens at a younger age emphasizes the need for their antioxidant supplementation in order to prevent pathological conditions.

The bioactive compounds being responsible for the abovementioned antioxidant effects in chickens, drinking water supplied with OMWW, were probably the polyphenols which are known for their antioxidant activity [9, 10]. The chemical analysis of Medoliva powder showed that it was rich in polyphenols, since TPC was the 10% *w*/*w* of the powder. Moreover, although the hydroxytyrosol levels (349.5 pg/ml) in plasma were low, it was shown that it can be absorbed by chickens' organism. Since this is the first study assessing the bioavailability of olive oil polyphenols in chickens, it is not possible to be compared with the other ones. However, studies on the bioavailability of olive oil polyphenols in human have also shown that polyphenols in their free forms present too low levels in plasma or urine due basically to the phase I/II xenobiotic metabolism [48]. Because of these low levels, the polyphenols' ability to exert bioactivities has been questioned. However, it has been suggested that (i) the metabolites derived from polyphenols' metabolism may also be bioactive and (ii) polyphenols may be freed from their conjugates intracellularly [48]. Finally, it should be taken into account that individual polyphenols may present in low levels but their bioactivities are usually attributed to synergistic effects between many different polyphenols [49].

5. Conclusions

This is the first study showing that supplementation of broiler chickens with polyphenols from OMWW through drinking water is an easy, cost-effective, and time-saving method for the enhancement of their antioxidant mechanisms (i.e., catalase activity, GSH, and TAC levels) and reduction of oxidative stress-induced damage (i.e., protein oxidation and lipid peroxidation). These findings present particular interest, since different diseases of farm animals have been associated with oxidative stress [3]. The most potent dose was that of 500 μg/ml powder (or 50 μg/ml polyphenols) from OMWW. It should also be taken into account that the exploitation of OMWW for developing high-added value products for animal supplementation is a solution for the environmental problems caused by OMWW.

Conflicts of Interest

The authors declare that there are no conflicts of interest.

Acknowledgments

The work was funded by the "Toxicology" MSc program in the Department of Biochemistry & Biotechnology at the University of Thessaly and by the Technological Educational Institute of Thessaly. This work was also partially supported by Grant (K. Golokhvast) of Russian Scientific Foundation (15-14-20032).

References

[1] B. Halliwell, "Role of free radicals in the neurodegenerative diseases: therapeutic implications for antioxidant treatment," *Drugs & Aging*, vol. 18, no. 9, pp. 685–716, 2001.

[2] M. Valko, D. Leibfritz, J. Moncol, M. T. Cronin, M. Mazur, and J. Telser, "Free radicals and antioxidants in normal

physiological functions and human disease," *The International Journal of Biochemistry & Cell Biology*, vol. 39, no. 1, pp. 44–84, 2007.

[3] J. Lykkesfeldt and O. Svendsen, "Oxidants and antioxidants in disease: oxidative stress in farm animals," *Veterinary Journal*, vol. 173, no. 3, pp. 502–511, 2007.

[4] R. P. Rhoads, L. H. Baumgard, J. K. Suagee, and S. R. Sanders, "Nutritional interventions to alleviate the negative consequences of heat stress," *Advances in Nutrition*, vol. 4, pp. 267–276, 2013.

[5] Y. P. Chen, X. Chen, H. Zhang, and Y. M. Zhou, "Effects of dietary concentrations of methionine on growth performance and oxidative status of broiler chickens with different hatching weight," *British Poultry Science*, vol. 54, no. 4, pp. 531–537, 2013.

[6] E. Oskoueian, N. Abdullah, Z. Idrus et al., "Palm kernel cake extract exerts hepatoprotective activity in heat-induced oxidative stress in chicken hepatocytes," *BMC Complementary and Alternative Medicine*, vol. 14, p. 368, 2014.

[7] K. Gerasopoulos, D. Stagos, S. Kokkas et al., "Feed supplemented with byproducts from olive oil mill wastewater processing increases antioxidant capacity in broiler chickens," *Food and Chemical Toxicology*, vol. 82, pp. 42–49, 2015.

[8] C. Manach, A. Scalbert, C. Morand, C. Rémésy, and L. Jiménez, "Polyphenols: food sources and bioavailability," *The American Journal of Clinical Nutrition*, vol. 79, no. 5, pp. 727–747, 2004.

[9] A. Scalbert, C. Manach, C. Morand, C. Rémésy, and L. Jiménez, "Dietary polyphenols and the prevention of diseases," *Critical Reviews in Food Science and Nutrition*, vol. 45, no. 4, pp. 287–306, 2005.

[10] S. Cicerale, L. Lucas, and R. Keast, "Biological activities of phenolic compounds present in virgin olive oil," *International Journal of Molecular Sciences*, vol. 11, no. 2, pp. 458–479, 2010.

[11] S. Makri, I. Kafantaris, D. Stagos et al., "Novel feed including bioactive compounds from winery wastes improved broilers' redox status in blood and tissues of vital organs," *Food and Chemical Toxicology*, vol. 102, pp. 24–31, 2017.

[12] A. M. Bode and Z. Dong, "Epigallocatechin 3-gallate and green tea catechins: united they work, divided they fail," *Cancer Prevention Research*, vol. 2, no. 6, pp. 14–517, 2009.

[13] A. Cárdeno, M. Sánchez-Hidalgo, and C. Alarcón-de-la-Lastra, "An up-date of olive oil phenols in inflammation and cancer: molecular mechanisms and clinical implications," *Current Medicinal Chemistry*, vol. 20, no. 37, pp. 4758–4776, 2013.

[14] E. Scoditti, C. Capurso, A. Capurso, and M. Massaro, "Vascular effects of the Mediterranean diet-part II: role of omega-3 fatty acids and olive oil polyphenols," *Vascular Pharmacology*, vol. 63, no. 3, pp. 127–134, 2014.

[15] A. Mujahid, N. R. Pumford, W. Bottje et al., "Mitochondrial oxidative damage in chicken skeletal muscle induced by acute heat stress," *The Journal of Poultry Science*, vol. 44, pp. 439–445, 2007.

[16] S. M. Paixao and A. M. Anselmo, "Effect of olive mill wastewaters on the oxygen consumption by activated sludge microorganisms: an acute toxicity test method," *Journal of Applied Toxicology*, vol. 22, no. 3, pp. 173–176, 2002.

[17] P. Paraskeva and E. Diamadopoulos, "Technologies for olive mill wastewater (OMW) treatment: a review," *Journal of Chemical Technology and Biotechnology*, vol. 81, article 475e1485, 2006.

[18] E. Frankel, A. Bakhouche, J. Lozano-Sánchez, A. Segura-Carretero, and A. Fernández-Gutiérrez, "Literature review on production process to obtain extra virgin olive oil enriched in bioactive compounds. Potential use of byproducts as alternative sources of polyphenols," *Journal of Agricultural and Food Chemistry*, vol. 61, no. 22, pp. 5179–5188, 2013.

[19] K. Gerasopoulos, D. Stagos, K. Petrotos et al., "Feed supplemented with polyphenolic byproduct from olive mill wastewater processing improves the redox status in blood and tissues of piglets," *Food and Chemical Toxicology*, vol. 86, pp. 319–327, 2015.

[20] V. L. Singleton, R. Orthofer, and R. M. Lamuela-Raventos, "Analysis of total phenols and other oxidation substrates and antioxidants by means of Folin–Ciocalteu reagent," *Methods in Enzymology*, vol. 299, pp. 152–178, 1999.

[21] Y. N. Reddy, S. V. Murthy, D. R. Krishna, and M. C. Prabhakar, "Role of free radicals and antioxidants in tuberculosis patients," *The Indian Journal of Tuberculosis*, vol. 51, pp. 213–218, 2004.

[22] H. Aebi, "Catalase in vitro," *Methods in Enzymology*, vol. 105, pp. 121–126, 1984.

[23] L. W. Oberley and D. R. Spitz, "Assay of superoxide dismutase activity in tumor tissue," *Methods in Enzymology*, vol. 105, pp. 457–464, 1984.

[24] A. Janaszewska and G. Bartosz, "Assay of total antioxidant capacity: comparison of four methods as applied to human blood plasma," *Scandinavian Journal of Clinical and Laboratory Investigation*, vol. 62, pp. 231–236, 2002.

[25] M. S. Keles, S. Taysi, N. Sen, H. Aksoy, and F. Akçay, "Effect of corticosteroid therapy on serum and CSF malondialdehyde and antioxidant proteins in multiple sclerosis," *The Canadian Journal of Neurological Sciences*, vol. 28, no. 2, pp. 141–143, 2001.

[26] N. Patsoukis, G. Zervoudakis, N. T. Panagopoulos, C. D. Georgiou, F. Angelatou, and N. A. Matsokis, "Thiol redox state (TRS) and oxidative stress in the mouse hippocampus after pentylenetetrazol-induced epileptic seizure," *Neuroscience Letters*, vol. 357, no. 2, pp. 83–86, 2004.

[27] B. Bayram, B. Ozcelik, S. Grimm et al., "A diet rich in olive oil phenolics reduces oxidative stress in the heart of SAMP8 mice by induction of Nrf2-dependent gene expression," *Rejuvenation Research*, vol. 15, no. 1, pp. 71–81, 2012.

[28] K. Hamden, N. Allouche, M. Damak, and A. Elfeki, "Hypoglycemic and antioxidant effects of phenolic extracts and purified hydroxytyrosol from olive mill waste in vitro and in rats," *Chemico-Biological Interactions*, vol. 180, no. 3, pp. 421–432, 2009.

[29] H. Zrelli, M. Matsuoka, S. Kitazaki, M. Zarrouk, and H. Miyazaki, "Hydroxytyrosol reduces intracellular reactive oxygen species levels in vascular endothelial cells by upregulating catalase expression through the AMPK-FOXO3a pathway," *European Journal of Pharmacology*, vol. 660, no. 2e3, pp. 275–282, 2011.

[30] L. Rubió, A. Serra, C. Y. Chen et al., "Effect of the co-occurring components from olive oil and thyme extracts on the antioxidant status and its bioavailability in an acute ingestion in rats," *Food & Function*, vol. 5, no. 4, pp. 740–747, 2014.

[31] M. J. Oliveras-López, J. J. Molina, M. V. Mir, E. F. Rey, F. Martín, and H. L. de la Serrana, "Extra virgin olive oil (EVOO) consumption and antioxidant status in healthy institutionalized elderly humans," *Archives of Gerontology and Geriatrics*, vol. 57, no. 2, pp. 234–242, 2013.

[32] T. Weinbrenner, M. Fito, R. de la Torre et al., "Olive oils high in phenolic compounds modulate oxidative/antioxidative status in men," *The Journal of Nutrition*, vol. 134, pp. 2314–2321, 2004.

[33] P. Rosignoli, R. Fuccelli, R. Fabiani, M. Servili, and G. Morozzi, "Effect of olive oil phenols on the production of inflammatory mediators in freshly isolated human monocytes," *The Journal of Nutritional Biochemistry*, vol. 24, no. 8, pp. 1513–1519, 2013.

[34] V. Tufarelli, V. Laudadio, and E. Casalino, "An extra-virgin olive oil rich in polyphenolic compounds has antioxidant effects in meat-type broiler chickens," *Environmental Science and Pollution Research International*, vol. 23, no. 7, pp. 6197–6204, 2016.

[35] L. A. Faine, H. G. Rodrigues, C. M. Galhardi et al., "Effects of olive oil and its minor constituents on serum lipids, oxidative stress, and energy metabolism in cardiac muscle," *Canadian Journal of Physiology and Pharmacology*, vol. 84, no. 2, pp. 239–245, 2006.

[36] M. Jacomelli, V. Pitozzi, M. Zaid et al., "Dietary extra-virgin olive oil rich in phenolic antioxidants and the aging process: long-term effects in the rat," *The Journal of Nutritional Biochemistry*, vol. 21, no. 4, pp. 290–296, 2010.

[37] S. B. Pajovic, J. Kasapovic, and J. Martinovic, "Superoxide dismutase activities in different tissues of female rats treated with olive oil," *Physiological Research*, vol. 46, no. 5, pp. 381–384, 1997.

[38] L. D. DeLeve and N. Kaplowitz, "Importance and regulation of hepatic glutathione," *Seminars in Liver Disease*, vol. 10, no. 4, pp. 251–266, 1990.

[39] K. Aquilano, S. Baldelli, and M. R. Ciriolo, "Glutathione: new roles in redox signaling for an old antioxidant," *Frontiers in Pharmacology*, vol. 26, no. 5, p. 196, 2014.

[40] R. Masella, R. Varì, M. D'Archivio et al., "Extra virgin olive oil biophenols inhibit cell-mediated oxidation of LDL by increasing the mRNA transcription of glutathione-related enzymes," *The Journal of Nutrition*, vol. 134, no. 4, pp. 785–791, 2004.

[41] A. Akbarian, J. Michiels, J. Degroote, M. Majdeddin, A. Golian, and S. De Smet, "Association between heat stress and oxidative stress in poultry; mitochondrial dysfunction and dietary interventions with phytochemicals," *Journal of Animal Science and Biotechnology*, vol. 28, pp. 7–37, 2016.

[42] O. Altan, A. Pabuçcuoğlu, A. Altan, S. Konyalioğlu, and H. Bayraktar, "Effect of heat stress on oxidative stress, lipid peroxidation and some stress parameters in broilers," *British Poultry Science*, vol. 44, no. 4, pp. 545–550, 2003.

[43] H. Lin, R. Du, and Z. Y. Zhang, "Peroxide status in tissues of heat-stressed broilers," *Asian-Australasian Journal of Animal Sciences*, vol. 13, pp. 1373–1376, 2000.

[44] K. Sahin, C. Orhan, M. Tuzcu, S. Ali, N. Sahin, and A. Hayirli, "Epigallocatechin-3-gallate prevents lipid peroxidation and enhances antioxidant defense system via modulating hepatic nuclear transcription factors in heat-stressed quails," *Poultry Science*, vol. 89, no. 10, pp. 2251–2258, 2010.

[45] A. Cardinali, S. Pati, F. Minervini, I. D'Antuono, V. Linsalata, and V. Lattanzio, "Verbascoside, isoverbascoside, and their derivatives recovered from olive mill wastewater as possible food antioxidants," *Journal of Agricultural and Food Chemistry*, vol. 60, no. 7, pp. 1822–1829, 2012.

[46] F. Rubio-Senent, B. de Roos, G. Duthie, J. Fernández-Bolaños, and G. Rodríguez-Gutiérrez, "Inhibitory and synergistic effects of natural olive phenols on human platelet aggregation and lipid peroxidation of microsomes from vitamin E-deficient rats," *European Journal of Nutrition*, vol. 54, no. 8, pp. 1287–1295, 2015.

[47] I. Kafantaris, B. Kotsampasi, V. Christodoulou et al., "Grape pomace improves antioxidant capacity and faecal microflora of lambs," *Journal of Animal Physiology and Animal Nutrition*, 2016.

[48] R. de la Torre, "Bioavailability of olive oil phenolic compounds in humans," *Inflammopharmacology*, vol. 16, no. 5, pp. 245–247, 2008.

[49] P. Pignatelli, A. Ghiselli, B. Buchetti et al., "Polyphenols synergistically inhibit oxidative stress in subjects given red and white wine," *Atherosclerosis*, vol. 188, no. 1, pp. 77–83, 2006.

Hindawi
Oxidative Medicine and Cellular Longevity
Volume 2017, Article ID 4130967, 9 pages
https://doi.org/10.1155/2017/4130967

Research Article

Seabuckthorn Paste Protects Lipopolysaccharide-Induced Acute Lung Injury in Mice through Attenuation of Oxidative Stress

Leilei Du,[1,2] Xiaoxin Hu,[1] Chu Chen,[3] Tingting Kuang,[1] Hengfu Yin,[1] and Li Wan[2]

[1]*College of Ethnomedicine, Chengdu University of Traditional Chinese Medicine, Chengdu, China*
[2]*College of Pharmacy, Chengdu University of Traditional Chinese Medicine, Chengdu, China*
[3]*Sichuan Academy of Chinese Medicine Sciences, Chengdu, China*

Correspondence should be addressed to Li Wan; wanli8801@163.com

Received 15 May 2017; Accepted 9 July 2017; Published 16 August 2017

Academic Editor: Lin-sen Qing

Oxidative stress is one of the major mechanisms implicated in endotoxin-induced acute lung injury. Seabuckthorn paste (SP), a traditional Tibetan medicine with high content of polyphenols and remarkable antioxidant activity, is commonly used in treating pulmonary diseases. In the present study, the protective effects and possible underlying mechanisms of SP on lipopolysaccharide- (LPS-) induced acute lung injury in mice were investigated. It was found that body weight loss, lung tissue microstructure lesions, transvascular leakage increase, malondialdehyde augmentation, and the reduction of superoxide dismutase and glutathione peroxidase levels caused by LPS challenge were all consistently relieved by SP treatment in a dose-dependent manner. Moreover, accumulation of nuclear factor erythroid 2-related factor 2 (Nrf2) in lung nuclei caused by SP treatment was observed. Our study demonstrated that SP can provide significant protection against LPS-induced acute lung injury through maintaining redox homeostasis, and its mechanism involves Nrf2 nuclear translocation and activation.

1. Introduction

Acute lung injury (ALI) is a multifactorial process which occurs due to various environmental triggers that include those caused by direct and indirect lung injury. With persistent high morbidity and mortality owing to complicated pathogenesis and a pathological course, ALI has been drawing increasing attention as a critical disease in clinics. According to previous reports, ALI, induced either by hypoxic stress or by chemical irritation of endotoxin, is typically accompanied with alteration of redox homeostasis and oxidative damage to lipids, proteins, and DNA. Hypoxic stress significantly enhanced the oxidative stress markers such as free radicals and malondialdehyde, and it is accompanied with decreased levels of antioxidants such as glutathione, glutathione peroxidase, and superoxide dismutase [1, 2]. In the pathogenesis of lung injury caused by lipopolysaccharide (LPS), free radicals have been verified as the final causative molecules with both *in vitro* and *in vivo* evidences [3]. Trials involving antioxidant supplementation revealed consistent results, among which alleviated damage to macromolecules induced by high altitude or endotoxin was observed [1–3].

Seabuckthorn (*Hippophae rhamnoides* L., Elaeagnaceae) has been used for a long history in Tibetan folk medicine. It is considered as a valuable herb in treating certain diseases including pulmonary conditions and in easing syndromes in unacclimatized persons on ascent to high altitude. Traditionally, seabuckthorn berries are collected and stewed in water before the extracted solution is filtered and condensed into a paste (seabuckthorn paste (SP)), which is a common preparation used in clinical practice. The edible berries of seabuckthorn contain a wild variety of oxidation-resistant compounds including relative high contents of vitamins and polyphenols [4] and can serve as a desirable natural antioxidant mixture. Based on these facts, we hypothesized that administration of seabuckthorn paste may enhance the antioxidant defense system and thus provide protection against ALI.

The transcription factor Nrf2 (nuclear factor erythroid 2-related factor 2) is a major regulator of the adaptive

Table 1: Animal experimental protocol.

Mice	Analysis Items
Batch I ($n = 50$)	Body weight, lung water content
Batch II ($n = 50$)	Body weight, bronchoalveolar lavage fluid (BALF) analysis, histopathology, immunofluorescence
Batch III ($n = 50$)	Body weight, oxidative stress markers, western blot

Mice in each batch were divided into five groups: (i) normal control group, (ii) model group, (iii) high-dose SP group (200 mg/kg), (iv) medium-dose SP group (400 mg/kg), and (v) low-dose SP group (800 mg/kg) ($n = 10$ for each group).

response to oxidative stress and orchestrates the expression of a large battery of cytoprotective genes such as antioxidants, phase II enzymes, and membrane transporters [5]. Under quiescent conditions, the transcription factor Nrf2 interacts with the actin-anchored protein Keap1, largely localized in the cytoplasm. This quenching interaction maintains low basal expression of Nrf2-regulated genes. However, upon recognition of chemical signals imparted by oxidative and electrophilic molecules, Nrf2 is released from Keap1, escapes proteasomal degradation, translocates to the nucleus, and transactivates the expression of several dozen cytoprotective genes that enhance cell survival [6].

Therefore, the present study was undertaken to investigate the effects of seabuckthorn paste in LPS-induced ALI in mice and to explore the possible mechanism in a perspective of redox homeostasis through its influence on the Nrf2 pathway.

2. Materials and Methods

2.1. Plant Material. Well-ripened seabuckthorn berries were collected from a natural growth site of a hilly region in the eastern margin of the Tibetan Plateau (Ma'erkang, Sichuan Province, China). Voucher specimens (number MZC-SJ-20160915-00~08) of the plant material are preserved in the herbarium of Chengdu University of Traditional Chinese Medicine after botanical identification.

2.2. Preparation of Seabuckthorn Paste. According to traditional process, 1 kg of seabuckthorn berries was boiled in 5 L water for 30 min and the supernatant was decanted, and the residue was reboiled in fresh water. The process was repeated three times for complete extraction. All the supernatants were pooled and filtered through a muslin cloth and condensed on a heater to obtain SP. The yield of SP from fresh berries was 13.88%, and the water content was 33.52%, calculated gravimetrically.

2.3. Antioxidant Activity In Vitro. Free radical scavenging activity was studied using 1,1-diphenyl-2-picrylhydrazyl (DPPH) while the total radical scavenging capacity was determined by the 2,2-azinobis-(3-ethylbenzothiazoline-6-sulfonic acid) (ABTS) assay, according to the procedures described by Debnath et al. [7]. Also, hydroxyl radical scavenging capacity was evaluated by the method described by Hazra et al. [8]. Trolox was used as standard, and the ability to scavenge radicals was expressed as IC_{50}, which is defined as the concentration of the tested material required to cause a 50% decrease in initial DPPH/ABTS/hydroxyl radical concentration.

The contents of total polyphenols and total flavonoids in SP were determined by colorimetry according to the method described in previous reports [9, 10].

All measurements were performed in triplicate and reported as mean ± standard deviation (SD).

2.4. Animals. Six to eight-week-old male SPF KM mice weighing 20 ± 2 g were purchased from Dashuo Biotechnology Co Ltd. (Chengdu, China). The animals were maintained at 24 ± 0.5°C with food and water ad libitum. The experimental protocol is shown in Table 1. The study protocol was approved by the institute's animal ethical committee and conformed to the national guidelines on the use and care of laboratory animals.

After acclimatization for 2 days, the mice were randomly allocated into groups. The animals in the SP treatment groups received respective dose of SP, while the animals in the control and model groups received saline, once daily through intragastric route for seven consecutive days. On Day 8, the mice of all groups except for the control group were administered 10 mg/kg LPS (O55:B5) (Sigma, USA) intraperitoneally. The animals were sacrificed 10 h after LPS injection.

2.5. Body Weight Changes. The body weight of each mouse in each group was recorded before and 10 h after LPS injection, and body weight ratio was calculated by the formula: $R = (Wa - Wb)/Wb$, of which Wa and Wb represent body weight recorded 10 h after and immediately before LPS injection, respectively.

2.6. Bronchoalveolar Lavage Fluid (BALF) Analysis. A median sternotomy was performed for exposure of both lungs. The trachea was exposed and an intravenous infusion needle was inserted. The lungs were lavaged three times with 0.5 ml of ice-cold phosphate-buffered saline. Returned lavage fluid was pooled for each animal and centrifuged at 1000 ×g for 10 min at 4°C. The cell-free supernatants were harvested for total protein analysis using the BCA protein assay kit (Nanjing Jiancheng Bioengineering Institute, China).

2.7. Lung Water Content. Lung water content was used as an index to estimate the degree of pulmonary edema. After the animal was sacrificed, the lungs were excised en bloc, blot dried, and placed on preweighed glass plates. The wet weight of the tissue was registered immediately. Then the tissue was placed in an incubator at 80°C for 72 h to obtain a constant weight. After the dry weight of the tissue was registered, the

Table 2: DPPH, ABTS, and hydroxyl radical scavenging activities and total polyphenols/flavonoids contents of the seabuckthorn paste.

Sample	IC_{50} (μg/ml)[a]			Content (mg/g)	
	DPPH radical[b]	ABTS radical[b]	Hydroxyl radical[b]	Total polyphenols[b]	Total flavonoids[b]
SP	18.54 ± 0.78	9.75 ± 0.35	1.43 ± 0.10	191.5 ± 5.78	130.9 ± 4.25
Trolox[c]	5.39 ± 0.12	3.02 ± 0.11	1.07 ± 0.08	—	—

[a]IC_{50} (μg/ml): the concentration at which 50% is inhibited. [b]Each value is expressed as mean ± standard deviation ($n = 3$). [c]Trolox as positive control.

water content of the tissue was calculated according to the formula: lung water content (%) = (wet weight − dry weight)/dry weight × 100% [9].

2.8. Histopathologic Analysis. The lungs were harvested at 10 h after LPS administration and fixed with an intratracheal instillation of 1 ml buffered formalin (10%, pH 7.2). The lobe was further fixed in 10% neutral buffered formalin for 48 h at 4°C. The tissues were embedded in paraffin wax. The sections approximately 5 μm thick were stained with hematoxylin and eosin using a standard protocol and observed under a light microscope for histopathological changes such as alveolar septum lesion, inflammatory cell infiltration, and blood stasis.

2.9. Immunofluorescence Studies. Nuclear factor erythroid 2-related factor 2 (Nrf2) nuclear translocation in lung cells was determined by immunofluorescence technique described by Lindl and Sciutto [11]. The sections of the lung tissue prepared as mentioned above were deparaffinized and rehydrated through submersion in graded alcohols. Antigen retrieval was performed with 10 mM citrate buffer pH 6 for 5 min in a microwave oven. The antibody used for immunostaining the V5-tagged protein was anti-V5-FITC (Invitrogen), and for visualizing the endogenous protein, the cells were probed with Nrf2 antibody. The fluorescein isothiocyanate- (FITC-) conjugated anti-rabbit antibody was used as a secondary antibody. To visualize the nuclei, the cells were stained with DAPI. The fluorescent images were captured using appropriate filters in a Nikon inverted fluorescent microscope. The antibodies were achieved from Wuhan Servicebio Technology Co Ltd. (Wuhan, China).

2.10. Oxidative Stress Markers In Vivo. The lung samples were homogenized with KCl solution (0.154 mol/L) in ice-cold condition and centrifuged at 3000 ×g for 15 min at 4°C. The supernatants were immediately stored at −80°C until assayed for malondialdehyde (MDA), glutathione peroxidase (GSH-Px), and superoxide dismutase (SOD) using respective kits (Nanjing Jiancheng Bioengineering Institute, China) according to instruments provided by the manufacturer.

2.11. Western Blot Analysis. The lung tissue homogenate was centrifuged (12,000 ×g, 10 min, 4°C) and the supernatants were aspirated. Biochemical fractionation of the cells was done using the nuclear extract kit (Active Motif, USA) according to the manufacturer's instructions. Protein concentrations were determined by the Bradford method [12]. Proteins were loaded and transferred to a PVDF membrane (Millipore, USA). After being blocked, the membranes were incubated overnight at 4°C with anti-Nrf2 (1 : 1000, Millipore) antibodies. The membranes were then incubated for 1 h at room temperature with horseradish peroxidase- (HRP-) labeled goat anti-rabbit secondary antibody (1 : 4000, Vector, Burlingame, USA). The membranes were placed into a gel imaging system (Bio-Rad, ChemiDoc XRS, USA) and then exposed. The intensity of blots was quantified using the Quantity One analysis software (Bio-Rad, USA). Lamin B was used as an internal control.

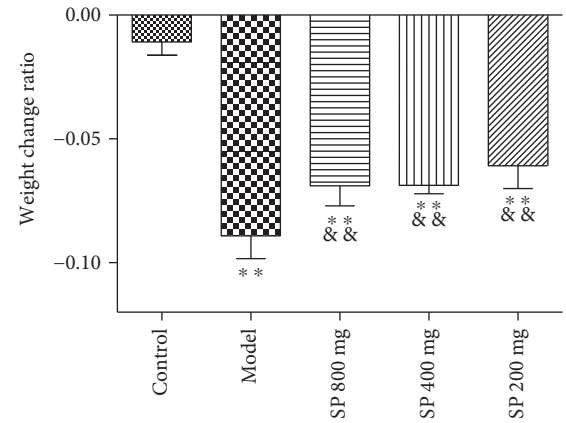

Figure 1: Body weight change ratios ($n = 30$). $^{**}P < 0.01$ versus control; $^{\&\&}P < 0.01$ versus model.

2.12. Statistical Analysis. Data were expressed as mean ± standard deviation. All statistical analysis was performed with SPSS 17.0 software package (SPSS Inc., Chicago, USA). Statistically significant differences between groups were determined by ANOVA followed by Tukey's test. The results were considered statistically significant if P values were <0.05.

3. Results

3.1. Antioxidant Activity In Vitro. The results of the three different methods to evaluate radical scavenging activities indicated that SP has strong antioxidant activity in the same order of magnitude with that of the positive control trolox. The values of IC_{50} are shown in Table 2.

3.2. Body Weight Change Ratio. LPS injection caused body weight loss in each treatment group. Ten hours after injection, the average weight of the model group was significantly reduced compared to that of the control group ($P < 0.01$). While SP provided protection to some extent, weight change ratios in all SP-treated groups were significantly decreased than that of the model group ($P < 0.01$), as shown in Figure 1. Low dose seemed to provide slightly better

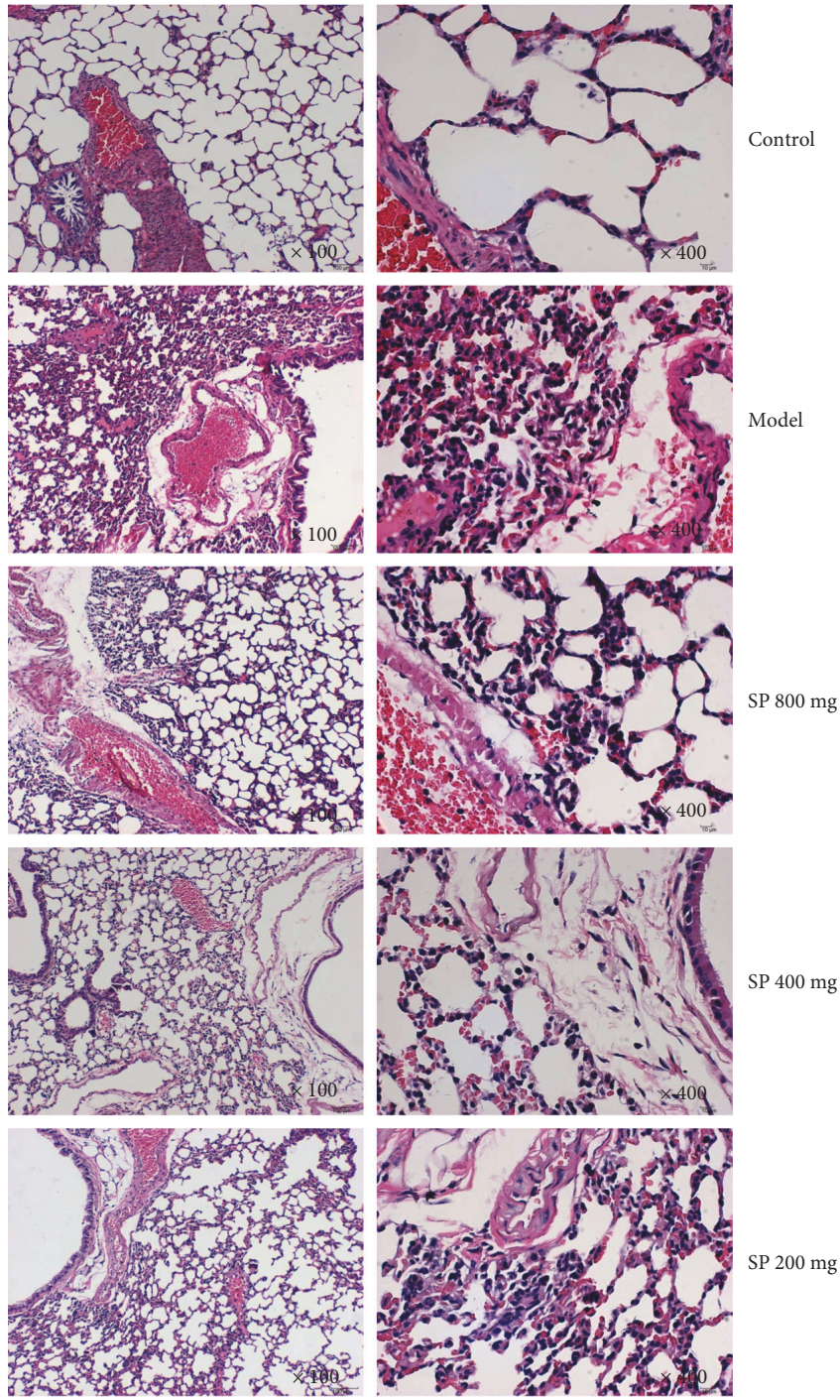

Figure 2: Effects of the seabuckthorn paste on the lung histopathological changes (hematoxylin-eosin stain, ×100 and ×400).

protection than medium and high dose (-0.061 ± 0.009, -0.069 ± 0.03, and -0.069 ± 0.008 for 200, 400, and 800 mg/kg dose, resp.). Whether the difference has practical significance is not clear yet.

3.3. Histopathologic Observations. As shown in Figure 2, the lung tissues from the control group represented normal structure without histopathologic changes under a light microscope. In the LPS-induced ALI mice of the model group, the lungs stained with hematoxylin-eosin indicated widespread alveolar wall thickness caused by edema, severe hemorrhage in the alveolus, alveolus collapse, and obvious inflammatory cell infiltration. In the SP-pretreated groups, the histopathologic lesions were minor compared with those in the model group.

3.4. Lung Water Content. The lung water content in normal control animals varied between 77.21% and 80.12% with a mean of $78.63 \pm 0.98\%$. The mean value of $80.48 \pm 0.73\%$ in mice of the model group was significantly higher ($P < 0.01$)

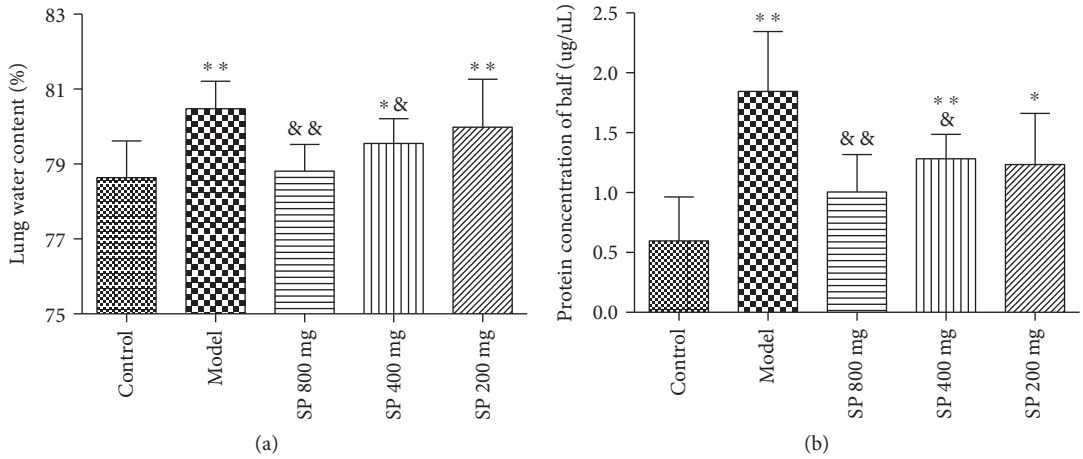

Figure 3: Effects of the seabuckthorn paste on the lung's transvascular leakage of fluid (a) and total proteins (b) ($n = 10$). $^{*}P < 0.05$ or $^{**}P < 0.01$ versus control; $^{\&}P < 0.05$ or $^{\&\&}P < 0.01$ versus model.

than that of the normal control group. The lung water contents in the SP 800 mg group and SP 400 mg group animals were both significantly lower ($P < 0.01$ and $P < 0.05$, $78.81 \pm 0.72\%$ and $79.55 \pm 0.66\%$ for 800 and 400 mg/kg dose, resp.) than that of the model group, while water content difference between the SP 200 mg/kg group and model group has no statistical significance. Animals in the 800 mg/kg SP group had substantial alleviation with no significant difference in water content comparing to that of the control group, as shown in Figure 3(a).

3.5. Total Protein Content in BALF. The mean BALF protein content in model animals was significantly higher (1.84 ± 0.50 mg/ml) ($P < 0.01$) as compared with the normal control values (0.60 ± 0.37 mg/ml). Pretreatment with SP provided remarkable protection against protein transvascular leakage, with BALF protein contents in high and medium SP dose groups significantly lower ($P < 0.01$ and $P < 0.05$, $1.00 \pm 0.31$and 1.28 ± 0.21 mg/ml for 800 and 400 mg/kg dose, resp.) than that of the model group, and the low SP dose group indicated a lower mean value yet without statistical significance (1.24 ± 0.43 mg/ml for 200 mg/kg dose), as shown in Figure 3(b). Notably, high dose of SP provided a strong protection that protein content in BALF in the 800 mg/kg group has no significant difference comparing to that of normal control animals.

3.6. Oxidative Stress Markers. LPS injection caused a significant increase ($P < 0.01$) (2.06 ± 0.36 nmol/mg) in the oxidative stress marker MDA levels in the lung homogenates than in the control group (1.22 ± 0.21 nmol/mg). The pretreatment of SP-attenuated MDA generation (1.66 ± 0.36, 1.83 ± 0.17, and 1.87 ± 0.14 nmol/mg for 800, 400, and 200 mg/kg dose, resp.) as compared with the model group and the difference between the 800 mg/kg group and model group have statistical significance ($P < 0.01$).

The levels of two antioxidant enzymes in the lung homogenates were significantly lower ($P < 0.01$) in the model group (4.37 ± 0.52 U/mg for SOD and 25.99 ± 2.81 μmol/mg for GSH-Px) than that of the control group (6.01 ± 0.65 U/mg for SOD and 36.00 ± 1.92 μmol/mg for GSH-Px). The pretreatment of animals with SP caused a marked increase in the level of SOD (5.61 ± 1.46, 5.43 ± 0.55, and 5.21 ± 0.66 U/mg for 800, 400, and 200 mg/kg dose, resp.) and GSH-Px (30.41 ± 4.40, 28.96 ± 3.97, and 31.34 ± 4.09 μmol/mg for800, 400, and 200 mg/kg dose, resp.) as compared with the model group. Statistical significance is evident in 400 mg/kg dose for SOD ($P < 0.01$) and also in 800 and 200 mg/kg dose for GSH-Px ($P < 0.01$).

These results are shown in Figure 4.

3.7. Lung Nrf2 Immunofluorescence Observations. As evident from Figure 5, immunofluorescence results showed varying degrees of enrichment of the Nrf2 protein both in the nuclear fraction and in the cytoplasmic fraction in lung cells upon a different dose SP treatment, comparing with control and model groups. The increased Nrf2 protein in the nucleus suggested translocation of the Nrf2 protein into the nuclei, which is considered as the starting point of Nrf2 pathway activation.

3.8. Nrf2 Protein Expression in Lung Nuclei. As Figure 6 shows, SP treatment caused increased Nrf2 accumulation in the nuclear fraction. Nuclear Nrf2 level in the model group (0.30 ± 0.03) has a significant increase compared to that of the control group (0.15 ± 0.06) ($P < 0.01$), while more pronounced increases were observed in the SP groups of different dose (0.47 ± 0.06, 0.42 ± 0.05, and 0.40 ± 0.07 for 800, 400, and 200 mg/kg dose, resp.), all with statistical significance compared to that of the model group ($P < 0.01$ versus model group).

4. Discussion

In the present study, we have demonstrated that traditional Tibetan medicine seabuckthorn paste has strong radical scavenging activities on par with trolox. Seabuckthorn berries contain high amount of polyphenols especially flavonoids,

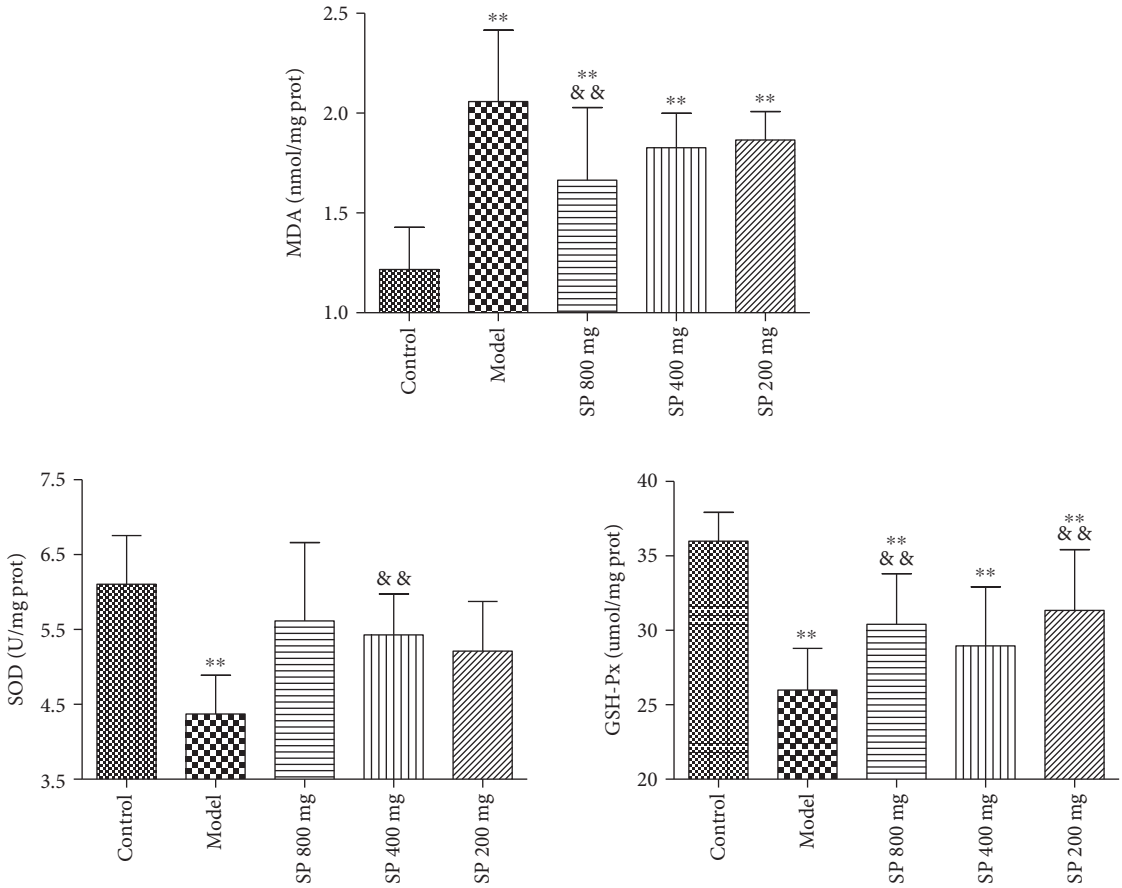

Figure 4: Effects of the seabuckthorn paste on the oxidative stress markers *in vivo* ($n = 10$). $^{**}P < 0.01$ versus control; $^{\&\&}P < 0.01$ versus model.

which are partly responsible for its potent antioxidative capacity. Our results consisted with previous reports that seabuckthorn is a desirable natural antioxidant resource possessing a variety of functions that improve health, such as alleviating atherosclerosis, reversing hyperthyroidism, reducing inflammation, relieving gastric ulcers, and preventing liver cirrhosis [13, 14]. However, the harvest of seabuckthorn berries is seasonal, and matured berries are easily to decay. In order to access this valuable medicine whenever necessary, Tibetans developed a process to make these berries into a paste, which could be stored for a long time conveniently. The oxidation resistance evaluation results in this study proved that the preparation of SP retains high content of polyphenols/flavonoids and potent antioxidative activities, thus may have health benefits similar to seabuckthorn berries.

LPS exposure causes general toxic responses including body weight loss and anorexia [15, 16], which were effectively reversed by SP pretreatment in the present study. As for local lesions, microstructure changes were observed in the lungs under LPS challenge, with obvious alleviation in the mice of SP treatment groups as per expectation. These results demonstrated that administration of SP in mice provided remarkable protection against LPS-induced acute lung injury. Previous studies showed that LPS exposure increased airway epithelium barrier paracellular permeability, associated with elevated levels of leakage for fluids, proteins, and other vascular components [17–19]. And the increased leakage contributes to diseases such as acute respiratory distress syndrome and pulmonary edema. Pretreatment with SP caused a marked decline in transvascular fluid leakage into the lungs besides curtailing leakage of proteins into the alveoli. These results suggest that SP may help maintain alveolar arterial capillary membrane integrity, thereby blocking pathological progress towards lethal conditions.

We explored the protection mechanism of SP on LPS-induced acute lung lesion in a perspective of redox homeostasis. High-dose exposure of LPS can trigger toxic inflammatory reactions through reactive oxygen and nitrogen species, and excessive production of these radicals is implicated to damage biomembranes, thereby compromising cell integrity and function and resulting in increased pulmonary capillary permeability [20–22]. Hence, the oxidative stress marker (MDA) and antioxidant enzymes (SOD, GSH-Px) in the lung homogenates of different groups of animals were measured. The increase in level of MDA and decrease in levels of SOD and GSH-Px caused by LPS stimulation were reversed in animals of SP treatment groups, indicating that SP could provide a significant protection against LPS-induced oxidative damage.

Based on the positive antioxidant results *in vivo*, we investigated the involvement of the Nrf2 pathway under SP

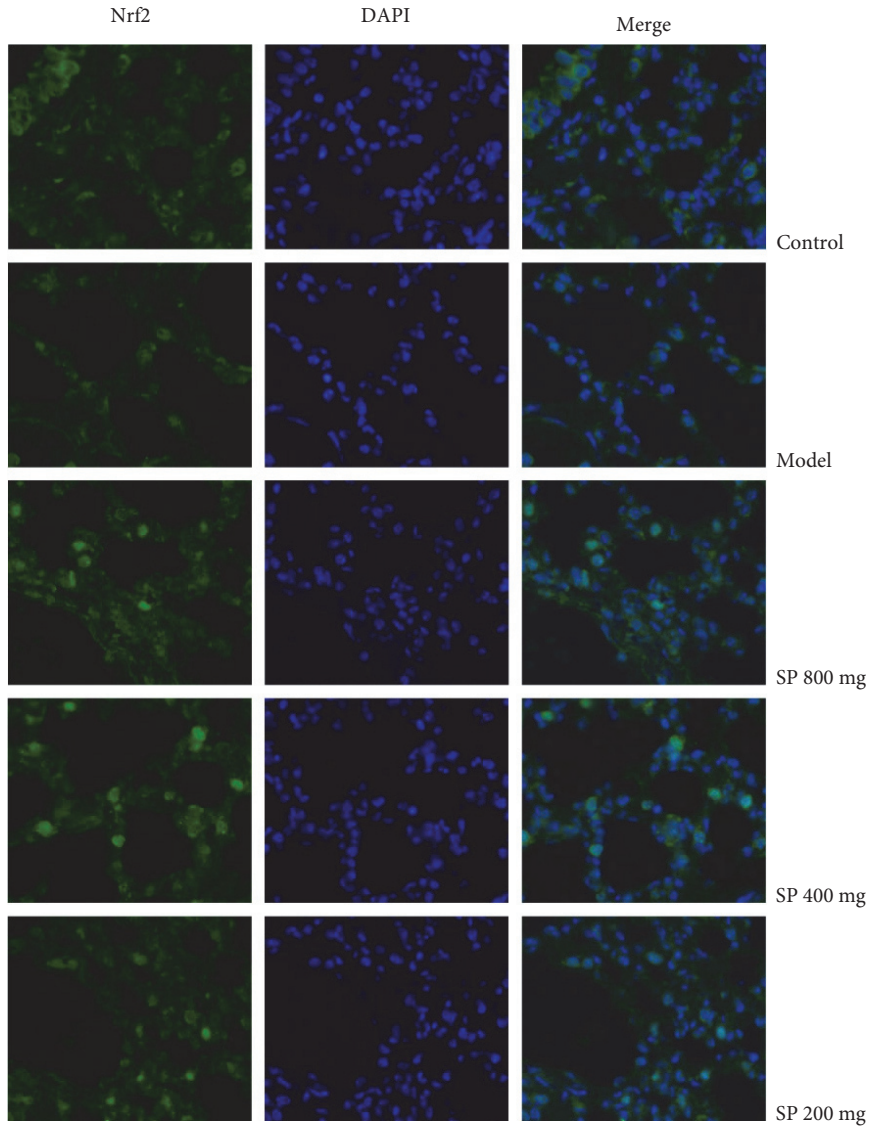

Figure 5: Effects of the seabuckthorn paste on Nrf2 nuclear translocation in lung cells (×400). Nrf2 localization was determined by immunofluorescence staining with anti-Nrf2 antibody followed by fluorescence-tagged secondary antibody. DAPI was used to visualize the nuclei in blue filter.

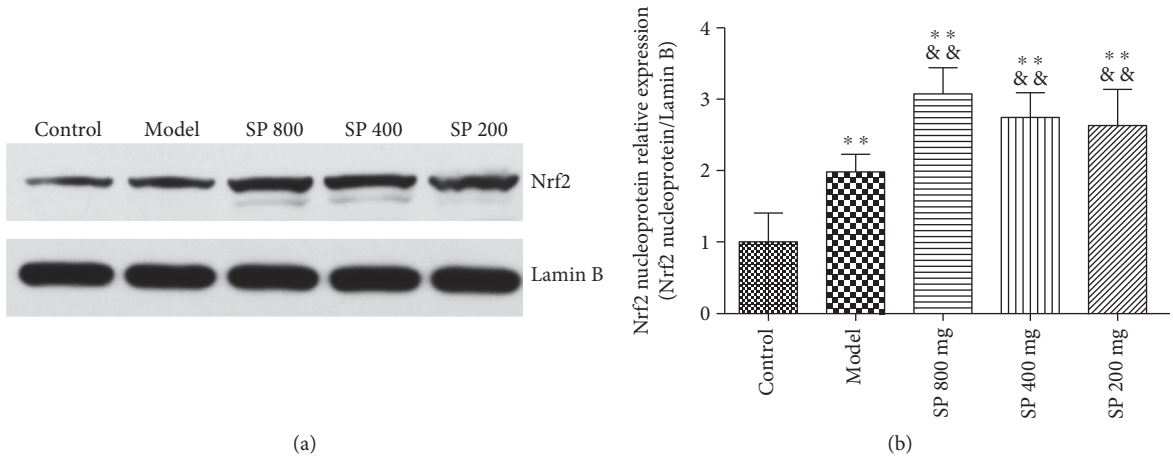

Figure 6: Effects of the seabuckthorn paste on the nuclear Nrf2 protein expression. Nuclear Nrf2 expression was detected by western blot (a) and the density of immunoreactive bands was analyzed (b). $^{**}P < 0.01$ versus control; $^{\&\&}P < 0.01$ versus model.

exposure. Nrf2 transcription factor is one of the most important antioxidant defense mechanisms that protect cells and tissues from various oxidative stresses. The accumulation of Nrf2 from the cytoplasm to nucleus is an essential signaling start for Nrf2 media regulation of antioxidant/detoxification enzymes [23, 24]. Immunofluorescence and western blot results in this study indicate that LPS stimulation increased the level of Nrf2 in the nuclei, as a stress response of the body defense system. And SP treatment resulted further elevation of Nrf2 accumulation in the nuclear fraction, confirming the occurrence of Nrf2 translocation and activation. Furthermore, dose-response relationships were observed in the assays. Therefore, the protective effect of SP on LPS-induced ALI is clearly associated with attenuation of oxidant stress, and the underlying mechanism through which SP exert antioxidant properties involves Nrf2 pathway activation.

In conclusion, we demonstrated that the seabuckthorn paste with relative high contents of polyphenols and flavonoids has potent antioxidant activities *in vitro* and *in vivo*. This traditional medicine can provide strong protection in mice against LPS-induced acute lung injury through maintaining redox homeostasis, and its mechanism involves Nrf2 nuclear translocation and activation.

Conflicts of Interest

The authors declare that they do not have any conflicts of interest.

Acknowledgments

The present research was supported by the National Natural Science Foundation of China (no. 81503361).

References

[1] T. Bakonyi and Z. Radak, "High altitude and free radicals," *Journal of Sports Science & Medicine*, vol. 3, no. 2, pp. 64–72, 2004.

[2] A. Dosek, H. Ohno, Z. Acs, A. W. Taylor, and Z. Radak, "High altitude and oxidative stress," *Respiratory Physiology & Neurobiology*, vol. 158, no. 2, pp. 128–131, 2007.

[3] K. Sato, M. B. Kadiiska, A. J. Ghio et al., "In vivo lipid-derived free radical formation by NADPH oxidase in acute lung injury induced by lipopolysaccharide: a model for ARDS," *The FASEB Journal*, vol. 16, no. 13, pp. 1713–1720, 2002.

[4] S. M. Sabir, H. Maqsood, H. Imran, M. Q. Khan, and A. Khaliq, "Elemental and nutritional analysis of sea buckthorn (Hippophae rhamnoides ssp. turkestanica) berries of Pakistani origin," *Journal of Medicinal Food*, vol. 8, pp. 518–522, 2005.

[5] O. A. Sawaf, T. Clarner, A. Fragoulis et al., "Nrf2 in health and disease: current and future clinical implications," *Clinical Science*, vol. 129, pp. 989–999, 2015.

[6] T. W. Kensler, N. Wakabayashi, and S. Biswal, "Cell survival responses to environmental stresses via the Keap1-Nrf2-ARE pathway," *Annual Review of Pharmacology and Toxicology*, vol. 47, pp. 89–116, 2007.

[7] T. Debnath, P. J. Park, N. C. Debnath, N. B. Samad, H. W. Park, and B. O. Lim, "Antioxidant activity of Gardenia jasminoides Ellis fruit extracts," *Food Chemistry*, vol. 128, pp. 697–703, 2011.

[8] B. Hazra, S. Biswas, and N. Mandal, "Antioxidant and free radical scavenging activity of Spondias pinnata," *BMC Complementary and Alternative Medicine*, vol. 128, pp. 63–72, 2008.

[9] J. Liu, C. Wang, Z. Z. Wang, C. Zhang, S. Lu, and J. Liu, "The antioxidant and free-radical scavenging activities of extract and fractions from corn silk (Zea mays L.) and related flavone glycosides," *Food Chemistry*, vol. 126, pp. 261–269, 2011.

[10] C. C. Chang, M. H. Yang, H. M. Wen, and J. C. Chern, "Estimation of total flavonoid content in propolis by two complementary colorimetric methods," *Journal of Food and Drug Analysis*, vol. 10, no. 3, pp. 178–182, 2002.

[11] K. A. Lindl and K. L. Sciutto, "Examining the endogenous antioxidant response through immunofluorescent analysis of Nrf2 in tissue," *Methods in Molecular Biology*, vol. 477, pp. 229–243, 2008.

[12] M. M. Bradford, "A rapid and sensitive method for the quantitation of microgram quantities of protein utilizing the principle of protein-dye binding," *Analytical Biochemistry*, vol. 72, no. 1-2, pp. 248–254, 1976.

[13] B. Yang and H. Kallio, "Composition and physiological effects of seabuckthorn (Hippophae) lipids," *Trends in Food Science & Technology*, vol. 13, pp. 160–167, 2002.

[14] S. M. Sabir, H. Maqsood, H. Imran, M. Q. Khan, and A. Khaliq, "Elemental and nutritional analysis of sea buckthorn (Hippophae rhamnoides ssp. turkestanica) berries of Pakistani origin," *Journal of Medicinal Food*, vol. 8, pp. 518–522, 2005.

[15] A. Cerami, Y. Ikeda, and N. L. Trang, "Weight loss associated with an endotoxin-induced mediator from peritoneal macrophages: the role of cachectin (tumor necrosis factor)," *Immunology Letters*, vol. 8, pp. 173–177, 1985.

[16] K. Lee, J. F. Ewing, and P. M. Sluss, "Effect of bacterial lipopolysaccharide on growth of murine bladder cancer, MBT-2," *Urological Research*, vol. 17, no. 5, pp. 285–288, 1989.

[17] H. Eutamene, V. Theodorou, F. Schmidlin et al., "LPS-induced lung inflammation is linked to increased epithelial permeability: role of MLCK," *European Respiratory Journal*, vol. 25, pp. 789–796, 2005.

[18] B. Yang, X. P. Li, and Y. F. Ni, "Protective effect of isorhamnetin on lipopolysaccharide induced acute lung injury in mice," *Inflammation*, vol. 39, no. 1, pp. 129–137, 2016.

[19] H. Zhang and G. Y. Sun, "LPS induces permeability injury in lung microvascular endothelium via AT_1 receptor," *Archives of Biochemistry and Biophysics*, vol. 441, no. 1, pp. 75–83, 2005.

[20] G. Kallapura, N. R. Pumford, X. H. Velasco, B. Hargisand, and G. Tellez, "Mechanisms involved in lipopolysaccharide derived ROS and RNS oxidative stress and septic shock," *Journal of Microbiology Research and Reviews*, vol. 2, no. 1, pp. 6–11, 2014.

[21] G. Vanita, G. Asheesh, S. Shalini, M. D. Harish, S. K. Grover, and K. Ratan, "Anti-stress and adaptogenic activity of L-arginine supplementation," *Evidence-Based Complementary and Alternative Medicine*, vol. 2, no. 1, pp. 93–97, 2005.

[22] J. Herget, J. Wilhelm, J. Novotna et al., "A possible role of the oxidant tissue injury in the development of hypoxic pulmonary hypertension," *Physiological Research*, vol. 49, no. 5, pp. 493–501, 2000.

[23] K. Sahin, C. Orhan, Z. Tuzcu, M. Tuzcu, and N. Sahin, "Curcumin ameloriates heat stress via inhibition of oxidative stress and modulation of Nrf2/HO-1 pathway in quail," *Food and Chemical Toxicology*, vol. 50, no. 11, pp. 4035–4041, 2012.

[24] J. W. Kaspar, S. K. Niture, and A. K. Jaiswal, "Nrf2:INrf2 (Keap1) signaling in oxidative stress," *Free Radical Biology and Medicine*, vol. 47, no. 9, pp. 1304–1309, 2009.

Hindawi
Oxidative Medicine and Cellular Longevity
Volume 2017, Article ID 7091904, 9 pages
https://doi.org/10.1155/2017/7091904

Research Article

Rosmarinic Acid Alleviates the Endothelial Dysfunction Induced by Hydrogen Peroxide in Rat Aortic Rings via Activation of AMPK

Hui Zhou,[1] Baocai Fu,[2] Bo Xu,[1] Xiangquan Mi,[3] Gang Li,[1] Chengjun Ma,[1] Jianxin Xie,[3] Ji Li,[1] and Zhenhua Wang[1]

[1]*Center for Mitochondria and Healthy Aging, College of Life Sciences, Yantai University, Yantai 264005, China*
[2]*Intensive Care Unit, Yantaishan Hospital, Yantai 264001, China*
[3]*School of Medicine, Shihezi University, Shihezi 832002, China*

Correspondence should be addressed to Ji Li; lijimelissafang@yahoo.com and Zhenhua Wang; zhenhuawang@tom.com

Received 7 April 2017; Revised 9 June 2017; Accepted 20 June 2017; Published 13 August 2017

Academic Editor: Jie Li

Endothelial dysfunction is the key player in the development and progression of vascular events. Oxidative stress is involved in endothelial injury. Rosmarinic acid (RA) is a natural polyphenol with antioxidative, antiapoptotic, and anti-inflammatory properties. The present study investigates the protective effect of RA on endothelial dysfunction induced by hydrogen peroxide (H_2O_2). Compared with endothelium-denuded aortic rings, the endothelium significantly alleviated the decrease of vasoconstrictive reactivity to PE and KCl induced by H_2O_2. H_2O_2 pretreatment significantly injured the vasodilative reactivity to ACh in endothelium-intact aortic rings in a concentration-dependent manner. RA individual pretreatment had no obvious effect on the vasoconstrictive reaction to PE and KCl, while its cotreatment obviously mitigated the endothelium-dependent relaxation impairments and the oxidative stress induced by H_2O_2. The RA cotreatment reversed the downregulation of AMPK and eNOS phosphorylation induced by H_2O_2 in HAEC cells. The pretreatment with the inhibitors of AMPK (compound C) and eNOS (L-NAME) wiped off RA's beneficial effects. All these results demonstrated that RA attenuated the endothelial dysfunction induced by oxidative stress by activating the AMPK/eNOS pathway.

1. Introduction

The vascular endothelium plays critical roles in maintaining the vascular structure and function [1]. In physiological states, the endothelium releases both relaxing and contracting factors including nitric oxide (NO), prostacyclin, and endothelin, which contribute to the local regulation of vascular tone and the coagulation [2].

Endothelial cells also secrete the reactive oxygen species (ROS), especially the hydrogen peroxide (H_2O_2), as the fast diffusion signal to recruit the leukocytes to the injury site and the endothelial NADPH oxidase is the main source of ROS [3]. Whereas excess ROS will result in oxidative stress which contributes to vascular dysfunction in cardiovascular events [4], diabetes [5], stroke [6], atherosclerosis [7], and so forth, it is becoming increasingly clear that oxidative stress contributed to the development of the macrovascular complications [8]. Indeed, recent studies have shown that the mechanism of endothelial dysfunction is largely due to the reduced bioavailability of endothelium-derived NO by oxidative stress [9]. The presence of ROS not only reduces the bioavailability of NO [10] but also results in the eNOS uncoupling which will result in more ROS formation [11].

Accumulating evidences from bench to bed support the free radical scavenging properties of phenolic antioxidants and the pharmacological activities against oxidative stress-mediated vascular disorders. Such (cases?) as resveratrol [12], curcumin [13], and the flavanol (−)-epicatechin [14] showed widely protective effects on the endothelial cells

in vivo and *in vitro*. Rosmarinic acid is one of the most potent antioxidants among the simple phenolic compounds [15]. Rosmarinic acid (α-O-caffeoyl-3, 4-dihydroxyphenyl lactic acid; RA) is a natural phenol antioxidant contained in some Labiatae family plants used in traditional medicine and phytotherapy such as *Perilla frutescens* (L.) Britt., *Salvia miltiorrhiza* Bge., *Rosmarinus officinalis* L., and *Lavandula angustifolia* Mill. RA possesses many bioactivities including antioxidative, astringent, anti-inflammatory, antimicrobial, antiangiogenic, antiviral, antirheumatic, antiallergic, antidepressant, antidiabetic, and antitumor effects [16]. Sotnikova et al. proved that RA improved the reactivity to phenylephrine of aortic rings and prevented the upregulation of IL-1β, TNF-α, and endothelin pathway in diabetic rats *in vivo* [8], while the effects on endothelium-dependent vasodilation were not investigated. Here, we established an oxidative injury with hydrogen peroxide (H_2O_2) and investigated the protective effects of RA on endothelium-dependent vasodilation mediated by acetylcholine (ACh) and the underlying mechanisms. Our results demonstrated that the protective activities of RA are mediated by an AMPK-eNOS signaling pathway.

2. Materials and Methods

2.1. Chemicals. Rosmarinic acid, acetylcholine (ACh), compound C,5-aminoimidazole-4-carboxamide-1-β-D-ribofuranoside (AICAR), apocynin, and diphenyliodonium were purchased from Sigma Chemical Co. (St. Louis, MO, USA); phenylephrine (PE) and *l*-N-nitro arginine methyl ester (L-NAME) were purchased from Aladdin Industrial Co. (Shanghai, China). The other reagents were of analytical purity.

2.2. Animals. Three-month-aged male Wistar rats (200–250 g) were obtained from the Animal Center of Shandong Luye Pharmaceutical Co. Ltd. (Yantai, China). The rats were maintained in a 12 h light/dark cycle and had free access to food and water. All experimental procedures were approved by the Institutional Animal Care and Use Committee of National Institute of Pharmaceutical Education and Research.

2.3. Preparation of Rat Aortic Rings. The thoracic aorta was isolated and placed in 4°C modified Krebs-Henseleit (K-H) solution (mM: NaCl, 118; KCl, 4.7; KH_2PO_4, 1.2; $MgSO_4$, 1.2; $NaHCO_3$, 25.0; $CaCl_2$, 2.5; D-glucose, 10.0. pH 7.4, [17]). The excess connective tissue was carefully cleaned and the aorta was cut into segments approximately 3 mm long. In some experiments, the aortic endothelium was removed by the paper clip. The tension of the aortic ring was recorded with a linear force transducer, and the K-H solution was aired with a 95% O_2 and 5% CO_2 mixture and maintained at 37°C. All the vessels were equilibrated for 1 h and the basic tension was adjusted to 2.0 g before the experiment. During the equilibration period, the K-H solution was replaced every 15 min. At the beginning of an experiment, the aortic rings were exposed to 80 mM KCl for 3 times until the responses were stable. The intact endothelium function was verified by the relaxation reaching more than 85% induced by ACh (10 μM) to induce in the precontracted aorta rings with PE (1 μM). The endothelium was considered effectively removed when the relaxation was less than 10% induced by ACh.

2.4. Endothelial Dysfunction Induced by H_2O_2 and the RA Treatment in Rat Aortic Rings. After 10 min equilibration with the new K-H solution, the aortic rings were pretreated with various concentrations of H_2O_2 (2.5, 5.0, and 10.0 mM) for 10 min. Following washout of H_2O_2, the aortic rings were depolarized with 80 mM KCl for 2 times. After returning to baseline tension, the rings were allowed to equilibrate for 20 min, and then the contraction were induced with PE (1 μM) till a stable plateau in tension. Then, each ring was exposed to increasing concentration of ACh (10^{-3}, 10^{-2}, 10^{-1}, 1, 5, 10, 50 μM) to generate a dose-dependent relaxation response. In the RA intervention experiment, the aortic rings were incubated with various concentrations (50.0 μM, 25 μM, 12.5 μM) of RA 10 min prior to exposure to 5 mM H_2O_2. Thereafter, a second vasodilation reactivity to ACh was obtained to evaluate the integrity of the endothelium after PE-induced contraction. In order to investigate the roles of AMPK in H_2O_2-induced endothelium dysfunction, the aortic rings were separately pretreated for 10 min with AMPK inhibitor (compound C) and AMPK activator (AICAR) before the exposure to H_2O_2 (5 mM).

2.5. Measurement of H_2O_2 Caused the Vasocontraction Impairment Mediated by Smooth Muscle Cells. In order to exclude the vasocontraction impairment mediated by smooth muscle cells injury, the vasoconstriction reactivity to PE was investigated after 5 mM H_2O_2 treatment in endothelial-intact (EC+) or endothelial-denuded (EC−) aortic rings.

2.6. Detection of O_2^- by NBT Reduction Assay. NBT reduction assay was performed as the method described previously [18]. Briefly, the aortic rings were incubated with the K-H solution containing 100.0 μM NBT for 1 h after the experiment. Subsequently, the HCl (0.5 mM) was added to stop the reaction. Then, the aortic rings were washed 3 times with PBS buffer; after they were minced and centrifuged at 20000g for 20 min on the part of the mixture of 40 mg/L diethylenetriaminepentaacetic acid, which was dissolved into 0.1 M NaOH and 0.1% SDS, the pellet was suspended in 0.5 mL of pyridine, along with being heated at 80°C for 1.5 h in order to extract formazan. The mixture was experienced a second centrifugation at 10000g for 10 min. Optical density (OD) was measured at 540 nm.

2.7. Cell Culture and Treatment. HAEC (human aortic endothelial cells) were purchased from Cell Bank, Shanghai Institutes for Biological Sciences, Chinese Academy of Sciences, Shanghai, and cultured in Dulbecco's Modified Eagle Medium (GIBCO) supplemented with L-glutamine, pyridoxine hydrochloride, 110 mg/L sodium pyruvate, 100 U/mL penicillin, and 100 μg/mL streptomycin and amphotericin at 37°C in a humidified atmosphere of 5% CO_2. Cells cultured up to six or fewer passages were first grown to confluence before exposure to H_2O_2 (5 mM) for 10 min, and stimulated

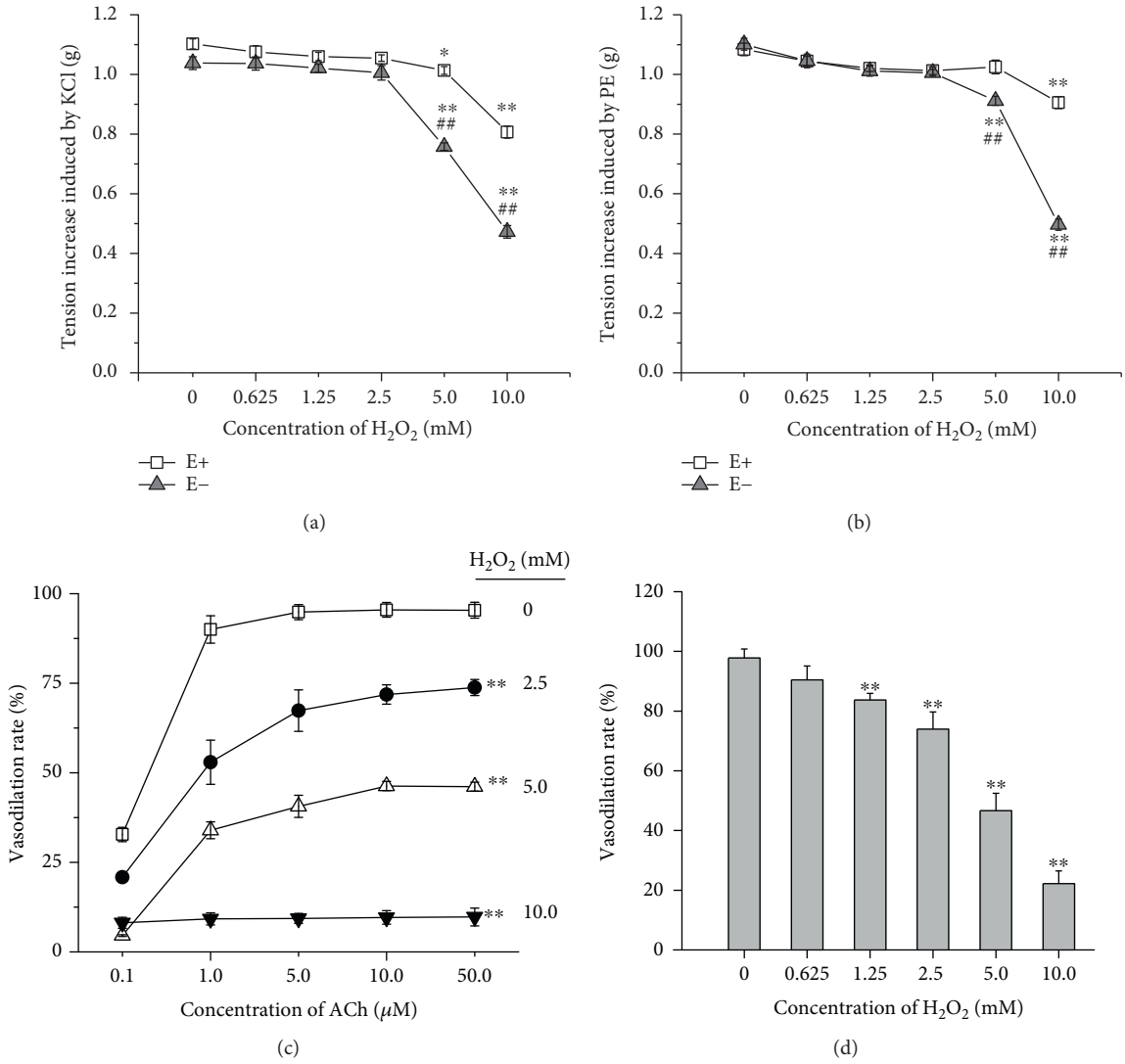

Figure 1: Effects of H_2O_2 exposure on PE- and KCl-induced contraction in rat aortic rings. (a) KCl induced contractile response in H_2O_2-treated aortic rings with (E+) or without (E−) endothelium. (b) PE induced contractile response in H_2O_2-treated aortic rings with (E+) or without (E−) endothelium. (c) ACh induced vasodilative response in H_2O_2-treated rat aorta with intact endothelium. (d) 5.0 mM H_2O_2 pulse treatment (10 min) induced the endothelium-dependent vasodilation impairments in rat aortic rings with intact endothelium. Data represents as means ± SD ($n = 6$). (a and b) $^{*}P < 0.05$, $^{**}P < 0.01$ versus the respective untreated group; $^{\#\#}P < 0.01$ versus the endothelium-intact aortic rings treated with the same concentration of H_2O_2; (c and d) $^{**}P < 001$ versus the untreated group.

by RA (50 μM) containing H_2O_2 (5 mM) for 10 min, to clarify the activity of AMPK on the expression of the phosphor-eNOS. Therefore, cells were treated with compound C (inhibitor of AMPK) with H_2O_2 and in the presence of RA for 10 min.

2.8. Western Blotting Assay. After lysis of the cells, the protein samples (25 μg/lane) were resolved by electrophoresis on 10% sodium dodecyl sulfate (SDS) polyacrylamide gels and then transferred to nitrocellulose membranes. The membranes were incubated in blocking buffers and then incubated with more of the following primary antibodies: anti-AMPK (1 : 1000, Cell Signaling Technology, MA, USA), anti-phospho-AMPK (Thr172) (1 : 1000, Cell Signaling Technology), anti-phospho endothelial nitric oxide synthase (eNOS, Ser1177), and anti-endothelial nitric oxide synthase (1 : 1000, Cell Signaling Technology). Thereafter, the membranes were washed and incubated with horseradish peroxidase-conjugated secondary antibodies. (1 : 2000, Cell Signaling Technology).

2.9. Statistical Analysis. Results were expressed as the mean ± SD for separated experiments and statistical analysis were made by paired Student's *t*-test or by one-way ANOVA for multiple factors analysis with SPSS 18.0 software. Differences were considered to be statistically significant when $P < 0.05$.

3. Results

3.1. Hydrogen Peroxide Exposure Affected the PE- and KCl-Induced Contraction. The cumulative addition of H_2O_2 to

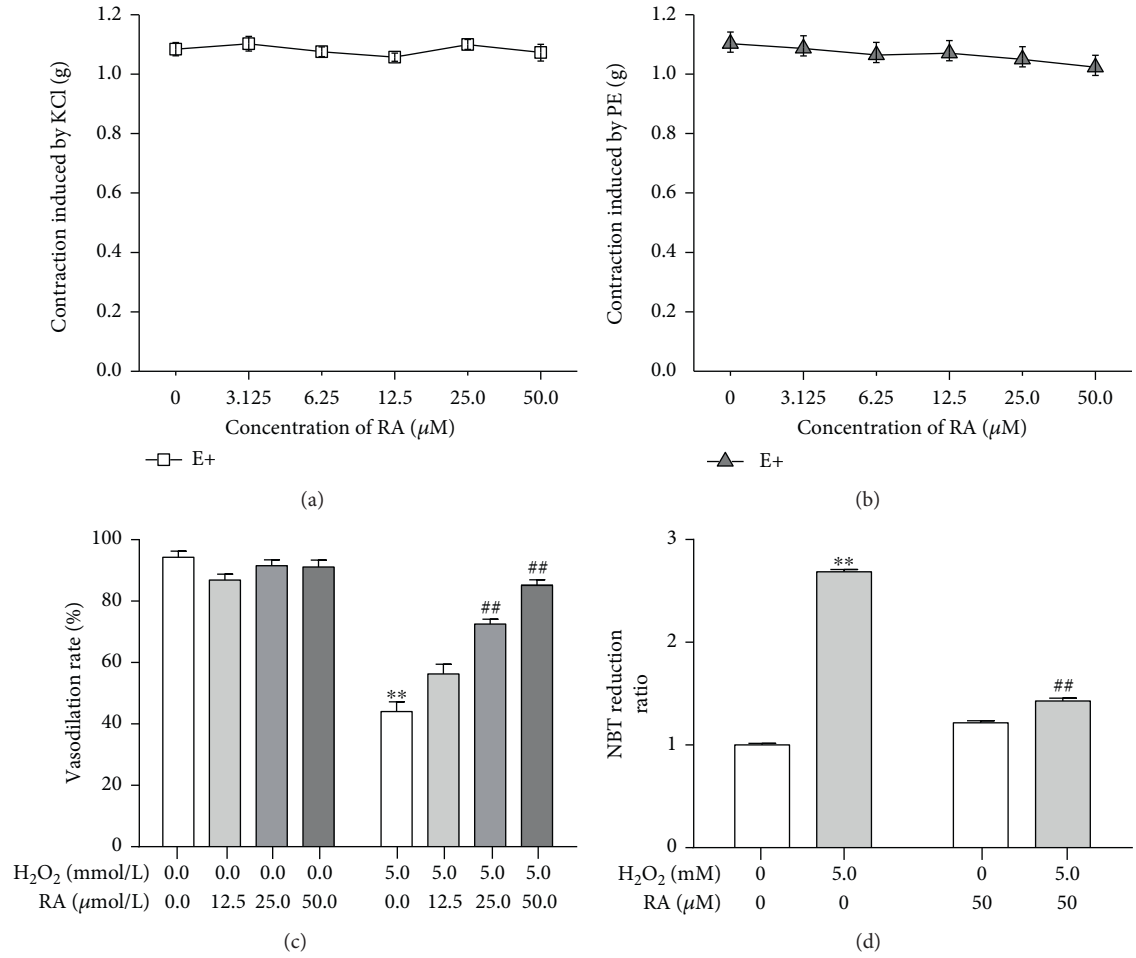

Figure 2: Rosmarinic acid alleviates the endothelial dysfunction induced by H_2O_2 in endothelium-intact rat aortic rings. (a) Rosmarinic acid (RA) pulse exposure showed no effect on the contraction induced by KCl in rat aortic rings. (b) Rosmarinic acid (RA) pulse exposure showed no effect on the contraction induced by PE in rat aortic rings. (c) Rosmarinic acid (RA) preincubation alleviated the endothelium-dependent vasodilation impairments induced by H_2O_2. (d) Rosmarinic acid (RA) cotreatment inhibited the NBT reduction induced by H_2O_2 in the endothelium-intact aortic rings. The results were expressed as the means ± SD ($n = 6$). $^{**}P < 0.01$ versus the untreated control group; $^{\#\#}P < 001$ versus the H_2O_2-treated group.

10.0 mM showed no obvious effect on the basal tension in endothelium-intact and endothelium-denuded aortic rings (data were not shown). The contraction response to PE or KCl was not affected till H_2O_2 reached 10.0 mM in endothelium-intact aortic rings. However, the 5.0 mM H_2O_2 pretreatment resulted in the significant decrease of the maximum contraction induced by PE or KCl in endothelium-denuded aortic rings (Figures 1(a) and 1(b)), which indicated that H_2O_2 induced more serious injury to the vascular smooth muscle in the endothelium-denuded aortic rings and the presence of the endothelium alleviated this injury.

A typical model regarding the concentration response curve of ACh-induced endothelium-dependent relaxation was impaired in H_2O_2-induced thoracic aorta compared with the control (Figures 1(c) and 1(d)) (control: $pD_2 = 7.00 \pm 0.05$, $E_{max} = 90\%$; 2.5 mM H_2O_2: $pD_2 = 5.88 \pm 0.12$, $E_{max} = 73\%$; 5 mM H_2O_2: $pD_2 = 4.52 \pm 0.22$, $E_{max} = 47\%$).

3.2. Effect of RA on H_2O_2-Induced Endothelium-Dependent Vasodilation Impairments in Rat Aortic Rings. The cumulative concentration of RA to 50 μM showed no effect on the contraction response to KCl or PE (Figures 2(a) and 2(b)), and the relaxation response to ACh (Figure 2(c)) in rat aortic rings as well, whereas it significantly alleviated the impairment of vasodilation reaction to ACh induced by H_2O_2 in a dose-dependent manner (Figure 2(c)) ($P < 0.01$). Because the oxidative stress mediates the endothelium injury and the NADPH oxidase is the main source of the endogenous reactive oxygen species, the $O_2^{\bullet-}$ generation in the aortic rings was examined by the NBT reduction. The 5 mM H_2O_2 treatment significantly promoted the generation of the reduced NBT (formazan) in isolated rat aortic rings, while the 50 μM RA almost entirely abolished the effect of H_2O_2 (Figure 2(d)).

3.3. eNOS Activation Was Involved in the Protection of RA against the Endothelial Dysfunction Induced by H_2O_2. Given

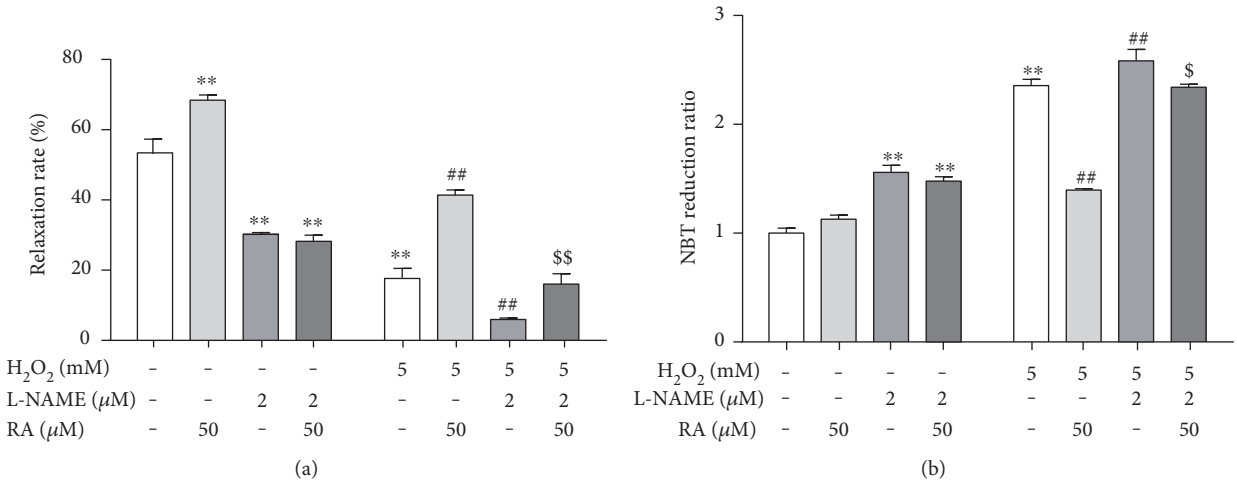

Figure 3: eNOS activation mediated the protection of rosmarinic acid on the endothelial dysfunction induced by H_2O_2 in rat aortic rings. The rat aortic rings were cotreated with eNOS inhibitor L-NAME (2.0 μM) and RA (50 μM) for 10 min, then exposed to H_2O_2 (5.0 mM) for another 10 min. The endothelial function was assessed by the endothelium-dependent vasodilation induced by acetylcholine (ACh, 10 μM) ($n = 6$). (a) The relative endothelium-dependent vasodilation rate after exposure to RA, eNOS inhibitor L-NAME, and H_2O_2 in rat aortic rings. (b) The NBT reduction after exposure to RA, eNOS inhibitor L-NAME, and H_2O_2 in rat aortic rings. Data are presented as the means ± SD ($n = 6$). $^{**}P < 0.01$ versus the untreated control group; $^{\#\#}P < 0.01$ versus the H_2O_2-treated group; $^{\$}P < 0.05$ and $^{\$\$}P < 0.01$ versus the H_2O_2- and RA-cotreated groups, respectively.

that NO is the most potent vasodilator and the modulator of intracellular oxidative status, and it is produced by the eNOS in endothelium [19], we explored the effect of eNOS activation in RA's protection against the endothelial dysfunction induced by H_2O_2. The pretreatment with the NOS inhibitor L-NAME alone significantly decreased the vasodilation induced by ACh (Figure 3(a)), while increased the NBT reduction (Figure 3(b)) in rat aortic rings. The L-NAME further increased the vasodilation impairment (Figure 3(a)), whereas it increased the NBT reduction (Figure 3(b)) in rat aortic rings induced by H_2O_2. Moreover, the L-NAME treatment abolished the RA's protection on the impairment of the endothelial-dependent relaxation injured by H_2O_2 (Figure 3(a)). And the decrease of NBT reduction induced by RA was also reversed by L-NAME in H_2O_2-treated aortic rings (Figure 3(b)).

3.4. AMPK Activation Was Involved in the Protection of RA against the Endothelial Dysfunction Induced by H_2O_2. AMPK is a crucial cellular energy sensor which senses change in the intracellular AMP/ATP ratio. It is also an intracellular stress sensor that is regulated by oxidative stress and other stresses that result in diminished cellular ATP levels. AMPK is one of the key modulators of eNOS in the endothelium and involved in the endothelial dysfunction induced by oxidative stress resulted from NADPH oxidase upregulation [20]. Here, we investigated the roles of AMPK in RA's protection to endothelial dysfunction induced by H_2O_2. As shown in Figure 4(a), compared with control, the response to ACh was similar to the AICAR- and RA-treated groups ($P < 0.01$). Similarly, activation of AMPK by AICAR decreased the NBT reduction. Whereas, the beneficial effect of RA on endothelium-dependent vasodilatation in rats was partly attenuated in the presence of compound C, a well-characterized AMPK inhibitor, reduced AMPK activity, and enhanced NBT reduction at 10 μM (Figure 4(b)). Furthermore, when compound C was combined with H_2O_2, it intensified the NBT reduction. Mechanistically, we found that AMPK activated and increased the protection of RA on endothelial dysfunction (Figure 4(b)).

3.5. RA Treatment Improved Endothelial Dysfunction in HAEC via AMPK/eNOS Pathway. In order to further ascertain the relationship of AMPK and eNOS in the RA's effect, the AMPK-eNOS signal pathway activation was investigated by their phosphorylation in human aortic endothelial cells (HAEC) *in vitro*. As shown in Figure 5, the expression levels of total AMPK and eNOS remained unchanged. And the 50 μM RA single treatment had no obvious effect on the AMPK and eNOS phosphorylation, while the 5 mM H_2O_2 treatment significantly downregulated the phosphorylation of AMPK and eNOS at Thr172 and Ser1177, respectively ($P < 0.01$), in HAEC cells. The cotreatment with RA significantly reversed the decrease of AMPK and eNOS phosphorylation induced by H_2O_2. The AMPK's inhibitor, compound C cotreatment, abolished the RA's upregulation of AMPK and eNOS phosphorylation in H_2O_2-treated HAEC cells. However, the AMPK agonist showed no more synergistic effect with RA. The results suggest that the AMPK phosphorylation played key roles in the protection effects of RA on H_2O_2-induced injury in HAEC.

4. Discussion

Endothelial dysfunction resulted from oxidative stress is the key initiating factor in almost all vascular events. Niethammer et al. found that the extracellular H_2O_2 generated by dual oxidase (Duox) reached 50 μM after 20 min of wounding near the wound margin in zebrafish larvae, which constructed a concentration gradient and mediated the rapid

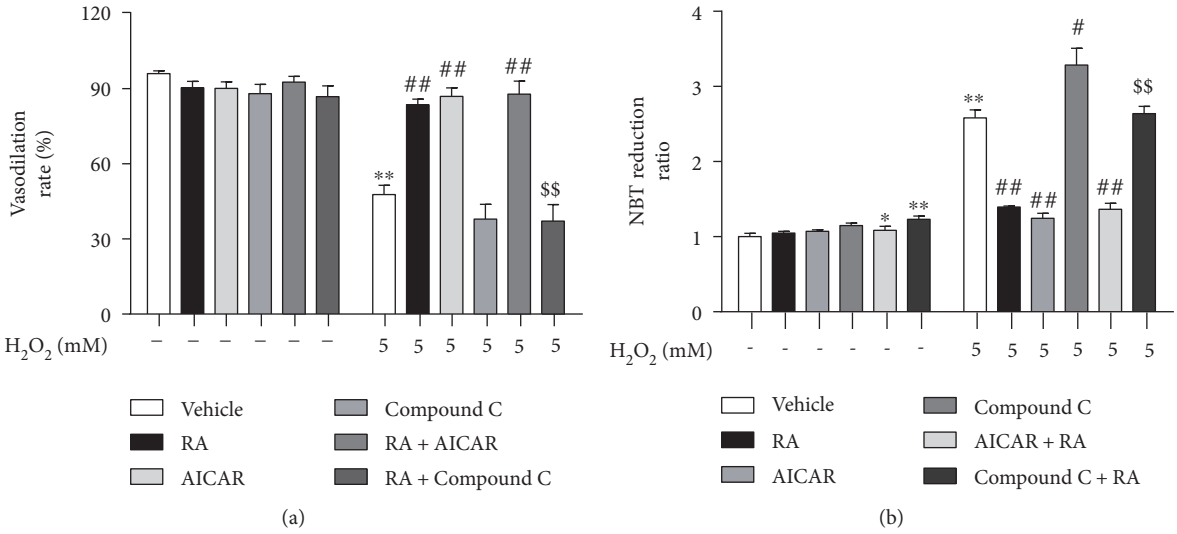

FIGURE 4: AMPK activation mediated the protection of rosmarinic acid against the endothelial dysfunction induced by H_2O_2 in rat aortic rings. The rat aortic rings were cotreated with AMPK activator AICAR (50 μM, 10 min) or inhibitor compound C (10 μM) and RA (50 μM) for 10 min, then exposed to H_2O_2 (5.0 mM) for another 10 min. The endothelium function was assessed by the endothelium-dependent vasodilation induced by acetylcholine (ACh, 10 μM). (a) The relative endothelium-dependent vasodilative rate after exposure to RA, AMPK modulator, and H_2O_2 in rat aortic rings. (b) The NBT reduction after exposure to RA, AMPK modulator, and H_2O_2 in rat aortic rings. Data are presented as the means ± SD ($n = 6$). $^{*}P < 0.05$ versus the untreated control group; $^{**}P < 0.01$ versus the untreated control group; $^{\#\#}P < 0.01$ versus the H_2O_2-treated group; $^{\$\$}P < 0.01$ versus the H_2O_2- and RA-cotreated groups.

recruitment of leukocytes to the wound [7]. Although the oxidative burst derived from the neutrophil activation in the inflammation will produce more ROS, there is no accurate concentration data of H_2O_2 reported. Here, we investigated the dose-effect relationship of H_2O_2 on the function of endothelium and vascular smooth muscle. In order to exclude the direct reaction of H_2O_2 with PE or ACh, the aortic rings were incubated in fresh K-H solution for 10 min and redepolarized with KCl after H_2O_2 pulse treatment for 10 min. The results showed that the vascular smooth muscle reactivity to PE or KCl in endothelium-denuded aortic rings were more vulnerable to H_2O_2 (at 5.0 and 10.0 mM) than in the endothelium-intact aortic rings (Figure 1), which indicated that the presence of endothelium protected the vascular smooth muscle from the oxidative injury induced by high concentration of H_2O_2. Moreover, the 2.5 mM H_2O_2 pretreatment resulted in the significant decrease of the vasodilative reaction to ACh, which demonstrated that the endothelial cells were more sensitive to H_2O_2 than the vascular smooth muscle cells.

The previous work of Sotnikova et al. proved that RA significantly improved the endothelium-dependent vasodilation in diabetic rat aorta, which might be mediated by its antioxidative and anti-inflammation properties [8]. The present study proves that RA improves the impairments of endothelial-dependent vasodilation caused by H_2O_2 in normal rat aorta (Figure 2). NADPH oxidase is the major source of reactive oxygen species in endothelial cells and vascular smooth cells [21]. Besides, it has been proved that endothelial-dependent relaxation was effectively improved after the deletion of Nox2, which implicates that the endothelial dysfunction might be associated with Nox2 overexpression [22]. H_2O_2-induced endothelial-dependent relaxation impairment is associated with the increased production of superoxide anion ($O_2^{\bullet-}$). It has been proved that H_2O_2 could activate NADPH oxidase in a dose- and time-dependent manner in respiration rate [23], and the oxidative injury to endothelium resulted from the excess ROS is the key mediator of endothelial impairment in atherosclerosis and diabetes [24]. Our work also proved that the pulse treatment with H_2O_2 significantly increased the NBT reduction in rat aorta and RA cotreatment significantly reversed the effects of H_2O_2, which demonstrates that the antioxidative activity is involved in the RA's protective effects on the endothelial function.

The endothelium-dependent vasodilation impairment is believed to be the consequence of a decreased bioavailability of nitric oxide (NO), an important endothelium-derived relaxing factor. The superoxide derived from NADPH oxidase could rapidly react with NO to form the stable peroxynitrite anion ($ONOO^-$), which will result in the decline of NO bioavailability. The other reason for NO signal dysfunction might lie in the eNOS expression and activation impairments. In our experiments, L-NAME partially decreased the phosphorylation of eNOS and antagonized the protective effects of RA on the endothelium dysfunction induced by H_2O_2, while it exacerbated the ROS formation in H_2O_2-treated rat aorta. These results revealed that the effects of RA might be associated with the NO synthesis.

In the recent years, AMPK is demonstrated to improve vascular function by activating eNOS [25]. In addition to regulating energy metabolism, AMPK exerts anti-inflammatory and antioxidative activities [26, 27]. Previous studies indicated that AMPK activation improved the endothelial

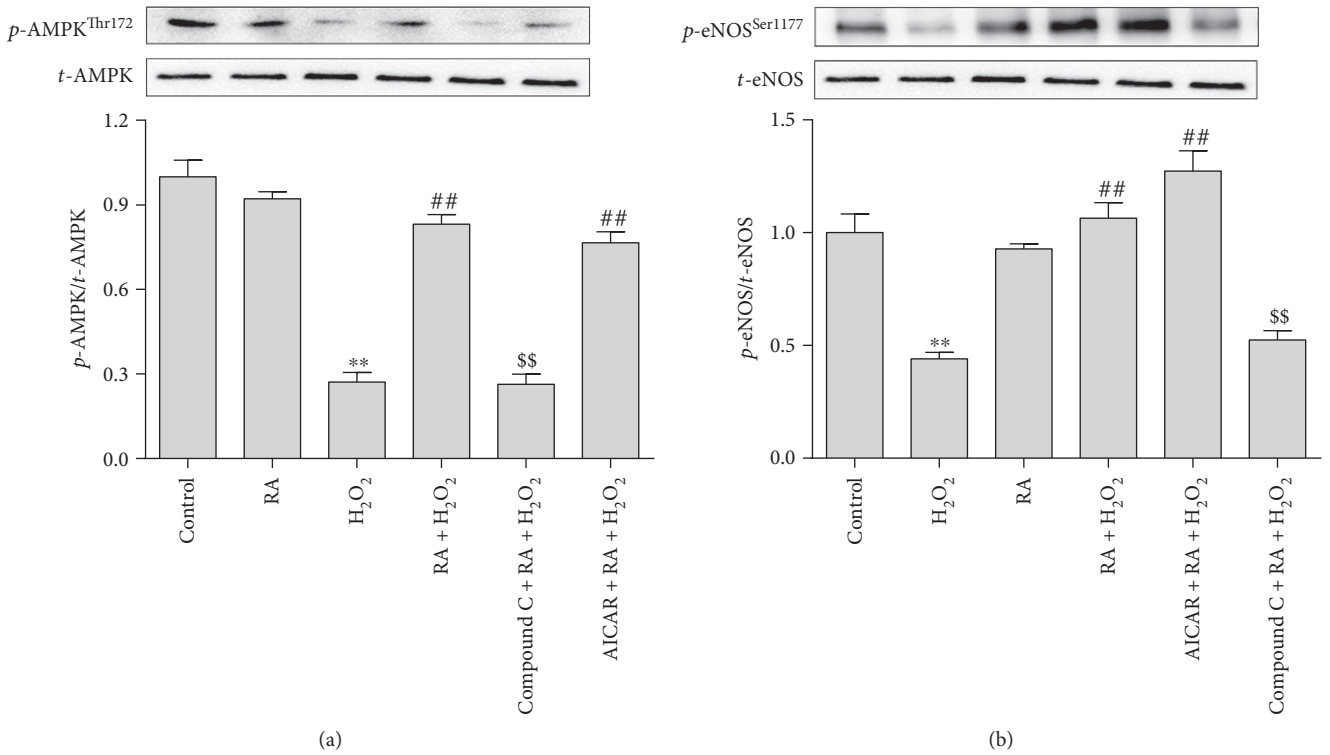

Figure 5: Rosmarinic acid induced the phosphorylation of AMPK and eNOS in HAEC cells. The HAEC cells were pretreated with the AMPK inhibitor compound C (10 μM) or activator AICAR (50 μM) combined with RA (50 μM) for 10 min prior to another 10 min exposure with H_2O_2 (5 mM). The total AMPK (*t*-AMPK), phosphorylated AMPK at Thr172 site (*p*-AMPK^{Thr172}), and the total eNOS (*t*-eNOS) and the phosphorylated eNOS at the Ser1177 site (*p*-eNOS^{Ser1177}) were determined by Western blot. The results is quantified as the relative ratio of the phosphorylated protein/total protein. The values are presented as the means ± SD; $n = 3$. $^{**}P < 0.01$ versus the untreated control group; $^{\#\#}P < 0.01$ versus the H_2O_2-treated group; $^{\$\$}P < 0.01$ versus the H_2O_2- and RA-cotreated groups.

function [28]. Here, we found that the AMPK agonist AICAR single treatment possessed the similar protective effects against endothelial dysfunction and oxidative stress induced by H_2O_2 in rat aorta as well as RA did, while the combination of RA and AICAR showed no further beneficial effect. The cotreatment with AMPK inhibitor compound C abolished the effects of RA, which further proved that the AMPK activation played a key role in the RA's effects. Hu et al.'s work revealed that H_2O_2 induced the bidirectional modulation in eNOS through the Akt and AMPK in a time- and dose-dependent way [29]. We also found that the Akt inhibitor LY294002 cotreatment significantly abrogates the RA's protection from the endothelium-dependent vasodilation impairments (Figure 1S available online at https://doi.org/10.1155/2017/7091904) induced by H_2O_2. And the RA significantly restored the phosphorylation downregulation at the Ser473 site of the Akt protein (Figure 2S). It indicated that the Akt signal pathway was involved in the RA's protective effects, while the interaction of AMPK and Akt in RA's effects needed to be investigated further.

In summary, this study demonstrated that RA significantly improved H_2O_2-induced endothelial dysfunction and the activation of AMPK-eNOS pathway was involved in the RA's effects. However, whether the modulating effects of RA is dependent on its direct activation of AMPK-eNOS pathway or its modulation on the oxidative status still remains unclarified in the present work. It needs further investigations to identify the underlying mechanisms of RA's protection on the endothelial function.

Abbreviations

RA: Rosmarinic acid
K-H: Krebs-Henseleit
AICAR: 5-Aminoimidazole-4-carboxamide-1-β-D-ribofuranoside
PE: Phenylephrine
ACh: Acetylcholine
EC+: Endothelium-intact aortic rings
EC−: Endothelium-denuded aortic rings
L-NAME: NG-nitro-L-arginine methyl ester
eNOS: Endothelial nitric oxide synthase
I/R: Ischemia and reperfusion
HAEC: Human aortic endothelial cells.

Conflicts of Interest

No potential conflicts of interest were disclosed.

Authors' Contributions

Hui Zhou, Baocai Fu, Zhenhua Wang, and Ji Li designed and conducted the study. Hui Zhou, Bo Xu, Xiangquan Mi, Gang Li, Chengjun Ma, and Jianxin Xie collected the data and

conducted the analysis. Hui Zhou, Bo Xu, Gang Li, Bo Xu, Chengjun Ma, Jianxin Xie, Zhenhua Wang, and Ji Li interpreted the data. Hui Zhou, Zhenhua Wang, and Ji Li wrote the manuscript. Hui Zhou and Baocai Fu contributed equally to this work.

Acknowledgments

This work is supported in part by the National Natural Science Foundation of China (21372190, 31470426), the Taishan Scholar Program of Shandong Province (tshw201502046), the "Personalized Medicines—Molecular Signature-based Drug Discovery and Development," the Strategic Priority Research Program of the Chinese Academy of Sciences (XDA12040320), and the Shuangbai Project of Yantai.

References

[1] C. R. Triggle and H. Ding, "A review of endothelial dysfunction in diabetes: a focus on the contribution of a dysfunctional eNOS," *Journal of the American Society of Hypertension*, vol. 4, no. 3, pp. 102–115, 2010.

[2] M. McIntyre, D. F. Bohr, and A. F. Dominiczak, "Endothelial function in hypertension," *Hypertension*, vol. 34, no. 4, pp. 539–545, 1999.

[3] P. Niethammer, C. Grabher, A. T. Look, and T. J. Mitchison, "A tissue-scale gradient of hydrogen peroxide mediates rapid wound detection in zebrafish," *Nature*, vol. 459, pp. 996–999, 2009.

[4] T. Heitzer, T. Schlinzig, K. Krohn, T. Meinertz, and T. Münzel, "Endothelial dysfunction, oxidative stress, and risk of cardiovascular events in patients with coronary artery disease," *Circulation*, vol. 104, no. 22, pp. 2673–2678, 2001.

[5] D. Giugliano, A. Ceriello, and G. Paolisso, "Oxidative stress and diabetic vascular complications," *Diabetes Care*, vol. 19, no. 3, pp. 257–267, 1995.

[6] Y. Higashi, K. Noma, M. Yoshizumi, and Y. Kihara, "Endothelial function and oxidative stress in cardiovascular diseases," *Circulation Journal*, vol. 73, no. 3, pp. 411–418, 2009.

[7] J. Davignon and P. Ganz, "Role of endothelial dysfunction in atherosclerosis," *Circulation*, vol. 109, no. 23, pp. III-27–III-32, 2004.

[8] R. Sotnikova, L. Okruhlicova, J. Vlkovicova et al., "Rosmarinic acid administration attenuates diabetes-induced vascular dysfunction of the rat aorta," *Journal of Pharmacy and Pharmacology*, vol. 65, no. 5, pp. 713–723, 2013.

[9] U. Förstermann, "Nitric oxide and oxidative stress in vascular disease," *Pflügers Archiv-European Journal of Physiology*, vol. 459, no. 6, pp. 923–939, 2010.

[10] T. C. Travaglia, R. C. Berger, M. B. Luz et al., "Low-salt diet increases NO bioavailability and COX-2 vasoconstrictor prostanoid production in spontaneously hypertensive rats," *Life Sciences*, vol. 145, pp. 66–73, 2016.

[11] C. Xu, F. Tang, M. Lu et al., "Astragaloside IV improves the isoproterenol-induced vascular dysfunction via attenuating eNOS uncoupling-mediated oxidative stress and inhibiting ROS-NF-κB pathways," *International Immunopharmacology*, vol. 33, pp. 119–127, 2016.

[12] Z. Ungvari, N. Labinskyy, P. Mukhopadhyay et al., "Resveratrol attenuates mitochondrial oxidative stress in coronary arterial endothelial cells," *American Journal of Physiology-Heart and Circulatory Physiology*, vol. 297, no. 5, pp. H1876–H1881, 2009.

[13] R. Motterlini, R. Foresti, R. Bassi, and C. J. Green, "Curcumin, an antioxidant and anti-inflammatory agent, induces heme oxygenase-1 and protects endothelial cells against oxidative stress," *Free Radical Biology and Medicine*, vol. 28, no. 8, pp. 1303–1312, 2000.

[14] E. J. Ruijters, A. R. Weseler, C. Kicken, G. R. Haenen, and A. Bast, "The flavanol (-)-epicatechin and its metabolites protect against oxidative stress in primary endothelial cells via a direct antioxidant effect," *European Journal of Pharmacology*, vol. 715, no. 1, pp. 147–153, 2013.

[15] M. A. Soobrattee, V. S. Neergheen, A. Luximon-Ramma, O. I. Aruoma, and T. Bahorun, "Phenolics as potential antioxidant therapeutic agents: mechanism and actions," *Mutation Research/Fundamental and Molecular Mechanisms of Mutagenesis*, vol. 579, no. 1-2, pp. 200–213, 2005.

[16] P. W. Peake, B. A. Pussell, P. Martyn, V. Timmermans, and J. A. Charlesworth, "The inhibitory effect of rosmarinic acid on complement involves the C5 convertase," *International Journal of Immunopharmacology*, vol. 13, no. 7, pp. 853–857, 1991.

[17] K. Kazama, K. Hoshino, T. Kodama, M. Okada, and H. Yamawaki, "Adipocytokine, progranulin, augments acetylcholine-induced nitric oxide-mediated relaxation through the increases of cGMP production in rat isolated mesenteric artery," *Acta Physiologica*, vol. 219, no. 4, pp. 781–789, 2017.

[18] M. Pourcyrous, C. W. Leffler, H. S. Bada, S. B. Korones, and D. W. Busua, "Brain superoxide anion generation in asphyxiated piglets and the effect of indomethacin at therapeutic dose," *Pediatric Research*, vol. 34, no. 3, pp. 366–369, 1993.

[19] M. L. Chang, J. S. Chang, W. Y. Yu et al., "*Polygonum viviparum* L. induces vasorelaxation in the rat thoracic aorta via activation of nitric oxide synthase in endothelial cells," *BMC Complementary and Alternative Medicine*, vol. 14, no. 1, p. 150, 2014.

[20] A. E. Dikalova, M. C. Góngora, D. G. Harrison, J. D. Lambeth, S. Dikalov, and K. K. Griendling, "Upregulation of Nox1 in vascular smooth muscle leads to impaired endothelium-dependent relaxation via eNOS uncoupling," *American Journal of Physiology-Heart and Circulatory Physiology*, vol. 299, no. 3, pp. H673–H679, 2010.

[21] V. E. Edirimanne, C. W. Woo, Y. L. Siow, G. N. Pierce, J. Y. Xie, and K. O, "Homocysteine stimulates NADPH oxidase-mediated superoxide production leading to endothelial dysfunction in rats," *Canadian Journal of Physiology and Pharmacology*, vol. 85, no. 12, pp. 1236–1247, 2007.

[22] E. Shafique, W. C. Choy, Y. Liu et al., "Oxidative stress improves coronary endothelial function through activation of the pro-survival kinase AMPK," *Aging (Albany New York)*, vol. 5, no. 7, pp. 515–530, 2013.

[23] E. A. Andronis, P. N. Moschou, I. Toumi, and K. A. Roubelakis-Angelakis, "Peroxisomal polyamine oxidase and NADPH-oxidase cross-talk for ROS homeostasis which affects respiration rate in *Arabidopsis thaliana*," *Plant Polyamines in Stress and Development*, vol. 5, p. 39, 2014.

[24] T. Mizuno, Y. Masuda, and K. Irie, "The *Saccharomyces cerevisiae* AMPK, Snf1, negatively regulates the Hog1 MAPK pathway in ER stress response," *PLoS Genetics*, vol. 11, no. 9, article e1005491, 2015.

[25] Y. Zhang, T. S. Lee, E. M. Kolb et al., "AMP-activated protein kinase is involved in endothelial NO synthase activation in response to shear stress," *Arteriosclerosis, Thrombosis, and Vascular Biology*, vol. 26, pp. 1281–1287, 2006.

[26] S. Bijland, S. J. Mancini, and I. P. Salt, "Role of AMP-activated protein kinase in adipose tissue metabolism and inflammation," *Clinical Science*, vol. 124, no. 8, pp. 491–507, 2013.

[27] S. Schuhmacher, M. Foretz, M. Knorr et al., "α1AMP-activated protein kinase preserves endothelial function during chronic angiotensin II treatment by limiting Nox2 upregulation," *Arteriosclerosis, Thrombosis, and Vascular Biology*, vol. 31, no. 3, pp. 560–566, 2011.

[28] H. Y. Tsai, C. P. Lin, P. H. Huang et al., "Coenzyme Q10 attenuates high glucose-induced endothelial progenitor cell dysfunction through AMP-activated protein kinase pathways," *Journal of Diabetes Research*, vol. 2016, Article ID 6384759, 14 pages, 2016.

[29] Z. Hu, J. Chen, Q. Wei, and Y. Xia, "Bidirectional actions of hydrogen peroxide on endothelial nitric-oxide synthase phosphorylation and function co-commitment and interplay of Akt and AMPK," *Journal of Biological Chemistry*, vol. 283, pp. 25256–25263, 2008.

Hindawi
Oxidative Medicine and Cellular Longevity
Volume 2017, Article ID 8192383, 11 pages
https://doi.org/10.1155/2017/8192383

Review Article

Salvianolic Acid Exerts Cardioprotection through Promoting Angiogenesis in Animal Models of Acute Myocardial Infarction: Preclinical Evidence

Long-jie Yu,[1] Ke-Jian Zhang,[1] Jia-Zhen Zhu,[1] Qun Zheng,[1] Xiao-Yi Bao,[1] Saroj Thapa,[1] Yan Wang,[1] and Mao-Ping Chu[2]

[1]*Department of Cardiology, The Second Affiliated Hospital and Yuying Children's Hospital of Wenzhou Medical University, Wenzhou 32500, China*
[2]*Children's Heart Center, The Second Affiliated Hospital and Yuying Children's Hospital of Wenzhou Medical University, Institute of Cardiovascular Development and Translational Medicine, Wenzhou Medical University, Wenzhou 325000, China*

Correspondence should be addressed to Yan Wang; wywzchina@sina.com and Mao-Ping Chu; chmping@hotmail.com

Received 27 February 2017; Revised 9 April 2017; Accepted 24 April 2017; Published 21 June 2017

Academic Editor: Pei Luo

Radix *Salviae miltiorrhizae*, danshen root (danshen), is one of the widely used Chinese herbal medicines in clinics, containing rich phenolic compounds. Salvianolic acid is the main active compound responsible for the pharmacologic effects of danshen. Here, we aimed to evaluate the effects of salvianolic acid on cardioprotection through promoting angiogenesis in experimental myocardial infarction. Studies of salvianolic acid in animal models of myocardial infarction were obtained from 6 databases until April 2016. The outcome measures were vascular endothelium growth factor (VEGF), blood vessel density (BVD), and myocardial infarct size. All the data were analyzed using Rev-Man 5.3 software. Ultimately, 14 studies were identified involving 226 animals. The quality score of studies ranged from 3 to 6. The meta-analysis of six studies showed significant effects of salvianolic acid on increasing VEGF expression compared with the control group ($P < 0.01$). The meta-analysis of the two salvianolic acid A studies and three salvianolic acid B studies showed significantly improving BVD compared with the control group ($P < 0.01$). The meta-analysis of five studies showed significant effects of salvianolic acid for decreasing myocardial infarct size compared with the control group ($P < 0.01$). In conclusion, these findings demonstrated that salvianolic acid can exert cardioprotection through promoting angiogenesis in animal models of myocardial infarction.

1. Introduction

Ischemic heart disease (IHD) remains the leading cause of death worldwide [1]. According to the World Health Organization report, 740 million people die of IHD annually all around the world, accounting for the death of 13.2% of the total population [2]. Myocardial infarction (MI) is one of the main manifestation of IHD, which makes myocardial necrosis or apoptosis in a short time [3], leading to heart failure with a poor prognosis [4]. It has been ranked as the leading cause of death in IHD [5].

In recent years, there are many types of treatments for MI, such as reducing incidence of coronary atherosclerosis [6], antithrombotic therapy including vitamin K antagonists [7], antiplatelet therapy with low-dose aspirin [8], and clopidogrel [9]. In addition, invasive vascular reconstruction is widely used, which improves coronary perfusion, such as percutaneous coronary intervention (PCI) and coronary artery bypass grafting (CABG) [10]. In the short term, clinical interventions and treatments of MI have achieved positive effectiveness [11]. However, the side effect of drugs such as lipid-lowering drugs leading to skeletal muscle, metabolic and neurological adverse events [12], antithrombotic therapy [13] and/or anti-platelet therapy [14] leading to bleeding, and the high incidence rate of restenosis or stent thrombosis limits the long-term success of treatment [15]. Thus, the promotion of therapeutic angiogenesis as a new treatment strategy has been proposed. Angiogenesis appears in all

vascularized organs during the whole embryonic development stage, formatting of new blood vessels from preexisting ones [16]. Although ischemia leads to endogenous myocardial angiogenesis, it cannot reach the effect to maintain normal capillary density [17]. Therefore, therapeutic stimulation of angiogenesis has been regarded as an effective treatment for myocardial ischemia [18].

Radix *Salviae miltiorrhizae*, danshen root (danshen), the dried root of *Salvia miltiorrhiza* Bge., known as a popular traditional Chinese herbal medicine, has been widely used and well received for the treatment of coronary artery diseases, such as angina pectoris and MI [19]. Salvianolic acid is the main active compound responsible for the pharmacologic effects of danshen [20] and exerts the significant cardiovascular protection [21]. Currently, various studies have indicated its significant function of promoting angiogenesis [22].

The use of preclinical systematic review can more systematically evaluate the efficacy, identify an area for testing in further animal experiments, provide reliable information about the drugs study, and list the base of future clinical research [23]. However, currently, there is no systematic review in this area. Thus, the aim of this study is to evaluate the effects of salvianolic acid on cardioprotection through promoting angiogenesis in animal experiments of MI.

2. Methods

2.1. Search Strategies. We searched studies of salvianolic acid in animal models of acute myocardial infarction from PubMed, EMBASE, Chinese National Knowledge Infrastructure (CNKI), VIP information database, and Wanfang Data information site from inception to April 2016. The search term used was "danshen OR *Salvia miltiorrhiza* OR Salvianolic acid OR Daiclzein" AND "myocardial infarction OR Myocardial Ischemia OR myocardialischemia OR myocardial infarct OR myocardial stems." All the research objects were limited to animals.

2.2. Inclusion/Exclusion Criteria. We included studies about the effect of salvianolic acid on animal models with myocardial infarction, in which the outcome measures were vascular endothelium growth factor (VEGF) and/or blood vessel density (BVD). To prevent bias, inclusion criteria were prespecified as follows: (1) acute myocardial infarction (AMI) experimental model was induced by ligating of the left anterior descending coronary artery (LAD); (2) experimental drug was Salvianolic acid; and VEGF and/or BVD (3) is the primary outcome measurement and (4) is compared with control animal models receiving saline or no treatment. Prespecified exclusion criteria were treatment with single danshen or danshen-based prescription, a nonmyocardial infarct model, no control group, and duplicate publications.

2.3. Data Extraction. Two authors independently extracted data as follows: (1) publication year and the first author's name; (2) the information of experimental animals including number, species, sex, weight, and age; (3) a model of myocardial infarction; (4) the time of giving experimental drug; (5) the type and the administration methods of anesthetic; (6) the characteristics of treatment used in the experimental group containing the types of salvianolic acid, administration method, and duration of treatment; (7) the primary outcome measures, other outcome measures, and timing for outcome assessments; and (8) side effect. If there were many different time point outcomes, only the last was recorded. Likewise, if the experimental animals received different doses of the drug, only the highest dose was recorded. If the primary data were incomplete, further information was retrieved by contacting with authors. For each comparison, we extracted the mean value and standard deviation from each experimental and control group of every study. Discrepancies were resolved after discussion between the two authors.

2.4. Quality Assessment. We evaluated the methodological quality of the included studies using the ten-item scale [24] with minor modification as follows: (a) peer-reviewed publication; (b) control of temperature; (c) random allocation to treatment or control; (d) blinded induction of model; (e) blinded assessment of outcome; (f) use of anesthetic without significant intrinsic vascular protection activity; (g) appropriate animal model (aged, diabetic, or hypertensive); (h) sample size calculation; (i) compliance with animal welfare regulations; and (j) statement of potential conflict of interests. Every item was given one point. Two authors independently evaluated the study quality, and the final result was identified by discussion when countering disagreement.

2.5. Statistical Analysis. All the data of VEGF and BVD were considered as continuous data, and then, we used the standard mean difference (SMD) with the random effect model to assess the comprehensive results, because of the heterogeneity between multistudies. Then we utilized I^2 statistic to estimate heterogeneity. The significance of differences between n groups was estimated by partitioning heterogeneity and by using the $\chi 2$ distribution with $n-1$ degrees of freedom (df), where n equals the number of groups. The publication bias was expressed by a funnel plot. Probability values of 0.05 were considered significant. We utilized RevMan version 5.3 to carry out the meta-analysis.

3. Results

3.1. Study Inclusion. We searched 573 potentially relevant studies, and 315 were excluded because of duplication. After screening titles and abstracts, 73 studies were excluded because of a nonanimal study, clinical trial, case report, comments, or review. By reading the full text of the remaining articles, 135 studies were excluded because of at least one of the following reasons: (1) the outcome measures did not include VEGF and/or BVD; (2) nonmyocardial infarct model; (3) treatment with single danshen or danshen-based prescriptions; (4) no control group; and (5) duplicate publications. Ultimately, 14 eligible studies were included in qualitative synthesis and 11 eligible studies [25–38] in quantitative synthesis (Figure 1).

3.2. Study Characteristics. Fourteen studies with 226 animals were included. All the studies were published between 2004 and 2016, including four studies [25–27, 38] in English and

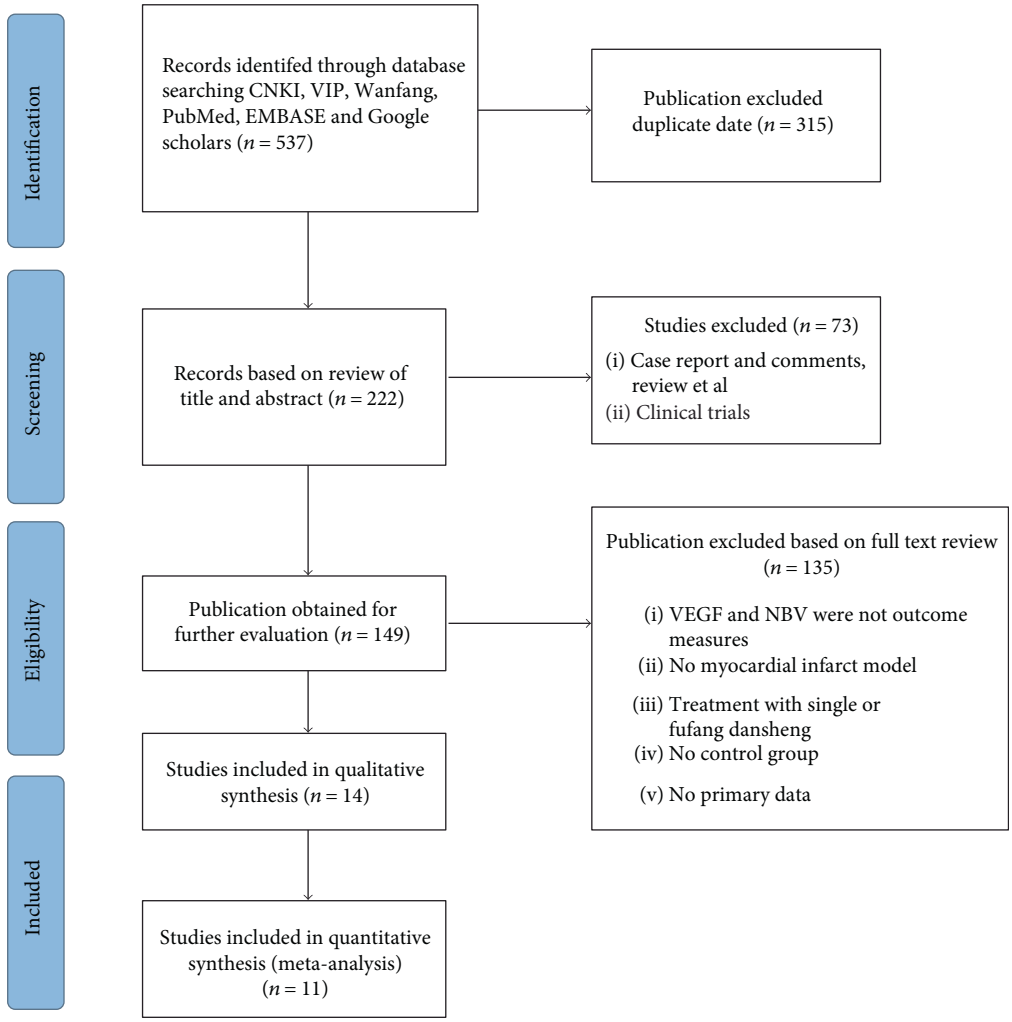

Figure 1: Flow diagram.

seven studies [29, 32–37], two online PhD theses [30, 31], and one online Master's thesis [28] in Chinese. A male/female Sprague Dawley rat, male Wistar rat, and male piglet model were used in 12 studies [25–31, 33, 34, 36–38], 1 study [35], and 1 study [32], respectively. All the myocardial infarction models were produced by ligation of the LAD. Twelve studies used blood vessel density (BVD) [26–35, 37, 38], ten studies [25–29, 31, 33, 34, 36, 38] used VEGF, and eight studies [25–27, 30, 31, 34, 35, 37] utilized myocardial infarct size as outcome measures. Anesthetic was reported in 13 studies, including pentobarbital ($n = 3$) [30, 34, 35], urethane ($n = 2$) [26, 28], chloral hydrate ($n = 4$) [25, 29, 31, 33], ether ($n = 2$) [36, 37], ketamine and diazepam ($n = 1$) [32], and hydrochloride ($n = 1$) [27], whereas one study [38] did not report the anesthetic. Seven studies [25, 26, 30, 34, 35, 37, 38] used salvianolic acid B, two studies [27, 31] used salvianolic acid A, and five studies [28, 29, 32, 33, 36] used mixed salvianolic acids. There were three administration methods, including intragastric administration ($n = 7$) [26, 28, 30, 33, 35–37], intravenous administration ($n = 5$) [25, 27, 31, 32, 34], and intraperitoneal administration ($n = 1$) [29]. The characteristics of the included studies are concluded in Table 1.

3.3. Study Quality. The quality score of studies ranged from 3 to 6. All studies were publications in a peer-reviewed journal or thesis. Five studies reported control of room temperature. All studies described random allocation to the groups. Thirteen studies used anesthetic without significant intrinsic vascular protection activity. No studies described a sample size calculation. Four studies reported a compliance with animal welfare regulations, and five studies mentioned a statement of potential conflict of interests. None of the studies described masked induction of appropriate animal models (aged, diabetic, or hypertensive). The methodological quality is concluded in Table 2.

3.4. Effectiveness

3.4.1. VEGF. Ten studies [25–29, 31, 33, 34, 36, 38] utilized VEGF as the outcome measure. The meta-analysis of six studies [26, 27, 29, 31, 34, 36] showed significant effects of salvianolic acid for increasing VEGF expression compared with the control group ($n = 101$, SMD 2.02, 95% CI: 1.45~2.59, $P < 0.00001$; heterogeneity $\chi 2 = 5.70$, $P = 0.34$, $I^2 = 12\%$), Figure 2. The subgroup analysis showed that

Table 1: Characteristics of the 15 included studies.

Study (years)	Species (sex, n = experimental/control group)	Weight	Model (method)	Time drug given	Anesthetic	Treatment group and administration methods	Control group	Angiogenesis outcome index	Intergroup differences (time)	Secondary outcome	Intergroup differences	Side effect
Chao et al. [25]	Male Sprague Dawley rats (8/8)	200–220 g	AMI	1 day after the surgery	Chloral hydrate [0.3 g/kg, (i.p.)]	Salvianolic acid B 24 mg/kg·4 h, i.v.	Normal saline	(1) VEGF	(1) $P < 0.001$; 8 h	(1) Myocardial infarct size	(1) $P < 0.001$; 8 h	No report
He et al. [26]	Male Sprague Dawley rats (15/15)	200–220 g	AMI	24 h after the surgery	Urethane [1.2 g/kg, intraperitoneally (i.p.)]	Salvianolic acid B 100 mg/kg·d, i.g.	Normal saline	(1) VEGF (2) BVD	(1) $P < 0.05$; 4 w (2) $P < 0.05$; 4 w	(1) Myocardial infarct size (2) LVSP (3) LVEDP (4) LVEF	(1) $P < 0.01$; 4 w (2) $P < 0.01$; 4 w (3) $P < 0.01$; 4 w (4) $P < 0.05$; 4 w	No report
Li et al. [27]	Male Sprague Dawley rats (5/5)	200–220 g	AMI	24 hours after the surgery	3.5% hydrochloride (3.5 mg/100 g, i.p.)	10 mg/kg/d salvianolic acid A i.v.	Normal saline	(1) BVD (2) VEGF	(1) $P < 0.05$; 7 d (2) $P < 0.001$; 7 d	(1) Myocardial infarct size	(1) $P < 0.01$; 1 w	No report
Yang [28]	Male Sprague Dawley rats (8/8)	180–200 g	AMI	1 week after the surgery	Urethane 1.2 g/kg, i.p.	Salvia extract (salvianolic acid B 20.6%; Danshensu 23.6%; protocatechualdehyde 3.9%) 100 mg/kg/d, i.g.	Normal saline	(1) VEGF (2) BVD	(1) $P < 0.05$; 60 d (2) $P < 0.05$; 60 d	(1) LVSP (2) LVEDP (3) IL	(1) $P < 0.05$; 60 d (2) $P < 0.05$; 60 d (3) $P < 0.05$; 60 d	No report
Fang [29]	Male Sprague Dawley rats (13/13)	220–260 g	AMI	3 days after the surgery	10% chloral hydrate (4 ml/kg, i.p.)	Salvianolate (main composition salvianolic acid B) 30 mg/kg·d, i.p.	Normal saline	(1) BVD (2) VEGF	(1) $P < 0.01$; 4 w (2) $P < 0.01$; 4 w	No	No	No report
Ma [30]	Male Sprague Dawley rats (10/10)	Three months Age	AMI	No report	3% pentobarbital 45 mg/kg, i.p.	Salvianolic acid B 1 g/(kg·d), i.g.	Normal saline	(1) BVD	(1) $P < 0.01$; 14 d	(1) Myocardial infarct size	(1) $P < 0.01$; 14 d	No report
Li [31]	Male Sprague Dawley rats (5/5)	200–220 g	AMI	1 day after the surgery	3.5% chloral hydrate (35 g/kg, i.p.)	Salvianolic acid A 10 mg/kg, i.v.	Normal saline	(1) BVD (2) VEGF	(1) $P < 0.001$; 1 w (2) $P < 0.001$; 1 w	(1) Myocardial infarct size (2) SDF-1 (3) MMP-9	(1) $P < 0.01$; 1 w (2) $P < 0.01$; 1 w (3) $P < 0.01$; 1 w	No report
Wang [32]	Male piglets (6/6)	28 ± 10 kg	AMI	1 day after the surgery	Ketamine, 20 mg/kg, and diazepam, 0.05 mg/kg, i.m.	Salvianolate (main composition salvianolic acid B) 400 mg, i.v.	Normal saline	(1) BVD	(1) $P < 0.01$; 4 w	(1) LVEF	(1) $P < 0.05$; 4 w	No report
Nuan-Liu [33]	Male Sprague Dawley rats (8/8)	200–240 g	AMI	2 days after the surgery	10% chloral hydrate i.p.	Salvia extract (main composition salvianolic acid B) 40 mg/kg·d, i.g.	Normal saline	(1) VEGF (2) BVD	(1) $P < 0.01$; 4 w (2) $P < 0.01$; 4 w	No	No	No report

Table 1: Continued.

Study (years)	Species (sex, n = experimental/control group)	Weight	Model (method)	Time drug given	Anesthetic	Treatment group and administration methods	Control group	Angiogenesis outcome index	Intergroup differences (time)	Secondary outcome	Intergroup differences	Side effect
Chen [34]	Male/female Sprague Dawley rats (8/8)	180–220 g	AMI	1 day after the surgery	3% pentobarbital 30 mg/kg i.p.	Salvianolic acid B 6.4 mg, i.v.	Normal saline	(1) VEGF (2) BVD	(1) $P < 0.01$; 2 w (2) $P < 0.01$; 2 w	(1) Myocardial infarct size (2) NO (3) NOS	(1) $P < 0.01$; 2 w (2) $P < 0.05$; 2 w (3) $P < 0.05$; 2 w	No report
Fang [35]	Male/female Wistar rats (10/10)	250 ± 50 g	AMI	6 days before the surgery	3% pentobarbital 30 mg/kg, i.p.	Salvianolic acid B 100 mg/(kg·d), i.g.	Normal saline	(1) BVD	(1) $P < 0.05$; 6 d	(1) Myocardial infarct size (2) Fibroblast	(1) $P < 0.01$; 6 d (2) $P < 0.01$; 6 d	No report
Ye [36]	Male Sprague Dawley rats (6/7)	240 ± 60 g	AMI	48 h after the surgery	Ether inhaler	Salvia extract (main composition salvianolic acid B (40 mg/kg·d), i.g.	Normal saline1	(1) VEGF	(1) $P < 0.01$; 8 w	No	No	No report
Pang [37]	Male Sprague Dawley rats (10/11)	180–220 g	AMI	24 h after the surgery	Ether inhaler	Salvianolic acid B 120 mg/(kg·d) i.g	Normal saline	(1) BVD	(1) $P < 0.05$; 2 w	(1) Myocardial infarct size (2) Ventricle thickness	(1) $P < 0.05$; 2 w (2) $P < 0.05$; 2 w	No report
Guo et al. [38]	Female SD rats (no report)	No report	AMI	No report	No report	80 μl of phosphate-buffered saline (PBS) alone and 5×10^6 salvianolic acid B pretreated MSC/d	80 μl of phosphate-buffered saline alone and 5×10^6 MSC/d	(1) BVD (2) VEGF	(1) $P < 0.01$; 4 w (2) $P < 0.05$; 4 w	No report	No report	No report

Note: LAD: the left anterior descending coronary artery; VEGF: vascular endothelium growth factor; LVSP: left ventricular systolic pressure; LVEDP: left ventricular end-diastolic pressure; IL: infarct length; LVEF: left ventricular ejection fraction.

Table 2: Risk of bias of the included studies.

Study	A	B	C	D	E	F	G	H	I	J	Total
Lin et al. [25]	√	√	√			√			√	√	**6**
He et al. [26]	√	√	√			√			√		**5**
Li et al. [27]	√	√	√			√			√		**5**
Yang [28]	√		√			√				√	**4**
Fang [29]	√	√	√			√					**4**
Ma [30]	√		√			√				√	**4**
Li [31]	√		√			√				√	**4**
Wang [32]	√		√			√					**3**
Liu [33]	√		√			√					**3**
Chen [34]	√		√			√					**3**
Fan [35]	√		√			√					**3**
Ye [36]	√		√			√					**3**
Pang [37]	√		√			√					**3**
Guo et al. [38]	√		√							√	**3**

Note: Studies fulfilling the criteria of: A: peer reviewed publication; B: control of temperature; C: random allocation to treatment or control; D: blinded induction of model; E: blinded assessment of outcome; F: use of anesthetic without significant intrinsic vascular protection activity; G: appropriate animal model (aged, diabetic, or hypertensive); H: sample size calculation; I: compliance with animal welfare regulations; J: statement of potential conflict of interests.

salvianolic acid A [27, 31] ($n = 20$, SMD 3.31, 95% CI: 1.72~4.90, $P < 0.0001$; heterogeneity $\chi 2 = 0.21$, $P = 0.65$, $I^2 = 0\%$), salvianolic acid B [26, 34] ($n = 42$, SMD 1.51, 95% CI: 0.81~2.21, $P < 0.0001$; heterogeneity $\chi 2 = 0.04$, $P = 0.84$, $I^2 = 0\%$), and a mixture of salvianolic acids [29, 36] ($n = 39$, SMD 2.28, 95% CI: 1.43 ~ 3.14, $P < 0.00001$; heterogeneity $\chi 2 = 0.55$, $P = 0.46$, $I^2 = 0\%$) were significantly increasing VEGF expression compared with the control group, respectively (Figure 3). After removing one study [34] that used female animals, the meta-analysis of five studies [26, 27, 29, 31, 36] that used male animals showed significantly increasing VEGF expression compared with the control group ($n = 89$, SMD 2.17, 95% CI: 1.52~2.82, $P < 0.00001$; heterogeneity $\chi 2 = 4.81$, $P = 0.31$, $I^2 = 17\%$), Figure 4. The remaining 4 studies [25, 28, 33, 38] failed to pool the analysis because of the absence of primary data, but all of them reported significant effects of salvianolic acid for increasing VEGF expression compared with the control group ($P < 0.05$ or $P < 0.01$).

3.4.2. BVD. Twelve studies [26–35, 37, 38] utilized BVD as the outcome measure, including salvianolic acid A [27, 31], salvianolic acid B [26, 30, 34, 35, 37, 38], and salvianolic acid mixture [28, 29, 32, 33]. The meta-analysis of the two salvianolic acid A studies [27, 31] showed significantly improving BVD compared with the control group ($n = 20$, SMD 3.56, 95% CI: 1.89~5.23, $P < 0.00001$; heterogeneity $\chi 2 = 0$, $P = 0.97$, $I^2 = 0\%$), Figure 5. The meta-analysis of the five salvianolic acid B studies [26, 30, 34, 35, 37] showed significantly improving BVD compared with the control group ($n = 107$, SMD 1.9, 95% CI: 0.9 ~ 2.9, $P = 0.0002$; heterogeneity $\chi 2 = 16.47$, $P = 0.002$, $I^2 = 76\%$). Owing to the significant statistical heterogeneity, we utilized subgroup analyses to explore the sources of the heterogeneity. Among the five included studies, three studies [30, 34, 35] used pentobarbital as anesthetic, one study [26] used urethane, and the last one [37] used ether. The meta-analysis of three studies [30, 34, 35] showed significant effects of salvianolic acid B for improving BVD compared with the control group ($n = 56$, SMD 2.83, 95% CI: 2.04~3.62, $P < 0.00001$; heterogeneity $\chi 2 = 0$, $P = 1$, $I^2 = 0\%$), Figure 6, suggesting that anesthetic was the potential cause of the heterogeneity. Additionally, after removing two studies [34, 35] which used female animals, the meta-analysis of three studies [26, 30, 37] showed significant effects of salvianolic acid B for improving BVD compared with the control group ($n = 71$, SMD 1.38, 95% CI:0.26~2.49, $P = 0.02$; heterogeneity $\chi 2 = 8.04$, $P = 0.02$, $I^2 = 75\%$). The reason of the high heterogeneity was possibly different anesthetics used. The remaining one salvianolic acid B study [38] failed to analyze because of the absence of primary data, but it also reported significant increasing BVD compared with the control group ($P < 0.05$). The meta-analysis of the 3 mixtures of salvianolic acid studies [29, 32, 33] showed significant effects for improving BVD compared with the control group ($n = 54$, SMD 8.46, 95% CI: 1.40~15.53, $P < 0.0001$; heterogeneity $\chi 2 = 19.78$, $P = 0.02$, $I^2 = 90\%$). The reason of the high heterogeneity might be that each of them had different types of salvianolic acid. The remaining one mixture of a salvianolic acid study [28] failed to pool the analysis because of the absence of primary data. However, all of them reported a positive effect on increasing BVD compared with the control group ($P < 0.05$ or $P < 0.01$).

3.4.3. Myocardial Infarct Size. Eight studies [25–27, 30, 31, 34, 35, 37] utilized myocardial infarct size as outcome measure. The meta-analysis of five studies [25, 27, 34, 35, 37] showed significant effects of salvianolic acid for decreasing myocardial infarct size compared with the control group ($n = 79$, SMD −2.16, 95% CI:−2.81~−1.51, $P < 0.00001$; heterogeneity $\chi 2 = 4.53$, $P = 0.34$, $I^2 = 12\%$), Figure 7. After removing one salvianolic acid A study [27], the meta-analysis of four salvianolic acid B studies [25, 34, 35, 37] showed significantly decreasing myocardial infarct size compared with the control group ($n = 69$, SMD −2.02, 95% CI:−2.63~−1.41, $P < 0.00001$; heterogeneity $\chi 2 = 0.63$, $P = 0.89$, $I^2 = 0\%$), Figure 8. After removing two studies [34, 35] that used female animals, the meta-analysis of three studies [25, 27, 37] showed significantly decreasing myocardial infarct size compared with the control group ($n = 47$, SMD −2.34, 95% CI:−3.67~−1.02, $P = 0.0005$; heterogeneity $\chi 2 = 4.36$, $P = 0.11$, $I^2 = 54\%$), Figure 9. The reason of the high heterogeneity was possibly the use of different types of salvianolic acid. The remaining three studies [26, 30, 31] failed to pool the analysis because of the absence of primary data, but all of them reported the significant effects of salvianolic acid for decreasing myocardial infarct size compared with the control group ($P < 0.05$ or $P < 0.01$).

4. Discussion

4.1. Summary of Evidences. To our knowledge, this is the first systematic review to estimate the effects of salvianolic acid for

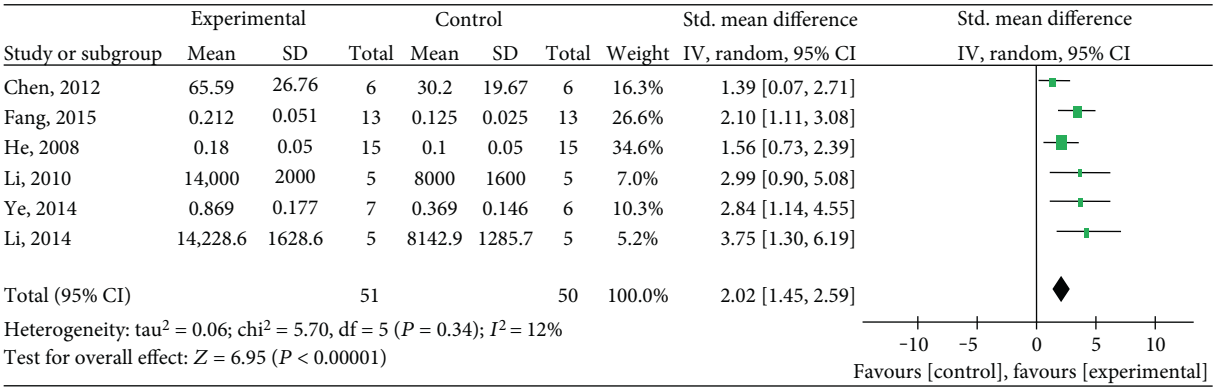

Figure 2: The forest plot: effects of salvianolic acid for increasing VEGF expression compared with the control group.

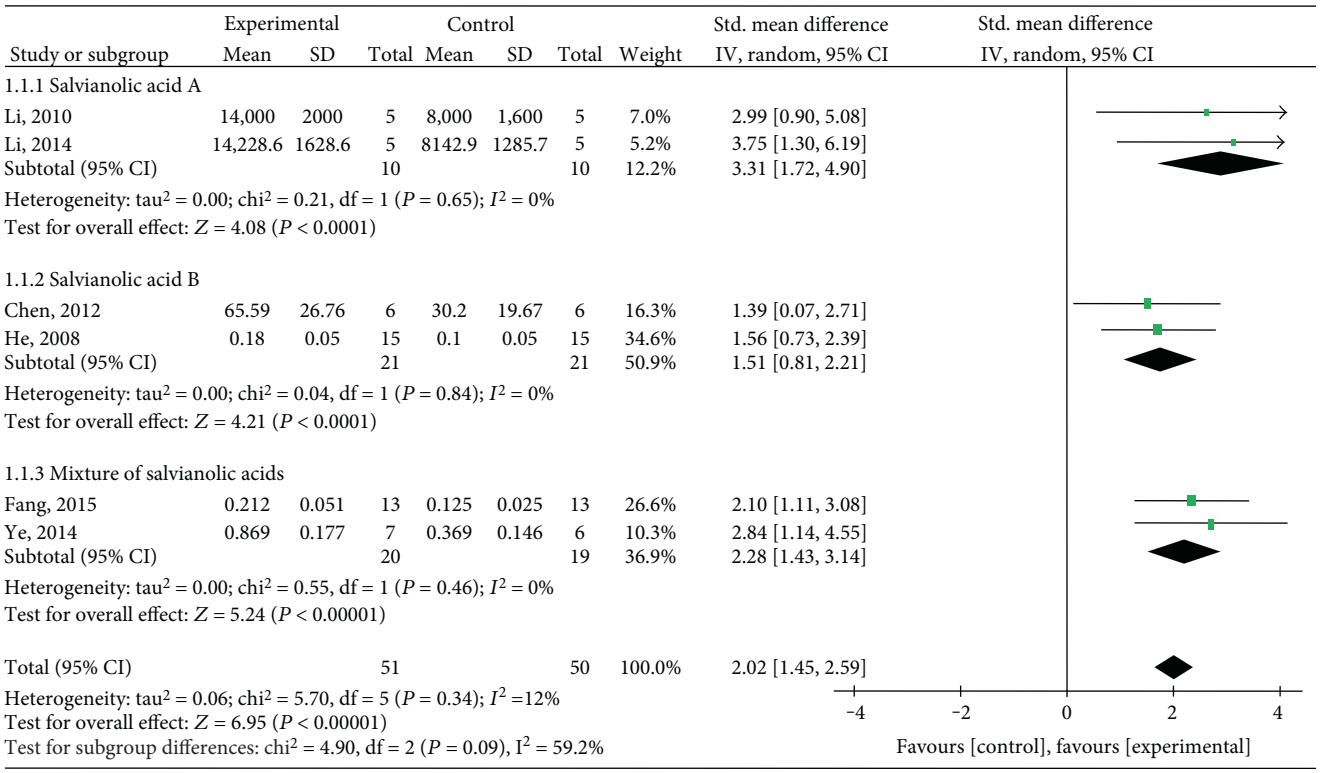

Figure 3: The forest plot: subgroup analysis of salvianolic acid A, salvianolic acid B, and a mixture of salvianolic acids for improving VEGF compared with the control group.

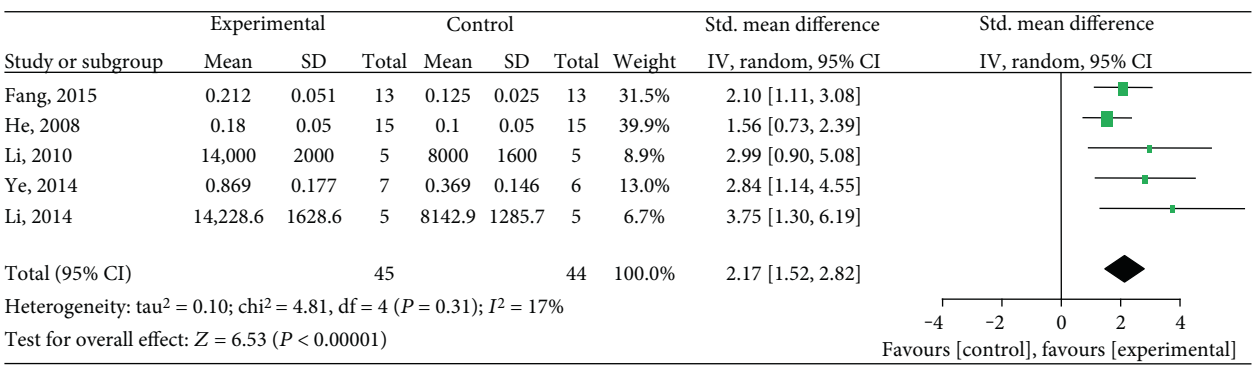

Figure 4: The forest plot: effects of salvianolic acid in male animals for increasing VEGF expression compared with the control group.

Study or subgroup	Experimental Mean	SD	Total	Control Mean	SD	Total	Weight	Std. mean difference IV, random, 95% CI
Li, 2010	13.8	2.4	5	4.8	2.2	5	50.6%	3.53 [1.19, 5.87]
Li, 2014	14	2.5	5	5.8	1.5	5	49.4%	3.59 [1.22, 5.96]
Total (95% CI)			10			10	100.0%	3.56 [1.89, 5.23]

Heterogeneity: tau^2 = 0.00; chi^2 = 0.00, df = 1 (P = 0.97); I^2 = 0%
Test for overall effect: Z = 4.19 (P < 0.00001)

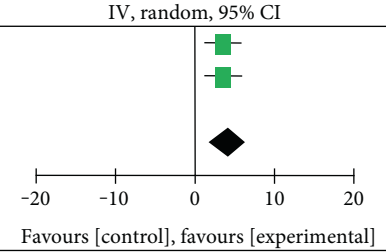

Figure 5: The forest plot: effects of salvianolic acid A for improving BVD compared with the control group.

Study or subgroup	Experimental Mean	SD	Total	Control Mean	SD	Total	Weight	Std. mean difference IV, random, 95% CI
Chen, 2012	30.2	5.07	8	15.6	4.62	8	27.6%	2.85 [1.35, 4.35]
Fan, 2004	51	11	10	26	5	10	36.4%	2.80 [1.50, 4.11]
Ma, 2006	4612	997.3	10	2374.8	381	10	35.9%	2.84 [1.52, 4.15]
Total (95% CI)			28			28	100.0%	2.83 [2.04, 3.62]

Heterogeneity: tau^2 = 0.00; chi^2 = 0.00, df = 2 (P = 1.00); I^2 = 0%
Test for overall effect: Z = 7.03 (P < 0.00001)

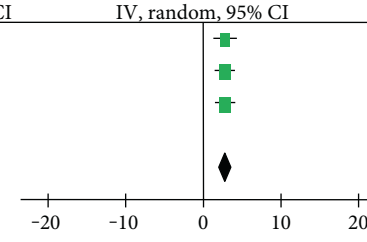

Figure 6: The forest plot: effects of salvianolic acid B that used pentobarbital as anesthetic for improving BVD compared with the control group.

Study or subgroup	Experimental Mean	SD	Total	Control Mean	SD	Total	Weight	Std. mean difference IV, random, 95% CI
Lin, 2016	8.96	1.76	8	21.25	7.72	8	22.3%	−2.08 [−3.36, −0.79]
Chen, 2012	5.74	2.02	6	14.84	5.4	6	16.6%	−2.06 [−3.57, −0.55]
Fan, 2004	7.13	1.96	10	15.46	4.38	10	25.2%	−2.35 [−3.55, −1.16]
Pang, 2008	13.52	1.925	10	18.091	3.002	11	32.1%	−1.72 [−2.75, −0.69]
Li, 2014	16	0.9	5	23	1.4	5	3.9%	−5.37 [−8.64, −2.10]
Total (95% CI)			39			40	100.0%	−2.16 [−2.81, −1.51]

Heterogeneity: tau^2 = 0.07; chi^2 = 4.53, df = 4 (P = 0.34); I^2 = 12%
Test for overall effect: Z = 6.49 (P < 0.00001)

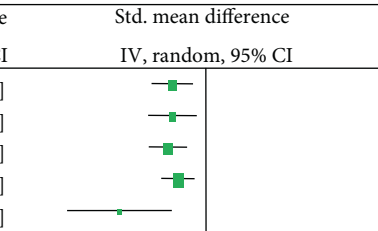

Figure 7: The forest plot: effects of salvianolic acid for decreasing myocardial infarct size compared with the control group.

Study or subgroup	Experimental Mean	SD	Total	Control Mean	SD	Total	Weight	Std. mean difference IV, random, 95% CI
Lin, 2016	8.96	1.76	8	21.25	7.72	8	22.7%	−2.08 [−3.36, −0.79]
Chen, 2012	5.74	2.02	6	14.84	5.4	6	16.3%	−2.06 [−3.57, −0.55]
Fan, 2004	7.13	1.96	10	15.46	4.38	10	26.1%	−2.35 [−3.55, −1.16]
Pang, 2008	13.52	1.925	10	18.091	3.002	11	35.0%	−1.72 [−2.75, −0.69]
Total (95% CI)			34			35	100.0%	−2.02 [−2.63, −1.41]

Heterogeneity: tau^2 = 0.00; chi^2 = 0.63, df = 3 (P = 0.89); I^2 =0%
Test for overall effect: Z = 6.49 (P < 0.00001)

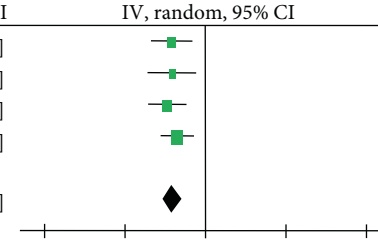

Figure 8: The forest plot: effects of salvianolic acid B for decreasing myocardial infarct size compared with the control group.

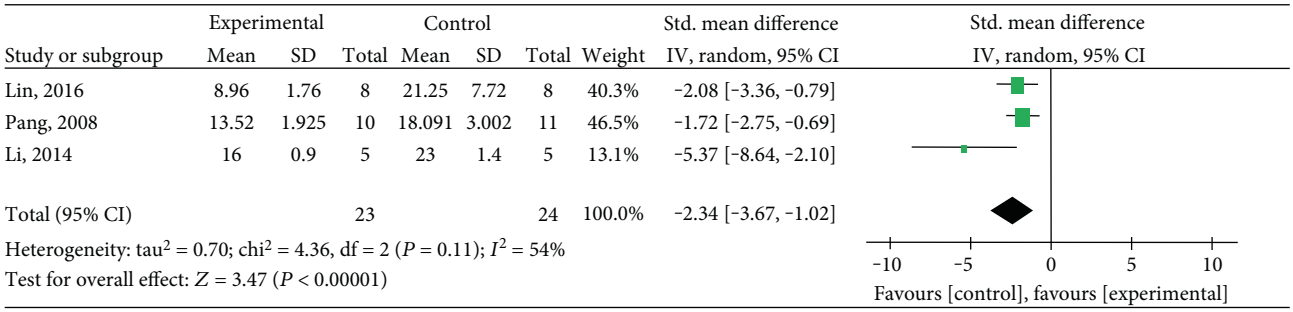

Figure 9: The forest plot: effects of salvianolic acid in male animals for decreasing myocardial infarct size compared with the control group.

experimental MI. Fourteen studies involving 226 animals were identified. The present study showed that salvianolic acid can reduce myocardial infarct size and promote the expression of VEGF and BVD in animal model experiments of MI, suggesting that salvianolic acid has cardioprotective function through promoting angiogenesis in the animal model of MI.

4.2. Limitations. First, we only searched English and Chinese databases, which may result in selective bias to some degrees [39]. Second, there are no negative studies, which may overestimate the effect to a certain degree [40]. Third, the methodological quality of included studies is generally poor, which ranges from 3 to 6. No study adopted blinded induction of model and blinded assessment of outcome. The poor methodological quality will be an inherent limitation of this systematic review, affecting the accuracy of the results [41]. MI generally occurs in patients associated with medical problems such as older age, diabetes, hypertension, and hyperlipidemia [42]. However, none of the studies adopted these appropriate animal models. Thus, we should treat present positive results cautiously because of the methodological flaws in some included studies. Finally, another weakness that should not be ignored is the heart protection of estrogen. There are two included studies [34, 35] adopting female animals. Although the specific mechanism remains unclear, the heart protection of estrogen has been observed both in clinical and in preclinical studies [43]. The sex of animals should be taken into account when designing animal experiment.

4.3. Implications. Angiogenesis is known as the process by which this plexus differentiates and gradually comes into being a network of functional capillaries. This step essentially is involved with the budding off of endothelial cells from the ends and lateral walls of the preexisting primitive endothelial tubules, resulting in the formation of a network of narrow capillary microvessels [44]. Clinical trials has showed that therapeutic angiogenesis make end-stage coronary artery disease patients to acquire improvements in exercise time and in symptoms of angina, as well as perfusion and left ventricular function [45]. Currently, therapeutic angiogenesis, as a new treatment of MI, has been a widespread recognition and affirmation [16–18]. This systematic review has showed that salvianolic acid can exert cardioprotection through promoting angiogenesis, making it as a potential candidate for clinical MI trials in the future.

There is no doubt that study quality is an important effect factor [41]. We suggest that further design of the studies carried out should refer to the ten-item scale [38] such as random allocation, blinded induction of model, blinded assessment of outcome, and use of anesthetic without significant intrinsic vascular protection activity. In addition, we should include appropriate animals because an unsuitable animal model may affect the validity of the experiments [46]. Myocardial infarction generally occurs in elderly patients with hypertension or hyperlipidemia [42], so using appropriate models can increase the accuracy of the results.

4.4. Conclusion. The salvianolic acid including salvianolic acid A, salvianolic acid B, and a mixture of salvianolic acids can reduce myocardial infarct size and promote the expression of VEGF and BVD in animal model experiments of MI, suggesting that salvianolic acid has cardioprotective function through promoting angiogenesis in the animal model of MI. However, the positive conclusion should be treated cautiously because of the methodological flaws.

Conflicts of Interest

The authors confirm that this article's content has no conflict of interest.

Authors' Contributions

Long-jie Yu, Ke-Jian Zhang, and Jia-Zhen Zhu contributed equally to this work.

Acknowledgments

This project was supported by the grant of the National Natural Science Foundation of China (81473491/H2902).

References

[1] M. S. Lauer, "Advancing cardiovascular research," *Chest*, vol. 141, no. 2, pp. 500–505, 2012.

[2] Organization WH, "World Health Organization report," May 2014, http://www.who.int/mediacentre/factsheets/fs310/zh/.

[3] K. Q. Luo, H. B. Long, and B. C. Xu, "Reduced apoptosis after acute myocardial infarction by simvastatin," *Cell Biochemistry and Biophysics*, vol. 71, no. 2, pp. 735–740, 2015.

[4] J. Hung, T. H. Teng, J. Finn et al., "Trends from 1996 to 2007 in incidence and mortality outcomes of heart failure after acute

myocardial infarction: a population-based study of 20,812 patients with first acute myocardial infarction in Western Australia," *Journal of the American Heart Association*, vol. 2, no. 5, article e000172, 2013.

[5] S. Mendis, K. Thygesen, K. Kuulasmaa et al., "World Health Organization definition of myocardial infarction: 2008-09 revision," *International Journal of Epidemiology*, vol. 40, no. 1, pp. 139–146, 2011.

[6] J. E. Dalen, J. S. Alpert, R. J. Goldberg, and R. S. Weinstein, "The epidemic of the 20th century: coronary heart disease," *The American Journal of Medicine*, vol. 127, no. 9, pp. 807–812, 2014.

[7] N. R. Patel, D. V. Patel, P. R. Murumkar, and M. R. Yadav, "Contemporary developments in the discovery of selective factor Xa inhibitors: a review," *European Journal of Medicinal Chemistry*, vol. 121, pp. 671–698, 2016.

[8] Antithrombotic Trialists' (ATT) Collaboration, C. Baigent, L. Blackwell et al., "Aspirin in the primary and secondary prevention of vascular disease: collaborative meta-analysis of individual participant data from randomised trials," *Lancet*, vol. 373, no. 9678, pp. 1849–1860, 2009.

[9] L. R. Jackson, C. Ju, M. Zettler et al., "Outcomes of patients with acute myocardial infarction undergoing percutaneous coronary intervention receiving an oral anticoagulant and dual antiplatelet therapy: a comparison of clopidogrel versus prasugrel from the TRANSLATE-ACS study," *JACC. Cardiovascular Interventions*, vol. 8, no. 14, pp. 1880–1889, 2015.

[10] R. Kones, "Primary prevention of coronary heart disease: integration of new data, evolving views, revised goals, and role of rosuvastatin in management. A comprehensive survey," *Drug Design, Development and Therapy*, vol. 5, no. 1, pp. 325–380, 2011.

[11] H. M. Krumholz, S. L. Normand, and Y. Wang, "Trends in hospitalizations and outcomes for acute cardiovascular disease and stroke, 1999-2011," *Circulation*, vol. 130, no. 12, pp. 966–975, 2014.

[12] P. D. Thompson, G. Panza, A. Zaleski, and B. Taylor, "Statin-associated side effects," *Journal of the American College of Cardiology*, vol. 67, no. 20, pp. 2395–2410, 2016.

[13] K. Bledzka, S. S. Smyth, and E. F. Plow, "Integrin alphaIIbbeta3: from discovery to efficacious therapeutic target," *Circulation Research*, vol. 112, no. 8, pp. 1189–1200, 2013.

[14] G. Scharbert, L. Wetzel, W. C. Schrottmaier, J. B. Kral, T. Weber, and A. Assinger, "Comparison of patient intake of ticagrelor, prasugrel, or clopidogrel on restoring platelet function by donor platelets," *Transfusion*, vol. 55, no. 6, pp. 1320–1326, 2015.

[15] S. Bangalore, Y. Guo, Z. Samadashvili, S. Blecker, J. Xu, and E. L. Hannan, "Everolimus-eluting stents or bypass surgery for multivessel coronary disease," *The New England Journal of Medicine*, vol. 372, no. 13, pp. 1213–1222, 2015.

[16] A. Anisimov, D. Tvorogov, A. Alitalo, V. M. Leppanen, Y. An, and E. C. Han, "Vascular endothelial growth factor-angiopoietin chimera with improved properties for therapeutic angiogenesis," *Circulation*, vol. 127, no. 4, pp. 424–434, 2013.

[17] K. Albrecht-Schgoer, W. Schgoer, J. Holfeld, M. Theurl, D. Wiedemann, and C. Steger, "The angiogenic factor secretoneurin induces coronary angiogenesis in a model of myocardial infarction by stimulation of vascular endothelial growth factor signaling in endothelial cells," *Circulation*, vol. 126, no. 21, pp. 2491–2501, 2012.

[18] S. Banquet, E. Gomez, L. Nicol et al., "Arteriogenic therapy by intramyocardial sustained delivery of a novel growth factor combination prevents chronic heart failure," *Circulation*, vol. 124, no. 9, pp. 1059–1069, 2011.

[19] B. Jiang, J. Chen, L. Xu et al., "Salvianolic acid B functioned as a competitive inhibitor of matrix metalloproteinase-9 and efficiently prevented cardiac remodeling," *BMC Pharmacology*, vol. 10, no. 1, p. 10, 2010.

[20] Y. Joe, M. Zheng, H. J. Kim et al., "Salvianolic acid B exerts vasoprotective effects through the modulation of heme oxygenase-1 and arginase activities," *The Journal of Pharmacology and Experimental Therapeutics*, vol. 341, no. 3, pp. 850–858, 2012.

[21] J. H. Ho and C. Y. Hong, "Salvianolic acids: small compounds with multiple mechanisms for cardiovascular protection," *Journal of Biomedical Science*, vol. 18, no. 1, p. 30, 2011.

[22] T. P. Fan, J. C. Yeh, K. W. Leung, P. Y. Yue, and R. N. Wong, "Angiogenesis: from plants to blood vessels," *Trends in Pharmacological Sciences*, vol. 27, no. 6, pp. 297–309, 2006.

[23] S. P. Murphy and A. N. Murphy, "Pre-clinical systematic review," *Journal of Neurochemistry*, vol. 115, no. 4, p. 805, 2010.

[24] M. R. Macleod, T. O'Collins, D. W. Howells, and G. A. Donnan, "Pooling of animal experimental data reveals influence of study design and publication bias," *Stroke*, vol. 35, no. 5, pp. 1203–1208, 2004.

[25] C. Lin, Z. Liu, Y. Lu et al., "Cardioprotective effect of Salvianolic acid B on acute myocardial infarction by promoting autophagy and neovascularization and inhibiting apoptosis," *The Journal of Pharmacy and Pharmacology*, vol. 68, no. 7, pp. 941–952, 2016.

[26] H. He, M. Shi, X. Yang, X. Zeng, L. Wu, and L. Li, "Comparison of cardioprotective effects using salvianolic acid B and benazepril for the treatment of chronic myocardial infarction in rats," *Naunyn-Schmiedeberg's Archives of Pharmacology*, vol. 378, no. 3, pp. 311–322, 2008.

[27] Y. J. Li, C. L. Duan, and J. X. Liu, "Salvianolic acid A promotes the acceleration of neovascularization in the ischemic rat myocardium and the functions of endothelial progenitor cells," *Journal of Ethnopharmacology*, vol. 151, no. 1, pp. 218–227, 2014.

[28] X.-Z. Yang, *Therapeutic Effects and Mechanisms of Danshen on Large Myocardial Infarction in Rats*, [M.S. thesis], Zhejiang University, China, 2007.

[29] L.-Y. Fang, "Role of salvianolate in angiogenesis after acute myocardial infarction in rats," *International Journal of Cardiovascular Diseases*, vol. 42, no. 4, pp. 256–260, 2015.

[30] Y.-Y. Ma, *The Effects of Salidrosid and Salvianolic Acid B on Prnliferation,Migration and Apoptosis of Human Endothelial Progenitor Cells*, [Ph.D. thesis], Fudan University, China, 2006.

[31] Y.-J. Li, *Explorations on the Material Basis of pro-Angiogenic Actions of Shuangshentongguan and Underlying Mechanisms*, [Ph.D. thesis], Academy of Chinese Medical Sciences, China, 2010.

[32] M.-W. Wang, *Promotion of Heart Function and Collateral Blood Vessel of Salvianolate on Acute Myocardial Infarction in Swines*, Department of Cardiology, the First Affiliated Hospital of NJMi, Nanjing 210029, China, 2008.

[33] N. Liu, L. Yang, B.-y. Mao, G.-c. Xu, and S.-s. Ye, "Salvia extract promotes angiogenesis of myocardium in rats with myocardial infarction," *Chinese Journal of Pathophysiology*, vol. 31, no. 8, pp. 1490–1494, 2015.

[34] H.-X. Chen, "Effect of salvianolic acid B on angiogenesis of ischemic myocardium in myocardial ischemia rats," *Chinese Journal of Experimental Traditional Medical Formulae*, vol. 18, no. 20, pp. 180–183, 2012.

[35] Y.-C. Fang, Y. C. Fan, G. F. Zhao, and W. Z. Zhang, "Influence of salvianolic acid B on pathomorphology in myocardial infarction tats," *Journal of Tianjin University of Traditional Chinese Medicine*, vol. 23, no. 1, pp. 12–14, 2004.

[36] S.-S. Ye, "Effect of salvia extract on the expression levels of VEGF in rats with myocardial infarction," *Lishizhen Medicine and Materia Medica Research*, vol. 25, no. 5, pp. 1046–1048, 2014.

[37] X.-L. Pang, "The intervention effect of TCM on acute myocardial infarction in rats," *Tianjin Journal of Traditional Chinese Medicine*, vol. 25, no. 4, pp. 325–327, 2008.

[38] H. D. Guo, G. H. Cui, J. X. Tian et al., "Transplantation of salvianolic acid B pretreated mesenchymal stem cells improves cardiac function in rats with myocardial infarction through angiogenesis and paracrine mechanisms," *International Journal of Cardiology*, vol. 177, no. 2, pp. 538–542, 2014.

[39] G. H. Guyatt, A. D. Oxman, V. Montori et al., "GRADE guidelines: 5. Rating the quality of evidence—publication bias," *Journal of Clinical Epidemiology*, vol. 64, no. 12, pp. 1277–1282, 2011.

[40] A. Franco, N. Malhotra, and G. Simonovits, "Social science. Publication bias in the social sciences: unlocking the file drawer," *Science*, vol. 345, no. 6203, pp. 1502–1505, 2014.

[41] S. C. Landis, S. G. Amara, K. Asadullah et al., "A call for transparent reporting to optimize the predictive value of preclinical research," *Nature*, vol. 490, no. 7419, pp. 187–191, 2012.

[42] R. Blankstein, W. Ahmed, F. Bamberg et al., "Comparison of exercise treadmill testing with cardiac computed tomography angiography among patients presenting to the emergency room with chest pain: the Rule Out Myocardial Infarction Using Computer-Assisted Tomography (ROMICAT) study," *Circulation. Cardiovascular Imaging*, vol. 5, no. 2, pp. 233–242, 2012.

[43] G. P. van Hout, S. J. Jansen of Lorkeers, K. E. Wever et al., "Translational failure of anti-inflammatory compounds for myocardial infarction: a meta-analysis of large animal models," *Cardiovascular Research*, vol. 109, no. 2, pp. 240–248, 2016.

[44] J. S. Silvestre, D. M. Smadja, and B. I. Lévy, "Postischemic revascularization: from cellular and molecular mechanisms to clinical applications," *Physiological Reviews*, vol. 93, no. 4, pp. 1743–1802, 2013.

[45] S. B. Freedman and J. M. Isner, "Therapeutic angiogenesis for ischemic cardiovascular disease," *Journal of Molecular and Cellular Cardiology*, vol. 33, no. 3, pp. 379–393, 2001.

[46] N. A. Crossley, E. Sena, J. Goehler et al., "Empirical evidence of bias in the design of experimental stroke studies: a metaepidemiologic approach," *Stroke*, vol. 39, no. 3, pp. 929–934, 2008.

Hindawi
Oxidative Medicine and Cellular Longevity
Volume 2017, Article ID 3631565, 14 pages
https://doi.org/10.1155/2017/3631565

Research Article

Hepatoprotective Effect of Polyphenol-Enriched Fraction from *Folium Microcos* on Oxidative Stress and Apoptosis in Acetaminophen-Induced Liver Injury in Mice

Hongtan Wu,[1,2,3] Gang Zhang,[3,4] Lisen Huang,[1,2,3] Haiyue Pang,[1,2,3] Na Zhang,[5] Yupei Chen,[1,2,3] and Gueyhorng Wang[1,2,3]

[1]*Application Technique Engineering Center of Natural Cosmeceuticals, College of Fuijan Province, Xiamen Medical College, Xiamen, Fujian 361023, China*
[2]*Research Center of Natural Cosmeceuticals Engineering, Xiamen Medical College, Xiamen, Fujian 361023, China*
[3]*Fujian Provincial Key Laboratory of Biological Engineering on Traditional Herbs, Xiamen Medical College, Xiamen, Fujian 361023, China*
[4]*Technology and Engineering Center for Marine Biomedical Resource Utilization, Xiamen Medical College, Xiamen, Fujian 361023, China*
[5]*Department of Pharmacy, Xiamen Medical College, Xiamen, Fujian 361023, China*

Correspondence should be addressed to Gang Zhang; zg@xmmc.edu.cn and Gueyhorng Wang; wgh@xmmc.edu.cn

Received 21 November 2016; Revised 24 February 2017; Accepted 20 March 2017; Published 23 May 2017

Academic Editor: Jie Li

Folium Microcos (FM), the leaves of *Microcos paniculata* L., shows various biological functions including antioxidant activity and α-glucosidase inhibitory effect. However, its therapeutic potential in acute liver injury is still unknown. This study investigated the hepatoprotective effect and underlying mechanisms of the polyphenol-enriched fraction (FMF) from *Folium Microcos*. FMF exhibited strong free radical scavenging activities and prevented HepG2/Hepa1–6 cells from hydrogen peroxide- (H_2O_2-) induced ROS production and apoptosis in vitro. Antioxidant activity and cytoprotective effects were further verified by alleviating APAP-induced hepatotoxicity in mice. Western blot analysis revealed that FMF pretreatment significantly abrogated APAP-mediated phosphorylation of MAPKs, activation of proapoptotic protein caspase-3/9 and Bax, and restored expression of antiapoptotic protein Bcl2. APAP-intoxicated mice pretreated with FMF showed increased nuclear accumulation of nuclear factor erythroid 2-related factor (Nrf2) and elevated hepatic expression of its target genes, NAD(P)H:quinine oxidoreductase 1 (NQO1) and hemeoxygenase-1(HO-1). HPLC analysis revealed the four predominantly phenolic compounds present in FMF: narcissin, isorhamnetin-3-O-β-D-glucoside, isovitexin, and vitexin. Consequently, these findings indicate that FMF possesses a hepatoprotective effect against APAP-induced hepatotoxicity mainly through dual modification of ROS/MAPKs/apoptosis axis and Nrf2-mediated antioxidant response, which may be attributed to the strong antioxidant activity of phenolic components.

1. Introduction

The liver is a major organ that regulates homeostasis of metabolism and detoxifies metabolites/xenobiotics generated during drug exposure in the body [1]. Owing to these crucial functions, the liver is liable to damages caused by hepatotoxic chemicals, free radicals, and other reactive oxygen species (ROS) [2]. Overproduction of pro-oxidants/ROS in the liver can cause damage to structural and functional integrity of cells, leading to extensive liver injury [3]. Dysfunction of antioxidant/detoxification defense system is also considered to play a significant pathophysiological role in the development of liver diseases [4]. Therefore, developing hepatoprotective agents to reduce or eliminate ROS production and

to strengthen physiological antioxidant capability will be an effective strategy for fighting oxidative stress that causes liver damage and diseases.

Acetaminophen (N-acetyl-p-aminophenol, APAP), a commonly used analgesic and antipyretic drug, is widely used to investigate liver toxicity associated with oxidative stress and to evaluate therapeutic potential of drug candidates. APAP is usually safe and effective at therapeutic doses, but overdose of it can cause severe acute liver injury [5]. Mechanistically, APAP-induced hepatotoxicity is initiated by extensive formation of N-acetyl-p-benzoquinone imine (NAPQI), a reactive metabolite of APAP, which in turn depletes hepatic glutathione (GSH) and causes mitochondrial dysfunction and damage, resulting in overproduction of mitochondrial ROS [6, 7]. During APAP challenge, ROS generated from mitochondria and other sources not only causes cell damage via mechanisms involving lipid peroxidation with subsequent liver injury [8] but also activates many kinases, such as c-jun-N-terminal kinase (JNK), to aggravate degenerative progression in liver tissues [9]. Activated JNK binding to mitochondria further enhances ROS generation. In addition, JNK can phosphorylate several transcription factors, such as p53 and NF-κB, to accelerate hepatic apoptosis and inflammatory response [10, 11], ultimately leading to extensive oxidative stress and acute liver injury.

Therefore, rigorous control of ROS levels by antioxidant molecules and detoxifying enzymes plays a crucial role in maintaining intracellular redox homeostasis in response to oxidative insults. It has been demonstrated that nuclear factor erythroid 2-related factor (Nrf2) and its negative regulator kelch-like ECH-associated protein 1 (Keap1) serve as an important reaction axis for cells to combat oxidative stress [12]. Nrf2 belongs to the basic leucine zipper family of transcription factors and is implicated as a major regulator of antioxidant response element- (ARE-) mediated detoxification and antioxidant gene expression [13]. Under basal conditions, Nrf2 interacts with Keap1 and is retained in the cytoplasm. In response to oxidative stress, Nrf2 dissociates from Keap1 and translocates to the nucleus, where it binds to ARE in the upstream region and subsequently promotes transcription of its target genes, including NAD(P)H:quinine oxidoreductase 1 (NQO1), glutamate-cysteine ligase catalytic and modifier subunits (GCLC and GCLM), and heme oxygenase-1 (HO-1) [14]. Considerable research has demonstrated the involvement of Keap1-Nrf2-ARE signaling pathway in organ injuries caused by toxic stimuli. Mice deficient in Nrf2 showed high susceptibility to APAP-induced liver injury [15, 16]. On the contrary, hepatocyte-specific Keap1 knockout mice exhibited an increase in genes encoding for detoxifying enzymes and resisted hepatotoxicity [17]. Thus, agents that can activate Nrf2 may be beneficial in mitigating oxidative stress-induced liver injury.

Despite the increasing need for hepatoprotective agents to protect people from liver injury, only a limited number of efficacious and reliable drugs were used successfully, and some of them even possessed potential adverse effects. In recent years, numerous edible and medicinal plants around the world have drawn increasing attention as dietary supplements and therapeutic intervention strategies for their excellent health-promoting properties and being less harmless than synthetic agents [18–20]. *Microcos paniculata* L., belonging to the Malvaceae family, is mainly distributed in tropical and subtropical areas of South and Southeast Asia [21]. In China, its leaves, named as *Folium Microcos* (FM), are traditionally used as folk medicine and herbal tea materials for treatment of fever, heatstroke, indigestion, and diarrhea [22]. Previous phytochemical studies on FM validated the existence of various bioactive constituents, such as triterpenoids, flavonoids, and alkaloids with pharmacological effects [21–23]. However, there are few reports available to describe the potential effect of FM against liver injury and what kinds of compounds it is related to. Hence, the present study evaluated the effect of the polyphenol-enriched fraction (FMF) from FM on oxidative stress and APAP-induced hepatotoxicity and investigated the potential mechanisms. Moreover, the main components of FMF were identified and quantified by reversed phase high-performance liquid chromatography (RP-HPLC) to gain insights into the compounds responsible for its antioxidant and hepatoprotective effects.

2. Materials and Methods

2.1. Chemicals and Reagents. Acetaminophen (N-acetyl-p-aminophenol, APAP), 3-(4,5-dimethylthiazol-2yl)-2,5-diphenyltetrazolium bromide (MTT), 2′,7′-dichlorodihydrofluorescein diacetate (DCFH-DA), 1,1-diphenyl-2-picrylhydrazyl (DPPH), nitroblue tetrazolium (NBT), phenazine methosulfate (PMS), β-nicotinamide adenine dinucleotide, reduced disodium salt, trihydrate (β-NADH), hematoxylin, and eosin were purchased from Sigma-Aldrich (St. Louis, MO, USA); Trizol, PrimeScript™ RT Master Mix, and SYBR Green Master Mix were purchased from Takara Biotechnology (Dalian, China); Oligonucleotides were synthesized by Sangon Biotech (Shanghai, China); Gallic acid and ascorbic acid were purchased from Sangon Biotech (Shanghai, China); assay kits of alanine aminotransferase (ALT), aspartate aminotransferase (AST), lactate dehydrogenase (LDH), catalase (CAT), superoxide dismutase (SOD), malonaldehyde (MDA), reduced glutathione (GSH), and glutathione peroxidase (GSH-Px) were purchased from Nanjing Jiancheng Institute of Biotechnology (Nanjing, China); Nuclear and Cytoplasmic Protein Extraction Kit was purchased from the Beyotime Institute of Biotechnology (Shanghai, China); Dulbecco's minimum essential medium (DMED), fetal bovine serum (FBS), and penicillin/streptomycin were purchased from Invitrogen (Carlsbad, CA, USA). All other chemicals were of the highest grade available.

2.2. Plant Material, Extraction, and Preparation. Leaves of *Microcos paniculata* L. were purchased from Guangzhou Qingping Professional Market for Traditional Chinese Medicine, Guangdong, China. The concentrated solution (FME) was prepared according to the following procedures [24]: the air-dried leaves of FM (400 g) were powdered and boiled with 7000 mL of deionized water for 1 h. The decoction was filtered and then concentrated by a rotary evaporator with a water bath at 55°C. FME was filtered again before being

added to a Diaion HP-20 resin (Mitsubishi Chemical, Tokyo, Japan) column, which was then washed sequentially with two-column volumes of water and 75% aqueous ethanol. Sugars, proteins, and salts were removed by washing the column with water, and the eluate was named as FMW. Polyphenols were retained and then eluted with 75% aqueous ethanol, and the eluate was designated as FMF. Each eluate was concentrated by vacuum rotary evaporation. The concentrated solution was dried in a lyophilizer and then stored at 4°C. The yields of FMW and FMF were 20.0 and 10.9 g, respectively.

2.3. Determination of Total Polyphenols and Total Flavonoids. Total polyphenolic contents in the different fractions were measured by Folin-Ciocalteu method as gallic acid equivalents (GAE), expressed as milligrams of gallic acid per gram of fractions [25]. Briefly, aliquots of 1 mL samples or standard solutions were mixed with 1 mL of Folin-Ciocalteu reagent and allowed to react for 3 min. Then, 1 mL of 10% Na_2CO_3 solution was added to the mixture, and the distilled water was supplied to the final volume of 10 mL, followed by a thorough mixture and a further stand at 25°C for 2 h. Absorbance was detected at 760 nm, and total polyphenolic contents were calculated as GAE from a calibration curve ($y = 0.0575x + 0.159$, $R^2 = 0.9980$, 1–50 μg of gallic acid). Data were presented as the average of triplicate analyses.

Total flavonoids of the fractions were measured using a modified colorimetric method as rutin equivalents (RE), expressed as milligrams of rutin per gram of fractions [26]. Approximately 1 mL of samples or standard solutions were mixed with 0.2 mL of 5% $NaNO_2$ solution. After 5 min, 0.2 mL of 10% $AlCl_3$ solution was added, and the mixture was allowed to stand for another 5 min. Subsequently, the reaction solution was mixed with 0.6 mL of 4% NaOH solution, and 60% ethanol was immediately supplied to obtain a final volume of 10 mL, followed by thorough mixing and standing for another 10 min. Absorbance of the mixture was determined at 510 nm, and total flavonoid contents were calculated as RE according to a calibration curve ($y = 0.0051x + 0.0029$, $R^2 = 0.9999$, 1–50 μg of rutin). Data were presented as the average of triplicate analyses.

2.4. Measurement of Antioxidant Activities In Vitro. DPPH free radical scavenging activities of different fractions were evaluated based on a reported method [27]. One mL of samples at various concentrations was added to 1 mL of 100 μM freshly prepared DPPH radical methanol solution. Reaction mixtures were shaken vigorously and incubated at 37°C in the dark for 30 min, and an equal volume of methanol and DPPH served as a control. Absorbance was measured at 517 nm. Superoxide anion radical ($O_2^{\bullet-}$) scavenging activities of different fractions were determined using a modified method [28]. One mL of samples at various concentrations was successively mixed with 1 mL of 468 μM NADH, 60 μM PMS, and 156 μM NBT and then incubated at room temperature for 5 min. Absorbance of the mixture was determined at 560 nm, and an equal volume of methanol served as a control.

Scavenging activities were estimated based on percentages of scavenged DPPH and $O_2^{\bullet-}$, as shown by the following equation:

$$\text{Scavenging effect (\%)} = \frac{1 - (\text{absorbance of sample} - \text{absorbance of blank})}{(\text{absorbance of control} - \text{absorbance of blank})} \times 100\%. \quad (1)$$

2.5. Cell Culture and Treatment. Human hepatic carcinoma cell line (HepG2) and mouse hepatoma cell line (Hepa1–6) were purchased from American Type Culture Collection (ATCC, Manassas, VA, USA). Cells were cultured in DMEM supplemented with 10% FBS and 100 U/mL penicillin/streptomycin in humidified incubator at 37°C and 5% CO_2-enriched atmosphere. To determine the antioxidant effect of FMF in H_2O_2-induced oxidative stress model, cells were seeded in 96-well plates at an initial density of 2×10^4 cells/well to adhere overnight, incubated with various concentrations of FMF for 12 h, and then exposed to 400 μM H_2O_2 without changing the medium for 4 h [29]. Control cells were incubated with culture medium of equal volume.

2.6. Cell Morphology Assay. Cells were seeded in 96-well plates at an initial density of 2×10^4 cells/well to adhere overnight, incubated with various concentrations of FMF for 12 h, and then exposed to 400 μM H_2O_2 without changing the medium for 4 h. Cell morphology images were taken at the magnification of 100x [29].

2.7. Cell Viability Assay. Cell viability was measured by MTT assay [30], which is based on the conversion of MTT to dark-blue formazan crystals by mitochondrial dehydrogenase enzyme. In brief, 10 μL of 5 mg/mL MTT was added into each well and incubated at 37°C for 4 h. After incubation, the culture medium was removed from the wells and replaced with 150 μL DMSO. Plates were then vigorously shaken to ensure complete solubilization. Finally, absorbance of formazan was measured on a plate reader (Molecular Devices, Sunnyvale, CA) at 490 nm. Relative cell viability was calculated as absorbance of sample-treated cells divided by absorbance of untreated control cells.

2.8. Measurement of Intracellular ROS In Vitro. Intracellular ROS levels were measured by using a modified method with DCFH-DA as a fluorescent probe [31]. Cells were cultured in collagen-coated 96-well black plates with transparent bottoms, treated with FMF at different concentrations for 12 h, and then exposed to 400 μM H_2O_2 without changing the medium for 4 h. Cells were subsequently loaded with 10 μM DCHF-DA at 37°C for 30 min. After washing twice with PBS buffer, fluorescence intensity that is representative of intracellular ROS levels was detected at 485/20 nm excitation and 528/20 nm emission using a fluorescence microplate reader (Molecular Devices, Sunnyvale, CA).

2.9. Animals and Experimental Design. Male ICR mice weighing 22.5 ± 1.0 g were purchased from the Laboratory

Animal Center, Xiamen University (Xiamen, China). Mice were allowed to acclimate to laboratory conditions for 7 days prior to dosing and maintained in a temperature-controlled environment ($22 \pm 2^{\circ}$C) with a 12 h light-dark cycle, free access to water, and standard rodent chow. All methods were conducted in accordance with the National Institutes of Health Guidelines for the Care and Use of Laboratory Animals. All efforts were made to minimize the number of animals used and their suffering.

Mice were randomly divided into three groups and are as follows: Group 1, control group, given appropriate vehicle throughout the experiment; Group 2, APAP group, given 500 mg/kg body weight APAP; Group 3, APAP + FMF group, given different doses of FMF (100, 200, and 400 mg/kg body weight) prior to APAP administration.

Concretely, Groups 1 and 2 were given PBS, and Group 3 was orally administered with FMF once daily for 7 consecutive days. Two hours after the final administration, Group 1 was treated with appropriate vehicle, while Groups 2 and 3 were treated with APAP at a dose of 500 mg/kg body weight by intragastric administration. Mice were subsequently anesthetized for blood sample collection and then sacrificed to obtain liver tissues after 12 h APAP treatment. Serum samples were separated from the blood by centrifugation at 10,000 ×g for 10 min at 4°C and then kept at −80°C for bioassays. A portion of the liver was fixed by 4% paraformaldehyde for histopathological analysis, and the remaining tissues were flash-frozen in liquid nitrogen and stored at −80°C for further analysis.

2.10. Measurement of Biochemical Parameters in Serum. To assess liver injury caused by APAP administration, enzymatic activities of serum ALT, AST, and LDH were estimated by using the corresponding commercial kits (Nanjing Jiancheng Institute of Biotechnology, China). Results of ALT, AST, and LDH were expressed as units per liter (U/L).

2.11. Measurement of Hepatic Levels of GSH, GSH-Px, SOD, CAT, and MDA. Liver tissues were homogenized in ice-cold PBS buffer and then centrifuged at 10,000 ×g for 10 min at 4°C. Supernatants were collected for the measurement of hepatic MDA, GSH, GSH-Px, SOD, and CAT using the corresponding commercial kits (Nanjing Jiancheng Institute of Biotechnology, China). Results were corrected for their protein content.

2.12. Histopathological Analysis. Portions of the freshly obtained liver were fixed in 4% buffered paraformaldehyde phosphate solution for 24 h and then embedded in paraffin for sectioning [8]. Hematoxylin and eosin staining was performed on 5 μm paraffin sections according to a standard procedure and analyzed by light microscopy.

2.13. Preparation of Nuclear and Cytosol Fractions. Liver nuclear and cytosol extracts were prepared by using the Nuclear and Cytoplasmic Protein Extraction Kit (Beyotime Institute of Biotechnology, Shanghai, China) according to the manufacturer's protocols. Protein concentrations were determined by Bradford method using bovine serum albumin as a standard.

2.14. RNA Isolation, RT-PCR, and Quantitative Real-Time PCR Analyses. Total RNA was isolated from liver tissues using TRIzol reagent (Takara Biotechnology, Dalian, China) and then reversely transcribed to cDNAs using PrimeScript RT Master Mix (Takara) according to the manufacturer's instructions. Quantitative real-time PCR analysis was performed using SYBR Green Master Mix (Takara) in a Roche LightCycler® 480 System (Roche Group, Switzerland). GAPDH was analyzed in each sample as an internal control for normalization, and fold changes in mRNA expression were calculated by the Comparative-Ct Method ($\Delta\Delta$Ct method).

Forward and reverse primers used for specific genes are listed as follows: Bax: (Forward, 5′-TTTCATCCAGGATCGAGCAGG-3′ and Reverse, 5′-GCAAAGTAGAAGAGGGCAACCAC-3′); Bcl2: (Forward, 5′-GGCATCTTCTCCTTCCAG-3′ and Reverse, 5′-CTACCCAGCCTCCGTTAT-3′); GAPDH: (Forward, 5′-TGCCGCCTGGAGAAACCT-3′ and Reverse, 5′-TGAAGTCGCAGGAGACAACC-3′).

2.15. Western Blot Analysis. Frozen liver tissues were homogenized in lysis buffer with glass homogenizers, and protein concentrations were then determined. Proteins were separated by sodium dodecyl sulfate-polyacrylamide gel electrophoresis (SDS-PAGE), transferred onto polyvinylidene difluoride membranes, and then identified by immunoblot analysis with appropriate primary antibodies at a dilution of 1 : 1000. Antibodies against cleaved caspase-3 (9664), caspase-3 (9665), cleaved caspase-9 (9509), caspase-9 (9508), Bax (2772), Bcl2 (3498), phospho-JNK (4668), JNK (9252), phospho-ERK1/2 (4370), ERK1/2 (4695), GAPDH (2118), Nrf2 (12721), HO-1 (70081), Tubulin (2148), and Lamin B (13435) were purchased from Cell Signaling Technology (Beverly, MA, USA); antibodies against NQO1 (11451–1-AP) and CYP2E1 (19937–1-AP) were purchased from Proteintech Group (Wuhan, China). Horseradish peroxidase-conjugated antibodies to rabbit IgG (7074) or to mouse IgG (7076) (1 : 5000 dilution for each) were purchased from Jackson ImmunoResearch Laboratories (West Grove, PA, USA). Protein bands were visualized using a SuperSignal West Pico Kit (Thermo Fisher Scientific Pierce, IL, USA) according to the manufacturer's instructions.

2.16. HPLC Analysis of Main Compounds of FMF. Chemical composition of FMF was determined using HPLC. The analysis was performed using an HC-C_{18} column (5 μm, 150 mm × 4.6 mm id, Agilent Technologies, USA) on an Agilent 1260 series HPLC system equipped with a diode array detector, an autosampler, and an openLAB CDS ChemStation Workstation (Agilent Technologies). A gradient elution was performed by varying the proportion of solvent A (acetonitrile-methanol, 25 : 75, *v*/*v*) to solvent B (water, containing 0.1% formic acid), with a flow rate of 1.0 mL/min. The solvent gradient was as follows: 0–10 min from 5% to 25% A; 10–50 min from 25% to 28% A; 50–70 min from 28% to 28% A. The wavelength for UV detection was 360 nm, and the injection volume was 10 μL.

Table 1: Contents of total phenolics and total flavonoids of different *Folium Microcos* extracts.

Extract	Total phenolics (μg GAE/mg extract)	Total flavonoids (μg RE/mg extract)
FME	79.3 ± 1.1	175.8 ± 2.1
FMW	24.2 ± 2.5	36.0 ± 4.2
FMF	338.1 ± 8.4^{a}	519.3 ± 5.3^{a}

Results are shown as mean ± SD ($n = 3$). $^{a}p < 0.001$ compared with other extracts.

All separations were performed at 25°C. The lyophilized powder of FMF was dissolved in methanol at a concentration of 0.44 mg/mL. All samples and mobile phases were filtered through a 0.45 μm membrane filter (Millipore) and then degassed in an ultrasonic bath prior to use. Four different flavonoids, including vitexin, isovitexin, isorhamnetin-3-O-β-D-glucoside, and narcissin were investigated. Identification of these compounds was performed by comparing retention times (t_R) with those of commercial standards. The linear regression equation for each calibration curve was established by plotting the amount of each standard compound injected against the average peak area.

2.17. Statistical Analysis. All data were representative of at least three independent experiments. Results were shown as mean ± SD. Student's *t*-test was used for comparisons between two groups. Differences were considered significant at $p < 0.05$. Prism 6 software package (GraphPad Software Inc., USA) was employed for statistical tests and graphical presentation of data.

3. Results

3.1. Total Phenolic, Flavonoid Contents, and Antioxidant Activities of Different Extracts. Polyphenolic compounds are able to alleviate oxidative stress by exerting antioxidant activities or affecting the antioxidant defense system [32, 33]. Therefore, total phenolic contents of FME, FMW, and FMF were determined using Folin-Ciocalteu method. As presented in Table 1, FME, FMW, and FMF contained 79.3 ± 1.1, 24.2 ± 2.5, and 338.1 ± 8.4 μg GAE/mg extract, respectively. Similar results were observed from the determination of total flavonoid contents in FME, FMW, and FMF, with values reaching 175.8 ± 2.1, 36.0 ± 4.2, and 519.3 ± 5.3 μg RE/mg extract, respectively. This quantitative analysis demonstrated that FMF contained the highest content of total phenolics and total flavonoids, implying that FMF is a polyphenol-enriched fraction. Then, DPPH free radical and superoxide anion radical ($O_2^{\bullet-}$) scavenging systems were employed to evaluate the antioxidant potential of FME, FMW, and FMF. As shown in Figure 1 and Table S1 in Supplementary Material available online at https://doi.org/10.1155/2017/3631565, FMF exhibited a concentration-dependent scavenging activity against DPPH and $O_2^{\bullet-}$ radicals ranging from 10 μg/mL to 40 μg/mL, and this property was superior to those of other tested extracts. In addition, the difference in free radical scavenging activity was unremarkable between FMF and the positive control ascorbic acid in both detected systems, especially when the concentration was above 40 μg/mL. These results showed close connection between both total phenolic and flavonoid contents and antioxidant capacity, suggesting that polyphenol-enriched FMF from *Folium Microcos* may potentially provide protection against oxidative damage. Hence, FMF was selected for the following cell and animal studies.

3.2. Protective Effects of FMF on Oxidative Stress In Vitro. A H_2O_2-mediated oxidative stress model in HepG2 cells was established to investigate the effects of FMF on oxidative damage. As can be seen in Figure 2, H_2O_2 exposure caused severe oxidative stress, as evidenced by increased ROS production and high cellular mortality compared with those by the untreated control cells. Prominent morphological changes were also caused by H_2O_2 stimulation (Figure S1). However, the abovementioned alterations were significantly alleviated by FMF pretreatment in a dose-dependent manner. Similar results were observed in Hepa1–6 cells (Figures S2 and S3). Further cytotoxicity assay indicated that FMF hardly affected the viability of tested cells (Figure S4). Collectively, these in vitro data supported the therapeutic potential of FMF in modulating antioxidant responses.

3.3. FMF Inhibited APAP-Induced Liver Injury. Oxidative stress plays an initial and augmented role in the pathogenesis of APAP-induced hepatotoxicity [34]. Therefore, hepatoprotective effects of FMF were investigated in APAP-induced liver injury mice model. As depicted in Figure 3, mice treated with APAP (500 mg/kg body weight) showed evidence of severe liver injury, as indicated by remarkable increases in serum ALT, AST, and LDH activities. However, these APAP-caused increases were significantly and dose-dependently inhibited by FMF pretreatment (100, 200, and 400 mg/kg body weight). Histopathological analysis provided supportive evidence for biochemical parameters assay (Figure 4). The sections of liver samples taken from APAP-intoxicated mice revealed extensive histological changes in the form of remarkable gross necrosis, sinusoidal congestion, hemorrhage, and inflammatory cell infiltration. Interestingly, FMF pretreatment remarkably ameliorated APAP-induced liver injury, and administration of APAP along with FMF at a dose of 400 mg/kg body weight showed a near-normal appearance, suggesting that FMF can protect against APAP-induced hepatic damage.

3.4. FMF Reduced APAP-Induced Hepatic Oxidative Stress. Lipid peroxidation and antioxidant enzyme activities were measured to examine the role of FMF in APAP-induced oxidative damage. MDA, a major end product that forms during the final stages of lipid peroxidation, is generally recognized as a direct index of toxic processes caused by free radicals [35]. As shown in Figure 5, administration of APAP to mice remarkably elevated MDA levels as compared to the untreated normal group. The liver antioxidant capacity of mice was also sharply decreased, as manifested by the significant reduction in hepatic GSH, GSH-Px, SOD, and CAT activities, which are the major enzymatic or nonenzymatic antioxidants and regulators of tissues responsible for

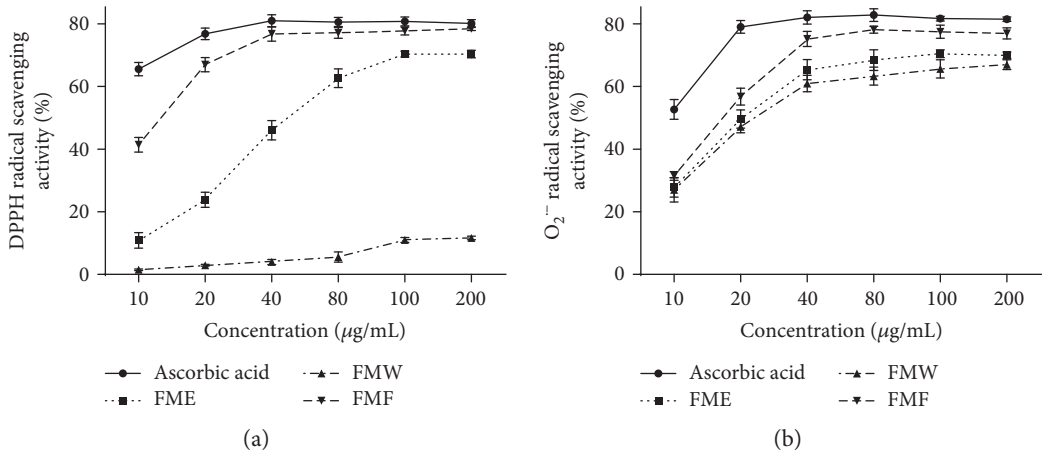

Figure 1: In vitro antioxidant activities of different extracts from *Folium Microcos*. (a) DPPH radical scavenging activity. (b) Superoxide anion radical ($O_2^{\bullet-}$) scavenging activity. FME, the concentrated solution; FMW, the fraction eluted with water; FMF, the fraction eluted with 75% ethanol. Results are shown as mean ± SD ($n = 3$).

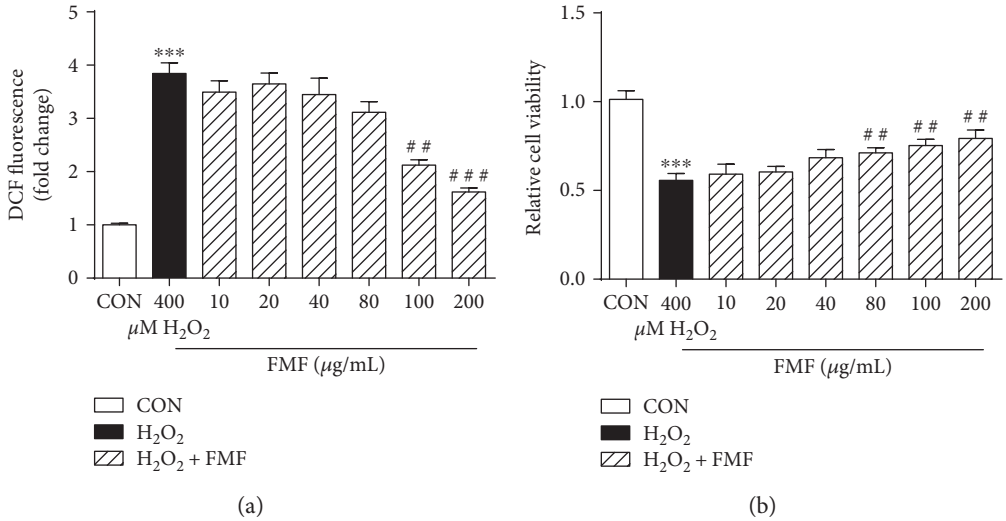

Figure 2: Effects of FMF on H_2O_2-mediated oxidative stress in HepG2 cells. Cells were treated with FMF (10, 20, 40, 80, 100, and 200 μg/mL) in the presence of 400 μM H_2O_2 for 4 h. (a) ROS formation was measured using a fluorescence microplate reader. (b) Cellular mortality was evaluated by MTT assay. Results are shown as mean ± SD ($n = 3$). $^{***}P < 0.001$ compared with the control group; $^{\#\#\#}P < 0.001$, $^{\#\#}p < 0.01$ compared with H_2O_2-intoxicated group.

intracellular redox homeostasis. However, the abovementioned alterations were effectively disputed by FMF pretreatment, clearly indicating the strong antioxidant capacity of FMF against APAP-induced liver injury.

3.5. FMF Ameliorated the Activation of ROS/MAPKs/Apoptosis Signaling and Facilitated Nrf2 Nuclear Translocation to Protect against APAP-Induced Hepatotoxicity. To determine the underlying mechanisms by which FMF alleviated APAP-induced acute liver injury, liver samples from mice treated with APAP with or without FMF pretreatment (400 mg/kg body weight) were homogenized for further western blot analysis. It is commonly recognized that APAP is converted to the highly reactive metabolite NAPQI by the hepatic cytochrome P450 system, especially CYP2E1, whose activity is critical for the development of APAP-induced hepatic injury [6, 7]. As presented in Figure 6(a), APAP treatment caused a significant increase in the expression level of CYP2E1. However, FMF pretreatment markedly suppressed APAP-induced elevation of CYP2E1. Many studies have illustrated the involvement of apoptosis in APAP-induced hepatotoxicity [36, 37]. Therefore, the expression of apoptosis-related proteins was determined. APAP administration significantly increased levels of cleaved caspase-3/9 and Bax and decreased Bcl2 protein expression. Nevertheless, these effects were prominently reversed by FMF pretreatment. Similar results were observed in mRNA levels of Bax and Bcl2 (Figure 6(b)). The activation of MAP kinases, especially the phosphorylation of JNK and ERK, can exacerbate APAP-induced mitochondrial oxidative stress and aggravate

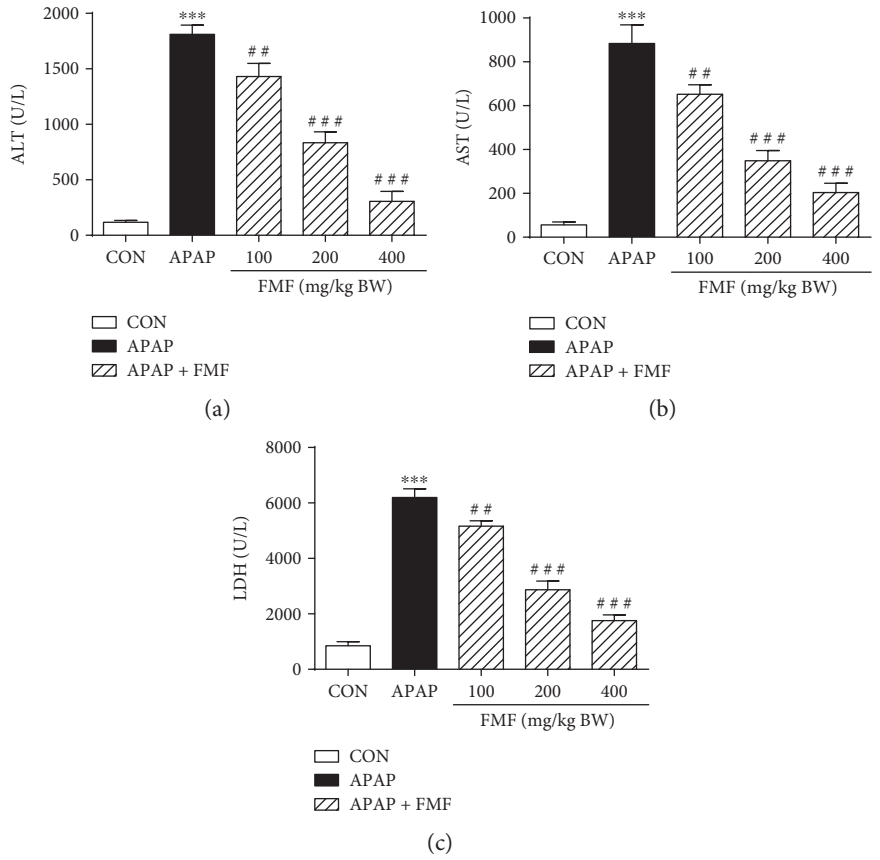

Figure 3: Effects of FMF on APAP-induced liver injury. Mice were intragastrically administered with either PBS or FMF at 100, 200, and 400 mg/kg body weight once daily for 7 consecutive days prior to single administration of APAP (500 mg/kg BW). Mice were killed at 12 h after APAP challenge. Activities of (a) ALT, (b) AST, and (c) LDH were measured in plasma samples by using the commercial kits. Results are shown as mean ± SD ($n = 8$ mice in each group). $^{***}p < 0.001$ compared with the control group; $^{###}p < 0.001$, $^{##}p < 0.01$ compared with APAP-intoxicated group.

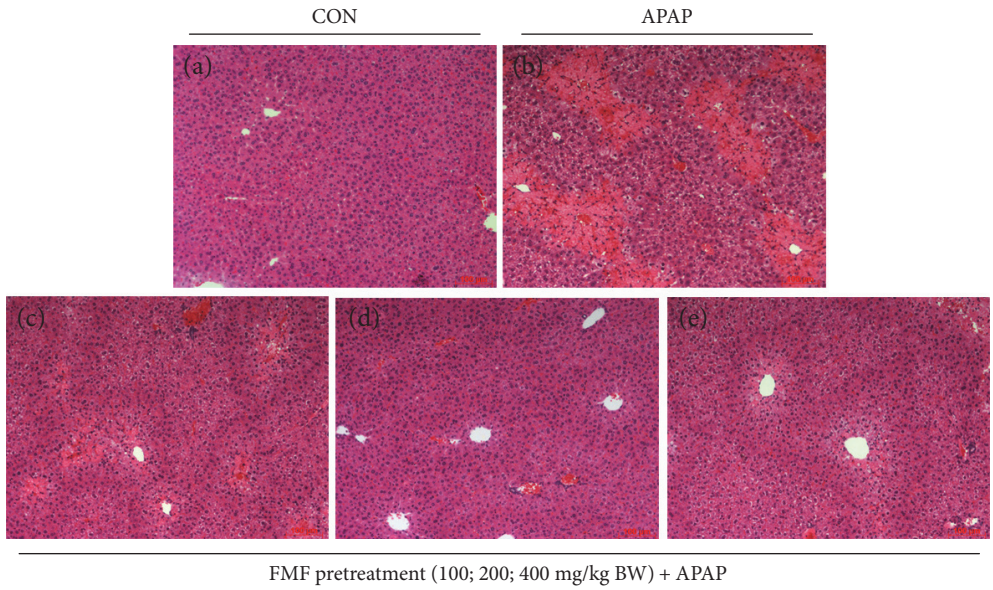

Figure 4: Effects of FMF on histological changes in APAP-intoxicated mice livers. Liver sections were stained with hematoxylin and eosin (original magnification of 100x). (a) Control group. (b) APAP-intoxicated group. (c) FMF (100 mg/kg BW) + APAP. (d) FMF (200 mg/kg BW) + APAP. (e) FMF (400 mg/kg BW) + APAP.

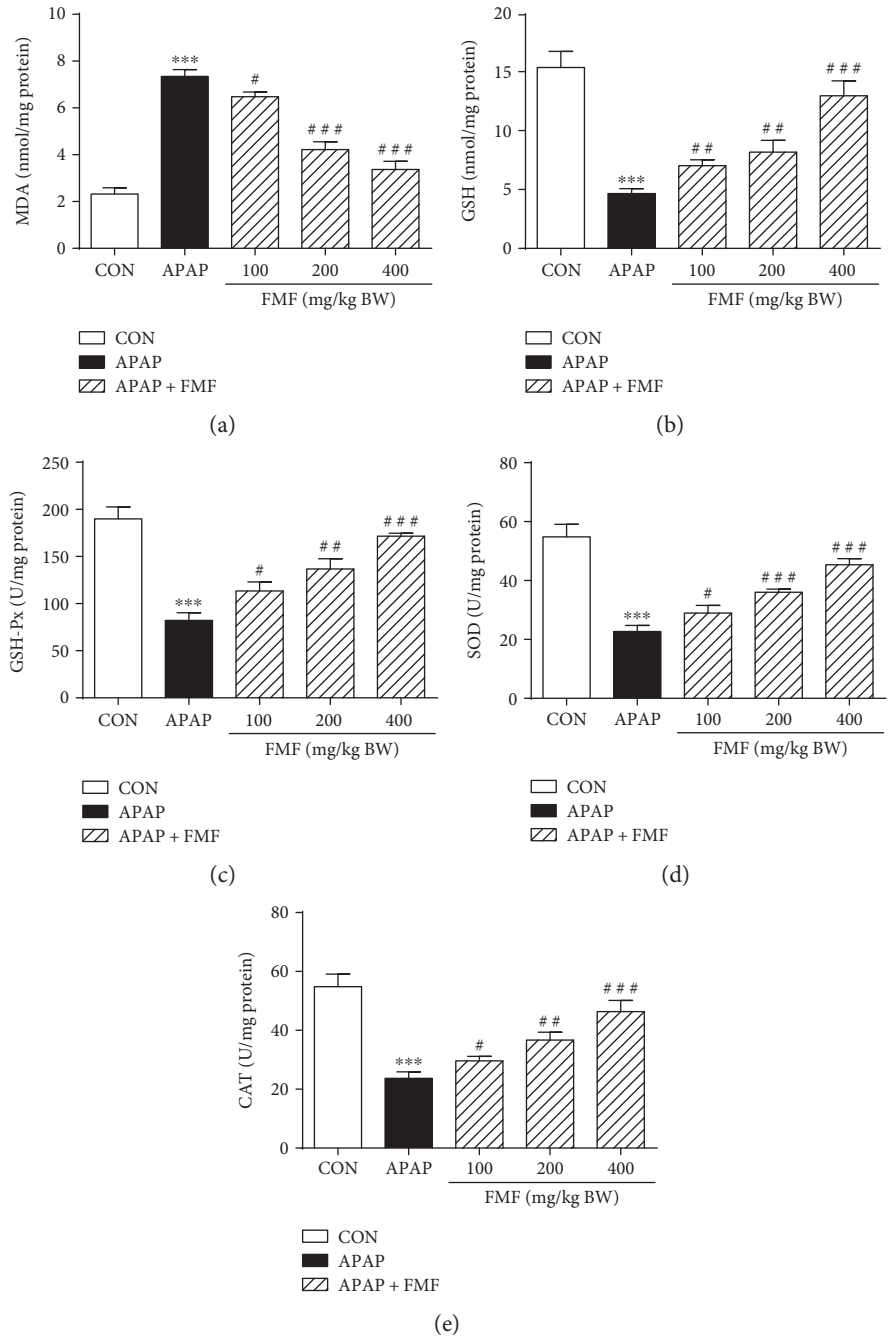

Figure 5: Effects of FMF on hepatic levels of MDA, GSH, GSH-Px, SOD, and CAT. Mice were intragastrically administered with either PBS or FMF at 100, 200, and 400 mg/kg body weight once daily for 7 consecutive days prior to single administration of APAP (500 mg/kg BW). Mice were killed at 12 h after APAP challenge. Liver samples were collected, and hepatic homogenates were used for the determination of (a) MDA, (b) GSH, (c) GSH-Px, (d) SOD, and (e) CAT levels by using the commercial kits. Results are shown as mean ± SD ($n = 8$ mice in each group). $^{***}p < 0.001$ compared with the control group; $^{###}p < 0.001$, $^{##}p < 0.01$, $^{#}p < 0.05$ compared with APAP-intoxicated group.

hepatic apoptosis [38]. As can be seen in Figure 6(a), administration of APAP to mice sharply increased levels of phosphorylated JNK and ERK. This was in good agreement with the results of previous studies. Interestingly, FMF pretreatment significantly inhibited APAP-mediated phosphorylation. Consequently, these results indicated that FMF alleviated APAP-induced hepatic apoptosis partially through inactivation of JNK/ERK MAPK pathway. Nrf2, which is a key sensor of oxidative stress, plays a protective role against APAP-induced hepatotoxicity by regulating the expression of intracellular detoxifying and antioxidant genes responsible for cytoprotective progress [12]. To examine whether FMF affects Nrf2 signaling, Nrf2 protein expression and nuclear accumulation were measured. As shown in Figure 7, despite a slight increase in Nrf2 protein level, the nuclear translocation of Nrf2 was suppressed after APAP intoxication. The

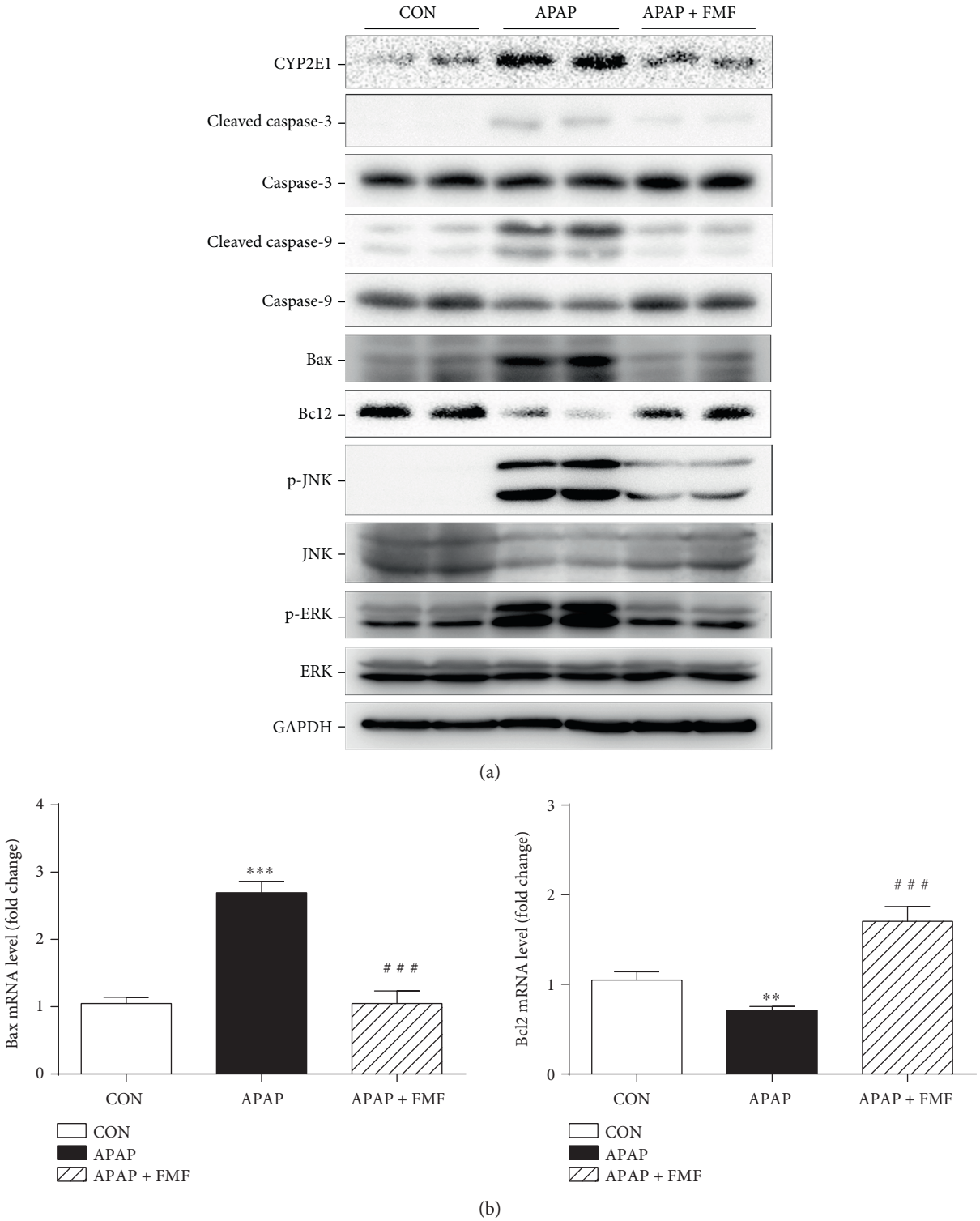

Figure 6: Effects of FMF on APAP-induced cell death-related gene expression. (a) Total cellular protein from liver tissues was extracted, and protein levels of CYP2E1, cleaved caspase-3/9, caspase-3/9, Bax, Bcl2, p-JNK, JNK, p-ERK, and ERK were determined by western blot. GAPDH was used as an endogenous control. (b) Total RNA from liver tissues was isolated and reverse-transcribed into cDNA for quantitative real-time PCR analysis of Bax and Bcl2 mRNA levels. GAPDH was used as an endogenous control. Results are shown as mean ± SD ($n = 3$). $^{***}p < 0.001$, $^{**}p < 0.01$ compared with the control group; $^{\#\#\#}p < 0.001$ compared with APAP-intoxicated group.

hypothesis that APAP treatment repressed the transcriptional activity of Nrf2 was further supported by declined expression levels of two Nrf2 target genes (NQO1 and HO-1). However, the suppression caused by APAP administration was dramatically restored by FMF pretreatment. Furthermore, FMF treatment may to some extent promote

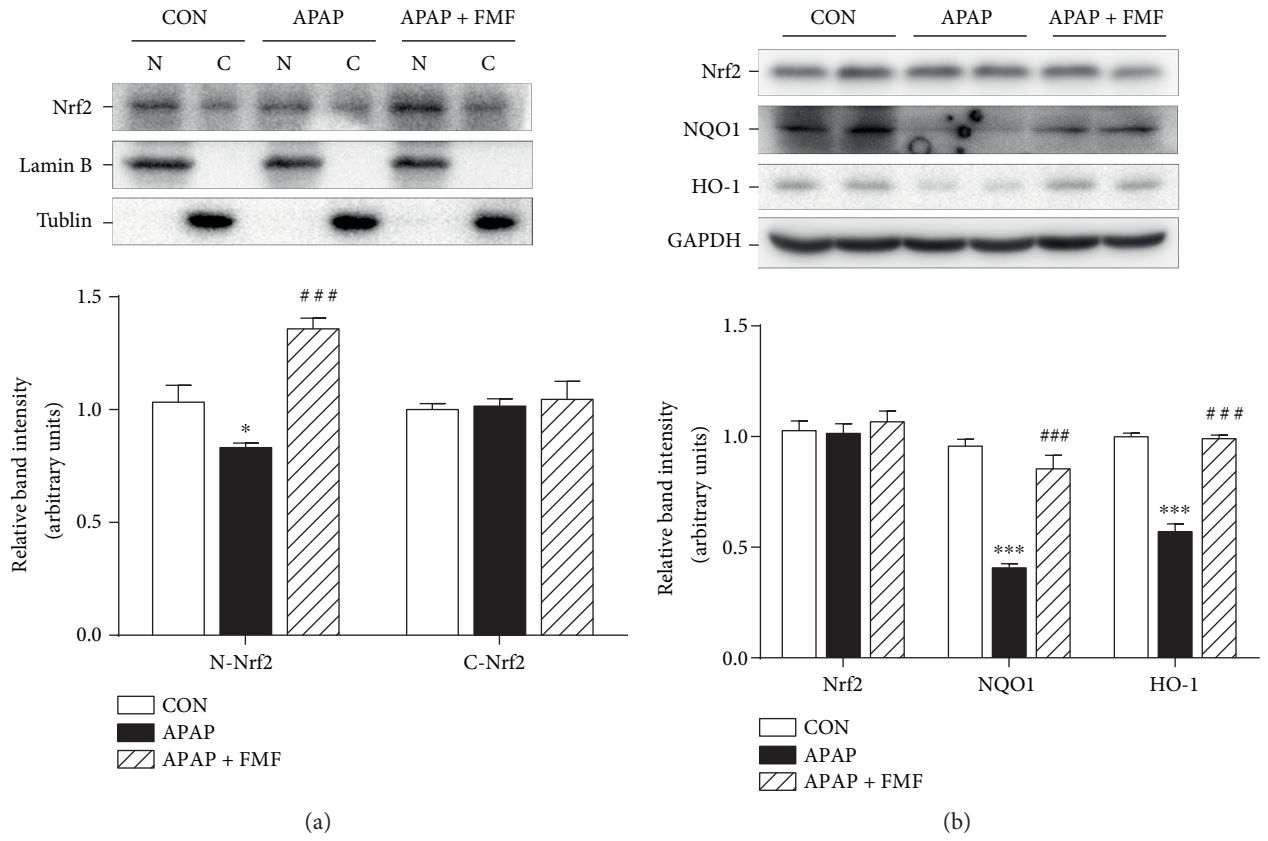

Figure 7: Effects of FMF on Nrf2 nuclear translocation and its target gene expression. (a) Nuclear and cytoplasmic extracts of liver tissues were prepared and protein level of Nrf2 was determined by western blot. Lamin B and tubulin were used as endogenous controls for nucleus and cytoplasm, respectively. (b) Total cellular protein from liver tissues was extracted, and protein levels of Nrf2, NQO1, and HO-1 were determined by western blot. GAPDH was used as an endogenous control. Relative intensity of the immunoreactive bands was analyzed and results are shown as mean ± SD ($n = 3$). $^{***}p < 0.001$, $^{*}p < 0.05$ compared with the control group; $^{\#\#\#}p < 0.001$ compared with APAP-intoxicated group.

Nrf2 nuclear translocation and its target gene expression, as verified by experiments in Hepa1–6 cells (Figure S5). Taken together, these data suggested that administration of FMF augmented Nrf2 nuclear accumulation, resulting in an enhanced antioxidant defense system to protect against APAP-induced oxidative injury.

3.6. Characterization of Chemical Composition of FMF. HPLC analysis was conducted to identify and quantify the major polyphenolic compounds present in FMF. HPLC chromatograms of standards and samples were shown in Figure S6. Under proposed HPLC analytical conditions, a good baseline separation was obtained for all the analytes, and four flavonoid glycosides, including vitexin, isovitexin, isorhamnetin-3-O-β-D-glucoside, and narcissin, were identified by comparing their retention times (21.3, 24.6, 45.3, and 47.2 min, resp.) with those of authentic standards. Quantitative data were calculated from their respective standard curves (Table S2). As shown in Figure S6 (b) and Table S2, narcissin (62.4 μg/mg) was identified as the major phenolic compound in FMF, followed by isorhamnetin-3-O-β-D-glucoside (11.3 μg/mg), isovitexin (10.6 μg/mg), and vitexin (10.4 μg/mg).

4. Discussion and Conclusions

In the present study, we demonstrate that the polyphenol-enriched fraction (FMF) from *Folium Microcos* has a preventive effect on APAP-induced hepatic apoptosis and oxidative injury. APAP-induced hepatotoxicity, as an experimentally convenient and clinically relevant animal model, is widely used to investigate liver injury associated with oxidative stress caused by ROS and other free radicals [39]. Previous studies on APAP toxicity have documented that oxidative stress is the major mechanism involved in the development of hepatotoxicity, and extensive defects of antioxidant defense systems were also observed in APAP-intoxicated tissues [34]. Currently, N-acetylcysteine (NAC), as a precursor of the antioxidant glutathione (GSH), serves as the primary and FDA-approved antidote for APAP poisoning. However, its efficacy is limited because of therapeutic window and adverse effects [40, 41]. Therefore, it is of great importance to develop effective therapeutic agents with little or no side effect.

Polyphenolic compounds, which are most abundantly present in green teas and herbal teas, have drawn increasing attention for their medicinal functions and health benefits,

and the widely accepted mechanism behind these properties involves the reduction of oxidative stress by scavenging free radicals [42]. To our knowledge, no report links hepatoprotective effects with phenolic constituents of *Folium Microcos*. In this study, the polyphenol-enriched fraction (FMF) from *Folium Microcos* exerted a strong antioxidant property in DPPH and $O_2^{\bullet-}$ scavenging assays (Figure 1) and prevented H_2O_2-induced ROS production and cell death (Figure 2). The considerable antioxidant effect of FMF, which is mainly attributed to the high content of polyphenol constituents, implies the potential of *Folium Microcos* in the prevention or attenuation of oxidative stress-mediated liver injury. This hypothesis was further verified by suppressing APAP-induced liver damage in mice pretreated with FMF. Our data showed significant increases in levels of serum ALT, AST, and LDH, which are considered as sensitive indicators of liver tissue damage, after APAP administration, as reported previously (Figure 3) [7, 10]. However, FMF pretreatment substantially prevented these elevations, suggesting that FMF not only preserved structural and functional integrity of hepatic cellular membrane but also protected liver tissues against toxic effects of APAP. Histopathological examination provided visual evidence for hepatoprotective effects of FMF, as manifested by the restoration toward histomorphological variations (Figure 4).

It is commonly recognized that enhanced lipid peroxidation and decreased functioning of enzymatic or nonenzymatic antioxidant defense systems are the major characteristics of APAP-induced hepatotoxicity [6]. In this study, administration of APAP to mice dramatically reduced liver antioxidant capacity, as characterized by remarkable increase in MDA content and decrease in hepatic levels of SOD, CAT, GSH-Px, and GSH, which are often regarded as indicators of oxidative stress response [6, 7, 10]. However, FMF pretreatment distinctly reversed the changes in parameters of hepatic oxidative damage (Figure 5). Collectively, together with histopathological evidence, the results of biochemical parameters assays in serum and liver tissue demonstrated that the protective effect of FMF on APAP-induced liver injury may result from the modification of endogenous antioxidant defense systems.

Accumulating evidence has demonstrated that hepatic apoptosis plays a central role in APAP-induced hepatotoxicity [36, 37]. In this process, ROS derived from APAP bioactivation directly activates JNK through MAPK pathway. Together with ROS, activated JNK can stimulate the expression of proapoptotic proteins and block the function of antiapoptotic proteins, leading to serious hepatotoxicity and cell apoptosis [38]. It was also reported that inhibition of JNK or hepatocyte-specific JNK knockout mice prevented the development of mitochondrial oxidative stress and decreased hepatic apoptosis and liver injury [43, 44]. Consistent with previous results, the present study showed that APAP administration caused severe impairment of antioxidant defense systems and activation of MAPK pathway. However, these alterations could be substantially reversed by FMF pretreatment (Figures 5 and 6), suggesting significant potential of FMF to protect against oxidative stress-induced hepatic apoptosis. Members of the caspase and Bcl2 families have been proposed to be crucial regulators of apoptotic response mediated by many agents. Several studies have also confirmed prominent apoptotic characteristics in APAP-intoxicated liver tissues, as evidenced by release of cytochrome c from the mitochondria, decreased Bcl2/Bax ratio, and increased activities of caspase-3, 6, 8, and 9 [45, 46]. In our hands, during APAP challenge, FMF pretreatment significantly disputed the conversion of caspase-3/9 into active forms, enhanced Bcl2 level, and reduced Bax expression in protein and mRNA levels, implying that actions of FMF against APAP-induced liver injury may be through the suppression of apoptosis (Figure 6). On this basis, our results indicated that in the presence of FMF, the decrease in ROS-mediated activation of MAPKs might act in conjunction with the reductive effect on apoptosis axis, resulting in attenuated oxidative stress and increased cell survival in response to APAP challenge.

Upon oxidative stress, the antioxidant defense system in organisms is frequently activated to provide protection against oxidative damage by maintaining cellular redox homeostasis [47]. Numerous studies have demonstrated the active involvement of Nrf2 in oxidative stress-mediated hepatotoxicity induced by APAP treatment [12–17]. To explore the possible mechanism of hepatoprotection, the present work investigated inductive effects of FMF on the activation of Nrf2 signaling. Our results revealed that FMF pretreatment reinforced Nrf2 nuclear accumulation and delayed its nuclear exclusion in response to APAP, resulting in enhanced transcriptional activities. The positive regulation of FMF on Nrf2 signaling was further manifested by the restoration of APAP-induced reduction of phase-2 enzymes, including NQO1 and HO-1 (Figure 7 and Figure S5), both of which are the major regulators that play critical roles in the elimination of ROS and toxic metabolites derived from the redox process in liver tissues. NQO1 enzymatically reduces NAPQI and prevents mitochondrial dysfunction caused by APAP [48]. HO-1 catalyzes the cleavage of heme to form biliverdin and diminishes intracellular ROS production [49]. Consequently, our results demonstrated that FMF enhanced hepatic defense system through the activation of Nrf2-mediated antioxidant and detoxifying gene expression to protect against APAP-induced liver injury.

In the current study, the main polyphenols present in FMF were identified and quantified by HPLC analysis to gain insights into the major active constituents responsible for its antioxidant and hepatoprotective effects. HPLC analysis clearly showed that narcissin (62.4 μg/mg) was identified to be the prominent phenolic compound in FMF, followed by isorhamnetin-3-O-β-D-glucoside (11.3 μg/mg), isovitexin (10.6 μg/mg), and vitexin (10.4 μg/mg) (Figure S6 and Table S2). Narcissin and isorhamnetin-3-O-β-D-glucoside share the same basic parent structure of isorhamnetin, which has been demonstrated to be not only an effective antioxidant agent but also a candidate drug for the prevention and treatment of liver diseases [50]. Isorhamnetin was reported to be efficacious in protecting hepatocytes against oxidative stress through the activation of AMPK pathways [51]. A recent study verified the hepatoprotective function of isorhamnetin in attenuating liver fibrosis by inhibiting TGF-β/Smad and

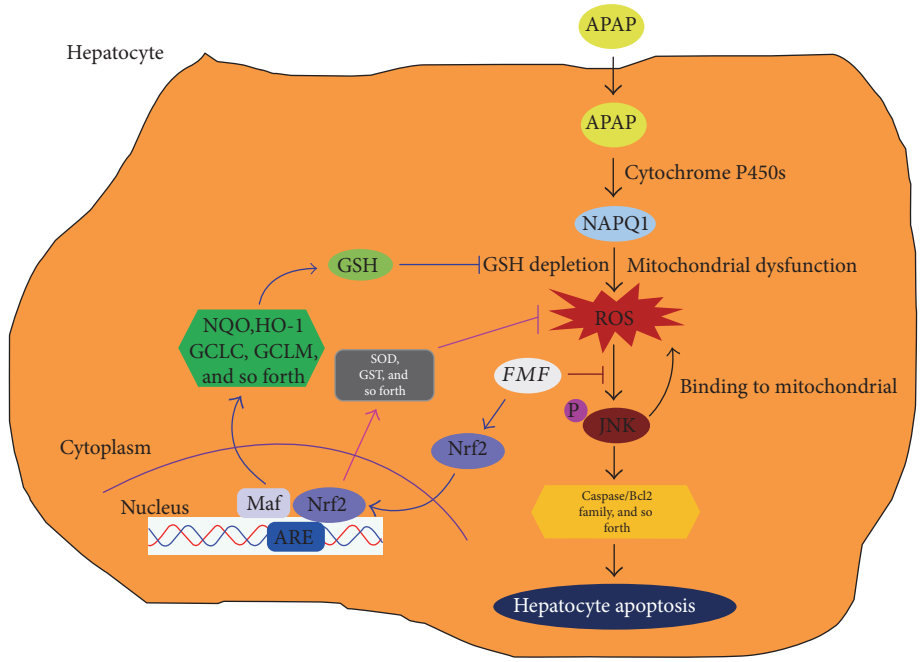

Figure 8: A proposed working model on how the polyphenol-enriched fraction (FMF) from *Folium Microcos* alleviates APAP-induced liver injury. After administration into the hepatocyte, APAP is first metabolized by cytochrome P4502E1 (CYP2E1) and generates NAPQI, which in turn depletes hepatic GSH and causes mitochondrial dysfunction, resulting in overproduction of ROS. ROS generated from mitochondria and other sources can cause the phosphorylation of JNK, which binds to the mitochondria, leading to enhanced ROS generation. Activated JNK can also phosphorylate transcription factors (e.g., c-Jun and NF-κB) as well as members of the caspase and Bcl2 families to accelerate hepatocyte apoptosis, culminating in severe liver damage. Coadministration of FMF not only alleviated the changes in ROS/MAPKs-mediated apoptotic signaling cascade during APAP challenge but also promoted Nrf2 nuclear translocation and enhanced Nrf2-mediated antioxidant defense system, ultimately leading to reduced oxidative stress and cell death.

Nrf2 signalings [52]. It was also shown that narcissin possessed significant antioxidant effects on non-enzyme-induced lipid peroxidation in isolated microsomes and increased hepatic cell viability in both CCl_4- and t-BuOOH-induced injury models [53]. Isorhamnetin-3-O-β-D-glucopyranoside was described to alleviate the adverse effects of hepatic ethanol ingestion by enhancing the activities of alcohol-oxidizing enzymes, microsomal ethanol-oxidizing system, and aldehyde dehydrogenase [54]. Vitexin, isovitexin, and vitexin- and isovitexin-enriched extracts also showed antioxidant or hepatoprotective activities [55–57]. Therefore, the presence of narcissin, isorhamnetin-3-O-β-D-glucoside, vitexin, and isovitexin in FMF from *Folium Microcos* may be the main bioactive compounds contributing to its antioxidant and hepatoprotective properties. This assumption requires further verification and will be discussed in our future studies.

In conclusion, the current study demonstrates for the first time the hepatoprotective role of FMF in liver tissues as a critical crossroad in cascade reactions triggered by APAP challenge via dual modification of the apoptosis signaling through the effects on ROS/MAPKs axis and Nrf2-mediated antioxidant defense system response (Figure 8). Collectively, our data strongly revealed the clinical potential of the polyphenol-enriched fraction from *Folium Microcos* as a natural and functional food ingredient for the prevention of oxidative stress-induced hepatic injury.

Conflicts of Interest

The authors declare that there is no conflict of interests regarding the publication of this paper.

Authors' Contributions

Hongtan Wu and Gang Zhang contributed equally to this work.

Acknowledgments

The study was supported by the Doctor Startup Fund Project of Xiamen Medical College (KX1513; K2016-09) and the Educational and Scientific Research Program for Young Scholar Sponsored by Educational Department of Fujian Province (JA14422) and the grant from the Xiamen Municipal Bureau of Science and Technology (3502Z20153032; 3502Z20161229).

References

[1] F. Yan, Q. Y. Zhang, L. Jiao et al., "Synergistic hepatoprotective effect of *Schisandrae* lignans with *Astragalus* polysaccharides on chronic liver injury in rats," *Phytomedicine*, vol. 16, no. 9, pp. 805–813, 2009.

[2] H. Jaeschke, G. J. Gores, A. I. Cederbaum, J. A. Hinson, D. Pessayre, and J. J. Lemasters, "Mechanisms of hepatotoxicity," *Toxicological Sciences*, vol. 65, no. 2, pp. 166–176, 2002.

[3] S. H. Chan, M. H. Tai, C. Y. Li, and J. Y. Chan, "Reduction in molecular synthesis or enzyme activity of superoxide dismutases and catalase contributes to oxidative stress and neurogenic hypertension in spontaneously hypertensive rats," *Free Radical Biology & Medicine*, vol. 40, no. 11, pp. 2028–2039, 2006.

[4] R. Zhu, Y. Wang, L. Zhang, and Q. Guo, "Oxidative stress and liver disease," *Hepatology Research*, vol. 42, no. 8, pp. 741–749, 2012.

[5] A. M. Larson, J. Polson, R. J. Fontana et al., "Acetaminophen-induced acute liver failure: results of a United States multicenter, prospective study," *Hepatology*, vol. 42, no. 6, pp. 1364–1372, 2005.

[6] R. N. Jadeja, N. H. Urrunaga, S. Dash, S. Khurana, and N. K. Saxena, "Withaferin-A reduces acetaminophen-induced liver injury in mice," *Biochemical Pharmacology*, vol. 97, no. 1, pp. 122–132, 2015.

[7] E. Song, J. Fu, X. Xia, C. Su, and Y. Song, "Bazhen decoction protects against acetaminophen induced acute liver injury by inhibiting oxidative stress, inflammation and apoptosis in mice," *PLoS One*, vol. 9, no. 9, article e107405, 2014.

[8] L. Tian, X. Shi, L. Yu, J. Zhu, R. Ma, and X. Yang, "Chemical composition and hepatoprotective effects of polyphenol-rich extract from *Houttuynia cordata* tea," *Journal of Agricultural and Food Chemistry*, vol. 60, no. 18, pp. 4641–4648, 2012.

[9] B. Saberi, M. D. Ybanez, H. S. Johnson, W. A. Gaarde, D. Han, and N. Kaplowitz, "Protein kinase C (PKC) participates in acetaminophen hepatotoxicity through c-jun-N-terminal kinase (JNK)-dependent and -independent signaling pathways," *Hepatology*, vol. 59, no. 4, pp. 1543–1554, 2014.

[10] Y. Ding, Q. Li, Y. Xu et al., "Attenuating oxidative stress by paeonol protected against acetaminophen-induced hepatotoxicity in mice," *PLoS One*, vol. 11, no. 5, article e0154375, 2016.

[11] H. Schroeter, C. S. Boyd, R. Ahmed et al., "c-Jun N-terminal kinase (JNK)-mediated modulation of brain mitochondria function: new target proteins for JNK signalling in mitochondrion-dependent apoptosis," *The Biochemical Journal*, vol. 372, no. Part 2, pp. 359–369, 2003.

[12] W. Wang, C. Guan, X. Sun et al., "Tanshinone IIA protects against acetaminophen-induced hepatotoxicity via activating the Nrf2 pathway," *Phytomedicine*, vol. 23, no. 6, pp. 589–596, 2016.

[13] Y. M. Jiang, Y. Wang, H. S. Tan et al., "Schisandrol B protects against acetaminophen-induced acute hepatotoxicity in mice via activation of the NRF2/ARE signaling pathway," *Acta Pharmacologica Sinica*, vol. 37, no. 3, pp. 382–389, 2016.

[14] L. M. Aleksunes, A. L. Slitt, J. M. Maher et al., "Induction of Mrp3 and Mrp4 transporters during acetaminophen hepatotoxicity is dependent on Nrf2," *Toxicology and Applied Pharmacology*, vol. 226, no. 1, pp. 74–83, 2008.

[15] A. Enomoto, K. Itoh, E. Nagayoshi et al., "High sensitivity of Nrf2 knockout mice to acetaminophen hepatotoxicity associated with decreased expression of ARE-regulated drug metabolizing enzymes and antioxidant genes," *Toxicological Sciences*, vol. 59, no. 1, pp. 169–177, 2001.

[16] K. Chan, X. D. Han, and Y. W. Kan, "An important function of Nrf2 in combating oxidative stress: detoxification of acetaminophen," *Proceedings of the National Academy of Sciences of the United States of America*, vol. 98, no. 8, pp. 4611–4616, 2001.

[17] H. Okawa, H. Motohashi, A. Kobayashi, H. Aburatani, T. W. Kensler, and M. Yamamoto, "Hepatocyte-specific deletion of the keap1 gene activates Nrf2 and confers potent resistance against acute drug toxicity," *Biochemical and Biophysical Research Communications*, vol. 339, no. 1, pp. 79–88, 2006.

[18] O. Ulicna, M. Greksak, O. Vancova et al., "Hepatoprotective effect of rooibos tea (*Aspalathus linearis*) on CCl_4-induced liver damage in rats," *Physiological Research*, vol. 52, no. 4, pp. 461–466, 2003.

[19] E. Joubert, E. S. Richards, J. D. Merwe, D. De Beer, M. Manley, and W. C. Gelderblom, "Effect of species variation and processing on phenolic composition and in vitro antioxidant activity of aqueous extracts of Cyclopia spp. (*Honeybush Tea*)," *Journal of Agricultural and Food Chemistry*, vol. 56, no. 3, pp. 954–963, 2008.

[20] S. Paul, M. A. Islam, E. M. Tanvir et al., "Satkara (*Citrus macroptera*) fruit protects against acetaminophen-induced hepatorenal toxicity in rats," *Evidence-Based Complementary and Alternative Medicine*, vol. 2016, Article ID 9470954, p. 11, 2016.

[21] P. C. Still, B. Yi, T. F. Gonzalez-Cestari et al., "Alkaloids from *Microcos paniculata* with cytotoxic and nicotinic receptor antagonistic activities," *Journal of Natural Products*, vol. 76, no. 2, pp. 243–249, 2013.

[22] Y. G. Chen, P. Li, R. Yan et al., "Alpha-glucosidase inhibitory effect and simultaneous quantification of three major flavonoid glycosides in *Microctis folium*," *Molecules*, vol. 18, no. 4, pp. 4221–4232, 2013.

[23] S. X. Feng, L. D. Lin, H. H. Xu, and X. Y. Wei, "Two new piperidine alkaloids from the leaves of *Microcos paniculata*," *Journal of Asian Natural Products Research*, vol. 10, no. 11-12, pp. 1155–1158, 2008.

[24] T. Itoh and Y. Furuichi, "Lowering serum cholesterol level by feeding a 40% ethanol-eluted fraction from HP-20 resin treated with hot water extract of adzuki beans (*Vigna angularis*) to rats fed a high-fat cholesterol diet," *Nutrition*, vol. 25, no. 3, pp. 318–321, 2009.

[25] V. L. Singleton and J. A. Rossi, "Colorimetry of total phenolics with phosphomolybdic-phosphotungstic asit reagents," *American Journal of Enology and Viticulture*, vol. 16, no. 3, pp. 144–158, 1965.

[26] J. Zhishen, T. Mengcheng, and W. Jianming, "The determination of flavonoid contents in mulberry and their scavenging effects on superoxide radicals," *Food Chemistry*, vol. 64, no. 4, pp. 555–559, 1999.

[27] K. Zhu, H. Zhou, and H. Qian, "Antioxidant and free radical-scavenging activities of wheat germ protein hydrolysates (WGPH) prepared with alcalase," *Process Biochemistry*, vol. 41, no. 6, pp. 1296–1302, 2006.

[28] M. Nishikimi, N. A. Rao, and K. Yagi, "The occurrence of superoxide anion in the reaction of reduced phenazine methosulphate and molecular oxygen," *Biochemical and Biophysical Research Communications*, vol. 46, no. 2, pp. 849–854, 1972.

[29] C. Guo, S. Liu, P. Dong et al., "Akbu-LAAO exhibits potent anti-tumor activity to HepG2 cells partially through produced H_2O_2 via TGF-beta signal pathway," *Scientific Reports*, vol. 5, p. 18215, 2015.

[30] M. B. Hansen, S. E. Nielsen, and K. Berg, "Re-examination and further development of a precise and rapid dye method for

measuring cell growth/cell kill," *Journal of Immunological Methods*, vol. 119, no. 2, pp. 203–210, 1989.

[31] L. Liu, H. Xie, X. Chen et al., "Differential response of normal human epidermal keratinocytes and HaCaT cells to hydrogen peroxide-induced oxidative stress," *Clinical and Experimental Dermatology*, vol. 37, no. 7, pp. 772–780, 2012.

[32] H. Shimoda, J. Tanaka, M. Kikuchi et al., "Walnut polyphenols prevent liver damage induced by carbon tetrachloride and δ-galactosamine: hepatoprotective hydrolyzable tannins in the kernel pellicles of walnut," *Journal of Agricultural and Food Chemistry*, vol. 56, no. 12, pp. 4444–4449, 2008.

[33] V. M. Moo-Huchin, M. I. Moo-Huchin, R. J. Estrada-Leon et al., "Antioxidant compounds, antioxidant activity and phenolic content in peel from three tropical fruits from Yucatan, Mexico," *Food Chemistry*, vol. 166, pp. 17–22, 2015.

[34] M. R. McGill, C. D. Williams, Y. Xie, A. Ramachandran, and H. Jaeschke, "Acetaminophen-induced liver injury in rats and mice: comparison of protein adducts, mitochondrial dysfunction, and oxidative stress in the mechanism of toxicity," *Toxicology and Applied Pharmacology*, vol. 264, no. 3, pp. 387–394, 2012.

[35] X. Yang, C. Dong, and G. Ren, "Effect of soyasaponins-rich extract from soybean on acute alcohol-induced hepatotoxicity in mice," *Journal of Agricultural and Food Chemistry*, vol. 59, no. 4, pp. 1138–1144, 2011.

[36] G. E. Kass, P. Macanas-Pirard, P. C. Lee, and R. H. Hinton, "The role of apoptosis in acetaminophen-induced injury," *Annals of the new York Academy of Sciences*, vol. 1010, no. 1, pp. 557–559, 2003.

[37] B. Hu and L. M. Colletti, "CXC receptor-2 knockout genotype increases X-linked inhibitor of apoptosis protein and protects mice from acetaminophen hepatotoxicity," *Hepatology*, vol. 52, no. 2, pp. 691–702, 2010.

[38] C. Latchoumycandane, C. W. Goh, M. M. Ong, and U. A. Boelsterli, "Mitochondrial protection by the JNK inhibitor leflunomide rescues mice from acetaminophen-induced liver injury," *Hepatology*, vol. 45, no. 2, pp. 412–421, 2007.

[39] H. Jaeschke, M. R. McGill, C. D. Williams, and A. Ramachandran, "Current issues with acetaminophen hepatotoxicity—a clinically relevant model to test the efficacy of natural products," *Life Sciences*, vol. 88, no. 17-18, pp. 737–745, 2011.

[40] K. J. Heard, "Acetylcysteine for acetaminophen poisoning," *The New England Journal of Medicine*, vol. 359, no. 3, pp. 285–292, 2008.

[41] E. A. Sandilands and D. N. Bateman, "Adverse reactions associated with acetylcysteine," *Clinical Toxicology (Philadelphia, Pa.)*, vol. 47, no. 2, pp. 81–88, 2009.

[42] A. S. Darvesh, R. T. Carroll, A. Bishayee, W. J. Geldenhuys, and C. J. Van der Schyf, "Oxidative stress and Alzheimer's disease: dietary polyphenols as potential therapeutic agents," *Expert Review of Neurotherapeutics*, vol. 10, no. 5, pp. 729–745, 2010.

[43] N. Hanawa, M. Shinohara, B. Saberi, W. A. Gaarde, D. Han, and N. Kaplowitz, "Role of JNK translocation to mitochondria leading to inhibition of mitochondria bioenergetics in acetaminophen-induced liver injury," *The Journal of Biological Chemistry*, vol. 283, no. 20, pp. 13565–13577, 2008.

[44] B. K. Gunawan, Z. X. Liu, D. Han, N. Hanawa, W. A. Gaarde, and N. Kaplowitz, "c-Jun N-terminal kinase plays a major role in murine acetaminophen hepatotoxicity," *Gastroenterology*, vol. 131, no. 1, pp. 165–178, 2006.

[45] A. Kumari and P. Kakkar, "Lupeol prevents acetaminophen-induced in vivo hepatotoxicity by altering the Bax/Bcl-2 and oxidative stress-mediated mitochondrial signaling cascade," *Life Sciences*, vol. 90, no. 15-16, pp. 561–570, 2012.

[46] D. Dong, L. Xu, X. Han et al., "Effects of the total saponins from *Rosa laevigata* Michx fruit against acetaminophen-induced liver damage in mice via induction of autophagy and suppression of inflammation and apoptosis," *Molecules*, vol. 19, no. 6, pp. 7189–7206, 2014.

[47] Q. Ma and X. He, "Molecular basis of electrophilic and oxidative defense: promises and perils of Nrf2," *Pharmacological Reviews*, vol. 64, no. 4, pp. 1055–1081, 2012.

[48] J. S. Moffit, L. M. Aleksunes, M. J. Kardas, A. L. Slitt, C. D. Klaassen, and J. E. Manautou, "Role of NAD(P)H:quinone oxidoreductase 1 in clofibrate-mediated hepatoprotection from acetaminophen," *Toxicology*, vol. 230, no. 2-3, pp. 197–206, 2007.

[49] N. G. Abraham and A. Kappas, "Pharmacological and clinical aspects of heme oxygenase," *Pharmacological Reviews*, vol. 60, no. 1, pp. 79–127, 2008.

[50] J. H. Yang, B. Y. Shin, J. Y. Han et al., "Isorhamnetin protects against oxidative stress by activating Nrf2 and inducing the expression of its target genes," *Toxicology and Applied Pharmacology*, vol. 274, no. 2, pp. 293–301, 2014.

[51] G. Z. Dong, J. H. Lee, S. H. Ki et al., "AMPK activation by isorhamnetin protects hepatocytes against oxidative stress and mitochondrial dysfunction," *European Journal of Pharmacology*, vol. 740, pp. 634–640, 2014.

[52] J. H. Yang, S. C. Kim, K. M. Kim et al., "Isorhamnetin attenuates liver fibrosis by inhibiting TGF-beta/Smad signaling and relieving oxidative stress," *European Journal of Pharmacology*, vol. 783, pp. 92–102, 2016.

[53] R. Gevrenova, M. Kondeva-Burdina, N. Denkov, and D. Zheleva-Dimitrova, "Flavonoid profiles of three *Bupleurum* species and in vitro hepatoprotective of activity *Bupleurum flavum* Forsk," *Pharmacognosy Magazine*, vol. 11, no. 41, pp. 14–23, 2015.

[54] J. M. Hur, S. H. Park, J. W. Choi, and J. C. Park, "Effects of extract and isorhamnetin glycoside from *Brassica juncea* on hepatic alcohol-metabolizing enzyme system in rats," *Natural Product Sciences*, vol. 18, no. 3, pp. 190–194, 2012.

[55] T. Liu, X. H. Yu, E. Z. Gao et al., "Hepatoprotective effect of active constituents isolated from mung beans (*Phaseolus radiatus* L.) in an alcohol-induced liver injury mouse model," *Journal of Food Biochemistry*, vol. 38, no. 5, pp. 453–459, 2014.

[56] J. H. Kim, B. C. Lee, G. S. Sim et al., "The isolation and antioxidative effects of vitexin from *Acer palmatum*," *Archives of Pharmacal Research*, vol. 28, no. 2, pp. 195–202, 2005.

[57] C. M. Lin, C. T. Chen, H. H. Lee, and J. K. Lin, "Prevention of cellular ROS damage by isovitexin and related flavonoids," *Planta Medica*, vol. 68, no. 4, pp. 365–367, 2002.